Molecular Dynamics Simulation Study for Investigating the Role of Trimethylamine-N-Oxide in Stabilizing Protein Conformation

A Thesis Submitted

in Partial Fulfillment of the Requirements

for the Degree of

DOCTOR OF PHILOSOPHY

by

Rahul Sarma

to the

Department of Chemistry

Indian Institute of Technology Guwahati, India

November, 2013

Dedicated to
my beloved parents

Declaration

I hereby declare that the matter manifested in this thesis "*Molecular Dynamics Simulation Study for Investigating the Role of Trimethylamine-N-Oxide in Stabilizing Protein Conformation*" is the result of research carried out by me in the Department of Chemistry, Indian Institute of Technology Guwahati, India under the supervision of Dr. Sandip Paul.

In keeping with the general practice of reporting scientific observations, due acknowledgement has been made wherever the work described is based on the findings of other investigators.

Rahul Sarma
IIT Guwahati

Certificate

It is certified that the work contained in this thesis entitled, "*Molecular Dynamics Simulation Study for Investigating the Role of Trimethylamine-N-Oxide in Stabilizing Protein Conformation*" has been carried out by Rahul Sarma for the Degree of Doctor of Philosophy under my supervision and the same has not been submitted elsewhere for a degree.

Dr. Sandip Paul
Thesis Supervisor
Department of Chemistry
Indian Institute of Technology Guwahati
Guwahati-781039, India

Preface

Over the past few years, the osmolyte trimethylamine-N-oxide (TMAO) has generated considerable research interest to the community of biophysicists and biochemists for its ability to stabilize proteins and nucleic acids, correct medicinally significant issues, such as prion aggregation and cellular folding defects, and counteract protein denaturation by urea, heat, and pressure. Although TMAO's protein protecting ability under harsh environmental conditions is well-established and interest in how TMAO exerts its stabilizing effect has remained very active, what is still unknown is the mechanism by which TMAO exactly stabilizes proteins and offset pressure- and urea-conferred protein denaturation. The entitled thesis seeks to address this issue by means of classical molecular dynamics simulations.

It is my great pleasure to express here few words of appreciation to the people who actually made this thesis a reality and an unforgettable experience for me. I wish, in particular, to express profound gratitude and sincere respect to my thesis supervisor Dr. Sandip Paul for his excellent guidance, constant encouragement, unstinting inspiration, and amicable cooperation during the course of this work. In my countless discussion sessions with him which I am going to treasure forever, he not only showed how science and its challenges could be made interesting to ease out a solution, but also taught me the way this fun conveyed to the others. I am indebted to Prof. Arun Chattopadhyay, Prof. Gopal Das, Dr. Debasis Manna, and Dr. Manabendra Sarma for periodically assessing my work and providing valuable suggestions for its improvement. My sincere thanks go to all other faculty members in the department for their kind help at various stages of my doctoral work.

I am grateful to Dhruba Da (Dr. Dhruba Jyoti Kalita), Renjith Da, Somnath Da (currently in France), and Bhaskar Da for their help and cheerful association, which were very much available in times of need. No words will be sufficient to express my feelings to labmates Subrata, Bhanita, Gargi, and Shubhadip whom I consider a part of my life. I am truly grateful to them for taking the time to listen to many questions arising in my mind and sharing their knowledge about computer simulations. They read several parts of the thesis and made suggestions for its betterment. I owe a lot to my friends Aswini, Apurba, Jiban, Naba, Jayanta, Subrata, Suraj, Paramartha, Harikrishna, Debashis, and Nirmali,

and all other research scholars in the department for their lively company during my stay in IITG.

I take this opportunity to express my sincere thanks to all my teachers in school, college, and university days for helping and encouraging me in various aspects of life and academics. All of my learning from them will be an asset in every walk of my life. I am grateful to the institute and also Council of Scientific and Industrial Research (CSIR), India for the financial support.

Many thanks go at last but certainly not the least to my family for their understanding, encouragement, and patience in my every endeavor. This thesis would not have seen the light of this day without their great wishes, immense patience, and great sacrifice. A famous quote reads- "Every journey begins with a single step"- and today, only because of my family, I move a step uphill towards my zenith.

Rahul Sarma

November 2013

"A scientific truth does not triumph by convincing its opponents and making them see the light, but rather because its opponents eventually die and a new generation grows up that is familiar with it."

– Max Planck

Outline of the Thesis

Chapter 1

Introduction

"Protein unfolding simulations are coming of age. They can be expected to fairly reliably depict protein folding/unfolding transition states, intermediate states, and denatured states, provided explicit solvent and good simulation techniques are employed. Simulations provide a molecular framework for the interpretation of experimental protein folding studies, and they are readily amenable to validation by comparison with experiment."

— V. Daggett *Chem. Rev.* **106**, 1898 (2006)

■ PROTEIN DENATURATION AND COUNTERACTION

The in-depth knowledge of environment effects on protein structure, stability, and function has been drawing the attention of many researchers. Proteins are known to show structural changes at high pressure. Numerous studies indicated that, in contrast to the heat-denatured proteins, pressure-denatured proteins are relatively compact [1]. Negative volume change upon pressure unfolding has been observed and, most likely, arises from combination of some compensating factors that include elimination of internal cavities and voids upon disruption of folded structures and exposure of hydrophobic and polar moieties [2-4]. In a nuclear magnetic resonance (NMR) study, the hydrogen exchange rate of proteins was found to be higher under high pressure conditions, suggesting protein denaturation through the penetration of water molecules into the tightly packed hydrophobic core of proteins [5]. In fact, water penetration into the protein interior at high pressure has been considered as a primary driving force for pressure-induced protein structural transition [2, 6-15]. The molecular dynamics (MD) simulations of the protein ubiquitin by Day and García [13] showed that the high pressure structure has more penetrating water molecules than the low pressure structure, providing evidence for the water penetration model; but they did not observe any structural transition of proteins. Recently, Imai and Sugita [15] reproduced the experimentally observed structural transition of ubiquitin, an opening of a central cleft, by 1 μs MD simulations at three pressures of 1, 3000, and 6000 bar. Combining their results with those in a previous thermodynamic study [16], they concluded that water penetration is the primary driving force for protein denaturation under high pressure. A similar conclusion, "the main driving force of protein denaturation at high pressures is the decrease of the hydrophobic effect," was made by Grigera and McCarthy in their MD study of effect of high pressure on the protein apomyoglobin [14].

In a series of studies by Kinoshita and co-workers, it was argued that water molecules in the bulk are extremely crowded at high pressure and penetration into the protein interior increases their total entropy in the system, favoring the pressure-denatured structure [17-19]. Significant collapse of water second shell was seen in some recent studies [20, 21]. Using small-angle X-ray scattering (SAXS) in combination with a liquid state theoretical approach, Schroer *et al.* [22] studied the influence of pressure on the structure and protein-protein interaction potential of dense protein solutions. They reported that the structural change of water structure at high pressure leads to a modification of the structure and intermolecular interaction potential of the protein lysozyme. On these grounds, it is reasonable

to assume that water penetration into protein interior and consequent dissolution of hydrophobic groups is associated with structural change of water caused by high hydrostatic pressures.

Protein denaturation occurs not only from changes in thermodynamic variables such as temperature and pressure, but is also caused by variation in pH, extracellular salt, and other co-solutes. Natural osmolytes, small organic molecules accumulated by organisms in response to osmotic stress, are known to affect the stability, structure, and function of proteins. In particular, it has been known for many years that a high concentration of urea, which is one of the most commonly available osmolytes, can cause protein denaturation in solution [23, 24] and hence can inhibit many important biological processes. Based on many experimental and theoretical studies, two mechanisms, 'indirect' and 'direct' interaction models, have been posited for urea-conferred protein denaturation. The indirect mechanism presumes that urea acts as a structure breaker for water so as to enhance hydration of protein sites [25-32]. On the other hand, the direct mechanism hypothesizes that urea molecules preferentially bind to protein through their stronger interactions with protein backbone or side-chains than water [33-47]. Despite the extensive studies from both experiment and theory in the past several decades, it is not clear whether the direct or indirect effect provides the driving force in urea-induced protein denaturation. In the meantime, combining the observations obtained from MD simulations of two peptides, chicken villin headpiece (HP-35) and its mutant, with those from previous simulation studies on a number of β-hairpins [32, 48] as well as on the hydration of the hydrophobic carbon nanotube [31], Gao and co-workers concluded that urea denaturation of proteins involves both direct and indirect effects [49]. A MD simulation study of the protein chymotrypsin inhibitor 2 (CI2) in 8 M urea by Bennion and Daggett [50] also indicated the importance of both direct and indirect mechanisms in urea-conferred denaturation. Urea can alter water structure and dynamics, making it free to act as the primary denaturant early in unfolding, thereby providing a link between the direct and indirect effects. The range of opinions is, however, very broad and interest in how urea causes protein denaturation remains strong even today.

Organisms also accumulate some other osmolytes that counteract protein perturbation induced by harsh environmental stresses. In terms of their effects on the functional activity of proteins, these osmolytes can be classified either as 'compatible' or 'counteracting' [51, 52]. Compatible osmolytes stabilize proteins without substantially affecting protein functional activity, whereas counteracting osmolytes are believed to cause changes

in protein function. Certain amino acids (e.g. proline and glycine) and polyols (e.g. trehalose, sucrose, and sorbitol) are representatives of compatible osmolytes and protect proteins against high temperature, freezing, anhydrobiosis etc. Counteracting osmolytes, on the other hand, consist of the methylamine class of osmolytes (trimethylamine-N-oxide [TMAO], betaine etc.) and can counteract deleterious effects of urea, inorganic ion, and hydrostatic pressure. TMAO (chemical structure shown below) represents the extreme

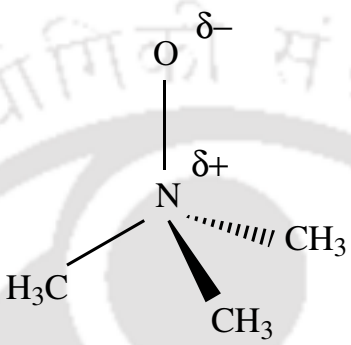

among the counteracting osmolytes and has generated considerable research interest to the community of biophysicists and biochemists over the past few years. This compound is particularly known for its ability to stabilize proteins [53, 54] and nucleic acids [55], correct medicinally significant issues, such as prion aggregation [56] and cellular folding defects [57], and protect proteins in perturbing conditions [23, 58-62]. TMAO's ability to counteract urea-induced protein denaturation at urea to TMAO concentration ratio of 2:1 has been extensively confirmed in a variety of protein systems and has also been demonstrated for nucleic acids in the form of bacterial tRNA, and more interestingly, this is the ratio generally found in tissues containing high urea levels [58, 60, 61]. For deep sea animals, Yancey [61] reported a linear increase of TMAO concentration with depth of the sea both among different species and within the same species. The common osmolytes of shallow relatives, e.g., urea in skates, were replaced by high levels of TMAO and the typical 2:1 concentration ratio of urea to TMAO in shallow elasmobranchs was found to be altered by a 1:2 urea:TMAO ratio in a species from 3 km depth [61]. These findings led Yancey to suggest that TMAO might act as a pressure counteractant. TMAO was indeed observed to offset pressure-inhibition of stability of several lactate dehydrogenase homologous, polymerization of actin, enzyme-substrate binding for two enzymes, and growth of living yeast cells [61]. Recent SAXS studies also provided evidence for the counteracting effect of TMAO against pressure [59, 62].

The question of significant interest is then, how does TMAO cause protein stabi-

lization and protect proteins at high pressure or in highly concentrated urea solution? A large number of studies have been devoted in this direction, but the mechanism has remained somewhat elusive. Multiple proposals have been put forward that include protein stabilization by preferential exclusion of TMAO [53, 63-66] through alteration of water structure [31, 32, 67] to preferential solvation of TMAO by water and urea [68]. TMAO's depletion from the protein surface is a well-captured phenomenon [63-66, 69, 70]. However, the preferential exclusion model does not explain the role of water in solvation of protein sites. Due to the exclusion of TMAO from the proximity of the protein surface, inclusion of water in the surface of the protein becomes inevitable (termed as preferential hydration). If the protein residues are considered to be better hydrated in TMAO solution as compared to pure water or if there is little difference in protein hydration shell between pure water and TMAO solution, then, the question is, why does an unfolded protein shift to its folded state in the presence of TMAO? Clearly, the preferential exclusion model alone is not sufficient to answer this question. Again, simulation studies indicated a small enhancement in the concentration of TMAO molecules in the vicinity of hydrophobic solutes as well as of hydrophobic polymer [71] and decaalanine peptide [72] in binary TMAO solution. Therefore, better accommodation of TMAO near the hydrophobic surface of protein is not unlikely. Interaction of TMAO with positively charged side-chains as well as with the peptide backbone through its hydrated form has also been suggested in the literature [73-76].

In solution, TMAO was found to interact strongly with water to form di- and/or tri-hydrated TMAO complexes [67, 68, 77, 78]. So the preferential solvation model in which water and urea prefer to solvate TMAO over protein residues seems useful at first instance, and corresponding to this model, a decrease in the number of protein−water hydrogen bonds [72, 73] and dehydration of a carbon nanotube [31] were observed in TMAO solution. However, the same was not applicable in the case of urea. TMAO did not show much affect on protein−urea interaction [72, 73], consistent with the experimental findings that the efficiency of an osmolyte to act on the protein is not interferred by the presence of a second osmolyte [79, 80]. Again, although enhancement of water structure by TMAO in the form of stronger water−water hydrogen bonds and long-range spatial ordering of the solvent was observed in previous simulation studies [31, 32, 67, 68], and TMAO effect on protein hydration through its indirect effect on water structure has been proposed [31, 67, 68, 73, 78, 81-84], by no means is the model sufficient to explain the mechanism of action of TMAO. Different measures of water structure have been found to display opposite trends

in the presence of TMAO, highlighting the limitations of arguments that relate enhanced or decreased water structure to macromolecular thermodynamics [67, 71, 72].

Thus, how TMAO stabilizes proteins and counters the pressure- and urea-conferred protein denaturation remains to be an important unanswered question in protein science. The entitled thesis seeks to address this issue by means of classical MD computer simulations. Rather than extrapolating the results from binary TMAO solution at ambient pressure condition to urea/TMAO mixture or high pressure conditions, we focus on both binary and ternary solutions of urea and TMAO as well as on binary TMAO solutions under high pressure conditions. Our simulation works and concluding remarks are presented in the following five chapters. The rest part of the current chapter is organized as follows. The basic techniques of MD simulation that is employed in our work are outlined in the next section. More details of the applications of these techniques for specific systems are given in later chapters. This is followed by a brief description of the work presented in the current thesis.

■ METHODOLOGY

We consider an N-particle system characterized by the following Hamiltonian

$$H = \sum_{i=1}^{N} \frac{p_i^2}{2m} + U(\mathbf{r}^N) \tag{1.1}$$

where m is the mass of each particle, p_i is the momentum of the i-th particle and $U(\mathbf{r}^N)$ is the total potential energy of the system which includes the all particle-particle interactions. The coordinates of the particles are denoted by $\mathbf{r}^N = \{\mathbf{r}_1, \cdots, \mathbf{r}_N\}$. The position and velocity of the i-th particle is represented by $\mathbf{r}_i$ and $\mathbf{v}_i$, respectively. The method of molecular dynamics consists of solving the equation

$$\ddot{\mathbf{r}}_\mathbf{i} = \frac{\mathbf{F_i}}{m_i}(\mathbf{r_1}, \mathbf{r_2}, ...\mathbf{r_N}) \tag{1.2}$$

where $i = 1, 2, ...N$, m_i is the mass of i-th particle and $\mathbf{F}_i$ is the force acting on particle i. This equation is obtained easily from the Lagrangian

$$L = \frac{1}{2}\sum_{i=1}^{N} m_i \mathbf{v_i}.\mathbf{v_i} - \frac{1}{2}\sum_{i=1}^{N}\sum_{j\neq i}^{N} u(r_{ij}) \tag{1.3}$$

where the potential U has been assumed to be the sum of pair potentials u_{ij}. The Lagrangian equation of motion is

$$\frac{d}{dt}(\frac{\partial L}{\partial \dot{q}_i}) - \frac{\partial L}{\partial \dot{q}_i} = 0 \tag{1.4}$$

It is clear from Eq. 1.4 that the dynamics of particles is described by 3N number of second order differential equations.

It is also possible to write down the Hamiltonian (H) for the system and solve the the Hamiltonian equations of motion

$$\dot{\mathbf{q}}_k = \frac{\partial H}{\partial p_k} \tag{1.5}$$

$$\dot{\mathbf{p}}_k = -\frac{\partial H}{\partial q_k} \tag{1.6}$$

where $\mathbf{q}_k$ and $\mathbf{p}_k$ represent generalized coordinates and momenta. For a system with pair-wise interaction potential, the Hamiltonian is

$$H = \frac{1}{2}\sum_{i=1}^{N} m_i \mathbf{v_i}.\mathbf{v_i} + \frac{1}{2}\sum_{i=1}^{N}\sum_{j\neq i}^{N} u(r_{ij}) \tag{1.7}$$

and Eqs. 1.5 and 1.6 yield

$$\dot{\mathbf{r}} = \frac{\mathbf{p_i}}{m_i} \tag{1.8}$$

$$-\dot{\mathbf{p}}_i = -\nabla \mathbf{u} = \mathbf{F_i} \tag{1.9}$$

where i=1,2,....N. There are now $6N$ first order differential equations to be solved.

The equations of motion are usually integrated by using finite difference methods. The Verlet algorithm is one of the most commonly used algorithms used for this purpose [85]. Its implementation is straightforward too. Consider the Taylor's expansion for the position at time $(t + \Delta t)$:

$$\mathbf{r}(t+\Delta t) = \mathbf{r}(t) + \dot{\mathbf{r}}(t)\Delta t + \ddot{\mathbf{r}}(t)\frac{\Delta^2 t}{2!} + ... \tag{1.10}$$

$$\mathbf{r}(t-\Delta t) = \mathbf{r}(t) - \dot{\mathbf{r}}(t)\Delta t + \ddot{\mathbf{r}}(t)\frac{\Delta^2 t}{2!} + ... \tag{1.11}$$

Addition of the above two equations gives

$$\mathbf{r}(t+\Delta t) = -\mathbf{r}(t-\Delta t) + 2\mathbf{r}(t) + \ddot{\mathbf{r}}(t)\Delta^2 t + ... \tag{1.12}$$

If the positions of the particles are known for at least two successive time steps then it is possible to predict its position at time $(t + \Delta t)$. We will also need to compute velocities and these can be obtained from

$$\mathbf{v}(t) = \frac{\mathbf{r}(t+\Delta t) - \mathbf{r}(t-\Delta t)}{2\Delta t} \tag{1.13}$$

This simple algorithm has several advantages. It is simple and the force on the particles need to be computed only once in each time step. In the present work, we have employed

the so-called leap-frog scheme which is a slight modification of the basic Verlet algorithm [85]. The leap-frog scheme consist of the following two equations

$$\mathbf{r}(t+\delta t) = \mathbf{r}(t) + \delta t \mathbf{v}(t+\frac{1}{2}\delta t) \tag{1.14}$$

$$\mathbf{v}(t+\delta t) = \mathbf{v}(t-\frac{1}{2}\delta t) + \delta t \cdot \mathbf{r}(t) \tag{1.15}$$

In the algorithm, the velocity equation is implemented first and then the position equation. The equations of motion can also be solved by using other schemes such as the predictor-corrector methods [85].

In the present work, we will deal with dipolar molecules where both position and orientation and the corresponding velocities need to be considered. For rigid molecules, it is natural to divide molecular motion into translation of the centre of mass and rotation about the centre of mass. The translational motion is handled by the methods described above. The rotational motion is governed by the torque τ_i. The orientation of a rigid molecule can be specified by three Euler angles ϕ, θ and ψ. These angles specify the relation between an axis system fixed in space and one fixed with respect to the body. When the angular equations of motion are written directly in terms of the derivatives of the Euler angles, they suffer from a serious drawback. A divergence occurs when θ approaches 0 or π [85]. In order to overcome this problem, Evans [86] proposed the use of quaternion parameters as generalized angular coordinates. Quaternions give well-behaved equations of motion. The basic simulation algorithm involving quaternions has been described by Evans and Murad [87]. The four quaternions q_0, q_1, q_2 and q_3 satisfy the constraint

$$q_0^2 + q_1^2 + q_2^2 + q_3^2 = 1 \tag{1.16}$$

and they are related to the Euler angles by the following relations [85]

$$\begin{aligned} q_0 &= \cos\frac{1}{2}\theta\cos\frac{1}{2}(\phi+\psi) \\ q_1 &= \sin\frac{1}{2}\theta\cos\frac{1}{2}(\phi-\psi) \\ q_2 &= \sin\frac{1}{2}\theta\sin\frac{1}{2}(\phi-\psi) \\ q_3 &= \cos\frac{1}{2}\theta\sin\frac{1}{2}(\phi+\psi) \end{aligned} \tag{1.17}$$

The rotation matrix $\mathbf{A}$ which connects a vector in space fixed coordinate frame to the one in the body fixed frame is given by

$$\mathbf{A} = \begin{pmatrix} q_0^2+q_1^2-q_2^2-q_3^2 & 2(q_1q_2+q_0q_3) & 2(q_1q_3-q_0q_2) \\ 2(q_1q_2-q_0q_3) & q_0^2-q_1^2+q_2^2-q_3^2 & 2(q_2q_3+q_0q_1) \\ 2(q_1q_3+q_0q_2) & 2(q_2q_3-q_0q_1) & q_0^2-q_1^2-q_2^2+q_3^2 \end{pmatrix}$$

The quaternions satisfy the following equations of motion

$$\begin{pmatrix} \dot{q_0} \\ \dot{q_1} \\ \dot{q_2} \\ \dot{q_3} \end{pmatrix} = \frac{1}{2} \begin{pmatrix} q_0 & -q_1 & -q_2 & -q_3 \\ q_1 & q_0 & -q_3 & q_2 \\ q_2 & q_3 & q_0 & -q_1 \\ q_3 & -q_2 & q_1 & q_0 \end{pmatrix} \begin{pmatrix} 0 \\ \omega_x^b \\ \omega_y^b \\ \omega_z^b \end{pmatrix}$$

where ω_α^b is the α-th component of angular velocity of a molecule in its body-fixed frame. The angular velocity is conveniently calculated from the torque in the space fixed frame and then it is converted to the body fixed frame with the help of the rotation matrix. The above equations are well-behaved and can be solved by Gear predictor-corrector method [85]. A leap-frog algorithm for quaternions has also been formulated [85, 88] and is employed in the present work.

The force field implemented in this work is pair-additive and has the following form:

$$u_{ij}^{LJ}(r_{ij}) = 4\epsilon_{ij}\left[\left(\frac{\sigma_{ij}}{r_{ij}}\right)^{12} - \left(\frac{\sigma_{ij}}{r_{ij}}\right)^{6}\right] \tag{1.18}$$

with two parameters: σ, the diameter, and ϵ, the well depth. In a simple approach to tackle the long-range charge-charge interaction, the pair-wise potential is supplemented with the appropriate Coulomb potential:

$$u_{ij}^{Coulomb}(r_{ij}) = \frac{q_i q_j}{4\pi\epsilon_o r_{ij}} \tag{1.19}$$

where q_i, q_j are the charges and ϵ_o is the permittivity of free space.

Chapter 5 treats intramolecular interactions (bond stretching, bond-angle, dihedral angle interactions etc.) as well by adding a function $U_{intramolecular}$ to the potential function:

$$\begin{aligned} U_{intramolecular} &= \sum_{bonds} K_b(b_{ac}-b_{eq})^2 \\ &+ \sum_{angles} K_\theta(\theta_{ac}-\theta_{eq})^2 \\ &+ \sum_{dihedrals} \frac{V_n}{2}(1+cos(n\phi-\delta)) \end{aligned} \tag{1.20}$$

In Eq. 1.20, b, θ, ϕ, and δ represent bond length, bond angle, dihedral angle, and phase angle, respectively, with subscripts ac and eq standing for actual and equilibrium,

respectively. K_b, K_θ, and V_n are the force constants for bond, bond angle, and dihedral angle.

■ PRESENT WORK

Because of its well-documented counteracting effect against protein denaturation by high pressure or urea and its unresolved issues concerning the mechanism, we perform simulations for investigating the role of TMAO in stabilizing protein conformation both at low and high pressures in the presence and absence of urea. Consequently, each of the chapters that describe our simulations (**Chapters 2-5**) is divided into two parts: Part A and Part B. Part A concentrates on protein stabilization in urea/TMAO mixture, whereas Part B focuses on the same at high pressure in binary TMAO solutions. **Chapters 2** and **3** deal with hydrophobicity of methane and neopentane, respectively, in the presence and absence of urea and TMAO at different pressures. While the small solute methane is computationally effective to understand hydrophobicity in aqueous environments, the relatively larger solute neopentane has been shown to display many of the characteristics that one expects to find only in very large hydrophobic objects. Each of these two chapters is organized into two parts. In Part A, we have examined the aggregation of non-polar solutes in pure water at 1 bar and then extended it to binary and ternary solutions of urea and TMAO at 1 bar. Two different models are used for both methane and neopentane to see the model dependency of hydrophobicity, if any. On the other hand, in Part B, hydrophobic aggregation is investigated in pure water as well as in aqueous solutions of increasing TMAO concentrations over a wide range of pressures relevant to protein denaturation. An insight picture of the pressure- and osmolyte-induced modification of hydrophobic interaction is obtained by examining direct interactions of the solute with solution species. Orientation of solution species in the close proximity of the solute is also investigated. The time-averaged normalized ratios of water oxygen, urea carbon, and TMAO nitrogen in different solutions are used to examine the preferential accumulation or depletion of solution species near the solute. This is followed by investigation of osmolyte solvation by water and its indirect effect on water structure. The familiar water oxygen−oxygen radial distribution function (rdf) is used to describe water structuring. Finally, the hydrogen bond properties and dynamics of water molecules in different spherical regions of a single hydrophobic solute are studied to describe water−water hydrogen bonding at discrete distances from the solute.

In **Chapter 4**, solvation characteristics of N-methylacetamide (NMA) are investigated thoroughly in the presence and absence of urea and TMAO at different pressures.

The solute NMA is of interest mainly because it is the smallest amide that contains the peptide linkage, the important fraction determining the extent of protein (de)stabilization by osmolytes, in addition to hydrophobic sites, and represents the typical solvent-exposed state of proteins. Part A of this chapter focuses osmolyte effects on NMA solvation at 1 bar pressure. Structural, energetic, and dynamical properties of NMA hydrogen bonds with solution species are investigated. To shed light on the counteracting mechanism, we have also examined here solvation of TMAO by water and urea and studied structural, energetic, and dynamical properties of various possible hydrogen bonds between solution species. In Part B, we have extended our examination of NMA hydration characteristics in pure water system at 1 bar to systems with high pressure and high TMAO concentration to see how the hydration of NMA atomic sites is affected by pressure and what the role of TMAO is on this pressure-induced modification of NMA hydration. Solvation of NMA by TMAO under high pressure conditions is then examined. This is followed by investigation of water structure in these different solution conditions. Water oxygen−oxygen rdf is used to describe water structuring. The hydrogen bond properties and dynamics of water molecules are also studied and the influence of increasing TMAO concentration on water structural and dynamical properties with increasing pressure is discussed.

Chapter 5 deals with solvation characteristics of a more realistic protein. Using two different conformations (helix and extended) of a 15-residue model peptide, we have investigated here direct interactions of peptide residues with solution species in pure water as well as in binary and ternary solutions of urea and TMAO at different pressures. In Part A, various site−site rdfs between the peptide and solution species are computed to see the solution structure near the peptide in pure water and also in binary and ternary solutions of osmolytes at 1 bar. Thereafter, we have given a close look on the solution compositions around the peptide. Finally, hydrogen bonding interactions between the peptide and solution species are investigated. Following important issues are addressed in Part B. First, what is the role of TMAO on the pressure-induced modification of peptide hydration? Can TMAO offset enhanced hydration of the peptide under high pressure conditions? Second, how does TMAO interact with peptide residues and water molecules at high pressure and what is the implication of TMAO solvation by water in pressure-induced modification of water structural properties? The thesis is ended in **Chapter 6** by presenting a summary of the results together with our view on TMAO's protein protecting action.

Chapter 2

Hydrophobicity of the Small Solute Methane

"The hydrophobic effect – the tendency for oil and water to segregate – is important in diverse phenomena, from the cleaning of laundry, to the creation of micro-emulsions to make new materials, to the assembly of proteins into functional complexes. This effect is multifaceted depending on whether hydrophobic molecules are individually hydrated or driven to assemble into larger structures. Despite the basic principles underlying the hydrophobic effect being qualitatively well understood, only recently have theoretical developments begun to explain and quantify many features of this ubiquitous phenomenon."

– D. Chandler *Nature(London)* **437**, 640 (2005)

Hydrophobic interactions are important in a variety of aqueous systems [89-91], the most important example being in proteins where the initial stage of folding is caused by the collapse and aggregation of strongly hydrophobic amino acid residues. Because of its well-recognized importance in protein folding as well as in other biological self-assembly processes such as micelle formation, lipid membrane formation, and molecular recognition, a large number of studies have been devoted to elucidate the molecular origin of the hydrophobic effect (hydrophobic hydration and the solvent-mediated attraction of nonpolar substances to aggregate in aqueous solution with respect to that which they would have in a nonpolar solvent). All facets of the hydrophobic effect are, however, not well understood even for the smallest hydrophobic solute, methane, and many of the issues concerning the hydrophobic effect are either controversial or unresolved. Consequently, experimental and theoretical endeavors to understand the behavior of methane in water are still going on.

In this chapter, we have included a report on the hydrophobicity of methane in aqueous solutions of urea and TMAO at low and high pressures. The chapter is organized into two parts. In Part A, the effects of urea and TMAO on hydration and association of methane molecules are discussed. On the other hand, we explore the effects of TMAO on pressure-modulated hydrophobicity of methane in Part B.

Part A:

Methane in Water and Aqueous Solutions of Urea and TMAO

Overview: Influences of urea and TMAO on hydrophobic interactions of methane in aqueous solutions are investigated by performing MD simulations. In this study, we have used two different models of methane: one is of single united site (UA), and the other contains 5-sites (AA). Both osmolytes are found to have negligible influence on association of methane regardless of the methane model used. Dehydration of methane takes place in the presence of urea and/or TMAO, and few osmolyte molecules occupy the space around methane. It is also found that urea molecules are expelled slightly from the solvation shell of methane, whereas TMAO interacts preferentially with methane through its hydrophobic methyl groups. In solution, both water and urea solvate TMAO. We also find the collapse of the water second shell by urea and water structure enhancement by TMAO. Investigation of water−water hydrogen bond properties in different spherical regions of a single methane molecule shows that the average number of water−water hydrogen bonds does not change significantly with distance. Number of water−water hydrogen bonds reduces in the presence of osmolyte, and osmolytes, TMAO in particular, enhance the life-time of these bonds.

■ INTRODUCTION

Aqueous solutions of small nonpolar molecules such as methanes have been studied in detail to understand the hydrophobic effect [92-94]. While some computational investigations were concerned with pairs [95, 96], triplets [97], or quadruplets [98] of methane molecules, others focused on simulations of a larger number of nonpolar solutes [99-101] and aggregation of such solutes [102]. The experimentally observed solvation free energy for methane in neat water is close to 8.5 kJ mol^{-1} [103, 104]. The value was estimated to be 8.7 and 9.3 kJ mol^{-1} for SPC and SPC/E water, respectively, from simulations [105]. The standard free energy of pairing for two methanes has also been estimated. Zhang and McCammon [96] employed a brute-force simulation of two methane molecules, which included hundreds of association and dissociation events, for this purpose. They found a value of about 3 kJ mol^{-1}, which was reproduced later by Raschke *et al.* [102] by calculating the free energy associated with the growth of a cluster of n methanes:

$$m_n + m_1 \rightleftharpoons m_{n+1} \tag{2.1}$$

using the relation:

$$\Delta G_{growth} = -k_B T ln \frac{[m_{n+1}]C_0}{[m_n][m_1]} \tag{2.2}$$

where k_B, T, and C_0 are the Boltzmann's constant, temperature, and unit of concentration required to make the fraction unitless, respectively. It has been found that methane aggregation and cluster formation become favorable only at cluster sizes of at least 5 methane molecules [40, 102], and consequently, Oostenbrink and van Gunsteren [40] concluded that a direct investigation of the hydrophobic effect based on dimers [95, 96] or small clusters [97, 98] is questionable.

In view of the importance of side-chain hydrophobic interactions in the stability of proteins and to reduce complex interactions of protein residues with solution species, the effect of urea on the hydrophobic effect in such model systems has also been studied for single nonpolar solutes [106] and pairs of solutes [107-109]. In contradiction to the hypothesis that urea preferentially solvates the hydrophobic residues [46], the transfer free energy from pure water to aqueous urea solution was found to be positive for a single methane molecule [25, 106, 110]. Urea-induced enhancement of methane−methane association was also observed in previous MD studies [107, 108]. Oostenbrink and van Gunsteren [40] studied the aggregation of methane in water and the effect of urea on hydrophobic clustering by simulation for 13 systems of different sizes and compositions. Their simulations showed

that a high urea concentration does not reduce hydrophobic interaction; rather it enhances slightly the clustering of methane molecules. The effects of TMAO on the thermodynamics of hydration and interactions of methane were also investigated and the major conclusion was that, TMAO has a negligible effect either on the thermodynamic stability of contact and solvent-separated conformations relative to pure water [71].

As discussed above, there have been many simulation studies that investigate the hydrophobicity of methane in aqueous urea and TMAO solutions. However, previous studies did not consider the behavior of methane in urea/TMAO mixture. In this part, we deal with the solvation characteristics and solvent-mediated attraction of methane molecules in pure water as well as in binary and ternary solutions of urea and TMAO. Again, one interesting observation concerning the solvation of hydrophobic solute in water is the influence of solute model on its association. In particular, Lee and Van der Vegt [44] observed that, in TIP4P water, the contact minimum of neopentane−neopentane potential of mean force (PMF) is significantly deeper for the five-site model than that for the single-site LJ neopentane model. So two models of methane are considered to see model dependencies of methane association, if any. We first examine whether urea or TMAO has any significant effect on the aggregation of methane in aqueous solution by calculating methane−methane PMF. An insight picture of the influences of these two osmolytes on aggregation is obtained by examining their effects on the water structure and also their direct interactions with the hydrophobic solute. The familiar water oxygen−oxygen rdf is used to describe water structuring and osmolyte's interaction with methane is examined by calculating site−site rdfs as well as the fraction of osmolyte molecules around methane. Furthermore, we investigate the orientation of solution species with respect to the hydrophobic solute and focus on the hydrogen bond properties and dynamics of water molecules in different spherical regions of a single methane particle to describe water−water hydrogen bonding and to quantify the extent of water structuring at discrete distances from the solute.

In the next section, we have presented a description of the models and simulation method. Results are discussed thereafter, and this part is ended with a section whereof we have included our concluding remarks.

■ MODELS AND SIMULATION METHOD

Classical MD simulations of methane were carried out in four different systems: pure water, aqueous urea, aqueous TMAO, and mixed urea/TMAO solutions. Ten methane molecules were used as solute to investigate the influences of urea and TMAO on the association

tendency of methane in aqueous solutions. The simulation box contained 500 molecular species in all cases and osmolyte solutions were constructed by replacing water molecules with osmolyte. Table 2A-1 presents an overview of systems. Note that, for calculations of water−water hydrogen bond properties and dynamics as well as of water orientational distribution in different spherical regions of methane, we used a single methane molecule immersed in water (and osmolytes), and to keep the total number of molecules constant (500), we replaced 9 methane solutes by water molecules. In all of the simulations, the extended simple point-charge (SPC/E) model [111] was used for water, the so-called Duffy-Kowalczyk-Jorgensen (DKJ) model [112] was adopted for urea, and TMAO was described with a rigid version of model proposed by Kast *et al.* [113] Two different models were used for methane: single-site united-atom (UA) model [114] and 5-site (AA) model [115]. Hydrogens were implicit in the UA model and explicit in the AA model. All models employed were rigid, and the interaction between atomic sites of two different molecules was expressed as:

$$u_{\alpha\beta}(r_{\alpha\beta}) = 4\epsilon_{\alpha\beta}\left[\left(\frac{\sigma_{\alpha\beta}}{r_{\alpha\beta}}\right)^{12} - \left(\frac{\sigma_{\alpha\beta}}{r_{\alpha\beta}}\right)^{6}\right] + \frac{q_\alpha q_\beta}{r_{\alpha\beta}} \tag{2.3}$$

where $r_{\alpha\beta}$ is the distance between atomic sites α and β, and q_i is the charge of the site i. The LJ parameters $\sigma_{\alpha\beta}$ and $\epsilon_{\alpha\beta}$ were obtained by using the combining rules $\sigma_{\alpha\beta} = (\sigma_\alpha + \sigma_\beta)/2$ and $\epsilon_{\alpha\beta} = (\epsilon_\alpha\epsilon_\beta)^{1/2}$. The values of the LJ parameters and the partial charges for methane, urea, TMAO, and water are summarized in Table 2A-2.

Table 2A-1. Overview of Systems[a]

model	system	V(nm^3)	Ns	Nu	Nt	Nw	Mu	Mt
UA	$S_{UA,1}$	15.21	10	0	0	490	0	0
	$S_{UA,2}$	19.51	10	100	0	390	8.51	0
	$S_{UA,3}$	18.07	10	0	40	450	0	3.68
	$S_{UA,4}$	22.36	10	100	40	350	7.43	2.97
AA	$S_{AA,1}$	15.39	10	0	0	490	0	0
	$S_{AA,2}$	19.46	10	100	0	390	8.53	0
	$S_{AA,3}$	17.77	10	0	40	450	0	3.74
	$S_{AA,4}$	22.25	10	100	40	350	7.46	2.98

[a] V, N, and M represent box volume, number of molecules, and molar concentration, respectively. s, w, u, and t, respectively, refer to solute (methane), water, urea, and TMAO.

Table 2A-2. Lennard-Jones Parameters and Charges for the Models Considered[a]

species	atom type	σ(Å)	ϵ (kJ mol^{-1})	charge(e)
water	Ow	3.166	0.646	−0.8476
	Hw	—	—	+0.4238
urea	Cu	3.75	0.4365	+0.142
	Ou	2.96	0.873	−0.390
	Nu	3.25	0.7067	−0.542
	Hu	0.0	0.0	+0.333
TMAO	Ct	3.041	0.281	−0.26
	Nt	2.926	0.8314	+0.44
	Ot	3.266	0.6344	−0.65
	Ht	1.775	0.0769	+0.11
methane(UA)	me	3.70	1.234	0.0
methane(AA)	C	3.50	0.276	−0.24
	H	2.5	0.1261	+0.06

[a] e is the elementary charge.

The solution properties were investigated by performing MD simulations at 298 K and 1 bar in a cubic box of length L. The LJ interactions were spherically truncated at a radius of $L/2$ and the Ewald method [85] was used to treat the long-range electrostatic interactions. The quaternion formulation of the equations of rotational motion was employed, and for time integration, we used leap-frog algorithm with a time step of $10^{-15}s$. Periodic boundary condition was used to reduce edge effect. In the starting configuration, the molecules were located on a face-centered-cubic lattice with random orientations. MD simulations were performed first in isothermal-isobaric (NPT) ensemble to obtain the box volume corresponding to the desired pressure. The weak coupling scheme proposed by Berendsen *et al.* [116] was used to maintain the physical pressure. During this initial phase of the simulation, the box volume was allowed to fluctuate, and the average volume was determined at the end of the simulation. The so obtained box volume was used in subsequent canonical (NVT) ensemble simulation runs. Each system was equilibrated with velocity rescaling to fix the temperature. Finally, production runs were carried out for 10 ns and these are the results reported.

■ RESULTS AND DISCUSSION

Methane−Methane Pair Potentials of Mean Force. To study the aggregation of methane in aqueous solutions, we calculated methane−methane PMF using the relation:

$$W(r) = -k_B T \ln g_{ss}(r) \tag{2.4}$$

where $g_{ss}(r)$ is the solute−solute pair correlation function. The PMF curves, shown in Figure 2A-1, have characteristic shapes with contact and solvent-separated minima (denoted as CM and SSM, respectively) separated by a maximum (the BARR), revealing existence of associated and solvent-separated states of methane in aqueous solution. The CM (appears at ∼4 Å) is deeper than the SSM (appears at ∼7 Å). This indicates that a methane molecule prefers to be in direct contact with other methane moieties rather than to be separated by a solvent molecule. The two models of methane have similar depths of the CM and the SSM (Table 2A-3). Osmolyte does not show significant influence on the well depth of the CM. The PMF difference between the SSM and the CM increases in the presence of osmolyte, suggesting osmolyte-induced relative stabilization of the methane contact pair over the solvent-separated state. The relative stabilization is,

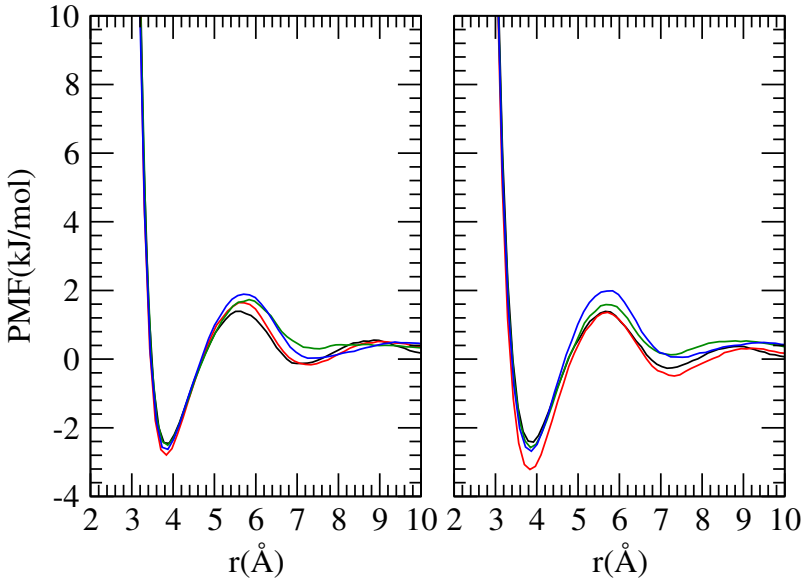

Figure 2A-1. *Methane−methane PMFs for the UA (left) and AA (right) models in water, aqueous urea, aqueous TMAO, and mixed urea/TMAO solutions.*

however, not very significant, and the effect of osmolytes urea and TMAO on the association of methane seems to be negligible.

Table 2A-3. PMF Values (in kJ mol^{-1}) at the CM, the SSM, and the BARR[a]

	UA				AA		
system	CM	BARR	SSM	system	CM	BARR	SSM
$S_{UA,1}$	−2.46	+1.39	−0.13	$S_{AA,1}$	−2.42	+1.39	−0.27
$S_{UA,2}$	−2.79	+1.64	−0.16	$S_{AA,2}$	−3.22	+1.36	−0.49
$S_{UA,3}$	−2.51	+1.73	+0.30	$S_{AA,3}$	−2.58	+1.59	+0.13
$S_{UA,4}$	−2.63	+1.89	+0.03	$S_{AA,4}$	−2.68	+1.99	+0.05

[a]The estimated standard deviations for all systems vary from 0.1 to 0.22 kJ mol^{-1}.

The observation that these two osmolytes have negligible influence on methane-methane interaction is validated further from calculation of association constant. The association constant, K_a, was calculated by integrating the PMF to the first maximum to understand the extent of association of methane in pure water and the effect of urea and TMAO on it.

$$K_a = 4\pi \int_0^{r_a} r^2 e^{-W(r)/k_B T} dr \tag{2.5}$$

The K_a values, presented in Table 2A-4, are almost identical in these systems (except for the system $S_{AA,2}$), revealing inability of urea and TMAO to alter hydrophobic interaction of small solutes.

Table 2A-4. Association Constant (K_a) for Methane

	UA		AA
system	$K_a(M^{-1})$	system	$K_a(M^{-1})$
$S_{UA,1}$	0.44	$S_{AA,1}$	0.47
$S_{UA,2}$	0.46	$S_{AA,2}$	0.59
$S_{UA,3}$	0.47	$S_{AA,3}$	0.48
$S_{UA,4}$	0.44	$S_{AA,4}$	0.48

Cluster Structure Analysis. In order to quantify the clustering of methane molecules in pure water and also in binary and ternary osmolyte solutions, we estimated average cluster size in our systems. We adopted the method first proposed for LJ fluid by Martinez *et al.* [117] and successfully employed later by Kokubo *et al.* [118] in their simulation study of aqueous urea solution. Each molecule was assigned as low, average, or high density clusters of its species depending upon the following relations:

- low if $n < n_0 - \delta$
- high if $n > n_0 + \delta$
- average if $n_0 - \delta \leq n \leq n_0 + \delta$

Note that, to calculate the number of molecules in the solvation sphere (n) excluding the reference particle, we integrated the methane−methane pair correlation function to the first minimum (rather than considering the instantaneous number of molecules around a test molecule) and for calculating the average number of molecules (n_0), we adopted the method proposed by Martinez *et al.* [117] δ was the fluctuation and in our case we set it to 20% of average number of molecules.

The results of our cluster structure analyses for the two methane models are shown in Table 2A-5. It is apparent from Table 2A-5 that for both models of methane, the

Table 2A-5. Methane Cluster Sizes for Different Systems[a]

model	system	n	n_0	δ	$n - n_o$	remark
UA	$S_{UA,1}$	0.48	0.49	0.10	−0.01	average
	$S_{UA,2}$	0.39	0.37	0.07	−0.02	average
	$S_{UA,3}$	0.43	0.46	0.09	−0.03	average
	$S_{UA,4}$	0.33	0.35	0.07	−0.02	average
AA	$S_{AA,1}$	0.50	0.49	0.10	0.01	average
	$S_{AA,2}$	0.50	0.40	0.08	0.10	high
	$S_{AA,3}$	0.45	0.43	0.09	0.02	average
	$S_{AA,4}$	0.36	0.37	0.07	−0.01	average

[a] n_0, n, and δ are the average number of methane molecules, number of methane molecules in the first coordination shell, and the fluctuation, respectively.

difference between n and n_0 values is very small both in pure water and in aqueous solutions of osmolyte. This difference is also close to the corresponding δ value indicating average sized clusters in these solutions. The average cluster size is slightly higher for the AA model in binary urea solution, and for other solutions the effect of osmolytes on the aggregation of methane molecules is negligible. These observations are consistent with our estimated K_a values for different solutions as discussed above.

Hydration of Methane. Molecular details of methane hydration were investigated by computing site−site rdfs between methane and water. For a further analysis, we also calculated the average number of water molecules around methane using the relation:

$$n_{\alpha\beta} = 4\pi\rho_\beta \int_0^{r_c} r^2 g_{\alpha\beta}(r) dr \tag{2.6}$$

where $n_{\alpha\beta}$ represents the number of atoms of type β surrounding atom α in a shell extending from 0 to r_c and ρ_β is the number density of β in the system.

Well-defined hydration shells for both models of methane can be seen in Figure 2A-2a. For the UA model, in pure water, the methane−water rdf starts to rise from zero at 2.9 Å and reaches the value of bulk density at 3.3 Å, for which $g(r) = 1$. Thus, exclusion of water molecules from the solvation shell of methane occurs below 3.3 Å. The first peak (the center of the first hydration shell) appears at about 3.6 Å and water density in this region is about 1.9 times the bulk water density. The first minimum, located at about 5.4 Å, indicates the outer limit of the first hydration shell of methane. The distribution functions are qualitatively similar for the two models of methane and about 20 water molecules are found in the first hydration shell of methane by integrating the rdf to the first minimum (Table 2A-6).

Osmolyte does not show any tendency to reduce water density in the vicinity of methane (Figure 2A-2a). Instead, water density increases around methane both in binary and ternary solutions of urea. Nonetheless, the number of water molecules in the first hydration shell of methane decreases in the presence of osmolyte (Table 2A-6). For binary urea solution, the dehydration is about 36%. TMAO, on the other hand, reduces the amount of water in the hydration sphere by about 21%. The dehydrating effect is obviously more pronounced for the urea/TMAO mixture, with the amount of water decreased by about 49%. Since some reduction in the hydration number of methane in aqueous osmolyte solutions arises from the reduced number density of water molecules in the osmolyte solution, we calculated the coordination numbers assuming that the only change with added osmolyte comes through the reduced number of water and these numbers are also given in Table

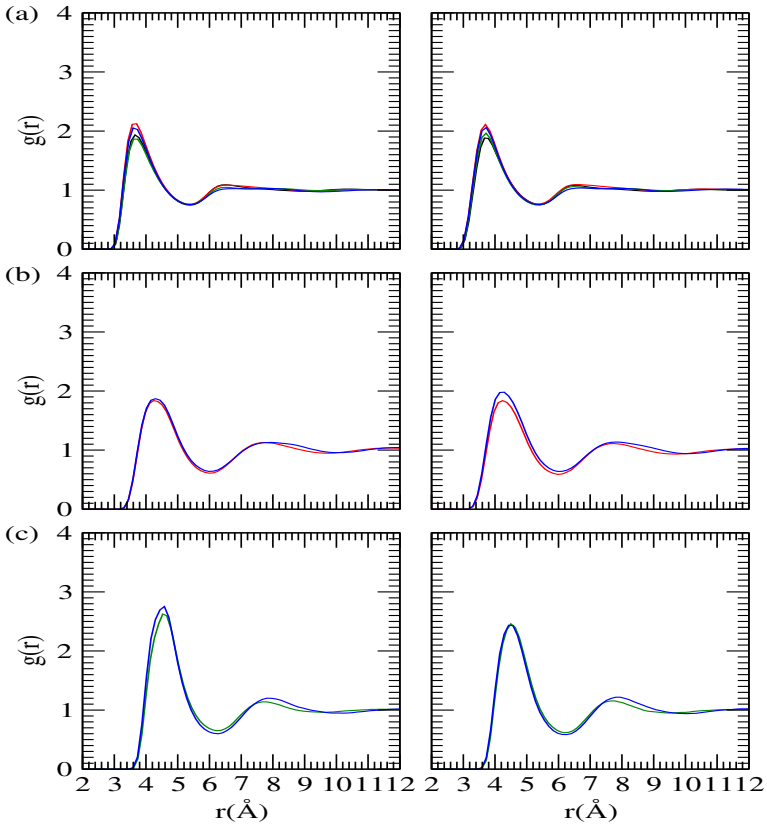

Figure 2A-2. *Distributions of water, urea, and TMAO central atoms (from a-c, respectively) around methane for the UA (left) and AA (right) models in water, aqueous urea, aqueous TMAO, and mixed urea/TMAO solutions.*

Table 2A-6. Hydration Number (Nw) for Methane[a]

UA		AA	
system	Nw	system	Nw
$S_{UA,1}$	20.14	$S_{AA,1}$	20.10
$S_{UA,2}$	12.84(16.03)	$S_{AA,2}$	12.75(16.00)
$S_{UA,3}$	15.87(18.50)	$S_{AA,3}$	16.09(18.46)
$S_{UA,4}$	10.31(14.39)	$S_{AA,4}$	10.32(14.36)

[a]Hydration numbers are obtained by integrating the rdf to the first minimum.

2A-6 in parentheses. The replacement of water by osmolyte from the first hydration shell of methane is clear from these values. Moreover, we find that the ratio of the first shell water molecules in pure water and in aqueous osmolyte solution is higher than the respective ratio of water molecules present in these systems, suggesting osmolyte-induced dehydration of methane. For example, for the UA model, the ratio of hydration waters in pure water ($S_{UA,1}$) and in binary urea solution ($S_{UA,2}$) is 1.57:1 which is higher than the ratio of total number of water molecules present in these systems (i.e., 1.25:1).

Osmolyte's Interaction with Methane. Site−site rdfs between methane and osmolyte molecules were computed first to investigate osmolyte's interaction with methane in different chemical environments. Figure 2A-2 depicts the distributions of osmolyte molecules (central atom only) around methane. Due to the larger excluded volumes for urea and TMAO molecules (vdW radii for water, urea, and TMAO are about 1.5, 2.2, and 2.95 Å [119], respectively), the osmolyte density around methane starts to rise from zero at a longer distance (relative to water). Interestingly, the first peak magnitude is slightly lower for urea than that for water, whereas TMAO has a much higher first peak than both water and urea. What these suggest is preference of methane for TMAO in its first solvation shell over water which, in turn, is preferred over urea.

Affinity of methane for osmolyte was also investigated by calculating the time-averaged normalized fractions of water oxygen, urea carbon, and TMAO nitrogen around methane. Following a recent study [120], the time-averaged normalized ratio, τ_i, of component i was defined as:

$$\tau_i(r) = \frac{n_i(r) \sum N_i}{N_i \sum n_i(r)} \tag{2.7}$$

where N_i is the total number of molecules of component i in the simulation box and n_i is the number of molecules of component i in the defined local domain of radius r. The summation goes over all of the species in the system. Clearly, τ_i is greater than 1 in case of preferential accumulation of i. Opposite to that, relative depletion of i leads to value lower than 1. The number of water and osmolyte molecules around methane were calculated using Eq. 2.6.

Figure 2A-3 shows the time-averaged normalized fraction of component i as a function of the radius of the spherical volume that defines the local volume around methane in binary and ternary solutions of urea and TMAO. Preferential accumulation of water in the close proximity of methane can be suggested immediately from the data in this figure. Also noticeable in Figure 2A-3 are the strong TMAO fraction around methane and the

weakest first peak (close to 1) for urea in both binary and ternary solutions. Thus, while methane shows a slight tendency to exclude urea from its solvation shell, it does have the tendency to interact with TMAO molecules. Note that urea-induced slight enhancement of methane clustering due to urea exclusion from methane solvation shell was suggested in previous simulation study [40].

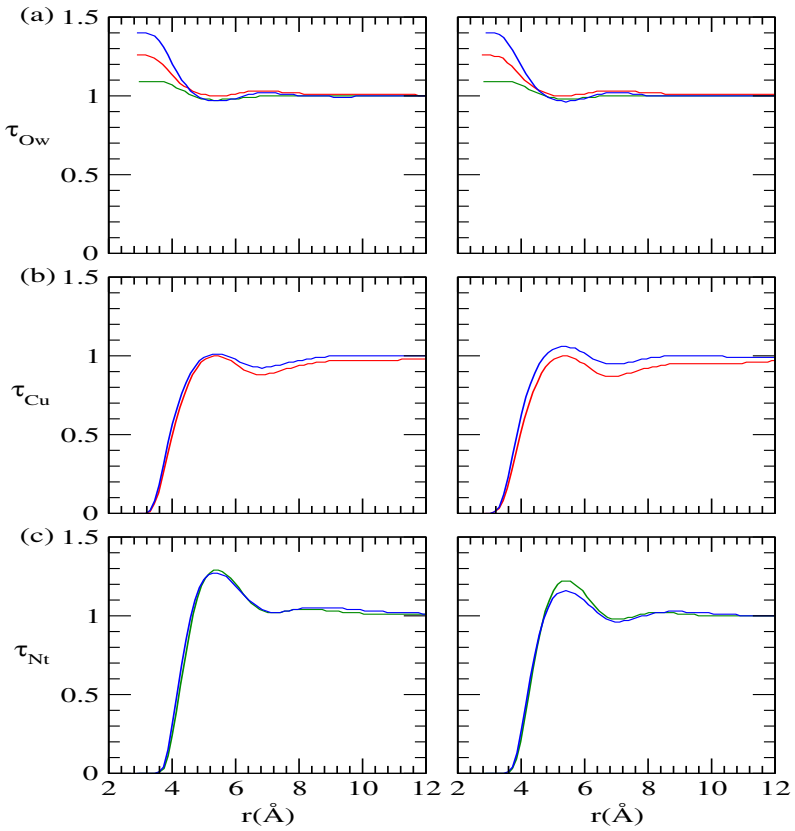

Figure 2A-3. *Time-averaged normalized fractions of water, urea, and TMAO central atoms (from a-c, respectively) as a function of the distance from methane for the UA (left) and AA (right) models in aqueous urea, aqueous TMAO, and mixed urea/TMAO solutions.*

We then examined the orientations of water and osmolyte near the methane moiety by computing all the rdfs involving methane, water, urea, and TMAO. These distribution functions are shown in Figure 2A-4 for the urea/TMAO mixture. The rdf profiles of water oxygen (Ow) and hydrogen (Hw) contain first peaks at similar positions, supporting the previously suggested typical surface-parallel orientation of water molecules in the vicinity of hydrophobic group [121-124]. There also arises a tail of hydrogen density at shorter separations, reflecting a slight preference of water hydrogens to come closer to the surface. The general behavior of these distribution functions is qualitatively similar for both models

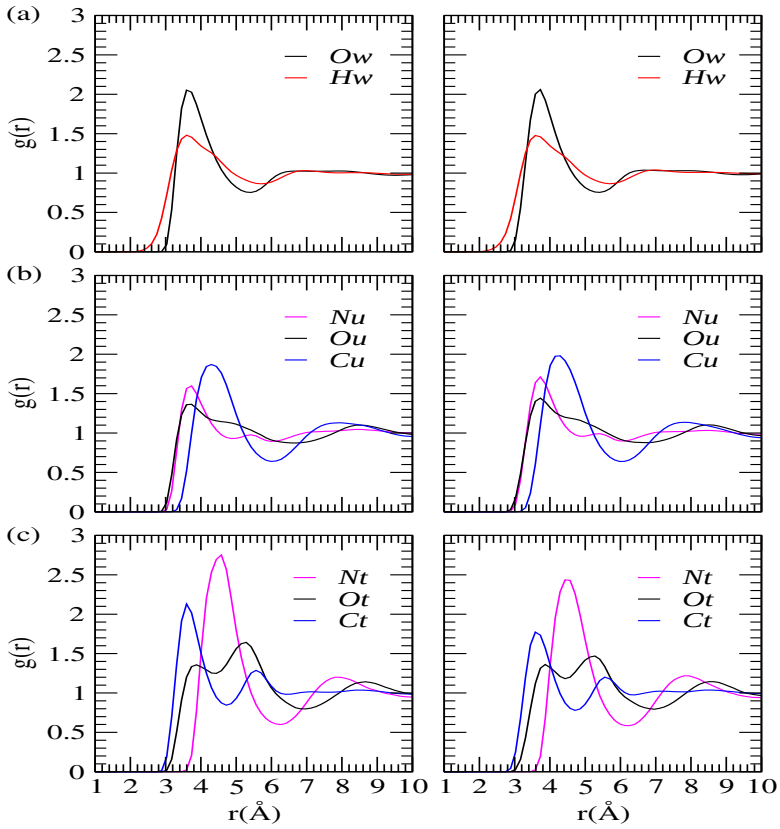

Figure 2A-4. *Selected site−site distribution functions showing orientations of water, urea, and TMAO molecules (from a-c, respectively) around methane for the UA (left) and AA (right) models in urea/TMAO mixture.*

of methane. For oxygen (Ou) and nitrogen (Nu) of urea, the rdf profiles show the first peak at similar locations with the Nu rdf consisting of a shoulder at a longer distance. The peak positions indicate direct interaction of methane with N- and O-atoms of urea molecules. Methane does not show any preference for urea N or O, as revealed by similar first peak heights for these two rdfs. The peak positions in solute−solvent rdfs involving TMAO (Ct followed by Nt followed by Ot) suggest the preference of TMAO methyl groups near the methane moiety. It is also interesting to observe nonzero oxygen density at shorter separations with a short-range shoulder to the first peak. These findings reveal that although TMAO molecules interact preferably with methane molecules through its methyl groups, its O-atom also has the tendency to form hydrogen bonds with solution species that are close to the methane moiety. Again, the first peak in methane−Ct rdf appears nearly at 3.6 Å which is close to the first peak position in methane−methane rdf (the CM in the PMF curve). The extreme closeness of these distances suggests that methane molecules can

act as 'substitute' for TMAO methyl groups. So, TMAO methyl groups help to associate methane molecules as well as reduce the interaction between methane molecules. These two opposing effects nullify the effects of each other leading to negligible effects of TMAO on methane aggregation.

Osmolyte Solvation and Its Effect on Water Properties. To assess the role of osmolytes urea and TMAO as water structure breaker [25-32] or maker [31, 32, 67, 68, 73, 78, 81-84] which, in turn, is supposed to lead to protein denaturation or stabilization, we studied the solvation characteristics of these two osmolytes in binary and ternary solutions and the consequent changes in water structural, energetic, and dynamical properties. More details will apear in **Chapter 4**. Selected site−site rdfs that reflect the structural aspects of the solution are shown in Figures 2A-5 and 2A-6. It is evident that the general features of $Ou - Hw$ and $Ow - Hu$ functions are similar to the $Ow - Hw$ rdf (Figure 2A-5). The qualitative similarity of these rdfs indicates that urea acts as both hydrogen bond donor and acceptor for water and appears to distribute locally in a pattern similar to the water molecules in bulk water. Although TMAO cannot donate its hydrogens to hydrogen bond acceptor sites, it does accept hydrogens from both water and urea as indicated by the first peak in the corresponding pair distribution functions ($Ot - Hw$ and $Ot - Hu$) located at about 1.8 Å. Note that the $Ot - Hw$ rdf is similar in shape to the corresponding water ($Ow - Hw$) and urea ($Ou - Hw$) functions, making it likely that TMAO simply 'fits' into the solution structure much as would urea molecules. Two additional points are worth noting from Figure 2A-5. First, in hydrogen bonding with water, urea is a better acceptor than a donor as indicated by the stronger peak in $Ou - Hw$ rdf relative to that in $Ow - Hu$ rdf. Second, the stronger peak in $Ot - Hw$ rdf reveals a much higher tendency of TMAO to accept hydrogens from water than from urea.

The first shell coordination numbers, which give the average number of hydrogen bonded neighbors, are presented in Table 2A-7 to shed more light on the nature of hydrogen bonding. Clearly, water loses some hydrogen bonds to identical species in the presence of osmolyte. The ratio of water hydrogen bonded neighbors is, however, close to the stoichiometric ratio of water molecules in the two systems. Moreover, the decrease in the number of hydrogen bonded water molecules in the osmolyte solution is compensated by hydrogen bonding with osmolyte and the total number of hydrogen bonded species per water molecule remains almost unchanged. Again, both urea and TMAO contain, on average, about 3 hydrogen bonded water molecules in the binary solutions. In the mixed

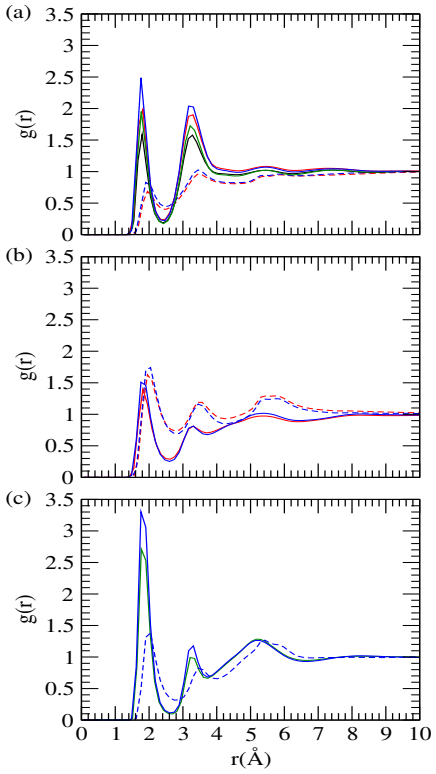

Figure 2A-5. *Selected site−site distribution functions that show hydrogen bonding interactions involving O-atoms of water, urea, and TMAO molecules (from a-c, respectively) for the UA model of methane in water, aqueous urea, aqueous TMAO, and mixed urea/TMAO solutions. Solid and dashed lines are for water and urea hydrogens, respectively.*

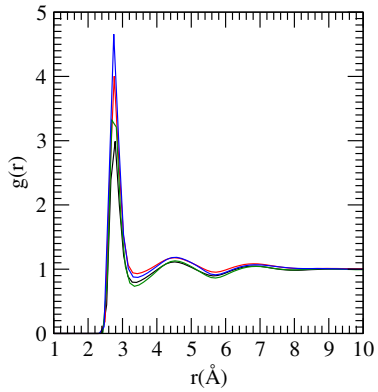

Figure 2A-6. *Water oxygen−oxygen rdfs for the UA model of methane in water, aqueous urea, aqueous TMAO, and mixed urea/TMAO solutions.*

osmolyte solution, some TMAO−water hydrogen bonds are replaced by TMAO−urea hydrogen bonds. Because of TMAO solvation by urea, number of urea−urea hydrogen bonds decreases in the presence of TMAO (the number reduces from 3.12 in $S_{UA,2}$ to 2.80 in $S_{UA,4}$). What these findings prove is, TMAO's ability to accept hydrogens of both water and urea. This TMAO solvation by water and urea has been considered as an important factor for TMAO-induced counteraction of urea-conferred protein denaturation [68, 125]. Calculation of energetic and dynamical properties of these hydrogen bonds introduces new insights, discussion of which is deferred until **Chapter 4**.

Table 2A-7. Coordination Numbers for Atom Pairs Involved in Hydrogen Bonding[a]

system	atom pair	W-W	W-U	W-T	U-W	U-U	U-T	T-W	T-U
$S_{UA,1}$	O-H	0.97	—	—	—	—	—	—	—
	H-O	0.97	—	—	—	—	—	—	—
	total	3.88	—	—	—	—	—	—	—
$S_{UA,2}$	O-H	0.75	0.13	—	0.73	0.39	—	—	—
	H-O	0.75	0.19	—	0.49	0.39	—	—	—
	total	3.00	0.90	—	3.42	3.12	—	—	—
$S_{UA,3}$	O-H	0.86	—	—	—	—	—	1.33	—
	H-O	0.86	—	0.12	—	—	—	—	—
	total	3.44	—	0.24	—	—	—	2.66	—
$S_{UA,4}$	O-H	0.69	0.13	—	0.65	0.35	—	1.00	0.22
	H-O	0.69	0.19	0.11	0.44	0.35	0.09	—	—
	total	2.76	0.90	0.22	3.06	2.80	0.36	2.00	0.88

[a]W, U, and T refer to water, urea, and TMAO, respectively. Numbers are with respect to the first species and the total is calculated by taking into account the number of hydrogen atoms in water and urea.

The indirect effect of osmolyte solvation on water structure was examined by computing water oxygen−oxygen rdf first. As observed previously by Wei *et al.* [32], we too observe the first and second peaks in $Ow - Ow$ rdf (Figure 2A-6), which characterize the hydrogen bonded first neighbor and the tetrahedrally located second neighbor, at about 2.8 and 4.5 Å, respectively. Both urea and TMAO enhance the first peak, indicating tightly coordinated water first shell in aqueous osmolyte solutions. On the other hand, while urea

leads to a shallower first valley and a less pronounced second peak, TMAO makes the first valley deeper and the second peak more pronounced. Such changes in $Ow - Ow$ rdf have been used as supporting evidence for a slight second-shell collapse of water structure by urea and water structure enhancement by TMAO [31, 32]. Height of the first peak increases further in urea/TMAO mixture and the first valley and the second peak become similar to that in pure water.

We investigated the structural, energetic, and dynamical properties of water−water hydrogen bonds at discrete distances from a methane molecule to assess the influence of solute/co-solute on water hydrogen bonding interactions. Three regions of width 1 Å each were considered: two near the solute surface (Regions I and II) and the third one at a relatively larger distance from the solute assuming bulk portion of the simulation cell (Region III: $10-11$ Å). For the AA model, Regions I and II were chosen to be $2.4-3.4$ and $3.4-4.4$ Å, respectively, whereas the same were $2.5-3.5$ and $3.5-4.5$ Å, respectively, for the UA model. The methods and the geometric criteria for hydrogen bond properties and dynamics calculations were adopted from previous works [126-131]. Two distinct molecules were considered to be forming a hydrogen bond $D-H\cdots A$ if the distances between D and A, and A and H were less than r_{DA} and r_{AH}, respectively, and simultaneously, the $H-D-A$ angle was less than 45°. We selected cut-off distances r_{DA} (=3.4 Å) and r_{AH} (=2.4 Å) according to the position of the first minimum of the appropriate rdf.

To investigate hydrogen bond dynamics, we defined a continuous hydrogen bond time correlation function, $S_{HB}(t)$, as:

$$S_{HB}(t) = \frac{< h(0)H(t) >}{< h >} \tag{2.8}$$

where h and H are two hydrogen bond population variables. If a particular tagged pair of particles is hydrogen bonded (according to the definition adopted above) at time t, h is unity, and is zero otherwise. In the case of H, if the tagged pair of particles remains continuously hydrogen bonded from initial period to time t, it takes a value of unity, and is zero otherwise. Clearly, $S_{HB}(t)$ describes the probability that a pair of particles, which was hydrogen bonded at $t = 0$, remains continuously bonded up to time t. The time integral of $S_{HB}(t)$, denoted as τ_{HB}, describes the average time that a hydrogen bond survives after it is chosen at $t = 0$. Because the hydrogen bonds are chosen randomly without imposing any condition on when they were created, τ_{HB} is the average persistence time (life-expectancy) of a randomly chosen hydrogen bond.

 In Table 2A-8, we have presented the average number of water−water hydrogen

bonds together with the energy and life-time of these bonds. The average number and life-time of hydrogen bonds do not change significantly with distance, though the hydrogen bonds are slightly more attractive in the vicinity of methane (by about 1 kJ mol^{-1}) as compared to the bulk region. The negligible change in water−water hydrogen bond number indicates that methane can 'fit' into the water cavities without disturbing the water hydrogen bonding network much. The addition of urea and/or TMAO reduces the average number of hydrogen bonded water molecules with a slight change in energy. Osmolytes, particularly TMAO, however, enhance the life-time of water−water hydrogen bonds. For example, the life-time increases from 1.38 ps in $S_{UA,1}$ to 1.88 ps in $S_{UA,3}$ and then to 2.04 ps in $S_{UA,4}$. Corroborative evidence for osmolyte-induced enhancement of the water−water hydrogen bond life-time can be seen in Figure 2A-7 which illustrates slower relaxation of $S_{HB}(t)$ in aqueous solutions of osmolyte. We note that our observation of the enhancement of hydrogen bonds in the presence of TMAO is in qualitative agreement with that reported by Bennion and Daggett [73].

Table 2A-8. Water−Water Hydrogen Bond Properties and Dynamics[a]

model	system	n_{HB}^{I}	n_{HB}^{II}	n_{HB}^{III}	E_{HB}^{I}	E_{HB}^{II}	E_{HB}^{III}	τ_{HB}^{I}	τ_{HB}^{II}	τ_{HB}^{III}
UA	$S_{UA,1}$	3.62	3.76	3.78	-19.69	-19.53	-18.74	1.42	1.50	1.38
	$S_{UA,2}$	2.73	2.90	2.88	-19.50	-19.66	-18.83	1.61	1.57	1.57
	$S_{UA,3}$	3.25	3.35	3.43	-20.24	-19.87	-19.28	1.90	1.93	1.88
	$S_{UA,4}$	2.51	2.60	2.51	-20.15	-19.93	-19.27	1.85	1.91	2.04
AA	$S_{AA,1}$	3.59	3.72	3.75	-19.60	-19.70	-18.77	1.50	1.45	1.39
	$S_{AA,2}$	2.87	3.01	2.88	-19.68	-19.62	-19.03	1.59	1.59	1.60
	$S_{AA,3}$	3.18	3.28	3.37	-20.31	-20.35	-19.45	1.98	1.97	1.99
	$S_{AA,4}$	2.70	2.84	2.74	-20.64	-20.04	-19.54	1.95	1.98	2.09

[a] n_{HB}, E_{HB}, and τ_{HB} represent average number, energy (in kJ mol^{-1}), and the life-time (in ps) of water−water hydrogen bond, respectively. Regions I, II, and III are defined in the text.

The fraction of water molecules (f_n) that engage in n number of hydrogen bonds with identical species are shown in Figure 2A-8 for the three selected regions. For both models of methane in pure water, most of the water molecules are 3- and 4- coordinated with relatively lower fractions of 2- and 5-coordinated water molecules. As compared to water in the

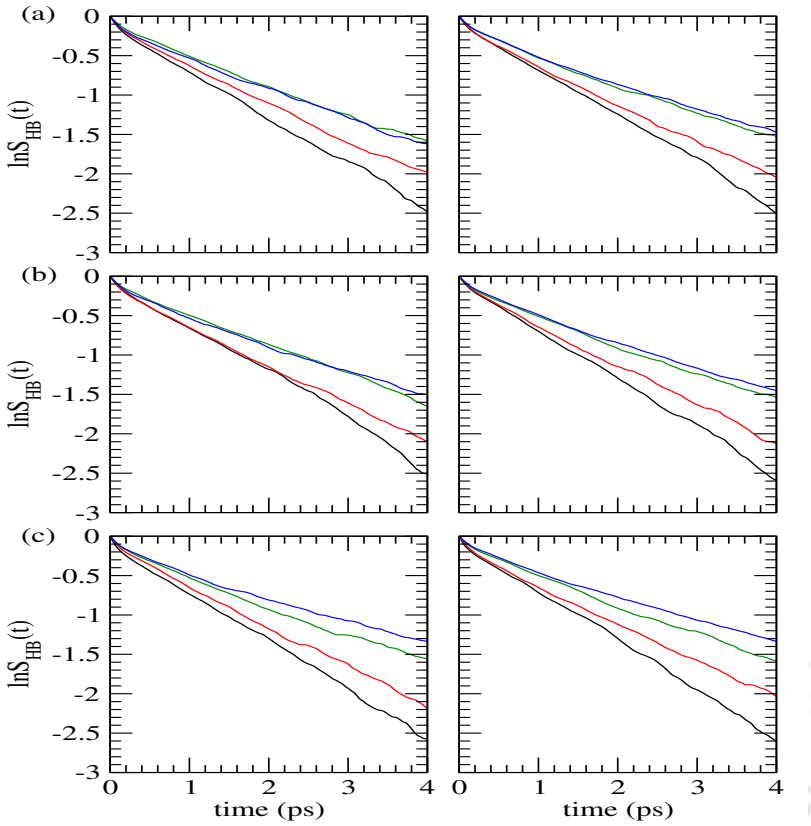

Figure 2A-7. *Time dependence of the continuous water−water hydrogen bond correlation function in Regions I, II, and III (from a-c, respectively) for the UA (left) and AA (right) models of methane in water, aqueous urea, aqueous TMAO, and mixed urea/TMAO solutions. Regions I, II, and III are defined in the text.*

bulk (Region III), the fraction of lower coordinated water molecules (f_2 and f_3) increases, and that of higher coordinated water molecules (f_4 and f_5) decreases slightly in the vicinity of the solute (Regions I and II), suggesting that water loses some of its identical nearest neighbors near the hydrophobic solute surface. The effect of osmolyte on water−water hydrogen bond number is dramatic, reducing the number of 4- and 5-coordinated water molecules while increasing the number of 2- and 3-coordinated water molecules. The comparatively large enhancement of 2-coordinated water molecules and the reduction of 4-coordinated water molecules are clearly related to the number of osmolytes that has to be accommodated in the cavities of water molecules. Of significant importance is the number of 3-coordinated water molecules which do not show any dependence on the number of osmolyte molecules. What we assume is that the central water molecule of these 3-coordinated water molecules acts as hydrogen donor to the osmolyte. A relation of these findings with

the hydration of methane can then be imagined in which water solvates urea and TMAO (mainly through hydrogen bonds) and at the same time increases the water−water hydrogen bond life-time, thereby making itself less available to solvate hydrophobic groups, which is consistent with our coordination number analysis showing the dehydration of methane in aqueous osmolyte solutions.

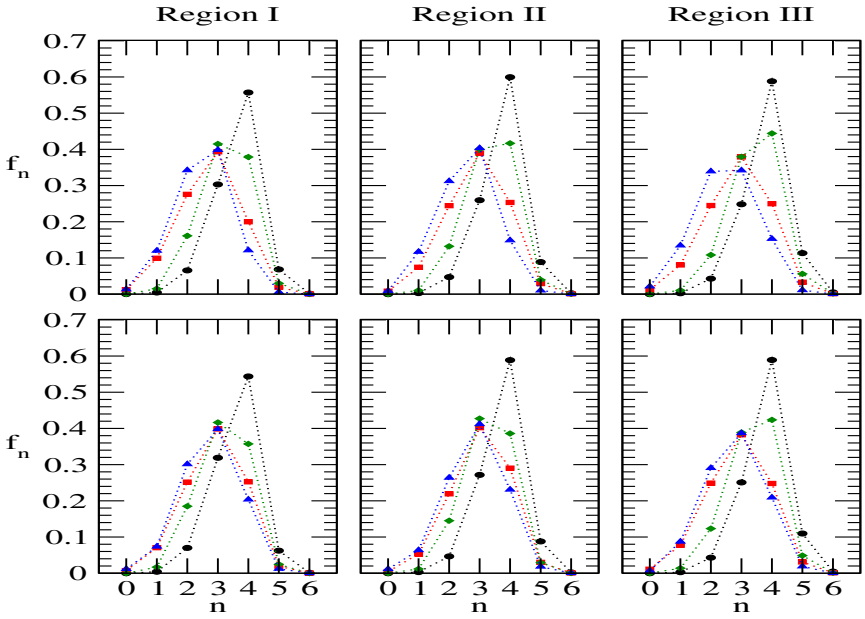

Figure 2A-8. *Fraction of water molecules that engage in n number of hydrogen bonds with identical species in different spherical shells around methane in water, aqueous urea, aqueous TMAO, and mixed urea/TMAO solutions. The top panel is for the UA model, and the bottom panel is for the AA model. Regions I, II, and III are defined in the text.*

Orientational Distributions. It is known that the orientational symmetry of bulk water breaks in the presence of liquid−solid or liquid−vapor interfaces [132-135]. Because water loses its orientational symmetry near the solute surface, our interest was to monitor the orientation of water molecules with respect to their distances from the hydrophobic methane center of mass and how the presence of osmolytes influences this distribution. To see this, we calculated the distribution function of the angle formed (θ) between water dipole vector ($\hat{\mu}$) and the unit vector ($\hat{\mathbf{u}}$) pointing from the oxygen atom of water toward the center of the methane molecule (see Figure 2A-9). We studied the water orientational distribution around methane in different regions. The regions considered were identical to those used for water−water hydrogen-bond properties and dynamics calculations. In Figure 2A-10,

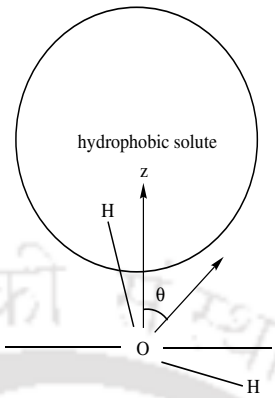

Figure 2A-9. *Angle (θ) between the dipole vector of a water molecule and the unit vector pointing from the oxygen atom of water toward the hydrophobic solute center.*

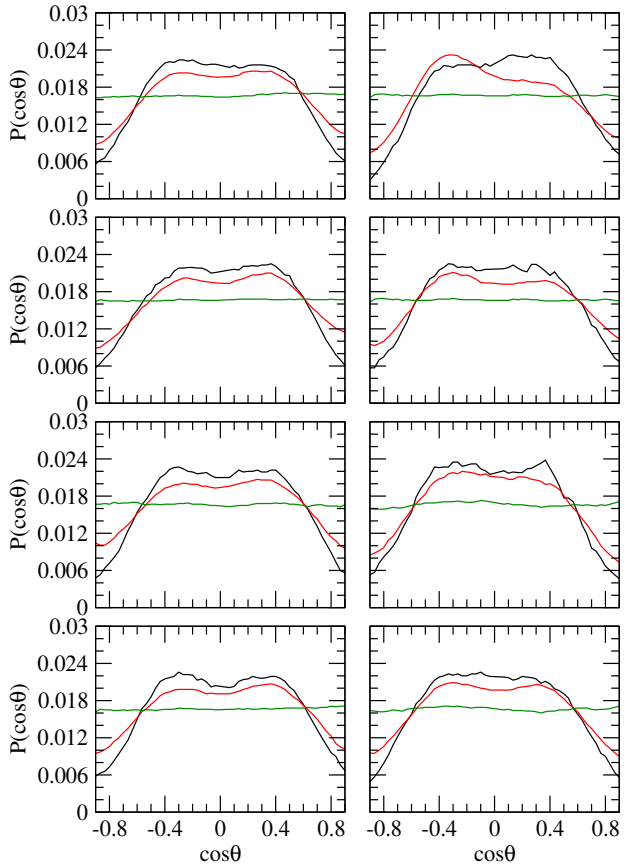

Figure 2A-10. *Orientational distribution of water for Regions I, II, and III in water, aqueous urea, aqueous TMAO, and mixed urea/TMAO solutions (from top to bottom, respectively). The left panel is for the UA model of methane and the right panel is for the AA model. Regions I, II, and III are defined in the text.*

we have shown the results of the normalized probability function $P(cos\theta)$ as a function of $cos\theta$ for the methane UA and AA models. Focusing on the orientational distribution of water in methane−water system first, we find that, as expected, there is no preferred orientation of water molecules far away (Region III) from the solute molecule. In the interfacial regions (Region I and II), however, the probability function is nonuniform which shows an orientational structure of interfacial water molecules near to the hydrophobic surface. Water dipoles in these regions prefer to oscillate in between +0.57 and −0.57; or, in other words, water dipoles make angles in the range $55-124^{\circ}$ with the unit vector. With increasing the distance from the solute molecule, these distribution functions become flatter, which is expected. Osmolyte does not have any notable influence on the orientational distribution of water.

■ SUMMARY AND CONCLUSIONS

We investigated hydrophobic interactions of methane and also the structure of the solution in the presence and absence of urea and TMAO using two different models of methane: UA and AA. The two models of methane behaved very similarly in pure water and in aqueous osmolyte solutions. Surface-parallel orientation of water near the methane moiety and osmolyte-induced dehydration of methane were observed. TMAO interacted with methane through its hydrophobic methyl groups adopting a side-on orientation that allowed its polar oxygen atom to form favorable hydrogen bonds with solution species near the methane molecule. On the other hand, although interaction between methane and urea was observed, methane showed lower affinity for urea than water. In other words, urea molecules were slightly expelled from the solvation shell of methane. Both osmolytes were, however, found to have negligible influence on aggregation of methane.

The water orientational profile calculations suggested anisotropic orientation of water molecules near to hydrophobic surface. The dipole vector of a water molecule in this region oscillated between 55 and 124° with the unit vector. As we move further away from the solute surface, this distribution became flatter, and as expected, there was no preferred orientation of water molecules at the bulk region. Only a slight change in the orientational profiles of water was observed in the presence of osmolytes.

Investigation of water−water hydrogen bond properties in different spherical regions of a single methane molecule did not show much difference in the average number of hydrogen bonds between hydration waters and water molecules in the bulk. However, methane hydration waters did have reduced number of identical nearest neighbors that

engage in hydrogen bonding interactions. The number of identical nearest neighbors reduced further upon addition of osmolyte. TMAO was seen forming hydrogen bonds with both water and urea and also reducing relaxation of water−water hydrogen bonds. Note that, the solvation of TMAO by water and TMAO's ability to enhance water structure are consistent with dehydration of methane in the presence of TMAO; but the expected higher aggregation of methane molecules on the face of methane dehydration does not happen due to the direct interaction of TMAO with methane molecules.

In the context of proteins, the present study shows insignificant effects of urea and TMAO on association of small hydrophobic groups to explain their role as protein stabilizer or destabilizer. Their effect on association of large hydrophobic groups will be treated in **Chapter 3**.

Part B:

TMAO's Effect on Hydrophobicity of Methane at High Pressure

Overview: Classical MD simulations are performed to explore the effects of increasing TMAO concentrations on the pressure-induced modification of hydrophobic interaction. Such systems are of interest because pressure increases the dissolution of hydrophobic protein interior, causing protein denaturation, and TMAO acts to offset the protein denaturing effect of high hydrostatic pressures. Methane molecules are chosen as model of hydrophobic solutes. The concentrations of TMAO range from 0 to 4 M, and for each system, simulations are performed at four different pressures ranging from 2 to 8 kbar. Compressed water shell in the vicinity of methane is observed at high pressure and TMAO is found to offset the pressure-induced slight dissolution of methane. Also observed are preferential accumulation of TMAO near the hydrophobic moiety and TMAO-induced dehydration of hydrophobic solute. From hydrogen bond properties and dynamics calculations, it is found that pressure increases average number of water−water hydrogen bonds, reducing their life-times. In contrast, TMAO reduces water−water hydrogen bond number but enhances their life-times.

■ INTRODUCTION

Water penetration into the protein interior at high pressure is a well-established phenomenon, and because protein interior is largely composed of hydrophobic residues, of fundamental importance in the context of pressure-induced protein denaturation is understanding the influence of pressure on hydrophobic hydration and the hydrophobic interaction of nonpolar solutes in water. Pressure effects on hydrophobicity of simple nonpolar solute have been studied in detail [7, 99, 136-142]. In a pioneer theoretical study, Hummer *et al.* [7] showed that pressure destabilizes the contact configuration of nonpolar molecular groups relative to a solvent-separated configuration. The reported pressure-induced relative stabilization of the water-separated configuration of hydrophobic solute was in line with the protein unfolding at high pressure. Dissolution of aggregates of methane at high pressures was also observed by Wallqvist [138-140]. On the other hand, MC simulations by Payne *et al.* [141] showed that, the hydrophobic interaction between methane decreases only at pressures more than 5 kbar; in the moderate pressure regions (< 5 kbar), increasing pressure rather favors methane to stay together in water. In a MD simulation study of methane in TIP3P water, Ghosh *et al.* [99] found insignificant effect of pressure on the contact configuration of methane, while favoring its solvent-separated configuration. Thus, results of these simulations were in qualitative agreement with the predictions of information theory [7]. Positive activation volumes and the corresponding slowdown of interconversion between the associated and solvent-separated states of methane at high pressure was also reported in the literature [7, 99], in excellent agreement with the experimentally observed considerable slowing down of folding and unfolding rates of the protein staphylococcal nuclease (SNase) with increasing pressure [143]. Continuing further, MC simulations by Chau and Mancera [136] indicated that, as compared to bulk, water molecules have a smaller number of hydrogen bonds in the first hydration shell of methane and the number of water−water hydrogen bonds increases with increasing pressure. The effect of pressure on the angular distribution of water around methane was found to be insignificant in that study.

Unfortunately, while the deleterious effect of pressure on association of methane have been discussed extensively in the literature, the mode of action of TMAO against pressure-induced dissolution of methane molecules is yet to be investigated. TMAO was shown to have negligible effect on association tendency of methane molecules at 1 bar (see Part A). However, rather than extrapolating the results from ambient pressure conditions to high pressure conditions, it is expedient to focus on TMAO systems under high pressure

conditions for a better interpretation of the counteracting mechanism. Therefore, we raise the following important issues. First, what is the influence of TMAO on the pressure-induced dissolution of methane in aqueous solution? Do increasing TMAO contents offset dissolution of simple methane molecules under pressure? Second, how does TMAO interact with methane at high pressure? In the context of protein stabilization by TMAO at high hydrostatic pressures, these are not trivial questions at all, and this is our concern in the present study. Herein, we present results from MD simulations of methane in pure water and binary solution of increasing TMAO concentrations over a wide range of pressures. We first examine the aggregation of methane in aqueous solutions. An insightful picture of the influences of TMAO on pressure-modulated hydrophobic interaction is then obtained by examining its direct interaction with methane molecules. Finally, we focus on the hydrogen bond properties and dynamics of water molecules in different spherical regions of a single methane molecule to describe water−water hydrogen bonding at discrete distances from the solute. The influence of pressure on hydrogen bond dynamics with increasing TMAO concentration is also discussed in this section.

The models and simulation details are described briefly in the next section. The results are then discussed and, finally, the chapter is concluded with a brief summary.

■ MODELS AND SIMULATION METHOD

Classical MD simulations of methane were carried out in pure water and in aqueous solutions of TMAO at four different hydrostatic pressures ranging from 2 to 8 kbar. For the methane−water systems (denoted as $S_{me}0$), the central simulation cell contained 10 methane molecules immersed in 490 water molecules. Three independent TMAO solutions with TMAO mole fractions of 0.03, 0.06, and 0.08 (denoted as $S_{me}2$, $S_{me}3$, and $S_{me}4$, respectively) were constructed by replacing 15, 30, and 40 water molecules, respectively, with TMAO. The molarities of TMAO increased with increasing pressure, but remained roughly in the vicinity of 2, 3, and 4 M in the systems $S_{me}2$, $S_{me}3$, and $S_{me}4$, respectively. Note that for water−water hydrogen bond properties and dynamics calculations, a single solute was used, and to keep total number of molecules constant (500), we replaced 9 methane molecules by water molecules. The SPC/E model [111] was used for water, the UA model [114] was adopted for methane, and TMAO was described with a rigid version of model proposed by Kast *et al.* [113] The values of the LJ parameters and the partial charges for methane, water, and TMAO were tabulated in Table 2A-2. The interaction between atomic sites of two different molecules was expressed using Eq. 2.3.

The methods employed were identical to those discussed in Part A of this chapter.

■ RESULTS AND DISCUSSION

Methane−Methane Pair Potentials of Mean Force. Methane−methane PMFs, as obtained by using Eq. 2.4, are shown in Figure 2B-1. The two minima at about 4 (the CM) and 7 Å (the SSM) in pure water at 1 bar (see Part A), and also the barrier show a movement towards shorter distances at high pressure. The small inward shift of the CM can be attributed for the reduction in excluded volume of methane, whereas relatively larger inward movement of the SSM and the barrier are due to changes in the overall structure of the solvent water molecules. The well depth of the CM does not follow any regular trend with pressure, but the height of the barrier increases and the SSM becomes deeper with increasing pressure. Addition of TMAO to the system changes the methane−methane PMF only slightly, with the well depth of the CM shifting little downward while the barrier height shifts upward. Moreover, the well depth of the SSM shifts upward, suggesting probable removal of solvent molecules from the interstitial position of hydrophobic solute pair. Remember that the negligible influence of TMAO on methane−methane PMF was observed at 1 bar as well (Part A).

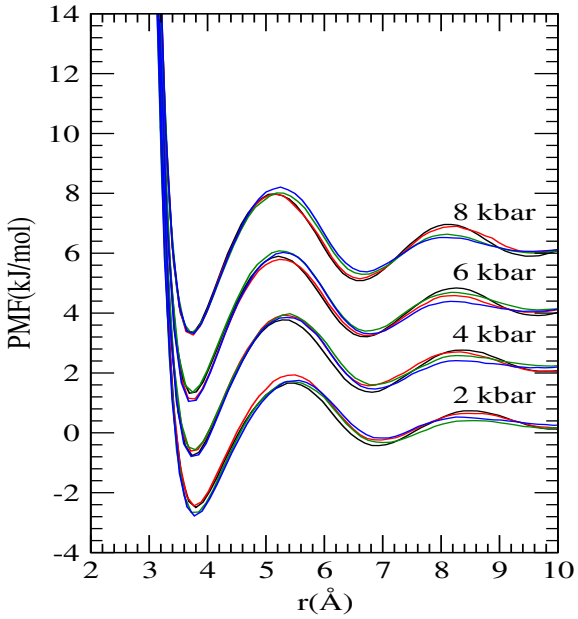

Figure 2B-1. *Methane−methane PMFs for systems* $S_{me}0$, $S_{me}2$, $S_{me}3$, *and* $S_{me}4$ *at different pressures. The curves are vertically translated for clarity.*

Figure 2B-2 depicts the relative changes of free energy of the desolvation barrier with respect to the CM (ΔW_u) and the SSM (ΔW_f), and also the free energy difference between the SSM and the CM ($\Delta W_{f\to u}$). It is notable here that the SSM and the CM states correspond loosely to unfolded and folded states of protein; in the context of dissolution of hydrophobic solutes in aqueous solution, $\Delta W_{f\to u}$ is related to thermodynamic

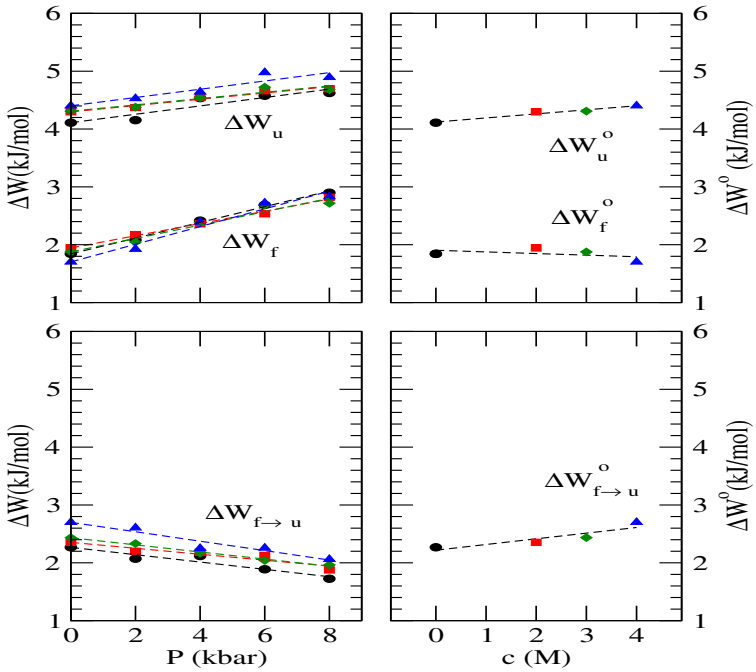

Figure 2B-2. *Left: Relative changes of the desolvation barrier with respect to the CM (ΔW_u) and the SSM (ΔW_f) (top), and the free energy difference between the SSM and the CM ($\Delta W_{f\to u}$) (bottom) as a function of pressure for systems $S_{me}0$, $S_{me}2$, $S_{me}3$, and $S_{me}4$. Right: The free energy change at 1 bar (obtained from linear extrapolations) as a function of TMAO concentration.*

stability of the associated state, or in other words, the association tendency of hydrophobic solutes in aqueous solution. Any perturbation that decreases the value of $\Delta W_{f\to u}$, will favor dissolution of hydrophobic solutes. On the other hand, from kinetic point of view, ΔW_u and ΔW_f correspond to the activation barriers for associated and solvent-separated states, respectively. Lower the value of ΔW_u, higher will be the hydrophobic dissolution propensity.

Focusing on the effect of high hydrostatic pressures in the absence of TMAO first, we observe that applied pressure enhances the activation barriers for both associated (ΔW_u) and solvent-separated states (ΔW_f) of methane (Figure 2B-2). The enhanced

activation barriers will favor both of these two states of methane and consequently, slow down the association and dissolution of hydrophobic solutes. The data in Figure 2B-2 also suggests relatively higher enhancement of activation barrier for association than that for solvent separation. The pressure derivatives of ΔW_u and ΔW_f at constant temperature give activation volumes for dissolution and association, respectively, and our estimated values of these activation volumes are $+0.73$ and $+1.36$ mL mol^{-1}, respectively. We note that positive activation volumes for associated and solvent-separated states were reported previously [7, 99]. The pressure-induced slowing down of association and dissolution of hydrophobic solutes are also consistent with experimentally observed considerable slow down of folding/unfolding kinetics of proteins with increasing pressure [143]. Inspection of the free energy difference between the SSM and the CM reveals that the relative stability of the solvent-separated state over the associated state increases at high pressure, suggesting pressure-induced dissolution of hydrophobic solutes. The pressure derivative of this free energy change ($(\partial(\Delta W_{f\rightarrow u})/\partial P)_T$) represents volume change ($\Delta v_{f\rightarrow u}$) associated with the breaking of each hydrophobic contact upon application of pressure. Our estimated value of $\Delta v_{f\rightarrow u}$ is -0.64 mL mol^{-1}, in excellent qualitative agreement with previous simulation results [99] and also with the predictions of information theory [7].

TMAO has negligible effect on ΔW_f but we find slight enhancement of ΔW_u. A slightly favorable associated state of methane over the solvent-separated state in the presence of TMAO is reflected in a relatively higher free energy gap between the CM and the SSM, shown in Figure 2B-2. Note that increasing pressure does not lead to a significant change in the relative stability of the solvent-separated state of methane over its associated state and TMAO can offset this slight reduction in free-energy difference between these two states.

In aqueous TMAO solutions, at ambient pressure condition, the degree of stabilization, m, of one state of hydrophobic solute relative to a second state can be investigated from the derivative of free energy change of the respective states (ΔW^o) at 1 bar with respect to molar concentration (c) of TMAO [144]. At a particular TMAO concentration, the value of ΔW° is estimated by extrapolating the corresponding ΔW vs P (pressure) plot to 1 bar pressure value:

$$\Delta W^\circ = \lim_{P\rightarrow 1bar} \Delta W(P) \tag{2.9}$$

For example, in the absence of TMAO, the change in free energy for associated to solvent-separated state transition at 1 bar ($\Delta W^\circ_{f\rightarrow u}$), obtained by extrapolating the $\Delta W_{f\rightarrow u}$ vs P plots to 1 bar, is found to be 2.27 kJ mol^{-1} (Figure 2B-2). Remember that this extrapolated

value of $\Delta W_{f\to u}$ at 1 bar pressure is close to the actual value of $\Delta W_{f\to u}$ (2.33 kJ mol^{-1}) in pure water (Part A). The difference between $\Delta W^{\circ}_{f\to u}$ and $\Delta W_{f\to u}$ (8 kbar) is 0.54 kJ mol^{-1}, i.e. the relative stability of the SSM increases by about 0.54 kJ mol^{-1} at 8 kbar pressure. For comparison, simulations by Ghosh *et al.* [99] using TIP3P water showed a net stabilization of the SSM (over the CM) by 0.81 kJ mol^{-1} at 8 kbar pressure. The value of m, obtained from the slope of $\Delta W^{o}_{f\to u}$ vs c plot (Figure 2B-2), is +0.10 kJ mol^{-1} M^{-1}, indicating slight strengthening of hydrophobic association in the presence of TMAO. Our simulation results thus reveal that a high concentration of TMAO can slow down the pressure-induced dissolution of small hydrophobic solutes.

Site−Site Radial Distribution Functions. To obtain molecular details of methane solvation, we computed, first, site−site rdfs between methane and solution species, and then the number of solution species around the hydrocarbon solute using Eq. 2.6.

Figure 2B-3 displays rdfs involving methane, water, and TMAO. Considering the hydration of methane in pure water first, we find that, compared to the bulk density, the water density increases in the first and second hydration spheres around the solute. The coordination number analysis shows an average of about 20 water molecules in the first hydration shell of methane at 2 kbar. The first maximum and minimum shift to shorter distances at high pressure, indicating inward movement of the first hydration shell. The monotonic increase of the first peak and decrease of the first minimum with pressure imply a movement of water molecules from the large-r side of the first hydration shell toward its short-r side. The water movement under pressure thus leads to a reduction in empty spaces in the close proximity of methane with higher water density in this region and also makes the hydration shell more structured. These results are in agreement with the general findings of an efficient packing of water molecules around the nonpolar solute at high pressure [99]. The coordination number analysis does not provide any evidence for pressure-induced enhancement of water molecules in the solvation shell of methane (Table 2B-1). The slight change in the first shell coordination number is likely due to the inward movement of first minimum in methane−water distribution function. Nonetheless, increased hydrophobic hydration is clear from the running coordination numbers of water molecules around the solute methane, displayed in Figure 2B-3, which reveals that within a specific cut-off distance, the number of water molecules increases around methane with increasing pressure. In aqueous solutions of TMAO, the first peak height and the position of first minimum in methane−water rdf remain unaffected. However, the number of water molecules in the solvation shell of

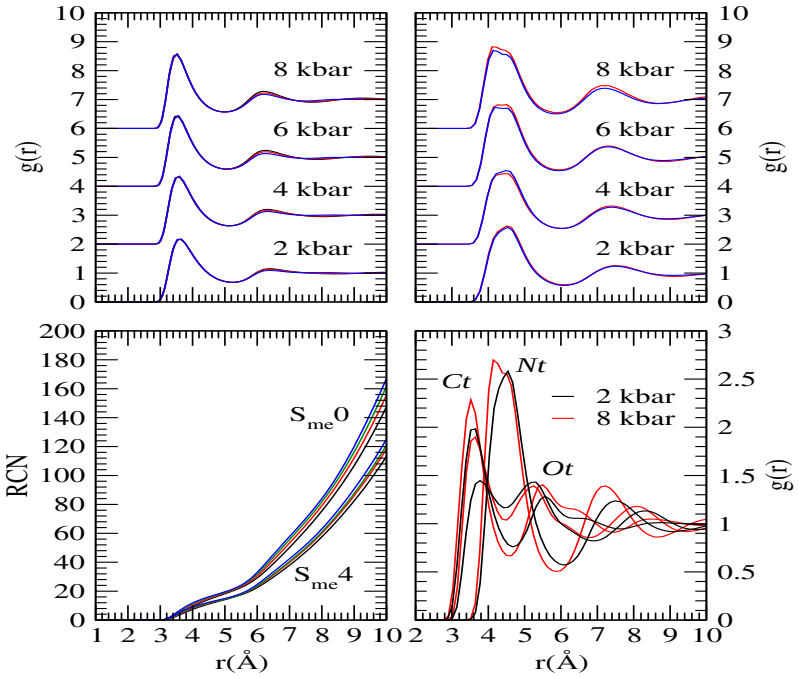

Figure 2B-3. *Top: Methane−water oxygen (left) and methane−TMAO nitrogen (right) rdfs for systems* $S_{me}0$, $S_{me}2$, *and* $S_{me}4$. *Bottom: Running coordination numbers of water oxygen around methane at 2, 4, 6, and 8 kbar pressures (left) and solute−solvent site−site distribution functions for TMAO for system* $S_{me}4$ *(right).*

methane decreases with increasing TMAO concentration (see Figure 2B-3 and Table 2B-1). Numbers given in parentheses in Table 2B-1 nullify the effect of reduced water number density and confirm methane dehydration in the presence of TMAO.

In Part A of this chapter, we examined the affinity of methane for water and TMAO in binary solution with TMAO mole fraction 0.08 at 1 bar and 298 K, and found preferential accumulation of TMAO near the methane moiety due to direct interaction between methane and TMAO methyl groups. Stronger first peak in methane−TMAO rdf as compared to that in methane−water rdf, shown in Figure 2B-3, suggests preference of methane to interact with TMAO over water at elevated pressures as well. This is confirmed further from the data in Figure 2B-4 which depicts the time-averaged normalized fraction of component i as a function of the radius of the spherical volume that defines the local volume around methane in solutions of increasing TMAO concentration at different pressures. Again, Figure 2B-3 indicates direct interaction of TMAO methyl groups with methane molecules. Note that the first peak of oxygen (Ot) density profile, which is responsible for hydrogen

Table 2B-1. Solvation Number for Methane[a]

system	P(MPa)	n_w	n_t	n_w/n_t
$S_{me}0$	200	20.17	—	—
	400	20.03	—	—
	600	19.95	—	—
	800	19.03	—	—
$S_{me}2$	200	18.29(19.55)	1.02	17.93(31.67)
	400	18.28(19.42)	0.97	18.85(31.67)
	600	17.87(19.34)	1.10	16.25(31.67)
	800	17.90(18.45)	1.08	16.57(31.67)
$S_{me}3$	200	16.57(18.94)	1.87	8.86(15.33)
	400	16.46(18.80)	1.92	8.57(15.33)
	600	16.39(18.73)	1.93	8.49(15.33)
	800	16.25(17.86)	1.95	8.33(15.33)
$S_{me}4$	200	15.24(18.52)	2.35	6.49(11.25)
	400	15.24(18.39)	2.37	6.43(11.25)
	600	14.82(18.32)	2.53	5.86(11.25)
	800	15.00(17.48)	2.43	6.17(11.25)

[a] n_w and n_t, respectively, represent number of water and TMAO molecules in the first solvation shell of methane. Numbers in parentheses in the fifth column are the bulk ratios.

bonding with water molecules near the methane moiety, becomes more pronounced at high pressure and the location of it shifts toward shorter distance. This change in the orientation of oxygen atom can be related directly to the enhanced hydration of methane at high pressure.

Table 2B-1 presents the average number of water and TMAO molecules in the first solvation shell of methane. We find that in the solvation shell, the number of water molecules decreases and that of TMAO molecules increases with increasing TMAO concentration. Interestingly, the water/TMAO ratio is always lower than the respective ratio in the bulk (presented within parentheses), providing further evidence for preferential solvation of methane by TMAO.

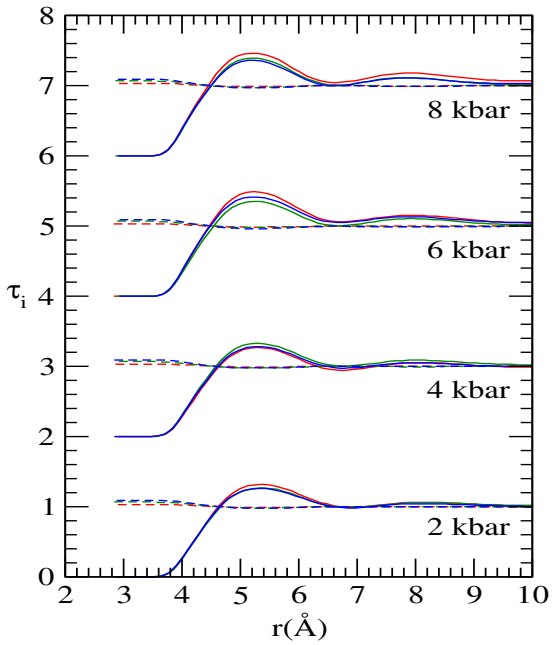

Figure 2B-4. *Time-averaged normalized fractions of water (dashed) and TMAO (solid) central atoms as a function of the distance from methane for systems $S_{me}2$, $S_{me}3$, and $S_{me}4$ at different pressures. The curves are vertically translated for clarity.*

Water−Water Hydrogen Bond Properties and Dynamics. MD simulations of methane in the presence and absence of TMAO at 1 bar showed TMAO-induced enhancement of water−water hydrogen bond life-time (see Part A). In view of its importance in hydration of methane, we made an attempt to study the influences of TMAO on structural, energetic, and dynamical properties of water−water hydrogen bonds at elevated pressures in different layers around the hydrophobic solute. Three regions were considered: two from the vicinity of methane (Region I: 2.5 – 3.5 Å and Region II: 3.5 – 4.5 Å) and the third from the bulk portion of the simulation cell (Region III: 10 – 11 Å). The methods and the geometric criteria for hydrogen bond properties and dynamics calculations were identical to those described in Part A.

In Table 2B-2, we have presented the average number of water−water hydrogen bonds per water molecule together with hydrogen bond life-time and energy of these bonds. The number of hydrogen bonds increases slightly with distance and the hydrogen bonds are slightly more attractive in the vicinity of the solute as compared to the bulk region, as observed previously near methane at 1 bar. With increasing pressure, due to efficient packing, the average number of hydrogen bonded water molecules increases with slight

decrease in hydrogen bond energy (less negative) and its life-time. For example, in Region I, the average number of water−water hydrogen bonds in pure water at 1 bar is 3.62 (see Part A), whereas the same for 8 kbar pressure is 3.96. The trend, i.e., the enhancement in the average number of water−water hydrogen bonds with increase of pressure is valid for other regions and for TMAO solutions as well. In contrast, TMAO reduces the average number of water−water hydrogen bonds, makes hydrogen bonding slightly more favorable, and enhances their life-times.

Table 2B-2. Water−Water Hydrogen Bond Properties and Dynamics[a]

system	P(MPa)	n_{HB}^{I}	n_{HB}^{II}	n_{HB}^{III}	E_{HB}^{I}	E_{HB}^{II}	E_{HB}^{III}	τ_{HB}^{I}	τ_{HB}^{II}	τ_{HB}^{III}
$S_{me}0$	200	3.74	3.83	3.87	-19.37	-19.24	-18.35	1.35	1.38	1.30
	400	3.83	3.91	3.94	-19.19	-18.95	-18.02	1.33	1.29	1.33
	600	3.90	3.99	4.01	-19.01	-18.67	-17.65	1.22	1.22	1.31
	800	3.96	4.04	4.08	-18.70	-18.27	-17.40	1.15	1.16	1.19
$S_{me}2$	200	3.43	3.56	3.74	-19.69	-19.61	-18.69	1.56	1.50	1.58
	400	3.65	3.73	3.75	-19.62	-19.26	-18.32	1.56	1.47	1.37
	600	3.65	3.74	3.83	-19.20	-18.95	-18.00	1.38	1.50	1.36
	800	3.74	3.82	3.87	-19.25	-18.94	-17.78	1.43	1.40	1.38
$S_{me}3$	200	3.52	3.58	3.53	-19.67	-19.36	-18.83	1.75	1.77	1.61
	400	3.58	3.66	3.59	-19.38	-19.16	-18.57	1.67	1.78	1.58
	600	3.43	3.52	3.71	-19.44	-19.46	-18.24	1.55	1.53	1.60
	800	3.60	3.67	3.69	-19.17	-18.82	-18.15	1.69	1.64	1.38
$S_{me}4$	200	3.27	3.36	3.44	-19.97	-20.01	-19.10	1.90	1.92	1.88
	400	3.35	3.43	3.49	-19.61	-19.65	-18.78	1.82	1.79	1.83
	600	3.36	3.44	3.54	-19.72	-19.50	-18.53	1.78	1.70	1.80
	800	3.51	3.59	3.57	-19.27	-18.97	-18.33	1.76	1.70	1.67

[a] n_{HB}, E_{HB}, and τ_{HB} represent average number, energy (in kJ mol^{-1}), and life-time (in ps) of water−water hydrogen bond, respectively. Regions I, II, and III are defined in the text.

The fraction (f_n) of water molecules that engage in n number of hydrogen bonds is illustrated in Figure 2B-5. Applied pressure increases the fraction of 5-coordinated water molecules and reduces the fraction of 3-coordinated water molecules, in excellent

agreement with previous MC simulation results for methane−water system at different pressures [136]. Thus, at high pressure, some of the water molecules are forced to occupy interstitial positions leading to an increase in the number of molecules with higher coordinated (5) hydrogen bonds at the expense of more stable lower coordinated (3) hydrogen bonds. On addition of TMAO, fraction of 2- and 3-coordinated water molecules increases with corresponding decrease of 4- and 5-coordinated water molecules. The enhancement of lower coordinated water molecules and the reduction of higher coordinated water molecules in the presence of TMAO were observed also at low pressure (Part A) and are correlated with the large size of TMAO molecule that has to be accommodated in the cavities of water molecules. The present results suggest that TMAO and pressure have counteracting effects on the water hydrogen bonding network. In a recent SAXS study of dense lysozyme solutions, Schroer *et al.* [62] predicted that it is the indirect effect of

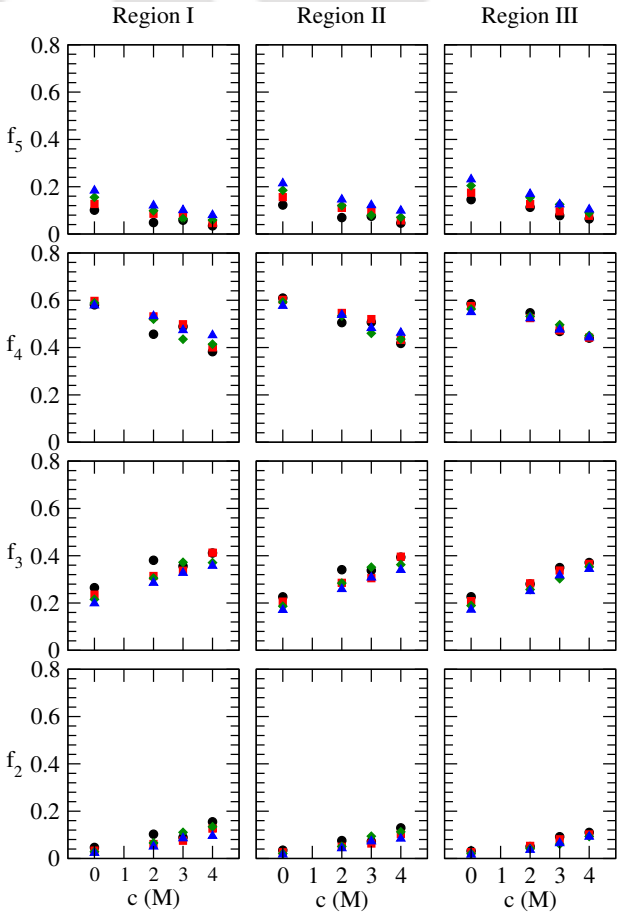

Figure 2B-5. *The fraction of water molecules that engage in n number of hydrogen bonds with identical species in the presence and absence of TMAO at 2, 4, 6, and 8 kbar pressures. Regions I, II, and III are defined in the text.*

TMAO on the water structure that plays a major role in protein stabilization by TMAO under high pressure conditions. To be specific, they suggested that TMAO increases the amount of strong hydrogen bonds of water, leads to a strengthening of hydrogen bond network structure, and thus counteracts pressure-induced denaturation of proteins. Our results lend support to their predictions.

■ SUMMARY AND CONCLUSIONS

Classical MD simulations were undertaken to investigate the effects of increasing TMAO concentration on the pressure-induced modification of hydrophobic interaction. Methane was chosen as model of hydrophobic solute and simulations were carried out for four independent TMAO solutions each at four different pressures relevant to protein denaturation. From PMF calculations, it was found that high pressure increased the stability of the solvent-separated state of hydrophobic solute with respect to its associated state. Also observed was efficient packing of water molecules around the hydrophobic solute at high hydrostatic pressure. TMAO was found to offset the pressure-induced slight dissolution of methane, reducing number of hydration waters. The preferential binding calculations showed that methane preferred to interact with TMAO molecules over water at elevated pressures as observed previously at low pressure.

Investigation of structural and dynamical properties of water−water hydrogen bonds in different layers around the solute molecule indicated slightly reduced number of hydrogen bonded identical neighbors in the vicinity of the solute as compared to the bulk region. High pressure enhanced water−water hydrogen bonding, favoring 5-coordinated hydrogen bonds and reducing energetically favorable 3-coordinated hydrogen bonds. On addition of TMAO, the average number of water−water hydrogen bond reduced, but there was a profound increase in hydrogen bond life-time. Moreover, TMAO increased the number of 2- and 3-coordinated water molecules, and reduced the number of 4- and 5-coordinated water molecules.

The present study reveals that TMAO and pressure have counteracting effects on the water structural properties. The effect of pressure on water structure is consistent with pressure-induced enhanced hydration (or dissolution) of hydrophobic groups which, in turn, is consistent with its role as protein destabilizer. There is, however, lack of a substantial effect of pressure on hydrophobicity of small methane molecules. Similarly, although TMAO's counteracting effect on pressure-conferred water crowding agrees with dehydration of hydrophobic solute in the presence of TMAO and TMAO seems to prevent

the slight pressure-induced dissolution of methane molecules, its effect on association of small solute is insignificant to describe it as a protein stabilizer. That is why, we shall dwell on TMAO's effect on pressure-modulated hydrophobicity of large solute in the next chapter.

Chapter 3

Assembly of Large Hydrophobic Solute

"When solute size is small, irrespective of the nature (whether attractive or repulsive) of the interaction between solute atom and solvent, water molecules are able to rearrange themselves to restore, at least in part, the hydrogen bond network without creating any dry cavity. For a large size hydrophobic solute, however, a fine balance among solute−solvent and solvent−solvent interactions and hydrogen bonding energies is required to determine whether cavitation or strict microscopic dewetting will occur."

– N. Choudhury and B. M. Pettitt *J. Am. Chem. Soc.* **127**, 3556 (2005)

Chapter 2 was concerned with the hydrophobicity of methane in pure water and the pressure- and osmolyte-induced modulation of this hydrophobicity. Although methane is a useful computational model to understand the behavior of hydrophobic groups in aqueous environments, it is intriguing to know the hydrophobicity of relatively larger nonpolar solutes. Understanding hydrophobicity of large solute is important not only because the introduction of a sufficiently large solute molecule into a bulk liquid can induce a depletion of solvent next to the solute molecule [133, 145-151], but also due to the fact that the effective size of nonpolar groups comprising the protein is larger than methane. Numerous studies concerning hydrophobicity have been reported with hydrophobic solute of different sizes as well as infinite plate models [90, 104, 133, 145, 148, 150, 152-189]. Usually, a small hydrophobic solute does not affect the water hydrogen bonding network considerably, but causes some restrictions in the spontaneous solvent fluctuations. A molecular level understanding that supports the assertion that a small hydrophobic unit can be accommodated into the spontaneous cavities present in water with some reorganization of the hydrogen bond network has emerged from a number of studies [100, 137, 147, 173-180]. So free energy of hydration of small solute is relatively low and the process is entropy dominated [90, 147, 174, 181, 182]. As the size of the solute increases, the ability to maintain the hydrogen bonding network reduces which causes an energetic cost in the system and the minimization of the energy loss also needs significant reorganization of water molecules [90, 133, 147]. As a result, the hydration process becomes increasingly unfavorable. Also critical in the context of hydrophobicity is the solute−solvent attractive interaction. Persistent hydration has been observed when the strength of solute−solvent interaction is very high [91, 148]. As the strength of this interaction reduces, the hydration behavior changes through a thin vapor-like interface [151, 183] to the complete dewetting [184, 185]. It was shown that an energetic gain from favorable solute−solvent interaction can overcome the energy cost due to the reduction in the number of hydrogen bonds [171]. Importance of solute−solvent interaction in hydration was indicated further by different solubility of propane, propene, and propyne in water despite their similarity in size [104].

On the other hand, aggregation of hydrophobic solutes can be described as reverse of hydration process and the driving force for aggregation arises, at least qualitatively, from the inverse thermodynamic properties to those of hydration. Thus, from the conventional wisdom of entropy driven hydrophobic hydration of small solute, their tendency to aggregate in water is expected to be entropy dominated process [186, 187]. There are many simulation studies showing the entropically stabilized contact pair of methane in water

[121, 177, 178, 188, 189]. In contrast, both enthalpic and entropic terms contribute in the clustering of large hydrophobic solutes in water. The enthalpy and entropy driven association of hydrophobic solute was demonstrated by Zangi in a MD simulation study of driving force for hydrophobic interaction at different length scales [156]. He showed that for small solutes, the driving force for association is 100% entropic and the enthalpic part rather favors dissociation of these solutes, while association of large hydrophobes are favored both enthalpically and entropically.

Keeping these in mind, in this chapter, we investigate the hydrophobicity of large solute in pure water and the pressure- and osmolyte-induced modulation of this hydrophobicity using neopentane as model of nonpolar solute. The main objectives are, first, to see how solute size (and model) changes the hydrophobicity and, secondly, to understand the influence of high pressure and osmolyte on hydrophobicity of large solute. The rest of the entitled chapter is divided into two parts. In Part A, we explore the influence of urea and TMAO on the assembly of neopentane molecules in aqueous environments. Effects of increasing TMAO concentration on pressure-induced modulation of neopentane aggregation are then presented in Part B.

Part A:

Neopentane in Water and Aqueous Solutions of Urea and TMAO

Overview: We deal here with the influences of urea and TMAO on the assembly of hydrophobic solute in aqueous solutions by performing MD simulations. The hydrophobic solute chosen in this study is neopentane which is considerably larger than a methane molecule. Two different models of neopentane are used: one is of single united site (UA), and the other contains 5-sites (AA). While the UA model of neopentane shows weak tendency for association in aqueous solutions, which is similar to the case of methane; significantly stronger association tendency is observed for the AA model, forming aggregate in water. Urea causes relative dispersion of neopentane aggregate, in accordance with urea-conferred protein denaturation. Dissolution of neopentane in binary urea solution occurs due to direct interaction between neopentane and urea molecules. A significant loss of water molecules in the solvation shell of neopentane is observed due to the existence of urea molecules in this region. TMAO does not show any tendency to enhance neopentane aggregation or to prevent urea-induced dispersion of neopentane, making it unlikely that TMAO stabilizes proteins and counteracts urea-induced denaturation by enhancing hydrophobic interaction. Not surprisingly though, TMAO interacts directly with neopentane molecules through its hydrophobic methyl groups and reduces number of water molecules near the neopentane surface.

■ INTRODUCTION

Neopentane, the simplest alkane with a quaternary carbon, is one of the three structural isomers with the molecular formula C_5H_{12} (pentanes), the other two being *n*-pentane and isopentane. So far, a large number of studies have been devoted to understand the behavior of neopentane in aqueous solutions. Solvation free energy of neopentane in neat water was found to be about 10 kJ mol^{-1} [104, 190], which is higher than that of methane ($\sim$ 8 kJ mol^{-1} [103, 104]) by about 2 kJ mol^{-1}. Employing MD simulation technique, Huang *et al.* [152] showed striking similarity in the orientational distribution of water molecules neighboring a neopentane molecule to that found next to a macroscopic hydrophobic surface. Much higher probability for contact pairing of neopentane than for solvent-separated pairing was indicated in that study, in contrast to previously observed less probable contact pairing of small molecule than solvent-separated pairing [173, 180, 191]. The density profile of water between a pair of neopentane molecules exhibited a kind of drying expected between two large hydrophobic surfaces brought close together, with the effect being more pronounced in the absence of solute−solvent attractions [152]. In addition to studies that focused on the neopentane pair PMFs in water [44, 153, 192, 193], also appears in the literature, simulation study performed with a larger number (8) of neopentane molecules, exhibiting a considerable propensity of neopentane self-aggregation in water [194].

With the aim of understanding the basic interactions responsible for protein folding and denaturation, solvation of neopentane in aqueous urea solution have also been investigated. Trzesniak *et al.* [106] reported solvation free energies of methane, ethane, propane, *n*-butane, isobutane, and neopentane in 6.9 M urea−water mixture obtained by MD simulations. A strong dependence of hydrocarbon transfer free energies on aliphatic hydrocarbon size was observed in that study, in accordance with other experimental and theoretical results [25, 108, 110]. Neopentane was found to be more soluble in urea than in water, in contrast to the unfavorable transfer of methane from water to urea−water mixture [25, 106]. Recently, Lee and Van der Vegt [44] investigated the influence of pair interaction of hydrophobic moieties using different models of neopentane, water, and urea molecules. Their calculations of equilibrium constant values of solvent-separated configuration relative to contact pair showed that, in aqueous urea solution, the equilibrium shifts significantly in favor of the solvent-separated configuration in comparison to the equilibrium in pure water. Examining the number density of water and urea molecules for the contact and solvent-separated pairs of neopentane, preferential interaction of urea with the nonpolar

solutes were observed [44], in agreement with previous simulation studies on hydrophobic solvation of aliphatic [106] and aromatic hydrocarbons [45] in urea solution. It was argued that the interstitial urea molecules interact through dispersion forces with two neopentane molecules at the same time, causing relative stabilization of the urea-separated pair [44]. MD simulations were also used to obtain PMFs for pairs of neopentane molecules in binary and ternary solutions of urea and TMAO [192, 193]. TMAO-induced reduction of the hydrophobic attraction both in water−TMAO and water−urea−TMAO solutions was indicated in those studies.

As discussed above, the effects of urea and TMAO on hydrophobic interaction between a neopentane pair have been studied previously [44, 192, 193]. However, to the best of our knowledge, there is no prior study that investigate the influences of urea and TMAO on the assembly of neopentane molecules in aqueous solutions. This issue is addressed in this part. We describe here the solvation characteristics of neopentane in binary and ternary solutions of urea and TMAO using 10 solute molecules. The solute−solute PMF is considered as a structural measure of aggregation. Again, the PMF between a neopentane pair in water and urea−water mixture was shown to be affected by the model of the solute used [44]. To see the model dependency, if any, we have used two models of neopentane. We first examine whether urea or TMAO has any significant effect on the aggregation of neopentane in aqueous solutions. To get deeper insight into how this aggregation is affected by these two osmolytes, we investigate their tendency to interact directly with neopentane and also study the changes in water structure. Finally, we give a close look on the orientation of water and also on the structural, energetic, and dynamical properties of water−water hydrogen bonds in different hydration shells of neopentane in the presence and absence of osmolytes.

The models and simulation details are briefly described in the next section. This is followed by a section whereof we discuss our results, and our conclusions are summarized in the last section.

■ MODELS AND SIMULATION METHOD

Classical MD simulations were carried out for neopentane in water, aqueous urea, aqueous TMAO, and mixed urea/TMAO solutions. The number of molecular species considered in different systems are presented in Table 3A-1. Note that, a single neopentane molecule was used for water−water hydrogen bond properties and dynamics calculations (as well as for water orientational profile calculations), and to keep the total number of molecules

constant, we replaced 9 neopentane molecules by water molecules. In all of the simulations, the SPC/E model [111] was used for water, the DKJ model [112] was adopted for urea, and TMAO was described with a rigid version of model proposed by Kast *et al.* [113] Two different models were used for neopentane: a single-site united-atom (UA) model [195] and a 5-site (AA) model [196]. In the AA model, the four methyl groups attached to the central carbon atom were considered as effective interaction sites. All models employed were rigid and the interaction between atomic sites of two different molecules was expressed using Eq. 2.3. The values of the LJ parameters and the partial charges for urea, TMAO, and water were summarized in Table 2A-2, and the same for neopentane are tabulated in Table 3A-2.

Table 3A-1. Overview of Systems[a]

model	system	V(nm^3)	Ns	Nu	Nt	Nw	Mu	Mt
UA	$S_{UA,1}$	16.39	10	0	0	490	0	0
	$S_{UA,2}$	20.83	10	100	0	390	7.97	0
	$S_{UA,3}$	19.18	10	0	40	450	0	3.46
	$S_{UA,4}$	23.79	10	100	40	350	6.98	2.79
AA	$S_{AA,1}$	16.20	10	0	0	490	0	0
	$S_{AA,2}$	20.35	10	100	0	390	8.16	0
	$S_{AA,3}$	19.10	10	0	40	450	0	3.48
	$S_{AA,4}$	23.12	10	100	40	350	7.18	2.87

[a]V, N, and M represent box volume, number of molecules, and molar concentration, respectively. s, w, u, and t, respectively, refer to solute (neopentane), water, urea, and TMAO.

Table 3A-2. Lennard-Jones Parameters and Charges for Neopentane[a]

model	atom type	σ(Å)	ϵ (kJ mol^{-1})	charge(e)
UA	np	6.15	3.496	0.0
AA	$C(central)$	3.80	0.209	0.0
	Me	3.96	0.6061	0.0

[a]e is the elementary charge.

The methods employed were identical to those described in **Chapter 2**. In short, we performed simulations at 298 K and 1 bar in a cubic box, initially, in the NPT ensemble to obtain the average volume of the simulation box corresponding to the desired pressure, and then in the NVT ensemble with the so obtained box volume. Production runs of 10 ns were carried out after equilibrating the system.

■ RESULTS AND DISCUSSION

Neopentane−Neopentane Pair Potentials of Mean Force. Figure 3A-1 presents the neopentane−neopentane PMFs as obtained by using Eq. 2.4. The primary minimum (the CM) in the PMF curve, which corresponds to the direct contact between two neopentane molecules, arises at a longer distance (about 6.6 Å for the UA model, e.g.) as compared to that in methane. This is due to the larger excluded volume of a neopentane molecule that prevents the center of a second species to penetrate in a specific region around the solute. Comparison of the PMF curve of neopentane with that of methane at 1 bar (reported in previous chapter) reveals similar association propensity for the neopentane UA model in water. On the other hand, the AA model of neopentane shows significantly higher association propensity of neopentane in water. For this particular model, the CM is significantly

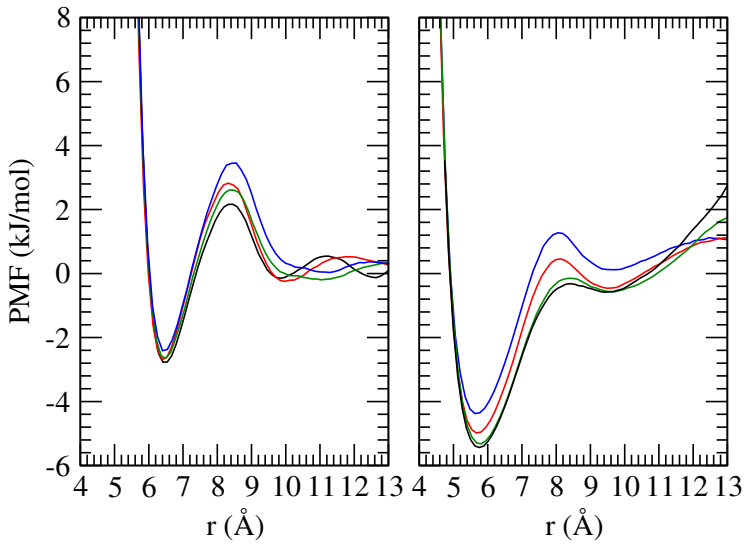

Figure 3A-1. *Neopentane−neopentane PMFs for the UA (left) and AA (right) models in water, aqueous urea, aqueous TMAO, and mixed urea/TMAO solutions.*

deeper, and the barrier between the contact and solvent-separated configurations is very weak (Table 3A-3). In pure water, the associated state is favored over the solvent-separated state by about 4.85 kJ mol^{-1}, which is much higher than the UA model (only 2.62 kJ mol^{-1}). This strong tendency for association leads to the formation of neopentane aggregate in the system. The small size of our simulation sample and the finite size of the aggregate makes the PMF to have a positive gradient that does not approach a value of zero at higher inter-particle distances. Note that a positive gradient in the PMF curve at larger solute separations was observed previously for larger nonpolar solutes [99, 197], whereas it was absent in case of methane (**Chapter 2**).

Neopentane molecules are relatively dispersed in aqueous urea solutions, as revealed by reduced well depth of the CM (Table 3A-3). The relative dispersion of neopentane in the presence of urea leads to reduction in the magnitude of the gradient appearing at large solute separations (for the AA model). Both models of neopentane, however, show only slight awareness of the presence of TMAO in the system and neopentane aggregation is not affected much in binary TMAO solution.

Table 3A-3. PMF Values (in kJ mol^{-1}) at the CM, the SSM, and the BARR[a]

	UA				AA		
system	CM	BARR	SSM	system	CM	BARR	SSM
$S_{UA,1}$	−2.77	+2.16	−0.15	$S_{AA,1}$	−5.43	−0.31	−0.58
$S_{UA,2}$	−2.68	+2.82	−0.24	$S_{AA,2}$	−4.98	+0.45	−0.46
$S_{UA,3}$	−2.64	+2.61	−0.19	$S_{AA,3}$	−5.32	−0.15	−0.57
$S_{UA,4}$	−2.41	+3.45	+0.03	$S_{AA,4}$	−4.37	+1.27	+0.12

[a]The estimated standard deviations for all systems vary from 0.03 to 0.27 kJ mol^{-1}.

In an attempt to understand the behavior of neopentane assembly more closely, we computed the association constant, K_a (using Eq. 2.5), and also analysed the cluster structure (see **Chapter 2** for method). The values of K_a for different systems simulated are presented in Table 3A-4 and Table 3A-5 displays the cluster structure analysis results for the two different models of neopentane. The data in Table 3A-4 clearly suggest strong association tendency for the AA model. We find that, in pure water, K_a takes the value of

4.4 M^{-1}, which is significantly higher than that observed for methane (**Chapter 2**). Additionally, the difference between n and n_0 is very high and this difference is much higher than the value of δ (Table 3A-5). Both urea and TMAO reduce the magnitude of K_a and the $n - n_0$ values get lowered in the presence of osmolyte. These confirm urea-induced dissolution of neopentane aggregate and TMAO's inability to prevent this dissolution.

Table 3A-4. Association Constant (K_a) for Neopentane

UA		AA	
system	$K_a(M^{-1})$	system	$K_a(M^{-1})$
$S_{UA,1}$	1.33	$S_{AA,1}$	4.43
$S_{UA,2}$	1.15	$S_{AA,2}$	3.37
$S_{UA,3}$	1.20	$S_{AA,3}$	4.20
$S_{UA,4}$	1.08	$S_{AA,4}$	2.56

Table 3A-5. Neopentane Cluster Sizes for Different Systems[a]

model	system	n	n_0	δ	$n - n_o$	remark
UA	$S_{UA,1}$	1.34	1.54	0.308	−0.20	average
	$S_{UA,2}$	0.92	1.16	0.232	−0.24	low
	$S_{UA,3}$	1.04	1.28	0.256	−0.24	average
	$S_{UA,4}$	0.75	1.10	0.220	−0.35	low
AA	$S_{AA,1}$	4.54	1.54	0.308	3.00	high
	$S_{AA,2}$	2.75	1.10	0.220	1.65	high
	$S_{AA,3}$	3.65	1.28	0.256	2.37	high
	$S_{AA,4}$	1.83	0.94	0.188	0.89	high

[a] n_0, n, and δ are the average number of neopentane molecules, number of neopentane molecules in the first coordination shell, and the fluctuation, respectively.

Hydration of Neopentane. Figure 3A-2a does not reveal any significant difference in hydration characteristics between methane (**Chapter 2**) and neopentane (UA model) in

pure water. The larger excluded volume of neopentane, however, causes shifting of water exclusion radius (the shortest distance at which $g(r) = 1$) and the subsequent hydration layers to larger distances. To be specific, for the UA model of neopentane, water exclusion occurs below 4.5 Å (against 3.3 Å for methane) and the first peak appears at about 5.0 Å (against 3.6 Å for methane). In contrast to the UA model, which has a well-defined first hydration shell with high water density at its center (~ 2 times the bulk water density), the propensity of water molecules to interact directly with neopentane decreases dramatically for the AA model in pure water. The water density around this particular neopentane model is very low; at the center of the first hydration shell (the first peak), density of water is only 1.1 times the bulk water density. This significantly small density of surrounding water molecules is correlated with the large aggregation of the AA model in pure water. The average hydration number of neopentane in pure water is 20 (Table 3A-6) which is

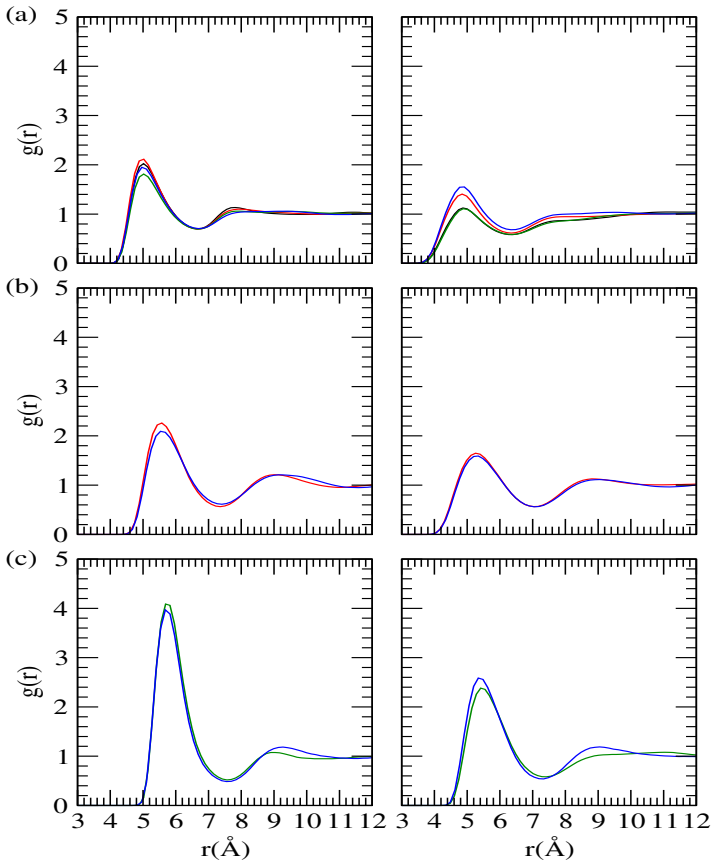

Figure 3A-2. *Distributions of water, urea, and TMAO central atoms (from a-c, respectively) around neopentane for the UA (left) and AA (right) models in water, aqueous urea, aqueous TMAO, and mixed urea/TMAO solutions.*

similar to that of methane (**Chapter 2**). Considering the much larger size of neopentane, this similarity is possible only due to the large aggregation of neopentane (as compared to methane for which the solute particles are largely dispersed in water), reducing the available space for water molecules around these solutes. This fact is supported by our observation that, for the UA model, the average hydration number (Table 3A-6) is much higher than that of methane (33 against 20).

It is clear from the data in Figure 3A-2a that the water density near the neopentane moiety (AA model) increases in the presence of urea (both binary and ternary solutions), perhaps due to urea-induced dispersion of neopentane molecules. Table 3A-6, however, suggests osmolyte-induced dehydration of neopentane molecules. Note that the dehydrating effect in the presence of urea is higher for the UA model of neopentane. For instance, the dehydration in binary urea solution is about 36% for the UA model vs 26% for the AA model. To nullify the effect of reduced water density in the system, coordination numbers were also calculated assuming that the only change with added osmolyte comes through the reduced number of water. These numbers, included in Table 3A-6 in parentheses, confirm the replacement of water by osmolyte from the first hydration shell of neopentane. Moreover, we find that the ratio of the first shell water molecules in pure water and in aqueous osmolyte solution is higher than the respective ratio of water molecules present in these systems, revealing osmolyte-induced dehydration of neopentane. For example, for the UA model, the ratio of hydration waters in pure water ($S_{UA,1}$) and in binary urea solution ($S_{UA,2}$) is 1.56:1 which is higher than the ratio of total number of water molecules present in these systems (i.e., 1.25:1).

Table 3A-6. Hydration Number (Nw) for Neopentane[a]

UA		AA	
system	Nw	system	Nw
$S_{UA,1}$	33.0	$S_{AA,1}$	20.2
$S_{UA,2}$	21.2(26.3)	$S_{AA,2}$	14.9(16.1)
$S_{UA,3}$	23.7(30.0)	$S_{AA,3}$	15.4(18.6)
$S_{UA,4}$	16.1(23.6)	$S_{AA,4}$	13.0(14.4)

[a]Hydration numbers are obtained by integrating the rdf to the first minimum.

Osmolyte's Interaction with Neopentane. Affinity of neopentane to interact with osmolytes can be seen in site−site rdfs between neopentane and osmolyte molecules, presented in Figure 3A-2. The peaks are narrower and sharper for the UA model of neopentane, indicating its better solvation as compared to the AA model. We find that, in progressing from water to urea to TMAO, the first peak in rdf grows back, demonstrating that in its first solvation shell, neopentane prefers TMAO over urea which, in turn, is preferred over water.

The relative accumulation or depletion of solution species in the vicinity of neopentane was investigated by calculating the time-averaged normalized ratio (τ_i) of component i defined in **Chapter 2**. Preference of neopentane for urea and TMAO over water is clearly visible in the τ_i profiles, displayed in Figure 3A-3. Remember that comparatively more TMAO molecules were observed in the vicinity of methane as well (**Chapter 2**). In contrast to neopentane, the small hydrophobic solute, however, showed a slight tendency

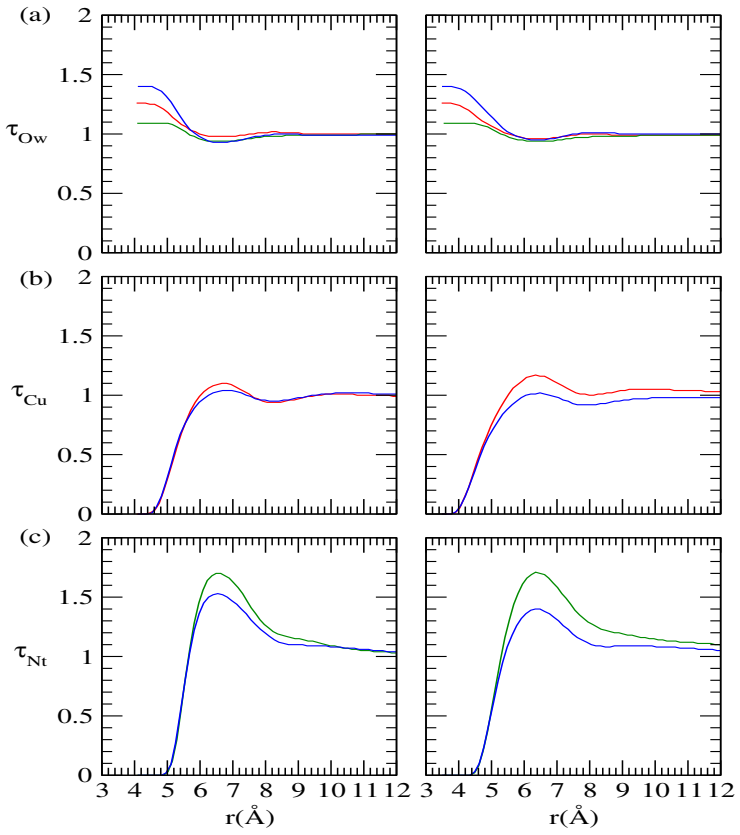

Figure 3A-3. *Time-averaged normalized fractions of water, urea, and TMAO central atoms (from a-c, respectively) as a function of the distance from neopentane for the UA (left) and AA (right) models in aqueous urea, aqueous TMAO, and mixed urea/TMAO solutions.*

to exclude urea from its solvation shell (**Chapter 2**). Similar observations were made previously by Trzesniak *et al.* [106] in their computer simulation studies on the solvation of aliphatic hydrocarbons in 6.9 M aqueous urea solution. The data in Figure 3A-3 also suggests a much better mixed solvation layer of neopentane in terms of water and osmolyte in the mixed osmolyte solution as compared to that in the binary solution.

The orientations of water and osmolyte near the neopentane moiety were examined by computing all the rdfs involving neopentane, water, urea, and TMAO. The general behaviors of these distribution functions, shown in Figure 3A-4 for the urea/TMAO mixture, are qualitatively similar to those observed in case of methane (**Chapter 2**), and reveal surface-parallel orientation of water and side-on orientations of urea and TMAO near the neopentane surface.

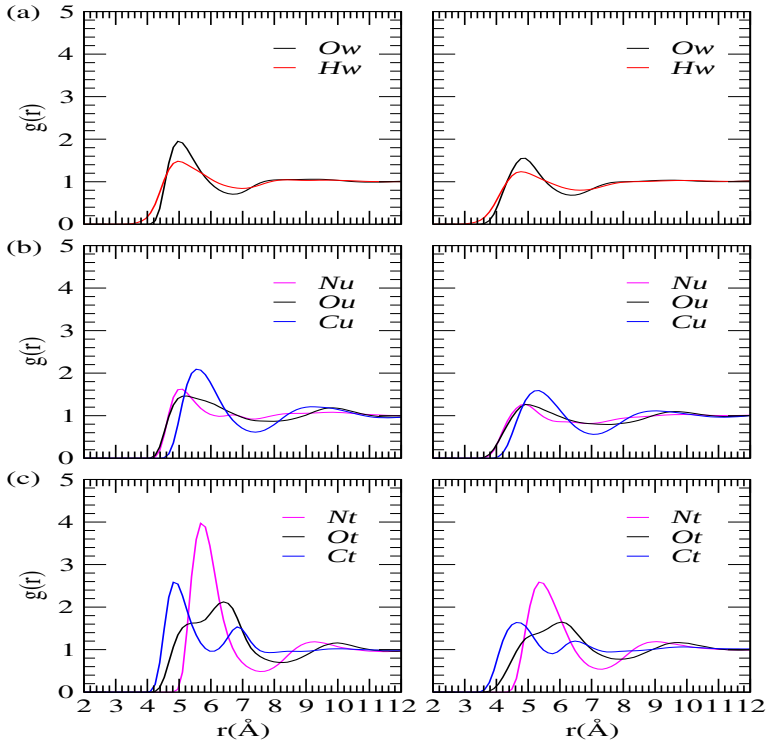

Figure 3A-4. *Selected site−site distribution functions showing orientations of water, urea, and TMAO molecules (from a-c, respectively) around neopentane for the UA (left) and AA (right) models in urea/TMAO mixture.*

Osmolyte Solvation and Its Effect on Water Properties. In previous chapter, we studied the solvation characteristics of urea and TMAO in binary and ternary solutions as well as the changes in water structural and dynamical properties to assess the influ-

ence of solute/co-solute on water structural, energetic, and dynamical properties. Selected site−site rdfs were computed and those were followed by hydrogen bond analysis. Both osmolytes were found to be well-solvated in aqueous solutions and an indirect effect of osmolyte solvation on water structure was evident in which urea broke the water second-shell slightly and TMAO enhanced the water structure. The data presented in Figures 3A-5 and 3A-6 and Table 3A-7 support those observations further.

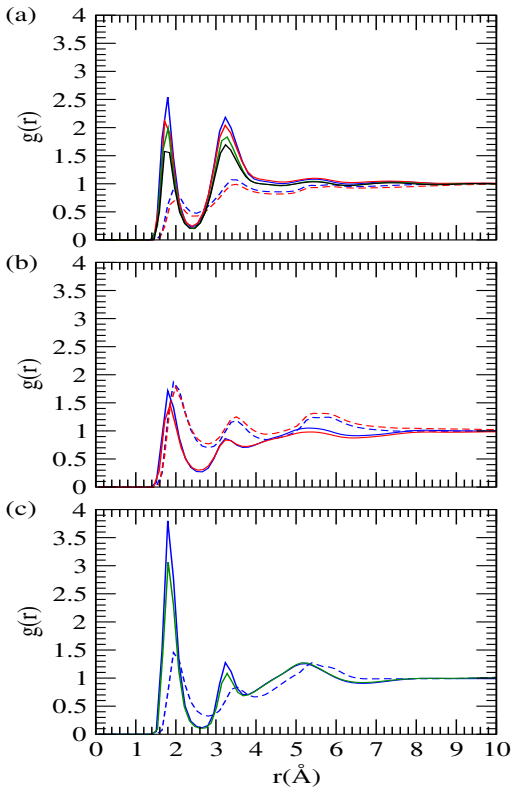

Figure 3A-5. *Selected site−site distribution functions that show hydrogen bonding interactions involving O-atoms of water, urea, and TMAO molecules (from a-c, respectively) for the UA model of neopentane in water, aqueous urea, aqueous TMAO, and mixed urea/TMAO solutions. Solid and dashed lines are for water and urea hydrogens, respectively.*

Structural, energetic, and dynamical properties of water−water hydrogen bonds at discrete distances from a neopentane molecule were investigated to see the influence of a relatively large hydrophobic solute as well as of osmolyte on water hydrogen bonding network. As in the case of methane, three regions of width 1 Å each were considered: two near the solute surface (Regions I and II) and the third one at a relatively larger distance from the solute assuming bulk portion of the simulation cell (Region III: 10 − 11 Å). For

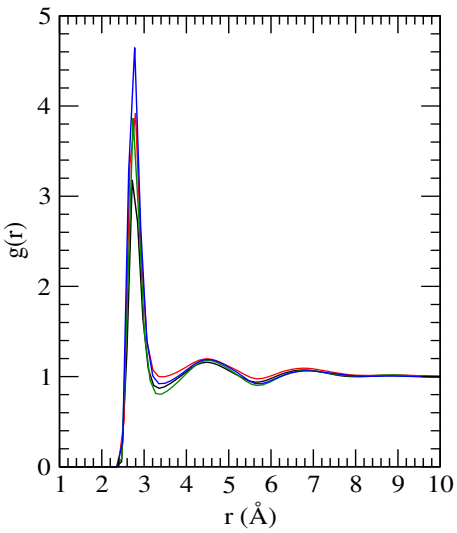

Figure 3A-6. *Water oxygen−oxygen rdfs for the UA model of neopentane in water, aqueous urea, aqueous TMAO, and mixed urea/TMAO solutions.*

Table 3A-7. Coordination Numbers for Atom Pairs Involved in Hydrogen Bonding[a]

system	atom pair	W-W	W-U	W-T	U-W	U-U	U-T	T-W	T-U
$S_{UA,1}$	O-H	0.93	—	—	—	—	—	—	—
	H-O	0.93	—	—	—	—	—	—	—
	total	3.72	—	—	—	—	—	—	—
$S_{UA,2}$	O-H	0.76	0.11	—	0.75	0.42	—	—	—
	H-O	0.76	0.19	—	0.43	0.42	—	—	—
	total	3.04	0.82	—	3.22	3.36	—	—	—
$S_{UA,3}$	O-H	0.89	—	—	—	—	—	1.30	—
	H-O	0.89	—	0.12	—	—	—	—	—
	total	3.56	—	0.24	—	—	—	2.60	—
$S_{UA,4}$	O-H	0.66	0.14	—	0.68	0.36	—	1.00	0.22
	H-O	0.66	0.19	0.11	0.48	0.36	0.09	—	—
	total	2.64	0.94	0.22	3.24	2.88	0.36	2.00	0.88

[a]W, U, and T refer to water, urea, and TMAO, respectively. Numbers are with respect to the first species and the total is calculated by taking into account the number of hydrogen atoms in water and urea.

the AA model, Regions I and II were chosen to be $3.2 - 4.2$ and $4.2 - 5.2$ Å, respectively; the same were $3.5 - 4.5$ and $4.5 - 5.5$ Å, respectively, for the UA model. The methods and the geometric criteria for hydrogen bond properties and dynamics calculations were identical to those described in **Chapter 2**.

The average number of water−water hydrogen bonds are presented in Table 3A-8 together with the energy and life-time of these bonds. From this table, we see that in the vicinity of the solute, the average number of water−water hydrogen bonds reduces in fraction as compared to that in the bulk region (Region III); however, the hydrogen bond becomes energetically more attractive near the solute. Osmolytes reduce number of water−water hydrogen bonds and, TMAO in particular, enhance their life-times. Although similar observations were made in the case of methane (**Chapter 2**), the number of hydrogen bonds broken near the neopentane surface is found to be higher than that of methane.

Table 3A-8. Water−Water Hydrogen Bond Properties and Dynamics[a]

model	system	n_{HB}^{I}	n_{HB}^{II}	n_{HB}^{III}	E_{HB}^{I}	E_{HB}^{II}	E_{HB}^{III}	τ_{HB}^{I}	τ_{HB}^{II}	τ_{HB}^{III}
UA	$S_{UA,1}$	3.41	3.59	3.74	-19.73	-19.74	-18.80	1.62	1.69	1.63
	$S_{UA,2}$	2.72	2.89	2.95	-19.85	-19.74	-18.85	1.76	1.78	1.68
	$S_{UA,3}$	3.03	3.20	3.46	-19.95	-20.17	-19.33	2.28	2.48	2.38
	$S_{UA,4}$	2.12	2.29	2.61	-19.35	-20.12	-19.38	2.59	2.68	2.68
AA	$S_{AA,1}$	3.44	3.63	3.71	-19.72	-19.74	-18.73	1.60	1.54	1.58
	$S_{AA,2}$	2.79	3.00	2.99	-19.93	-19.84	-18.81	1.88	1.83	1.75
	$S_{AA,3}$	3.06	3.19	3.37	-21.08	-20.27	-19.36	2.66	2.46	2.35
	$S_{AA,4}$	2.18	2.29	2.46	-20.88	-20.28	-19.75	2.76	2.77	2.67

[a] n_{HB}, E_{HB}, and τ_{HB} represent average number of water−water hydrogen bond, energy of the hydrogen bond (in kJ mol^{-1}), and the life-time (in ps), respectively. Regions I, II, and III are defined in the text.

Orientational Distributions. To see how the orientation of water molecules changes as we move away from the solute neopentane and the influences of osmolyte on this orientation, we calculated the distribution function of the angle formed (θ) between water dipole vector ($\hat{\mu}$) and the unit vector ($\hat{\mathbf{u}}$) pointing from the oxygen atom of water toward the center of the

neopentane molecule (see Figure 2A-9) considering three different regions (Regions I-III) of width 1 Å each (as defined above). In Figure 3A-7, we have presented the results of the normalized probability function P(cosθ) as a function of cosθ. In the vicinity of the solute, the probability function is nonuniform with the maximum value of P(cosθ) around cosθ=0. It means that the water dipoles are almost perpendicular to the line connecting the water oxygen to the neopentane center. The orientational distribution function in the vicinity of neopentane is relatively sharper than that of methane (**Chapter 2**), indicating influence of solute size on the distribution of water molecules. The orientational distribution function becomes flatter as we move away from the solute and the probability function is uniform in Region III, i.e., there is no preferred orientation of water molecules in the bulk phase as one would expect. The influence of osmolyte on water orientation is insignificant.

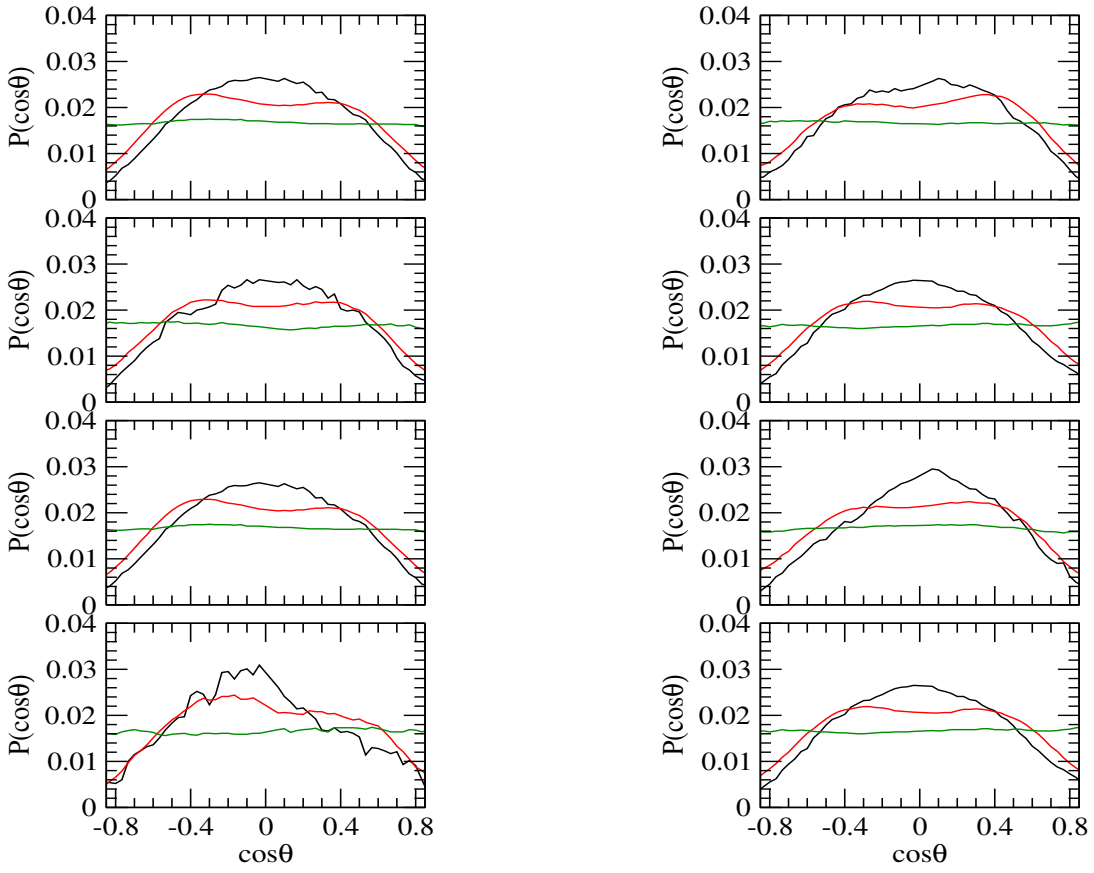

Figure 3A-7. *Orientational distribution of water for Regions I, II, and III in water, aqueous urea, aqueous TMAO, and mixed urea/TMAO solutions (from top to bottom, respectively). The left panel is for the UA model of neopentane and the right panel is for the AA model. Regions I, II, and III are defined in the text.*

■ SUMMARY AND CONCLUSIONS

Employing MD simulation technique, the solvation characteristics of neopentane and also the structure of the solution in the presence and absence of osmolytes were investigated. Two different models of neopentane were used: UA and AA. Significantly higher association tendency was observed for the AA model in aqueous solutions. However, there was not much difference in association propensity between methane and the UA model of neopentane. Both urea and TMAO interacted directly with neopentane, removing water molecules from the first solvation shell of neopentane; and we found preferential accumulation of these two osmolytes near the hydrophobic moiety. In the vicinity of neopentane, water molecules adopted the typical surface-parallel orientation, whereas side-on orientations of urea and TMAO were observed in that region. Urea dissolved aggregates of neopentane. On the other hand, TMAO was found to have negligible influence on aggregation of neopentane.

Investigation of water−water hydrogen bond properties in different spherical regions of a single neopentane molecule showed loss of hydrogen bonds between water molecules (in fraction) near neopentane. The hydrogen bonds, however, became attractive in the vicinity of the solute. In aqueous solutions of osmolyte, some of the water−water hydrogen bonds were replaced by osmolyte−water hydrogen bonds, and osmolytes, TMAO in particular, reduced relaxation of water−water hydrogen bonds.

From these results, we infer that urea interacts directly with large nonpolar groups comprising the protein and can dissolve protein hydrophobic assembly, causing protein denaturation. Direct interaction occurs also between TMAO and protein's hydrophobic residues, and it is unlikely that TMAO stabilizes proteins and counteracts urea-conferred protein denaturation by enhancing hydrophobic interaction.

Part B:

TMAO's Effect on Assembly of Neopentane at High Pressure

Overview: Employing MD simulation technique, solvation of neopentane is probed in aqueous solutions of increasing TMAO concentrations over a wide range of pressures relevant to protein denaturation. The concentrations of TMAO vary from 0 to 4 M and for each TMAO concentration, simulations are performed at five different pressures ranging from 1 bar to 8 kbar. Potentials of mean force are calculated and the relative stability of solvent-separated state over the associated state of hydrophobic solute are estimated. Results suggest that high pressure reduces association of neopentane. From computations of site−site rdf followed by analysis of coordination number, it is found that water molecules are tightly packed around the nonpolar particle at high pressure and the hydration number increases with increasing pressure. Neopentane interacts preferentially with TMAO over water and although hydration of neopentane reduces in the presence of this osmolyte, TMAO does not show any tendency to prevent the pressure-induced dispersion of neopentane moieties. Analysis of hydrogen bond properties and solvation characteristics of TMAO reveals that TMAO can form hydrogen bonds with water and prevent the pressure-induced crowding of water molecules.

■ INTRODUCTION

In **Chapter 2** of this thesis, we reviewed many studies that investigate the influence of pressure on hydration and association of methane molecules. Much less attention has been provided toward understanding pressure-modulated hydrophobicity of large solute. Ghosh *et al.* [99] performed MD simulations of large hydrophobic solutes ($\sim$ 35% larger in size compared to methane) in water at 1 bar and 8 kbar pressures. Significantly amplified effects of pressure on the PMF of larger solutes were observed in that study, although the qualitative picture remained similar to that observed for methane [99]. The long-lived aggregate of approximately 7-9 solutes (out of the 10 large hydrophobic solutes) that appear at 1 bar dissolved at 8 kbar pressure and at that extreme pressure, there existed only a tendency to form contact and solvent-separated pairs. No prior study on the effects of pressure on neopentane assembly has been reported either in pure water or in aqueous solutions of TMAO. Herein, we describe the solvation characteristics and solvent-mediated attraction of neopentane molecules in pure water and binary solutions of increasing TMAO concentrations over a wide range of pressures. We first examine TMAO's effect on the pressure-induced modifications of neopentane assembly. To get deeper insight of TMAO's mode of action, interaction of neopentane with the solution species is investigated by computing site−site rdfs, coordination numbers, and fractions of water and TMAO molecules in the vicinity of neopentane. The solvation characteristics of TMAO molecule at low and high pressures are also examined to cast light on the protein stabilizing action of TMAO. Finally, effects of pressure and TMAO on the hydration shell of neopentane are explored by computing water−water hydrogen bond properties and dynamics in different layers of a single neopentane molecule in the presence and absence of TMAO at different pressures.

The models and simulation details are briefly described in the next section. This is followed by a section whereof we discuss our results, and our conclusions are summarized in the last section.

■ MODELS AND SIMULATION METHOD

Classical MD simulations of neopentane were undertaken to probe the action of TMAO on pressure-induced modification of hydrophobic interaction. The concentration of TMAO in the systems simulated varied from 0 to 4 M and for each TMAO solution, simulations were carried out at 5 different hydrostatic pressures ranging from 1 bar to 8 kbar. Initially, the 0 M TMAO solution, denoted as $S_{np}0$, was constructed by inserting 10 neopentane molecules

in a simulation cell containing 490 water molecules. The water molecules were then replaced with TMAO (keeping total number of molecules fixed) to create three independent TMAO solutions with TMAO mole fractions of 0.03, 0.06, and 0.08 (denoted as $S_{np}2$, $S_{np}3$, and $S_{np}4$, respectively). Again, to examine water−water hydrogen bond properties and dynamics at discrete distances from the solute, 9 neopentane molecules were replaced by water molecules and hence, the simulation cell contained only one neopentane molecule in those systems.

In all of the simulations, the SPC/E model [111] was used for water, the AA model [196] was adopted for neopentane, and TMAO was described with a rigid version of model proposed by Kast *et al.* [113] All models employed were rigid and the interaction between atomic sites of two different molecules was expressed using Eq. 2.3. The values of the LJ parameters and the partial charges for water, TMAO, and neopentane were summarized in Tables 2A-2 and 3A-2.

The methods employed were identical to those described in **Chapter 2**.

■ RESULTS AND DISCUSSION

Neopentane−Neopentane Pair Potentials of Mean Force. Figure 3B-1 illustrates the neopentane−neopentane PMFs as obtained by using Eq. 2.4. Clearly, high pressure shifts the locations of the two minima (the CM and the SSM) and also of the barrier in the PMF toward shorter distances. The small inward shift of the CM can be attributed to the reduction in neopentane excluded volume, whereas much larger inward movement of the SSM and the barrier are due to changes in overall structure of the solvent. High pressure also reduces the well-depth of the CM and makes the barrier more pronounced. The magnitude of the gradient appearing at large solute separations decreases and the PMF value approaches to zero, indicating dispersion of neopentane at high pressure. We note that the inward movements of location of the CM, the SSM, and the barrier in the PMF profiles observed here are similar to those observed for methane (**Chapter 2**). On the other hand, the reduced well depth for the contact pair of neopentane at elevated pressure is in sharp contrast with that of methane. On increasing the pressure to 8 kbar, the relative stability of the contact configuration over the solvent separated state decreases by about 2.9 kJ mol^{-1}. The data presented in Figure 3B-1, on the other hand, do not provide any evidence for counteracting effect of TMAO against pressure-induced dissolution of neopentane molecules.

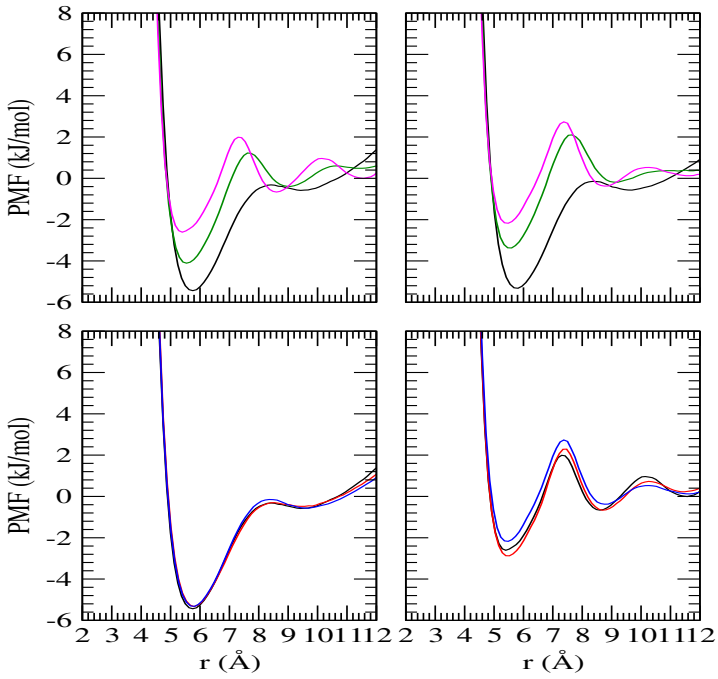

Figure 3B-1. *Neopentane−neopentane PMFs for systems $S_{np}0$ (left) and $S_{np}4$ (right) at 1, 4000, and 8000 bar pressures (top) and also at 1 (left) and 8000 (right) bar pressures for systems $S_{np}0$, $S_{np}2$, and $S_{np}4$ (bottom).*

Solvation of Neopentane. Figure 3B-2 displays rdfs that concern hydration of neopentane. As shown in Figure 3B-2, the rise in the neopentane−water rdf from zero does not change its position at elevated pressure. However, the water exclusion radius (the shortest distance at which $g(r) = 1$), the first and second peaks, and the first minimum show shifting to shorter distances. For example, water exclusion radius reduces from 4.6 to 4.2 and then to 4.0 Å as pressure increases from 1 through 4000 to 8000 bar. Significant variations in peak heights also occur at high pressure with the height of the first and second peaks increasing monotonically with pressure. These results indicate efficient packing of water molecules around the solute at high pressure. Table 3B-1 reveals pressure-induced enhancement of neopentane hydration number which is consistent with reduced clustering of neopentane at high pressure. We note that pressure-induced enhancement of water packing around the hydrophobic solute and consequent relative destabilization of hydrophobic contact was observed in case of methane as well (**Chapter 2**), and is in line with the notion

that nonpolar side-chains are more separated in a pressure-denatured structure than in the native one [9, 11, 198-202].

The height and location of the first peak remain almost unaffected on addition of TMAO (Figure 3B-2). Nonetheless, the coordination numbers suggest TMAO-induced removal of water molecules from the solvation shell of neopentane (Table 3B-1). Numbers given in parentheses in this table nullify the effect of reduced water number density and confirm neopentane dehydration in the presence of TMAO.

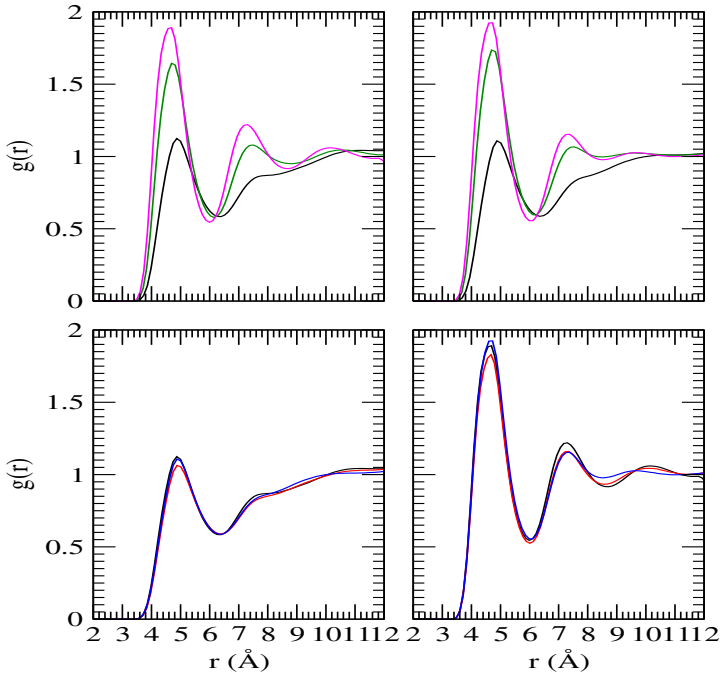

Figure 3B-2. *Site−site distribution functions involving neopentane and water (Ow) as a function of pressure (top) for systems $S_{np}0$ (left) and $S_{np}4$ (right) and also as a function of TMAO concentration (bottom) for 1 bar (left) and 8 kbar (right) pressures. Color codes are as in Figure 3B-1.*

Focusing on the interaction of TMAO with neopentane, we find that, as compared to that in neopentane−water rdf (Figure 3B-2), the first peak is stronger in neopentane-TMAO rdf (Figure 3B-3). This observation suggests that neopentane prefers to interact more with TMAO than with water. Also the first peak in neopentane−TMAO rdf increases with pressure and reduces with increasing TMAO concentration. The observation that TMAO is accumulated preferentially in the vicinity of neopentane is confirmed by the data in Figure 3B-4 that presents the time-averaged normalized fractions of water oxygen and TMAO nitrogen as a function of pressure as well as of TMAO concentration.

In Table 3B-1, we have presented the average number of TMAO molecules in the first solvation shell of neopentane. It can be seen easily that the number of TMAO molecules in the vicinity of neopentane increases with increasing TMAO concentration. The number also increases at high pressure, but the change is very small. This enhancement of TMAO molecules around neopentane is correlated with water exclusion from the neopentane surface.

Table 3B-1. Solvation Number for Neopentane[a]

system	P(MPa)	n_w	n_t	n_w/n_t
$S_{np}0$	0.1	20.2	—	—
	200	26.1	—	—
	400	26.1	—	—
	600	27.0	—	—
	800	28.8	—	—
$S_{np}2$	0.1	18.0(19.6)	1.6	11.25(31.67)
	200	24.1(25.3)	1.6	15.06(31.67)
	400	24.4(25.3)	1.8	13.56(31.67)
	600	24.2(26.2)	1.8	13.44(31.67)
	800	25.3(27.9)	1.8	14.06(31.67)
$S_{np}3$	0.1	16.0(19.0)	2.8	5.71(15.33)
	200	22.3(24.5)	2.7	8.26(15.33)
	400	22.1(24.5)	3.0	7.37(15.33)
	600	22.7(25.4)	3.3	6.88(15.33)
	800	23.7(27.0)	2.9	8.17(15.33)
$S_{np}4$	0.1	15.4	3.5	4.40(11.25)
	200	20.2(18.6)	3.8	5.32(11.25)
	400	21.1(24.0)	3.7	5.70(11.25)
	600	21.9(24.0)	3.8	5.76(11.25)
	800	22.5(26.5)	3.7	6.08(11.25)

[a] n_w and n_t, respectively, represent number of water and TMAO molecules in the first solvation shell of neopentane. Numbers in parentheses in the fifth column are the bulk ratios.

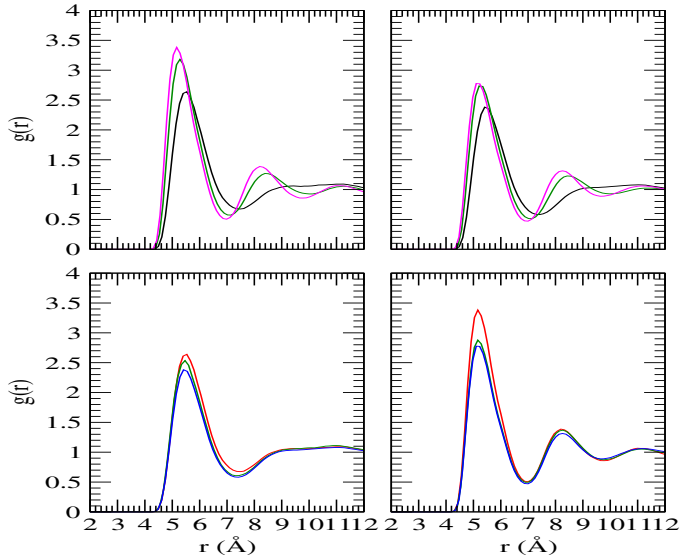

Figure 3B-3. *Site−site distribution functions involving neopentane and TMAO (Nt) for systems* $S_{np}2$ *(left) and* $S_{np}4$ *(right) at 1, 4000, and 8000 bar pressures (top) and also at 1 (left) and 8000 (right) bar pressures for systems* $S_{np}2$*,* $S_{np}3$*, and* $S_{np}4$ *(bottom).*

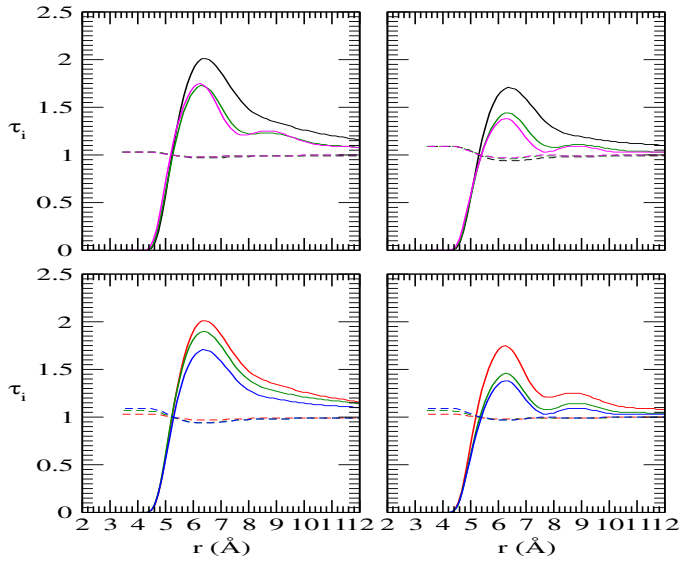

Figure 3B-4. *Time-averaged normalized fractions of water (dashed) and TMAO (solid) central atoms as a function of pressure (top) for systems* $S_{np}2$ *(left) and* $S_{np}4$ *(right) and also as a function of TMAO concentration (bottom) for 1 bar (left) and 8 kbar (right) pressures. Color codes are as in Figure 3B-3.*

Solvation of TMAO. Site−site distribution functions that describe solvation of TMAO atomic sites are shown in Figure 3B-5. Let us first consider the hydration of TMAO at 1 bar. The typical surface-parallel orientation of water molecules in the vicinity of hydrophobic group can be seen in $Ct - Ow$ and $Ct - Hw$ rdf profiles. There arises a tail of hydrogen density at shorter separation and the region of maximum density is similar for both oxygen and hydrogen of water. Note that the first peak in $Ct - Hw$ rdf is located at a slightly longer distance as compared to that in $Ct - Ow$ rdf, which is different from that observed in cases of methane (**Chapter 2**) and neopentane. This is, however, consistent with the results observed previously in simulations of TMAO solution at 1 bar [71]. On the other hand, the orientational characteristics of water molecules (preferred water hydrogen over water oxygen) near the TMAO oxygen are very similar to that near a negative ion or near a water oxygen in bulk water. The strong first peaks in $Ot - Ow$ and $Ot - Hw$ rdfs demonstrate strong affinity of TMAO for water coming through TMAO−water hydrogen bonding. The height of the first peak for $Ot - Hw$ rdf is much higher than that for $Ow - Hw$ rdf (Figure 3B-6). This immediately implies that

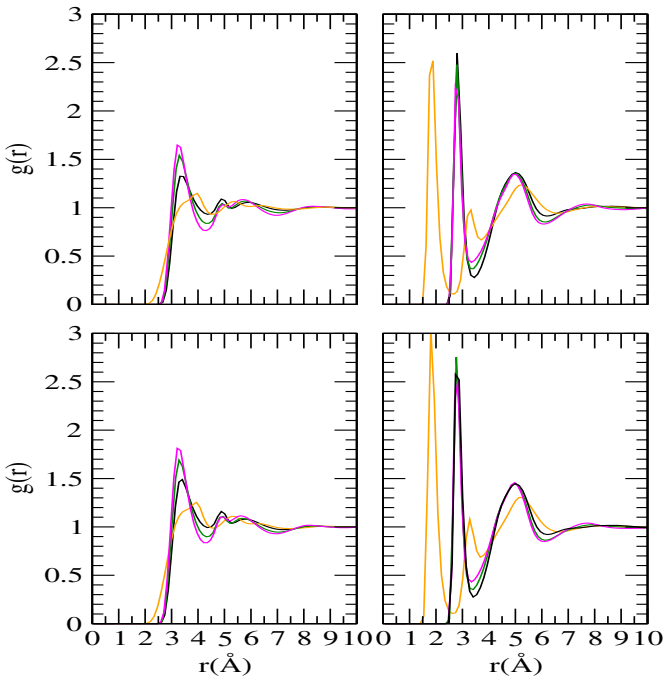

Figure 3B-5. *TMAO carbon−water oxygen (left) and TMAO oxygen−water oxygen (right) site−site rdfs for systems $S_{np}2$ (top) and $S_{np}4$ (bottom) at 1, 4000, and 8000 bar pressures. Orange colored lines are for TMAO carbon−water hydrogen (left) and TMAO oxygen−water hydrogen (right) rdf at 1 bar.*

water has higher tendency to be hydrogen bonded to a TMAO molecule than to a second water molecule. The next chapter provides additional evidences for much stronger hydrogen bonds between TMAO and water than those between water molecules.

Integration of the rdfs gives 7.1 and 2.7 water molecules in the first hydration shell of TMAO methyl group and oxygen atom, respectively, for the system $S_{np}4$ at 1 bar. These numbers are in broad concordance with previous studies [78, 203, 204]. Addition of these numbers results in a molecular hydration number of 24.0. Considering the fact that some of these water molecules are shared between different groups, the hydration number per TMAO molecule agrees well with Meersman *et al.* [204] Infrared spectroscopy study, on the other hand, showed only about 8.5 water molecules that are affected by TMAO [205]. It is not difficult to assume that only those water molecules will be affected that are in the close proximity of a TMAO molecule. To get the number of water molecules that are likely to be affected by a TMAO molecule, we then calculated the hydration number by integrating the corresponding rdf only to the first maximum (instead of using the first hydration shell). The numbers obtained by this method, for the system $S_{np}4$ at 1 bar, are 2.2 and 0.9 for TMAO methyl group and oxygen atom, respectively, yielding an average number of 7.5 water molecules in the vicinity of a TMAO molecule. This is in line with the experimental observation.

Water distribution around TMAO methyl group changes only slightly with increasing TMAO concentration. On the other hand, while the height of the first peak increases monotonically with pressure, the first minimum shows a downward movement. Additionally, the first peak and minimum shift to shorter distances at high pressure. These observations are very similar to those observed in case of neopentane hydration and reflect enhanced packing of water molecules around methyl groups of TMAO at high pressure.

Behavior of water in the vicinity of TMAO oxygen at high pressure is quite different from that in the vicinity of TMAO methyl groups. The first peak in $Ot - Ow$ rdf is not affected much at high pressure, but the first minimum shows an inward and upward movement, revealing a tendency of part of the hydration water to move toward large-r side of the first shell under high pressure conditions. To get insight into the nature of hydrogen bonding, we calculated the number of hydrogen bonded water molecules to TMAO oxygen by integrating the rdf to the first minimum. On average, about 3 water molecules are found that donate hydrogen atoms to TMAO oxygen, which is consistent with the notion that TMAO oxygen is hydrated by 2 to 3 water molecule [71, 72, 76, 78, 125, 204, 206]. Negligible enhancement in the number of hydrogen bonded water molecules is observed

at high pressure. On the other hand, although the number reduces per TMAO oxygen with increasing TMAO concentration, the total number of TMAO−water hydrogen bonds increases. For example, the total number of $Ow-Hw\cdots Ot$ hydrogen bonds for system $S_{np}2$ at 1 bar and 8 kbar are 41.40 (2.76 × 15) and 42.90 (2.86 × 15), respectively; whereas the same for system $S_{np}4$ at 1 bar and 8 kbar are 104.00 (2.60 × 40) and 110.40 (2.76 × 40), respectively. The examination of solvation characteristics of TMAO thus suggests that, TMAO is well solvated by water molecules and the number of water molecules required to solvate all TMAO molecules present in the system increases with increasing TMAO contents.

Water Structural and Dynamical Properties. An examination of possible effects of pressure and TMAO on hydrogen bonding network of water (Figure 3B-6) shows that the $Ow-Hw$ profiles are affected only slightly by pressure. From integration of the rdf to

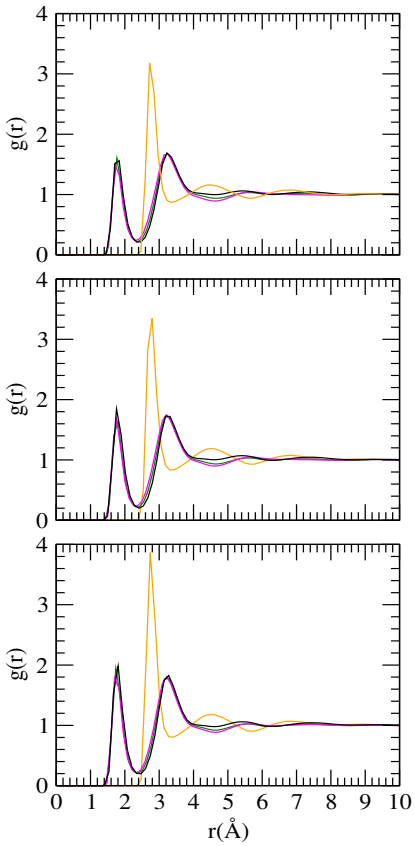

Figure 3B-6. *Water oxygen−water hydrogen site−site distribution functions for systems $S_{np}0$, $S_{np}2$, and $S_{np}4$ (from top to bottom, respectively) at 1, 4000, and 8000 bar pressures. Orange colored lines are for water oxygen−water oxygen rdf at 1 bar.*

the first minimum, it appears that each water molecule can form about 4 hydrogen bonds with identical species. Pressure does not affect the number of water−water hydrogen bonds, whereas TMAO reduces these hydrogen bonds by forming itself hydrogen bonds with water. Further insight into the nature of water−water hydrogen bonding interactions in aqueous solutions of TMAO as a function of TMAO concentration and pressure can be obtained by investigating the properties and dynamics of these hydrogen bonds in different layers around the hydrophobic solute. In an attempt to this, we considered two regions from the vicinity of the neopentane surface (Region I: 3.0−4.0 Å and Region II: 4.0−5.0 Å) and a third region was considered at a relatively larger distance from the solute assuming bulk portion of the simulation cell (Region III: 10.0−11.0 Å). The geometric criteria and the methods for hydrogen bond properties and dynamics calculations were identical to those described in **Chapter 2**.

In Table 3B-2, we have presented the average number of water−water hydrogen bonds per water molecule together with hydrogen bond life-time and energy of these bonds. We note that, at 1 bar pressure in pure water, the number of hydrogen bonded water molecules in the bulk region (Region III) is 3.78, which is in concordance with that obtained (about 3.45) by Huang *et al.* [152], taking into account the use of different water models (SPC/E vs SPC) and hydrogen bond criteria (45^o vs 30^o). Three points, visible from Table 3B-2, are: (a) number of water−water hydrogen bonds reduces in fraction in the vicinity of the solute as compared to the bulk region, (b) TMAO reduces the average number of water−water hydrogen bonds and makes hydrogen bonds slightly attractive, and (c) pressure enhances the average number of water−water hydrogen bonds and reduces water−water hydrogen bond energy. Pressure-induced reduction and TMAO-induced enhancement in water−water hydrogen bond life-time can also be seen from Table 3B-2. This modification of life-expectancy of water−water hydrogen bond is further reflected in the decay of continuous hydrogen bond time correlation function, $S_{HB}(t)$, with time, as shown in Figure 3B-7. This figure shows that the hydrogen bond decays slightly faster at high pressure and the decay is much slower for highly concentrated TMAO solution. These observations are supported by various other lines of research. TMAO-induced enhancement of water−water hydrogen bond life-time was reported in previous MD simulations [67, 68, 73]. Based on MD simulations on TMAO−water clusters, Wei *et al.* [32] suggested that TMAO strengthens the hydrogen bonds between water molecules and slows down the orientational relaxation of water significantly. They predicted that the methyl groups on TMAO are responsible for these effects. In their infra-red pump probe experiment studies

of water−TMAO mixture, Rezus and Bakker [81, 83] showed that the orientational mobility of water molecules near to TMAO methyl group is greatly reduced compared to bulk water molecules. Another experimental study suggested that the rotational dynamics of water molecules are slowed down in the presence of TMAO and as the concentration increases, the dynamics are further decelerated [78].

Table 3B-2. Water−Water Hydrogen Bond Properties and Dynamics[a]

system	P(MPa)	n_{HB}^{I}	n_{HB}^{II}	n_{HB}^{III}	E_{HB}^{I}	E_{HB}^{II}	E_{HB}^{III}	τ_{HB}^{I}	τ_{HB}^{II}	τ_{HB}^{III}
$S_{np}0$	0.1	3.37	3.63	3.78	-20.13	-19.51	-18.73	1.55	1.46	1.50
	200	3.56	3.76	3.88	-20.05	-19.41	-18.28	1.45	1.38	1.35
	400	3.67	3.87	3.96	-19.64	-18.92	-18.02	1.25	1.29	1.37
	600	3.72	3.94	4.02	-19.41	-18.85	-17.82	1.23	1.22	1.29
	800	3.82	3.98	4.06	-19.26	-18.58	-17.53	1.21	1.16	1.26
$S_{np}2$	0.1	3.25	3.48	3.65	-20.22	-19.91	-18.85	1.77	1.71	1.74
	200	3.26	3.48	3.68	-20.05	-19.96	-18.77	1.75	1.50	1.74
	400	3.47	3.65	3.79	-19.81	-19.39	-18.20	1.59	1.47	1.61
	600	3.57	3.73	3.84	-19.65	-19.20	-18.04	1.55	1.50	1.38
	800	3.52	3.69	3.87	-19.59	-19.09	-17.89	1.42	1.40	1.48
$S_{np}3$	0.1	3.12	3.34	3.49	-20.25	-19.90	-19.34	2.24	2.19	2.07
	200	3.12	3.33	3.59	-20.30	-20.05	-18.86	1.94	1.91	2.17
	400	3.34	3.48	3.63	-20.02	-19.77	-18.46	1.97	1.86	1.80
	600	3.42	3.55	3.68	-20.10	-19.50	-18.24	1.97	1.93	1.70
	800	3.39	3.51	3.71	-19.94	-19.55	-18.05	1.92	1.86	1.68
$S_{np}4$	0.1	2.92	3.17	3.44	-20.65	-20.34	-19.42	2.26	2.31	2.29
	200	3.10	3.20	3.40	-20.48	-19.92	-19.18	2.32	2.33	2.33
	400	3.27	3.44	3.55	-19.79	-19.61	-18.67	2.23	2.16	2.21
	600	3.27	3.41	3.52	-20.25	-19.73	-18.69	1.99	2.14	2.23
	800	3.29	3.43	3.62	-20.16	-19.55	-18.25	1.94	2.04	2.15

[a] n_{HB}, E_{HB}, and τ_{HB} represent average number, energy (in kJ mol^{-1}), and life-time (in ps) of water−water hydrogen bond, respectively. Regions I, II, and III are defined in the text.

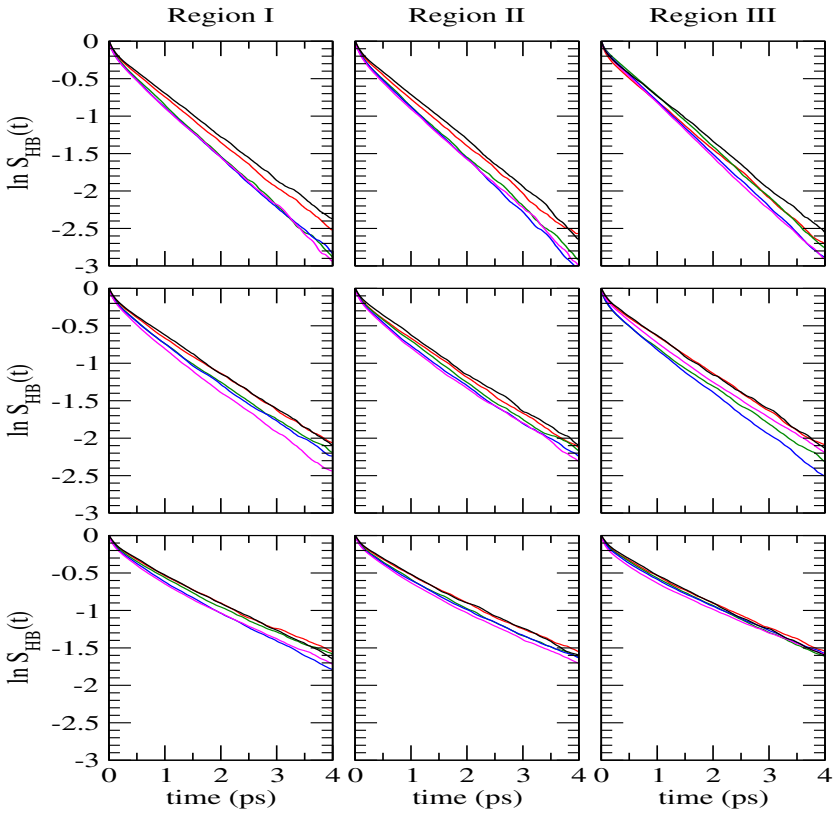

Figure 3B-7. *Time dependence of continuous water−water hydrogen bond correlation function as a function of pressure in different spherical shells of neopentane for systems $S_{np}0$, $S_{np}2$, and $S_{np}4$ (from top to bottom, respectively) at 1, 2000, 4000, 6000, and 8000 bar pressures. Regions I, II, and III are defined in the text.*

In Figure 3B-8, we have shown the fraction of water molecules that engage in n number of hydrogen bonds with identical species for all of the simulated systems. At a particular pressure, the perturbation in hydrogen bonding network of water molecules created by the relatively large neopentane molecule can be seen from the enhancement in the fraction of 2- and 3-coordinated water molecules while reducing the fraction of 4- and 5-coordinated water molecules in the vicinity of this hydrophobic solute (Regions I and II) as compared to the bulk region (Region III). This clearly suggests that water loses some of its identical nearest neighbors to accommodate the hydrophobic solute. Enhancement of pressure increases the fraction of higher coordinated (4 and 5) water molecules and reduces the fraction of lower coordinated (2 and 3) water molecules, indicating water crowding at high pressure. Note that the pressure-induced water crowding at high pressure was suggested to be a possible reason for water penetration (which relaxes wa-

ter crowding in the bulk) into the protein interior, causing protein denaturation [17-19]. We also find TMAO-induced reduction in the number of identical nearest neighbors of water molecules. The loss in the number of higher coordinated water molecules is correlated with the solvation of large TMAO molecules. The significant enhancement in the number of 2- and 3-coordinated water molecules and reduction in the number of 4- and 5-coordinated water molecules for the highest TMAO concentration investigated here provides corroborative evidence for our observation (from coordination number) that, the number of water molecules that solvate TMAO increases with increasing concentration of TMAO.

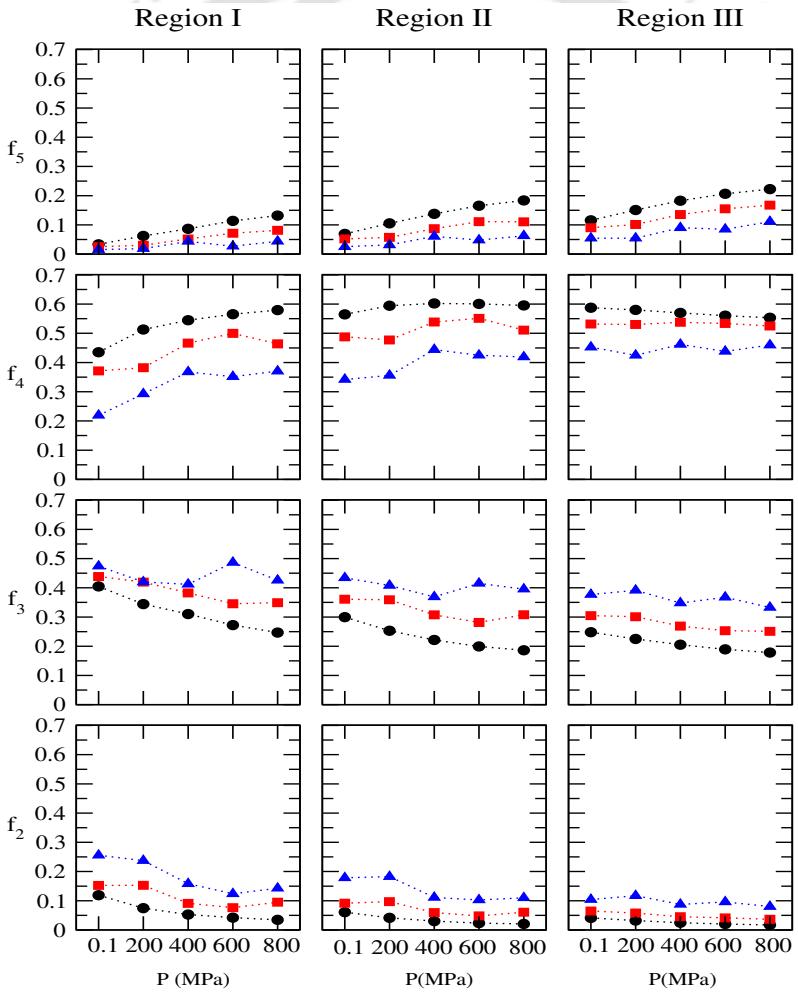

Figure 3B-8. *The fraction of water molecules that engage in n number of hydrogen bonds with identical species in different spherical shells of neopentane for systems* $S_{np}0$, $S_{np}2$, *and* $S_{np}4$. *Regions I, II, and III are defined in the text.*

■ SUMMARY AND CONCLUSIONS

We employed the MD simulation technique to investigate the effects of increasing TMAO concentration on the pressure-induced modification of neopentane aggregation. From PMF calculations, we found high propensity of neopentane for self-aggregation in pure water at 1 bar pressure. The comparatively large configurational volume of solvent-separated state generally prevents such kind of assembly of small solutes like methane. Dispersion of neopentane molecules were observed at high pressure. The effects of pressure on relative dispersion of hydrophobic solute were found to be amplified significantly for the larger solute. Supporting the notion that nonpolar side-chains are separated by water molecules at high pressure [7, 99, 138-141], our simulation results showed enhanced hydration of neopentane molecules at high pressure. Pressure-induced significant compression of neopentane hydration shell was also observed.

From calculations of water−water hydrogen bond properties and dynamics, we found water molecules losing some of its identical neighbors near the hydrophobic solute surface; the number of broken hydrogen bonds was higher than that in the case of smaller solute methane. It reveals that although a small solute such as methane can be accommodated in the water cavities with negligible disruption of hydrogen bonding network of water, the same is not possible for a relatively large solute. For water molecules, number of hydrogen bonded identical neighbors enhanced with pressure, indicating pressure-induced water crowding. This water crowding will definitely cause an entropic loss in the system. Then if we consider only the entropic part of free energy change, the pressure-induced relative stabilization of the solvent-separated state of neopentane as compared to its associated state can be interpreted simply as follows. As expected, at 1 atm, the entropic gain drives the association of neopentane in the system. With increasing pressure, water crowding increases thereby creating an entropic loss. To minimize the loss, water molecules show a tendency to occupy the space between two neopentane molecules. Because the movement of penetrating water molecules are also restricted near the solute surface, an entropic loss is expected in the vicinity of the solute. But, the entropic gain arising from the relaxation in movement of bulk water molecules can overcome this penalty and overall, the solute separation gives an entropic profit to the system. Here we note that the dominating contribution of translational entropy gain from relaxation of water molecules far away from the protein surface in overall entropic gain in the system during pressure denaturation is reported in the literature [17].

TMAO formed considerable number of hydrogen bonds with water (more than 2 hydrogen bonds per TMAO molecule). The number of identical nearest neighbor water molecules reduced in aqueous TMAO solution, but the hydrogen bonding network of water became stronger as was evident from stronger water−water hydrogen bond energies and enhancement of water−water hydrogen bond life-times. On the face of TMAO's direct interaction with water molecules and its water structure enhancing ability, we can expect TMAO to reduce the pressure-induced enhancement of hydrophobic hydration. Indeed, it was reflected in our coordination number analysis showing neopentane dehydration in aqueous solution of TMAO. TMAO, on the other hand, did not improve assembly of neopentane. This clearly indicates a role of direct interaction between neopentane and TMAO in neopentane dehydration.

Combining the results of this study with those obtained in **Chapter 2**, it is reasonable to conclude accumulation of TMAO near the hydrophobic side-chains of proteins both at low and high pressures in the presence or absence of urea. TMAO's accumulation reduces number of water molecules near the protein hydrophobic surface, but it does not have much affect on hydrophobic interaction and TMAO seems to be neutral toward association of protein hydrophobic groups. In all likelihood, TMAO exerts its protein stabilizing effect via the protein backbone. In the chapter that follows, we shall treat this side of TMAO's effect.

Chapter 4

Solvation of Protein Backbone

"The major factor which opposes and overrides the side chain preference for denaturation and results in the stabilization of proteins observed in osmolytes is the highly unfavorable exposure of polypeptide backbone on unfolding. ....The prevalence of the unfavorable transfer free energy of the peptide backbone, and the fact that the peptide backbone unit is the most numerous group in a protein, makes it an extremely important factor in influencing the character of protein conformations existing in both stabilizing and destabilizing solvents."

– Y. Liu and D. W. Bolen *Biochemistry* **34**, 12884 (1995)

The previous two chapters of the thesis dealt with hydrophobicity of hydrocarbons of different sizes: methane (**Chapter 2**) and neopentane (**Chapter 3**). Protein stability is, however, governed not only by hydrophobic interactions, but also by interactions like hydrogen bonding. A substantial part of the foundation of our present day understanding of biological structure and function is constructed by the wealth of conceptual ideas derived from the transfer free energy considerations, from which the importance of protein backbone solvation in governing the protein folding process has become apparent [54, 64, 69, 207-210]. In fact, the protein backbone was found to play the dominating role in determining the extent of protein (de)stabilization by osmolytes, with the side-chains playing only a minor role, and consequently, it was concluded that the osmolytes exert their effect on protein stability predominantly via the protein backbone [54, 64, 208, 209]. So there is a natural demand of investigation of backbone solvation in aqueous solutions.

In response to the demand, in this chapter, we turn our attention to backbone solvation using NMA as model of protein backbone. The solute NMA is the smallest amide that contains a single peptide group ($O = C - N - H$) terminated by methyl moieties on the carbonyl carbon and on the amide nitrogen and hence holds special status as a minimal model of the protein backbone with the advantage of being small enough to be accessible by both current experimental and computational techniques. In the work described in this chapter, we have used dilute NMA solutions to provide a sufficient number of NMA solvation sites for solution species avoiding NMA−NMA hydrogen bonds as much as possible. In other words, the systems considered here have negligible number of NMA−NMA hydrogen bonds and represent typical solvent-exposed states of proteins where protein backbone can freely interact with the surrounding solution species.

As before, the chapter is organized into two parts. Solvation characteristics of NMA in aqueous solutions of urea and TMAO are explored in Part A, and we discuss TMAO's effects on NMA solvation under high pressure conditions in Part B.

Part A:

Amide Solvation in Water and Aqueous Solutions of Urea and TMAO

Overview: To shed light on the solvation characteristics of protein backbone in the presence of osmolytes urea and TMAO, we have investigated here various structural, energetic, and dynamical properties of NMA solutions in binary and ternary solutions of urea and TMAO by employing the MD computer simulation technique. Analysis of solvation characteristics reveals dehydration of NMA and reduction in hydrogen bond number between NMA oxygen and water upon addition of TMAO. The effect of TMAO on NMA−urea hydrogen bonding interaction is found to be insignificant. Because TMAO cannot donate its hydrogen to NMA oxygen, total number of hydrogen bonds formed by NMA oxygen with solution species decreases in the presence of TMAO. In solution, TMAO is found to interact strongly with water and urea. Solvation of TMAO makes water hydrogen bonding network relatively stronger and also reduces relaxation of urea−water hydrogen bonds. Implications of these results toward osmolyte's influence on backbone solvation are discussed.

■ INTRODUCTION

Because of the simplicity as a model of the peptide linkage with its locally similar internal degrees of freedom and intermolecular bonding to those of polypeptide segments, the molecule NMA has been the subject of extensive experimental and theoretical investigations. The pure substance has been found to form interpeptide hydrogen bonds (known for stabilizing polypeptide secondary structures) [211], with solvent altering the strengths of these bonds [212]. In aqueous solution, NMA can act both as donor and acceptor, as revealed by UV Raman studies [213-216] and normal coordinates analysis [217]. Water hydrogen bonding to the carbonyl oxygen has been reported to be stronger than that of amide hydrogen [213-219]. Combining FT-IR spectroscopy with density functional theory (DFT) calculations for various solute concentrations of NMA in a water saturated solution of carbon tetrachloride, Köddermann and Ludwig [218] showed that the peptide−peptide interactions are stronger than the peptide−water interactions. On the other hand, approximately isoenergetic amide−amide and amide−water interactions were indicated in a separate study [220].

While the majority of work focused on the hydration of NMA in NMA−water mixtures providing useful information about backbone hydration, much less is known about the effects of co-solutes on this hydration. In 2010, Wei *et al.* [32] presented an analysis of the effects of three different co-solutes, two denaturants, urea and tetramethylurea (TMU), and one protectant, TMAO, on the hydration of NMA molecules on the basis of classical MD simulations. Their study showed that TMAO weakened the interaction between water and the carbonyl group, whereas both urea and TMU enhanced the same, the effects being in perfect accordance with their (co-solutes') effects on water−water interactions. The hydration of NH group was found to be weaker as compared to the CO group in pure water as well as in the presence of co-solute [32]. The authors did not address direct interactions between NMA and co-solute, and suggested TMAO- and TMU-induced enhancement of water−NH interaction a result of introduction to the system extra good proton acceptors (the CO group of TMU and the NO group of TMAO) without changing the proton donors, recruiting NH group as the proton donors [32].

To get better idea of backbone solvation, we investigate herein solvation characteristics of NMA in binary and ternary solutions of urea and TMAO. Various structural, energetic, and dynamical properties that describe NMA solvation are examined first. We then study the solvation of TMAO by water and urea with an attempt to dissect the

counteracting mechanism.

What follows in this part are brief description of the models and simulation method, discussion of the results obtained, and finally, our concluding remarks.

■ MODELS AND SIMULATION METHOD

We carried out classical MD simulations of NMA in pure water as well as in binary and ternary solutions of urea and TMAO. Twenty NMA molecules (mole fraction of 0.04) were used in all of the simulated systems. An overview of simulations is presented in Table 4A-1. Note that the total number of molecules was fixed at 500 in all cases and osmolyte solutions were constructed by replacing water molecules with osmolyte. We used the SPC/E model [111] for water, and described TMAO and NMA with rigid version of models proposed by

Table 4A-1. Overview of Simulations[a]

system	V(nm^3)	Ns	Nw	Nt	Nu	Mu	Mt
NW	16.77	20	480	0	0	0	0
NU	20.92	20	380	0	100	7.94	0
NT	19.65	20	440	40	0	0	3.38
NUT	23.69	20	340	40	100	7.01	2.80

[a]V, N, and M represent box volume, number of molecules, and molar concentration, respectively. s, w, u, and t, respectively, refer to solute (NMA), water, urea, and TMAO.

Kast *et al.* [113] and Jorgensen and Swenson [221], respectively. The so-called DKJ model [112] was adopted for urea. The interaction between atomic sites of two different molecules was expressed using Eq. 2.3. The values of the LJ parameters and the partial charges for urea, TMAO, and water were summarized in Table 2A-2, and those for NMA are tabulated in Table 4A-2.

For the details of the methods employed, one can go through **Chapter 2**. In brief, MD simulations were performed at 298 K in a cubic box, initially, in the NPT ensemble to obtain the average volume of the simulation box corresponding to the desired pressure, and then in the NVT ensemble with the so obtained box volume. After equilibration, production runs were carried out for 10 ns.

Table 4A-2. Lennard-Jones Parameters and Charges for NMA[a]

atom type	σ (Å)	ϵ (kJ mol^{-1})	charge (e)
C	3.75	0.439	+0.50
O	2.96	0.878	−0.50
N	3.25	0.711	−0.57
H	0.0	0.0	+0.37
$Me_1(CH_3-C)$	3.91	0.669	0.0
$Me_2(CH_3-N)$	3.80	0.711	+0.20

[a] e is the elementary charge.

■ RESULTS AND DISCUSSION

Interaction of NMA with Solution Species. As a part of investigation of NMA interactions with the solution constituents, we first computed site−site rdfs between NMA and solution species. Selected rdfs that reflect these interactions are shown in Figures 4A-1−4A-3.

Figure 4A-1 displays rdfs involving water oxygen (Ow) and different atomic sites comprising NMA. The hydration pattern of the carbonyl methyl group (Me_1) in pure water at 1 bar exhibits surface parallel orientation of water molecules around this hydrophobic group. It is adequately described by the site−site Me_1-Ow and Me_1-Hw rdf profiles with first peaks at similar positions. This behavior of water molecule is typical of hydrophobic hydration. As depicted in Figure 4A-1, the water distribution around Me_1 group is not as defined as that around a methane molecule (**Chapter 2**). This perturbation of water structure around NMA hydrophobic surface is supported by the findings that the solvent density around a methyl group in ethane is somewhat less layered than the solvent density around a methane molecule and also that water peaks are narrower and sharper for spherical molecules (methane, iso-butane, neopentane) than those for nonspherical molecules (ethane, propane, n-butane) [106, 222].

The second methyl group in NMA (Me_2) exhibits similar hydration characteristics (Figure 4A-1). However, the water distribution is slightly better defined in the vicinity of this group as revealed by an increase in first peak height and an inward movement of the first minimum in Me_2-Ow rdf.

The carbonyl oxygen and the amide hydrogen in NMA are expected to participate in hydrogen bonding interaction with water. This particular interaction, which should lead to different orientational behavior of water molecules near the carbonyl oxygen and amide hydrogen, is demonstrated in rdf profiles of NMA oxygen and hydrogen atoms (Figure 4A-1). In particular, for pure water, the contact peaks in $O-Hw$ and $O-Ow$ rdf profiles, which characterize the first neighbor, appear at about 1.8 and 2.8 Å, respectively, reflecting formation of hydrogen bond between carbonyl oxygen and water. On the contrary, as reflected in the peak positions (Ow followed by Hw), water oxygen is preferred near the amide hydrogen and water oxygen accept this amide hydrogen in NMA−water hydrogen bonding interaction (the first peak appears at the characteristic location of hydrogen bond formation).

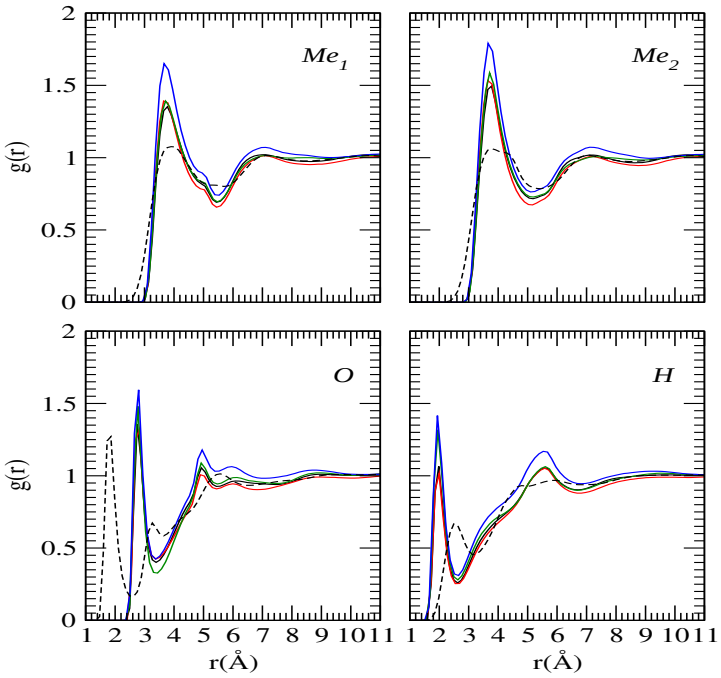

Figure 4A-1. *NMA−water oxygen (Ow) site−site distribution functions in water, aqueous urea, aqueous TMAO, and mixed urea/TMAO solutions. The dashed line is for water hydrogen (Hw) in pure water.*

Considering the effects of urea and TMAO alone (systems NU and NT), we see that urea has little effect on distribution of water in the vicinity of NMA atomic sites (Figure 4A-1). NMA−water rdfs show only slight awareness also of the presence of TMAO, except for the $H-Ow$ rdf in which the peak magnitude increases on addition of TMAO. In contrast to these, for the system containing both urea and TMAO, there is noticeable rise of water density around NMA atomic sites.

NMA−urea site−site rdfs are shown in Figure 4A-2. Note that the orientation of urea in the vicinity of the two hydrophobic methyl groups (Me_1 and Me_2) is similar to that observed in cases of methane (**Chapter 2**) and neopentane (**Chapter 3**). The Nu and Ou rdf profiles contain first peak at similar positions, indicating that there is no preference for urea oxygen or nitrogen near these hydrophobic groups. The location and height of the first peak in these rdfs also suggest direct interaction of urea with NMA methyl groups. Again, as expected from a hydrogen bonding perspective between urea and NMA, different orientational behaviors of urea molecules are observed near the carbonyl oxygen and amide

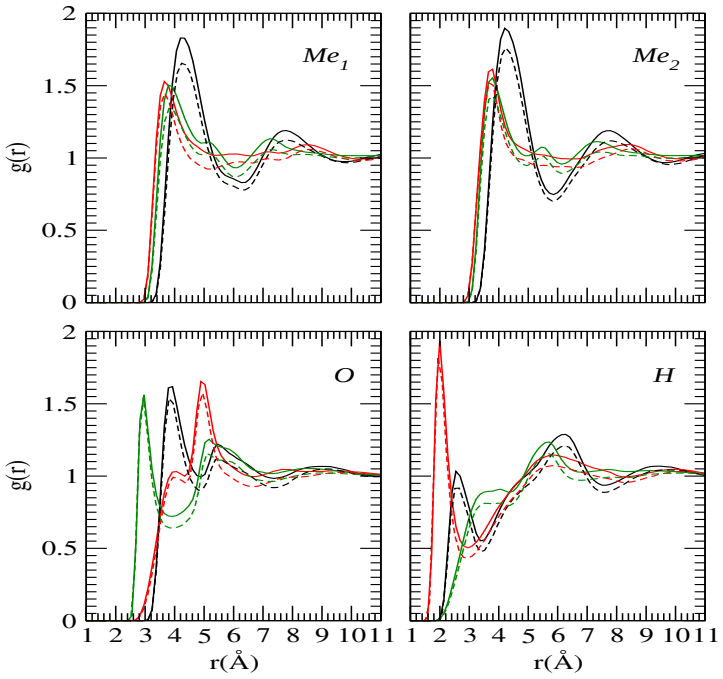

Figure 4A-2. *NMA−urea site−site distribution functions in aqueous urea (solid) and mixed urea/TMAO (dashed) solutions. Black, red, and green lines are for urea carbon (Cu), oxygen (Ou), and nitrogen (Nu), respectively.*

hydrogen in NMA. In particular, the peak positions (Nu followed by Cu followed by Ou) reflect the preference of urea nitrogen near the NMA oxygen. On the contrary, urea oxygen is preferred near the amide hydrogen and urea oxygen accepts this amide hydrogen in NMA−urea hydrogen bonding interaction. From Figure 4A-2, we see that the urea density reduces slightly upon addition of TMAO.

Figure 4A-3 exhibits solvation of NMA atomic sites by TMAO. A side-on orientation of TMAO near the NMA hydrophobic sites, as observed previously in cases of methane

(**Chapter 2**) and neopentane (**Chapter 3**), can be suggested immediately from the peak positions. The rdf profiles indicate a direct interaction between methyl groups in NMA and TMAO. Moreover, as in the case of urea, the amide hydrogen in NMA shows a significant preference for TMAO oxygen. In the vicinity of carbonyl oxygen, a preference of TMAO methyl group can be seen from Figure 4A-3. It is, however, necessary to mention that hydrogen bonding interaction between TMAO methyl hydrogen and NMA oxygen is unlikely, and although TMAO forms hydrogen bonds with NMA hydrogen (see $H - Ot$ rdf), the small first peak in $H - Nt$ rdf suggests weak solvation of amide group by TMAO. In the center of the first solvation shell of NMA hydrogen, density of TMAO is about 0.7 times the bulk density. Slightly weaker NMA−TMAO peaks are observed in urea/TMAO mixture.

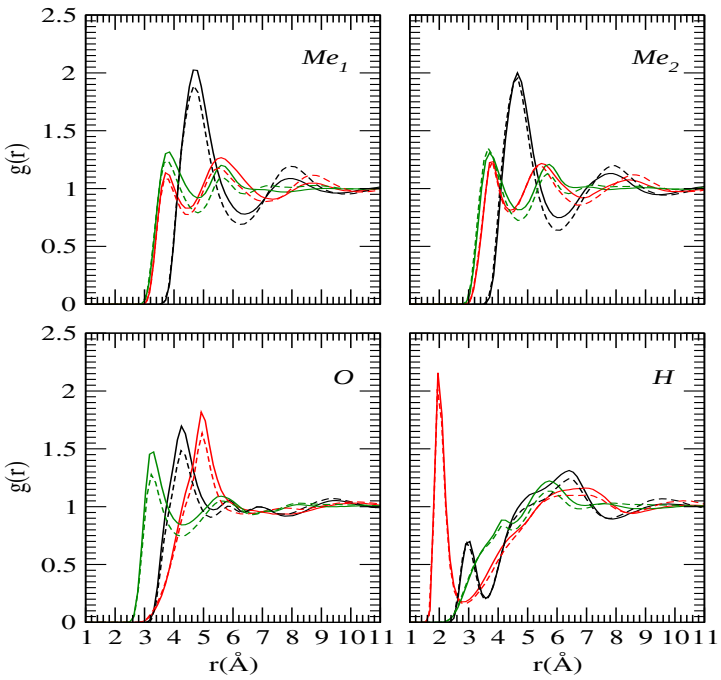

Figure 4A-3. *NMA−TMAO site−site distribution functions in binary (solid) and ternary (dashed) solutions of TMAO. Black, red, and green lines are for TMAO nitrogen (Nt), oxygen (Ot), and carbon (Ct), respectively.*

Further insight into the solvation of NMA was obtained by computing the average number of water and osmolyte molecules (central atom only) around the NMA atomic sites. The average number of molecules was calculated from the corresponding rdf using Eq. 2.6. The running coordination numbers for different atomic sites in NMA are shown in Figure 4A-4. Because urea and TMAO are significantly larger in size than water, exclusion

of these two osmolytes from a certain volume shell around the atomic sites of NMA is expected for purely geometric reasons, and this is reflected in larger radii of exclusion for these two osmolytes. The relatively closer approach of urea as compared to TMAO can be interpreted as better contact of NMA with urea than with TMAO. The point that also emerges from Figure 4A-4 is the replacement of a large number of water molecules in the solvation shell of each NMA atomic site by osmolyte. The total number of water

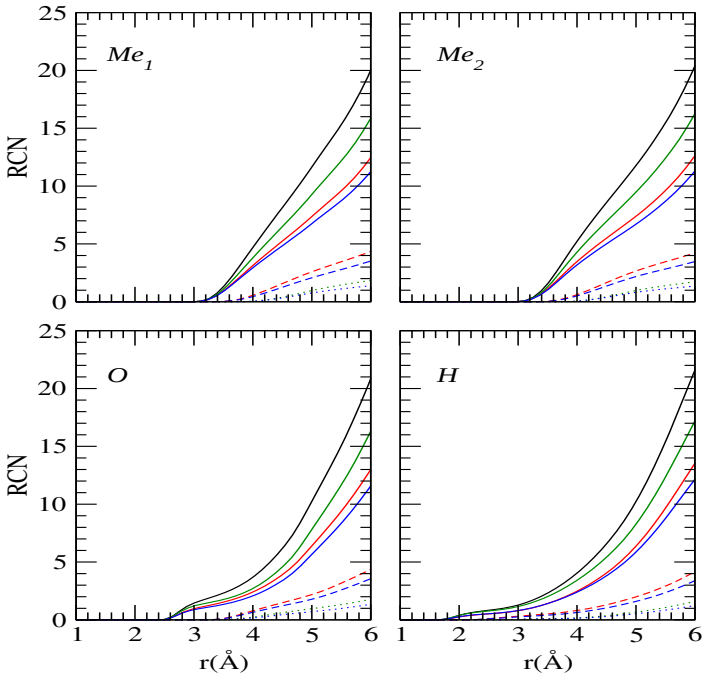

Figure 4A-4. *Running coordination numbers for different NMA atomic sites in water, aqueous urea, aqueous TMAO, and mixed urea/TMAO solutions. Solid, dashed, and dotted lines are for water, urea and TMAO, respectively.*

molecules in the solvation shell of NMA molecule is much higher in pure water than in aqueous solution of osmolyte (Figure 4A-5). Considering the effect of urea alone, i.e., in the absence of TMAO, we see that, in the solvation shell of radius 6 Å, NMA loses about 30 water molecules, and about 16 urea molecules enter in this particular region. This corresponds to replacement of about 2 hydration water by each urea molecule. Due to this higher exclusion of water, total number of solution species (water plus urea) in the NMA solvation shell is much higher in pure water than in urea solution (Figure 4A-5).

For the simulation of NMA in aqueous TMAO solution (system NT), we find that the existence of TMAO in the solvation shell leads to reduction in hydration water (Figure

4A-5). To be specific, each TMAO molecule can replace about 2.5 hydration water of NMA. However, since the number of TMAO molecules that enter in NMA solvation shell is significantly small (about 7 in contrast to about 16 for urea), NMA dehydration is lower in aqueous solution of TMAO in comparison to that of urea.

Comparison of the solvation number of NMA in urea/TMAO mixture with that in binary urea solution reveals removal of both water and urea from the solvation shell of NMA. Nonetheless, removal of urea is much less pronounced as compared to water.

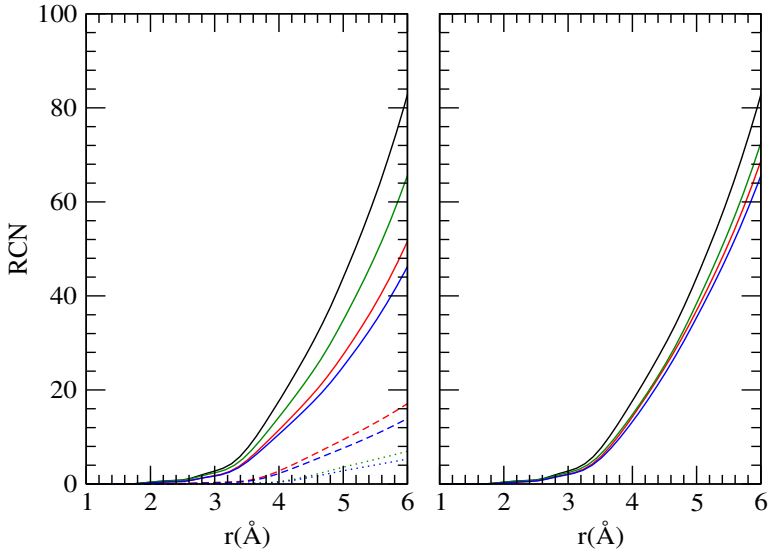

Figure 4A-5. *Left: Total number of water (solid), urea (dashed), and TMAO (dotted) molecules in the solvation shell of NMA as a function of distance. Right: Total number of solution species in the solvation shell of NMA as a function of distance. Results are for pure water, aqueous urea, aqueous TMAO, and mixed urea/TMAO solutions.*

The difference between the local environment of NMA and that of the bulk solution was investiagted by calculating the time-averaged normalized ratio (τ_i) of component i as defined in **Chapter 2.**

Figure 4A-6 shows the τ_i values for different atomic sites in NMA as a function of distance. The regions of preferential exclusion/accumulation of urea and TMAO are clearly visible in this figure. In the close proximity of the NMA atomic sites, τ_{Ow} is greater than 1, whereas τ_{Cu} and τ_{Nt} are lower than 1, implying preferential accumulation of water in this region. This is directly related to the larger excluded volumes of urea and TMAO that prevents a close approach of their central atoms. However, relatively larger number

of osmolyte molecules appear beyond this region. Comparing the component fractions of water and osmolyte in the binary solution with the ternary solution, we find relative deficit of osmolyte and excess of water around the NMA atomic sites in urea/TMAO mixture. From the data in Figure 4A-6, it is not hard to suggest a much better mixed solvation layer of NMA in terms of water and osmolyte in the mixed osmolyte solution as compared to that in the absence of a second osmolyte. TMAO is found to be excluded from the amide hydrogen and its relative exclusion increases slightly upon addition of urea.

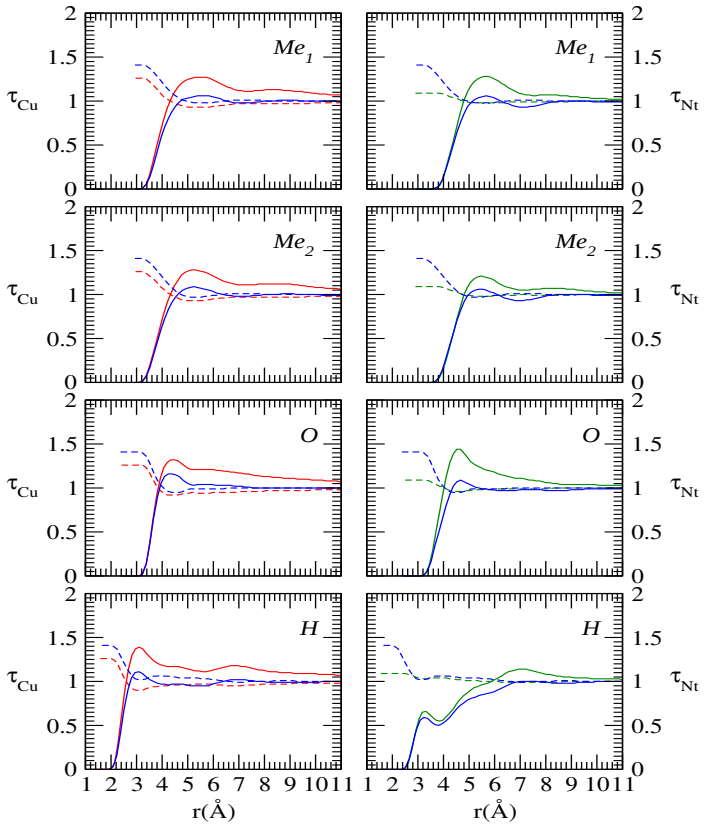

Figure 4A-6. *Time-averaged normalized fractions of urea (left) and TMAO (right) central atoms as a function of the distance from NMA atomic sites in aqueous urea, aqueous TMAO, and mixed urea/TMAO solutions. Dashed lines are for normaized fractions of water oxygen.*

For further characterization of NMA solvation, we investigated the structural, energetic, and dynamical properties of hydrogen bonds formed by NMA with solution species. The methods and the geometric criteria for hydrogen bond properties and dynamics calculations were identical to those described in **Chapter 2**. We selected cut-off distances according to the position of the first minimum of the appropriate rdf and these distances

are tabulated in Table 4A-3. We considered the five possible hydrogen bonds between NMA and solution species: $O\cdots HwOw$, $Ow\cdots HN$, $O\cdots HuNu$, $Ou\cdots HN$, and $Ot\cdots HN$. Note that hydrogen bonds in this study are abbreviated as $Im-Jn$ where I and J can be N (for NMA), W (for water), U (for urea), and T (for TMAO), and m and n can be a (for acceptor) and d (for donor). Further, hydrogen bonds are with respect to the first species. For example, the $O\cdots HwOw$ bond is abbreviated as $Na-Wd$ and the hydrogen bond number is with respect to NMA oxygen.

Table 4A-3. Cut-off Distances (in Å) for the Hydrogen Bonds Investigated[a]

		N-W	N-U	N-T	W-W	U-W	T-W	U-U	T-U
Donor	r_{DA}	3.26	3.52	3.48	3.39	4.52	3.48	4.24	3.81
	r_{AH}	2.62	2.94	2.82	2.37	2.51	2.69	2.80	2.80
Acceptor	r_{DA}	3.39	3.95	—	3.39	3.38	—	4.24	—
	r_{AH}	2.62	2.80	—	2.37	2.66	—	2.80	—

[a]N, W, U, and T represent NMA, water, urea, and TMAO, respectively. The terms, 'Donor' and 'Acceptor', in the first column are, respectively, for hydrogen bonds with first species behaving as donor and acceptor. r_{DA} and r_{AH} are defined in the text.

In Table 4A-4, we have presented the total (considering all 20 NMA molecules) number of hydrogen bonds formed between NMA and solution species together with energies of these bonds. Figure 4A-7, on the other hand, illustrates the fraction of NMA molecules that engage in n number of hydrogen bonds with solution species. In Figure 4A-7, we find that most of the carbonyl oxygens participate in 2 hydrogen bonds with water, although some of these are also 1- or 3-coordinated to water. On average, each NMA oxygen is found to have about 1.7 hydrogen bonds to water. The amide hydrogen remains satisfied by forming a single hydrogen bond to water molecule and the average number of $Nd-Wa$ hydrogen bonds per NMA is only 0.75. Thus, hydrogen bonding between NMA and water is solely dominated by carbonyl oxygen in NMA, which is not surprising. Table 4A-4 shows that out of the total 49 NMA−water hydrogen bonds in pure water, 34 goes to carbonyl oxygen, leaving only 15 for amide hydrogen.

In binary solution of urea, NMA molecules lose significant number of hydrogen bonds to water (Table 4A-4) and almost all of these hydrogen bonds are replaced by

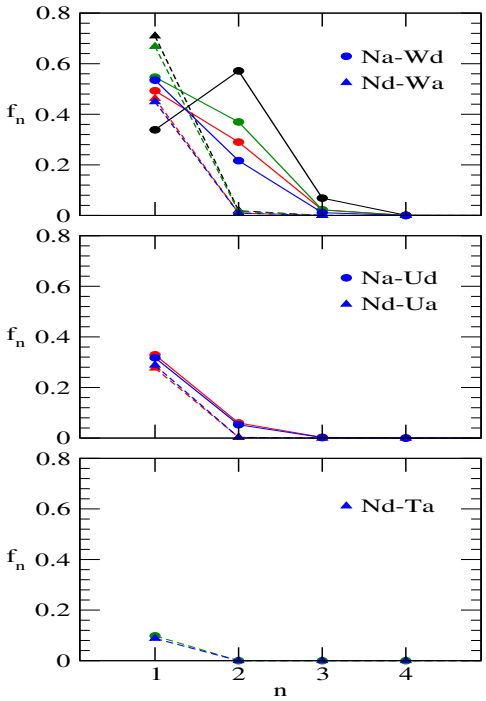

Figure 4A-7. *Fraction of NMA molecules that engage in n number of hydrogen bonds with water and osmolyte in water, aqueous urea, aqueous TMAO, and mixed urea/TMAO solutions. Hydrogen bond types are defined in the text and the numbers are with respect to the first species.*

Table 4A-4. Number of Hydrogen Bonds Formed by NMA with Solution Species[a]

system	Na-Wd	Nd-Wa	Na-Ud	Nd-Ua	Nd-Ta	total
NW	33.80	15.00	—	—	—	48.80
	(−20.02)	(−19.64)	(—)	(—)	(—)	
NU	22.60	9.60	9.00	5.60	—	46.80
	(−19.97)	(−19.88)	(−21.82)	(−28.92)	(—)	
NT	27.00	14.20	—	—	2.00	43.20
	(−20.75)	(−20.09)	(—)	(—)	(−36.28)	
NUT	20.00	9.40	8.40	5.80	1.80	45.40
	(−20.33)	(−20.02)	(−21.65)	(−29.26)	(−36.17)	

[a]Hydrogen bond energies (in kJ mol^{-1}) are given in parentheses. Hydrogen bond types are defined in the text.

NMA−urea hydrogen bonds, keeping total number of hydrogen bonds between NMA and solution species close to pure water system. Note that the effect of urea on NMA−water hydrogen bond number is dramatic for both amide hydrogen and carbonyl oxygen. In most cases, the two solvation sites of NMA oxygen are shared by one water molecule and one urea molecule (Figure 4A-7). Although there are some NMA oxygens that participate in 2 hydrogen bonds with water even in the presence of urea, the number is significantly lower than that in case of pure water. The average number of $Na - Wd$ hydrogen bonds per NMA reduces from about 1.7 in pure water to about 1.1 in binary urea solution and there arises about 0.5 $Na - Ud$ hydrogen bonds. What these results support is the direct interaction model for urea-conferred protein denaturation [33-47]. Urea removes water from the protein solvation shell and makes some favorable contact with protein residues, leading to protein unfolding.

Just like in the case of urea, addition of TMAO reduces average number of $Nd-Wa$ hydrogen bonds. The loss is, however, very small and is also well compensated by formation of few $Nd - Ta$ hydrogen bonds (Table 4A-4). We observe that average number of $Na-Wd$ bonds decreases dramatically upon addition of TMAO. With the fact that TMAO cannot form hydrogen bonds with carbonyl oxygen in NMA taken into consideration, the so observed large reduction in $Na - Wd$ hydrogen bonds is striking and likely the most significant. Figure 4A-7 shows that relative population of carbonyl oxygen that participate in 2 hydrogen bonds with water reduces in binary TMAO solution, whereas that participating in 1 hydrogen bond increases. Since TMAO is unable to compensate the loss of $Na - Wd$ hydrogen bonds, total number of hydrogen bonds between NMA and solution species reduces from about 49 in pure water to about 43 in binary TMAO solution (Table 4A-4).

It is interesting to observe that TMAO does not affect the number of NMA−urea hydrogen bonds and there is almost no change in the relative population of NMA molecules that participate in 1 and 2 hydrogen bonds with urea (Figure 4A-7). On the other hand, average number of NMA−water hydrogen bonds is lower in the urea/TMAO mixture as compared to binary urea solution (Table 4A-4). Remarkably, MD simulations of the protein CI2 by Bennion and Daggett [73] suggested that TMAO does not stabilize the native state by occluding urea from the solvation shell. Similarly, Kokubo *et al.* [72] did not observe disturbance of peptide−urea hydrogen bonds in urea/TMAO mixture. In contrast, these study showed dehydration of protein and a significant loss of peptide−water hydrogen bonds upon addition of TMAO [72, 73]. Again, from Figure 4A-7, it can be seen that

there is not much difference in relative population of hydrogen bonds for $Nd-Wa$ between binary and ternary solutions of urea. The largest differences arise only from a decrease in relative population of carbonyl oxygen that participate in 2 hydrogen bonds to water. On these grounds, it is reasonable to suggest here that unavailability of backbone oxygen to form hydrogen bonds with solution species is the most likely reason for protein stabilizing and counteracting ability of TMAO.

In Table 4A-4, we find that $Na-Wd$ hydrogen bond is weaker than the $Na-Ud$ bond by about 2 kJ/mol. The energy distribution curve is much broader for the latter, with some energetically strong hydrogen bonds (Figure 4A-8) and also the hydrogen bond relaxes slowly as compared to $Na-Wd$ both in binary and ternary solutions of urea (Figure 4A-9). Note that the relative population of high energy (more negative) bonds slightly

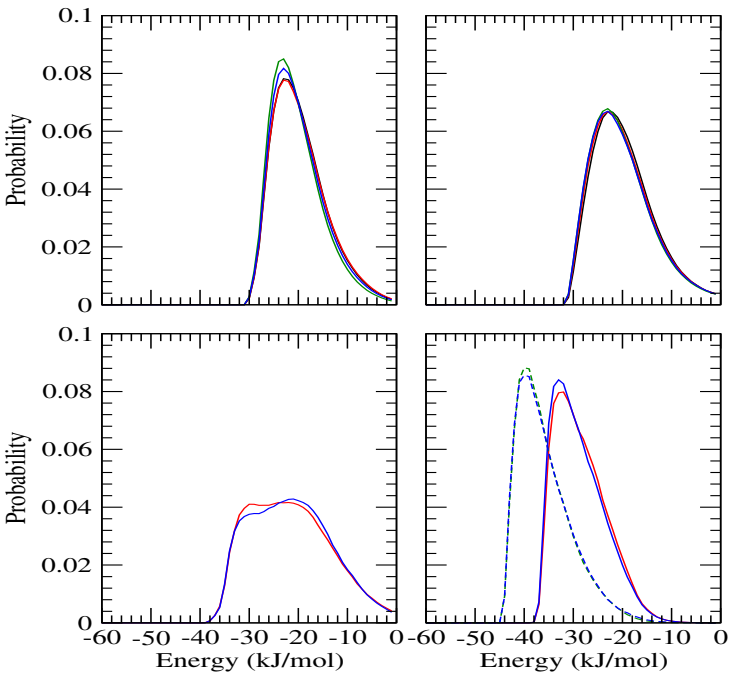

Figure 4A-8. *Probability distribution of hydrogen bond energies for oxygen (left) and hydrogen (right) of NMA with water (top) and urea (bottom) in water, aqueous urea, aqueous TMAO, and mixed urea/TMAO solutions. Dashed lines in bottom-right panel are for NMA−TMAO hydrogen bonds.*

increases for $Na-Wd$ and decreases for $Na-Ud$ upon addition of TMAO. The $Nd-Ta$ hydrogen bond is the strongest among the hydrogen bonds investigated here. For the urea/TMAO mixture, the $Nd-Ta$ bond is more attractive than the $Nd-Ua$ bond by about 7 kJ mol^{-1} which, in turn, is about 9 kJ mol^{-1} more attractive than the $Nd-Wa$

hydrogen bond. As revealed in Figures 4A-8 and 4A-9, on moving from $Nd-Wa$ through $Nd-Ua$ to $Nd-Ta$, the energy distribution curve shifts to more attractive region and the hydrogen bond relaxation becomes slower and slower. We note that magnitudes of these hydrogen bond energies do not change significantly on changing the system.

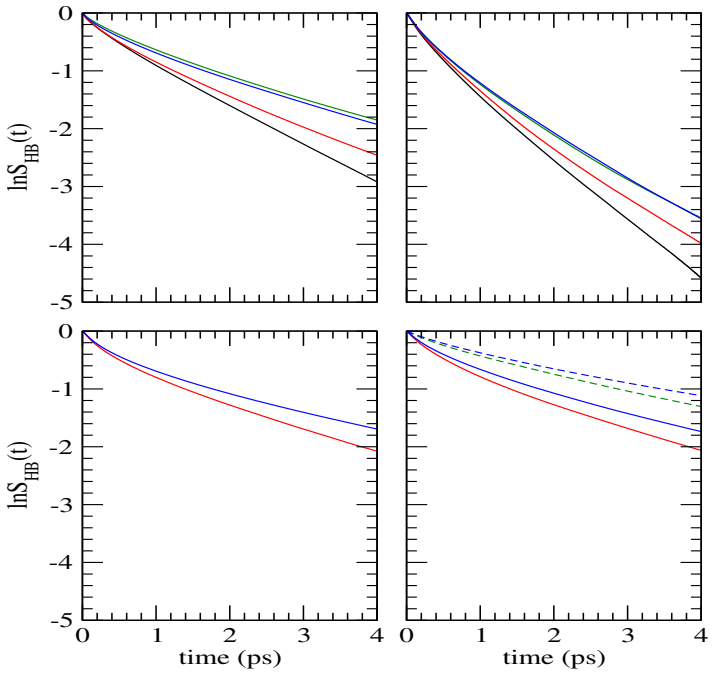

Figure 4A-9. *Time dependence of the continuous hydrogen bond correlation functions, $S_{HB}(t)$, for oxygen (left) and hydrogen (right) of NMA with water (top) and urea (bottom) in water, aqueous urea, aqueous TMAO, and mixed urea/TMAO solutions. Dashed lines in bottom-right panel are for NMA−TMAO hydrogen bonds.*

Thus, a thorough investigation of the solvation characteristics of NMA atomic sites in pure water, and in binary and ternary solutions of urea and TMAO reveals replacement of a large number of NMA hydration waters by these two osmolytes. While both urea and TMAO are found to interact directly with NMA atomic sites, NMA can make some better contact with urea than with TMAO. NMA loses some hydrogen bonds to water due to the inclusion of osmolyte in its solvation shell. The hydrogen bonds of NMA oxygen to water become stabilized in the presence of TMAO. But, the relative stabilization is not large and this energetic gain can be expected to overcome easily by the energetic cost due to the loss of large number of hydrogen bonds to water. Urea reduces the loss of NMA−water hydrogen bonds by forming hydrogen bonds with NMA hydrogen bonding sites, whereas TMAO

cannot form hydrogen bonds with NMA oxygen and hence shows its inability to compensate the loss of hydrogen bonds between NMA and water. What these findings suggest is that, unlike urea which can stabilize unfolded protein by forming hydrogen bonds with its backbone, TMAO prevents backbone oxygen from interacting efficiently with solution species, providing the pathway for TMAO-induced protein stabilization and counteraction. Two other possible pathways to investigate the underlying mechanism by which TMAO stabilizes protein and counteracts protein denaturation by urea are to examine the solvation of TMAO by water and urea (which eventually reduces availability of water and urea to solvate protein residues) and also the indirect effect of TMAO on water structure. In the following, we have discussed both of these two possibilities in aqueous NMA solutions in different environments.

Interactions between Solution Species. In an attempt to understand the origin of the counteracting effect of TMAO, we studied the solvation of both hydrophobic (methyl group) and hydrogen bonding (oxygen atom) sites of TMAO by water and urea and also examined the hydrogen bonding interactions between the solution components. Figure 4A-10 displays selected rdfs that show the solvation of TMAO by water and urea. We can see immediately that the first peak in $Ot-Ow$ rdf is much stronger than that in $Ct-Ow$ rdf, demonstrating strong affinity of TMAO for water coming through TMAO−water hydrogen bonding. Urea has little effect on the hydration shell of methyl group, but increases the first peak in $Ot-Ow$ rdf dramatically. So water molecules become tightly coordinated to TMAO oxygen upon addition of urea. However, the number of water molecules in the first hydration shell of TMAO methyl group decreases in urea/TMAO mixture (Table 4A-5). Similarly, TMAO oxygen loses about 0.7 first shell water molecules in the presence of urea, ultimately leading to overall loss of about 8 water molecules in the solvation shell of TMAO.

It is striking to note that the general features of the $Ct-Cu$ and $Ot-Nu$ functions are similar to those of the $Ct-Ow$ and $Ot-Ow$ rdfs. The qualitative similarity of these rdf pairs indicates that urea can solvate both hydrophobic and hydrogen bonding sites of TMAO as do water molecules. The density of urea near the TMAO methyl group is very similar to that of water, suggesting no preference of hydrophobic sites for water and urea. However, as reflected by the much stronger first peak in $Ot-Ow$ rdf than that in $Ot-Nu$, water interacts more with TMAO than does urea.

In Figure 4A-11, we have shown rdfs for atom pairs associated with hydrogen bonding. Following observations are made from this figure: (a) The first peak in $Ou-Hw$

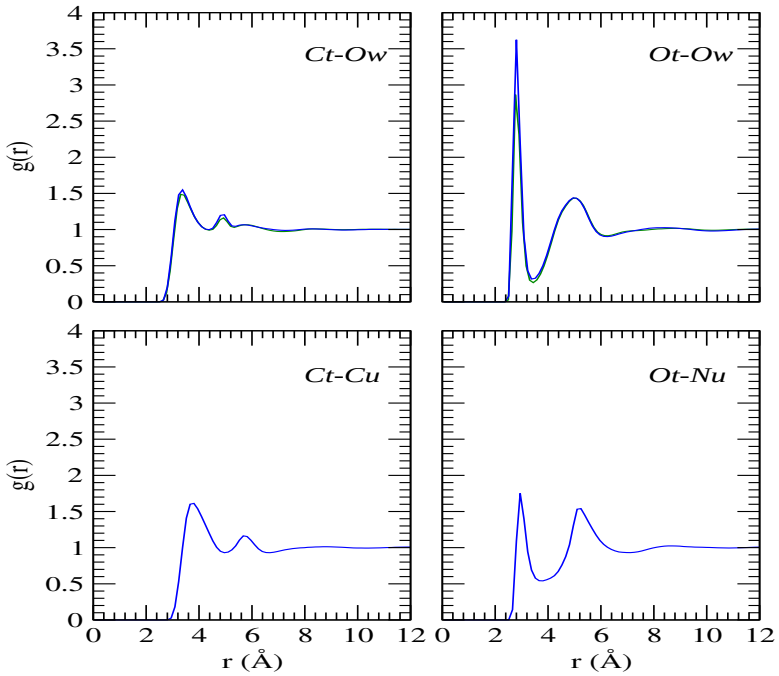

Figure 4A-10. *Selected site−site rdfs that show solvation of TMAO by water and urea in aqueous TMAO and mixed urea/TMAO solutions.*

Table 4A-5. Coordination Numbers for TMAO Atomic Sites[a]

atom pair	r_c(Å)	NT	NUT
$Ct - Ow$	4.4	7.0	4.5
$Ot - Ow$	3.4	2.7	2.0
$Nt - Ow$	6.3	23.5	15.1
$Ct - Cu$	5.0	—	2.0
$Ot - Nu$	3.8	—	1.2
$Nt - Cu$	6.4	—	4.7

[a] r_c is the integration distance. Numbers are with respect to first atomic site. For Nu, the actual number is multiplied by 2.0 to consider both nitrogen atoms in urea.

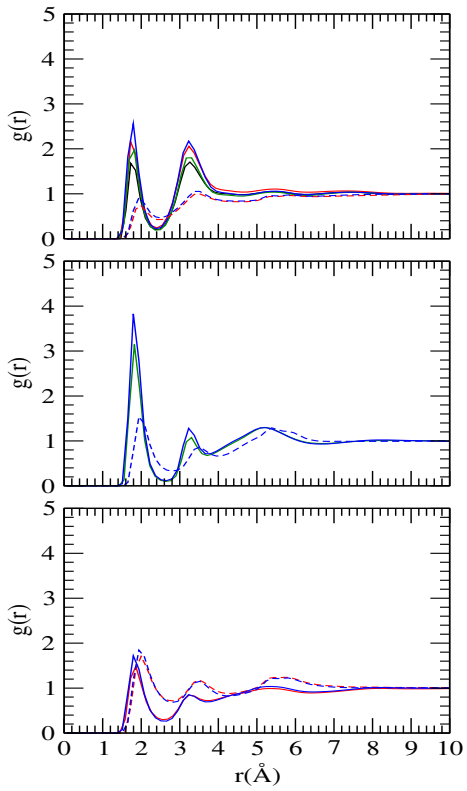

Figure 4A-11. *Selected site−site rdfs that show hydrogen bonding interactions involving O-atoms of water, urea, and TMAO molecules (from top to bottom, respectively) in water, aqueous urea, aqueous TMAO, and mixed urea/TMAO solutions. Solid and dashed lines are for water and urea hydrogens, respectively.*

rdf is much stronger than that in $Hu - Ow$, indicating that urea prefers to be a hydrogen bond acceptor rather than a donor in urea−water hydrogen bonds. (b) Relative to water hydrogen, first peaks are shifted outward for urea hydrogen. (c) Although both water and urea hydrogens are tightly coordinated to TMAO oxygen, tendency of TMAO oxygen for water hydrogen is much higher.

To obtain further insight into the nature of hydrogen bonding interactions, we computed the strength and number of the hydrogen bonds by adopting the geometric criteria defined in **Chapter 2**. The cut-off distances for the hydrogen bonds are listed in Table 4A-3.

Figure 4A-12 illustrates the fraction of molecules (f_n) that engage in n number of hydrogen bonds and the average number of hydrogen bonds per molecule are depicted in Table 4A-6. For pure water, most of the water molecules participate in either 3 or 4

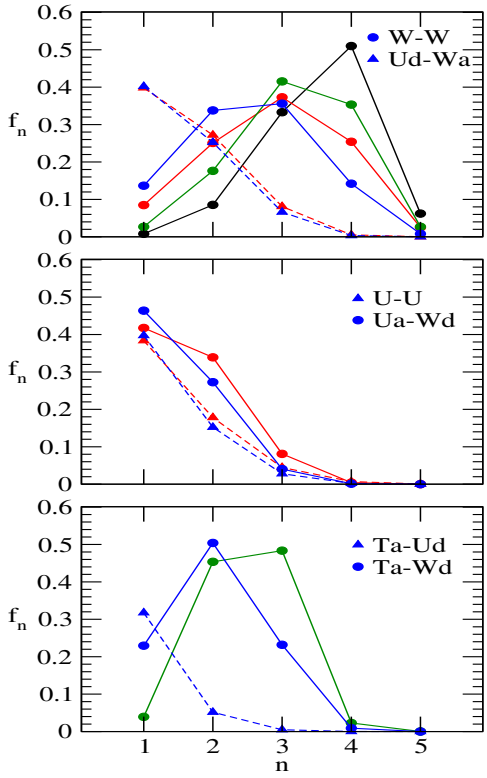

Figure 4A-12. *Fraction of molecules that engage in n number of hydrogen bonds with solution species in water, aqueous urea, aqueous TMAO, and mixed urea/TMAO solutions. Hydrogen bond types are defined in the text and the numbers are with respect to the first species.*

hydrogen bonds. Small fractions of water molecules are engaged in either 2 or 5 hydrogen bonds. The effect of osmolyte on water hydrogen bonding network is dramatic. It reduces the number of higher (4 and 5) coordinated water molecules and at the same time, increases the number of lower (1-3) coordinated water molecules. As a result, average number of water−water hydrogen bonds is reduced in aqueous solutions of osmolyte (Table 4A-6). Note that the changes are significantly pronounced for 2- and 4-coordinated water molecules, and are related to the number of osmolyte molecules that has to be accommodated in the cavities of water molecules.

In binary solution, majority of the urea oxygens are found to have either 1 or 2 hydrogen bonds to water (Figure 4A-12) and, on average, there are about 2.6 water molecules which are hydrogen bonded to each urea molecule (Table 4A-6). As revealed in Figure 4A-12, although self-association of urea molecules through hydrogen bonding is possible, urea prefers to form maximum number of hydrogen bonds with water molecules. The aver-

age number of urea−urea hydrogen bonds is significantly smaller than that of urea−water hydrogen bonds per urea molecule. Addition of TMAO to the system increases relative population of 1-coordinated water molecule and decreases those of 2- and 3-coordinated water molecule for oxygen of urea. Relative population of 1-coordinated water molecule to urea hydrogen remains similar in the ternary solution, whereas the fraction of 2- and 3-coordinated water molecules decreases. This ultimately leads to a reduction of about 0.3 urea−water hydrogen bonds in the urea/TMAO mixture. TMAO also breaks some urea−urea hydrogen bonds and so, although urea forms some hydrogen bonds with TMAO molecule (about 0.2 per urea), total number of hydrogen bonds per urea molecule reduces in the ternary osmolyte solution. These observations are consistent with direct interaction between urea and TMAO. In the absence of TMAO, urea hydrogens are free to interact with oxygens of water and urea. As TMAO is added, fraction of these hydrogen bonds are replaced by TMAO−urea hydrogen bonds.

Table 4A-6. Properties of Hydrogen Bonds Involving Water and Osmolyte[a]

		$W-W$	$Wa-Ud$	$Ua-Wd$	$U-U$	$Ta-Wd$	$Ta-Ud$
n_{HB}	NW	3.52	—	—	—	—	—
	NU	2.84	0.32	1.34	0.90	—	—
	NT	3.20	—	—	—	2.46	—
	NUT	2.51	0.33	1.12	0.79	1.96	0.42
E_{HB}	NW	−19.17	—	—	—	—	—
	NU	−19.26	−15.09	−20.42	−24.36	—	—
	NT	−19.73	—	—	—	−29.02	—
	NUT	−19.85	−15.25	−20.74	−24.69	−28.76	−29.59
τ_{HB}	NW	1.25	—	—	—	—	—
	NU	1.41	0.91	0.88	1.61	—	—
	NT	1.77	—	—	—	3.75	—
	NUT	1.98	1.14	1.22	2.03	3.92	2.65

[a] n_{HB}, E_{HB}, and τ_{HB} represent average number, energy (in kJ mol^{-1}), and life-time (in ps), respectively. Hydrogen bond types are defined in the text and hydrogen bond numbers are with respect to the first species.

In contrast to urea, majority of TMAO molecules participate in 3 hydrogen bonds with water (Figure 4A-12). Number of TMAO molecules engaged in 2 hydrogen bonds with water is also significant and, on average, there are about 2.5 water molecules that are found to be hydrogen bonded to TMAO oxygen. Upon addition of urea, the third hydrogen bond of TMAO oxygen to water is likely to be replaced by a new hydrogen bond between TMAO and urea. Each TMAO molecule now forms hydrogen bonds mostly with 2 water molecules and, on average, the total number of hydrogen bonds per TMAO molecule (2.5) remains similar to its binary solution.

The average energies and life-times of hydrogen bonds between these solution species are given in Table 4A-6. Figure 4A-13, on the other hand, shows the probability distributions of the hydrogen bond energies and time dependence of the hydrogen bond correlation functions. These results lead to several interesting observations. We see that urea has negligible effect on water−water hydrogen bond energy. Change in energy distribution is very small in binary urea solution. The water−water hydrogen bond relaxes slowly in the presence of urea (as compared to pure water) and the life-expectancy of this hydrogen bond increases slightly (from 1.25 ps in pure water to 1.41 ps in binary urea solution). These results do not provide any evidence for urea's ability to disturb water hydrogen bonding network. In fact, previous simulations showed enhancement of the first peak in $Ow-Ow$ rdf, indicating a tightly coordinated first shell of water, and only a slight collapse of the water second shell was noted (**Chapters 2** and **3**).

Effect of TMAO on water hydrogen bonding interaction is more pronounced. In particular, hydrogen bonds become more attractive (Table 4A-6) and the energy distribution shifts toward higher energy (more negative) side in aqueous solutions of TMAO, indicating water hydrogen bond network stabilization by TMAO. Water−water hydrogen bond relaxation is also much slower in the presence of TMAO and hydrogen bond life-time increases to 1.77 ps in binary TMAO solution.

Considering the case of urea−water interaction, we find that the $Ua-Wd$ bond is more attractive than the $Ud-Wa$ hydrogen bond and, in fact, the average energy for the latter (about -15 kJ mol^{-1}) is the lowest among the hydrogen bonds investigated in this study. For hydrogen bonds formed by urea oxygen with water hydrogen, energy distribution is very similar to that for water−water hydrogen bonds. In contrast, the distribution is broader for hydrogen bond between urea hydrogen and water oxygen, and the population of low-energy hydrogen bonds is significantly higher in this case. There is, however, no such differences between these two hydrogen bonds in terms of their relaxation with time

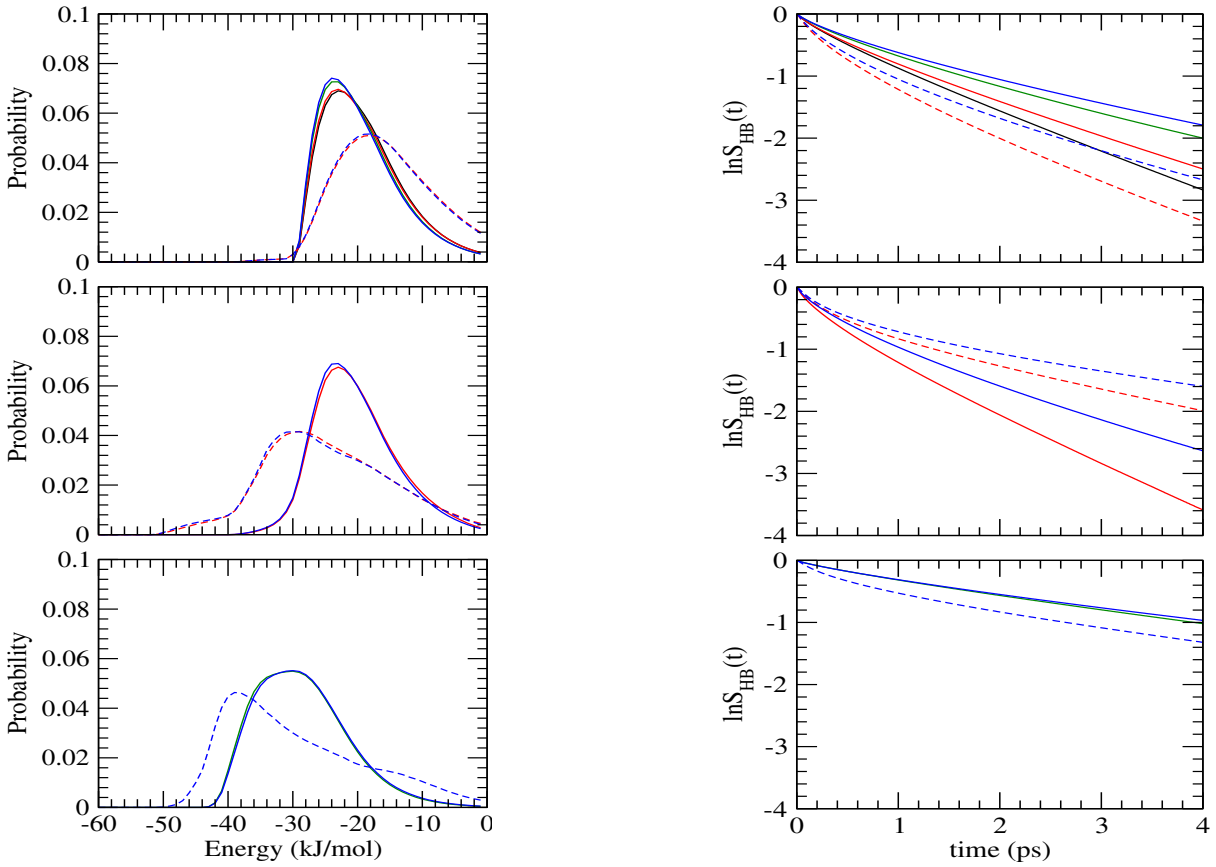

Figure 4A-13. *Probability distributions of hydrogen bond energies (left) and time dependence of the correlation functions, $S_{HB}(t)$, (right) for hydrogen bonds involving oxygen atoms of water, urea, and TMAO (from top to bottom, respectively) in water, aqueous urea, aqueous TMAO, and mixed urea/TMAO solutions. Solid and dashed lines are for water and urea hydrogens, respectively.*

and both have similar hydrogen bond life-times (about 0.9 ps in binary urea solution). Although there is negligible change of urea−water hydrogen bond energies in the presence of TMAO, relaxation of urea−water hydrogen bond becomes slower as TMAO is added to the system.

The hydrogen bonds formed by TMAO oxygen with both water and urea are energetically very strong (about -29 kJ mol^{-1}). For the ternary solution, the TMAO−water hydrogen bond is more attractive than the water−water and urea−water (urea acceptor) hydrogen bonds by about 9 kJ mol^{-1}. Similarly, the TMAO−urea hydrogen bond is about 5 kJ mol^{-1} more attractive than the urea−urea bond. The energy distributions show a

large population of these hydrogen bonds in high energy (more negative) regions. What is more, these hydrogen bonds decay very slowly in aqueous solutions. The average life-time of TMAO−water hydrogen bond is found to be 3.92 ps in the urea/TMAO mixture, which is about 2 times higher than that between water molecules for the same system. We note that significantly longer hydrogen bond life-time for a TMAO−water than for a water−water hydrogen bond has been widely reported in the literature [67, 68, 77, 78]. The MD simulations also predicted that TMAO−water hydrogen bonds are more attractive than water−water hydrogen bonds [68].

Hence, examining the solvation characteristics of TMAO, we find that both water and urea can solvate TMAO molecules and due to the existence of urea in its solvation shell, TMAO loses some hydration waters upon addition of urea. Solvation of TMAO by water, on the other hand, leads to relative stabilization of water hydrogen bonding network. These observations correspond well with previously observed solvation of TMAO by water and urea [68, 76, 125] and also with the water structure making ability of TMAO [31, 32, 67].

■ SUMMARY AND CONCLUSIONS

We investigated solvation characteristics of NMA in binary and ternary solutions of urea and TMAO to shed light on the backbone solvation in the presence of these two osmolytes. Computations of site−site rdfs indicated direct interactions of both urea and TMAO with NMA atomic sites. It was evident from analysis of solvation number that the number of TMAO molecules that enter in NMA solvation shell was significantly lower than that of urea, and due to the inclusion of osmolytes, NMA molecules were dehydrated in binary and ternary solutions of urea and TMAO. Both osmolytes were observed to replace a large number of water molecules in the solvation shell of each NMA atomic site, though the water removing ability of TMAO was slightly higher than that of urea (2.5 per TMAO against 2.0 per urea). Addition of a second osmolyte also reduced the number of the other osmolyte in the solvation shell, but the effect was much less pronounced in comparison to hydration water. The local environment of NMA was further explored by calculating the fraction of each component and it was observed that the solvation layer of NMA was better mixed in terms of water and osmolyte in urea/TMAO mixture as compared to that in binary osmolyte solution.

Investigation of structural, energetic, and dynamical properties of NMA hydrogen bonds with solution species showed that hydrogen bonding between NMA and water was largely dominated by carbonyl oxygen in NMA. Our results demonstrated replacement of

a large number of NMA−water hydrogen bonds by NMA−urea hydrogen bonds and the total number of hydrogen bonds between NMA and solution species was found to be similar in pure water and in binary urea solution. The two solvation sites in NMA oxygen (which were occupied by water alone in pure water) were shared by water and urea in aqueous urea solution. Hydrogen bonds between NMA and urea were found to be more attractive than those between NMA and water and the relaxation was also slower for the former. On the other hand, our analysis of hydrogen bond properties did not provide any evidence for the 'water structure breaking' capacity of urea. Rather, urea was found to slightly increase water−water hydrogen bond energy and life-time. All of our results are consistent with direct interaction model for urea-conferred protein denaturation, but do not support the indirect mechanism that presumes urea as a structure breaker for water, making water molecules free to interact with protein residues.

Just like urea, TMAO was observed to replace hydrogen bond between amide hydrogen and water (though the change was negligible). TMAO cannot donate its hydrogen to hydrogen bond acceptor sites; but strikingly, TMAO methyl groups showed tendency to occupy the space near NMA oxygen, reducing the number of hydrogen bonds between carbonyl oxygen and solution species. These lead us to suggest that, it is the unavailability of backbone oxygen to form hydrogen bonds with solution species that protects the native protein.

To shed light on the counteracting mechanism, we then examined solvation of TMAO by water and urea and also studied structural, energetic, and dynamical properties of various possible hydrogen bonds between solution species. Urea was seen to solvate both hydrophobic and hydrogen bonding sites in TMAO and because of its interaction with urea, TMAO lost some hydration waters upon addition of urea. TMAO oxygen, which participated in 2 to 3 hydrogen bonds with water in its binary solution, showed its inability to maintain these hydrogen bonds as urea was added and these hydrogen bonds were replaced by TMAO−urea hydrogen bonds. We observed that hydrogen bonds formed by TMAO with water and urea were very strong. In fact, these hydrogen bonds were found to be energetically much stronger than those between water and urea and also had high life-times. In addition to its direct interaction with water and urea, TMAO also showed an indirect effect on water−water and urea−water interaction in which it stabilized water hydrogen bonding network and also reduced relaxation of urea−water hydrogen bonds.

In the context of proteins, the present study provides a clear indication of the importance of backbone oxygen in determining the extent of osmolyte-induced protein

(de)stabilization. While the denaturant urea forms energetically favorable hydrogen bonds with backbone oxygen, TMAO cannot donate its hydrogen to backbone oxygen and hence shows its inability to compensate for the loss of a significant number of hydrogen bonds between backbone oxygen and water that is caused by occupancy of TMAO methyl groups near the backbone oxygen. Thus, the total number of favorable contacts of backbone oxygen with solution species is reduced upon the addition of TMAO (as compared to pure water). TMAO induces protein folding because the compact state has more energetically favorable interactions (intrabackbone plus few backbone−solvent) than the extended state (only backbone−solvent). What is more, folding of protein in aqueous TMAO solution allows TMAO to maximize the number of favorable contacts with water in the bulk and also to stabilize the water hydrogen bonding network. The picture does not change even in the urea/TMAO mixture. As compared to binary urea solution, in which the protein prefers its solvent-exposed state to maximize favorable contacts with solution species, the number of efficient interaction sites for the backbone oxygen is reduced as TMAO is added. Since the relative stability of the unfolded state gained by backbone−solvent interactions is overcome by various intrabackbone plus few backbone−solvent interactions in the folded state, the protein adopts a (folded) structure in ternary solutions of urea and TMAO that is similar to that in pure water. The only difference is that some urea molecules now appear in close proximity of the protein. The highly favorable interactions of TMAO with water and urea in the bulk give further stability to the system that contains the folded protein. Hence, in all likelihood, the inefficient interaction of backbone oxygen with solution species in the presence of TMAO plays the most important role in the ability of TMAO to stabilize proteins and offset protein denaturation by urea. A note of caution, however, is that, although hydrogen bond number provides a useful measure to describe protein stability, there are several other factors effective in protein stabilization. A systematic study with proteins will be needed to get to the conclusion of the counteracting mechanism.

Part B:

TMAO's Effect on Amide Solvation at High Pressure

Overview: We report here MD computer simulation results for aqueous solutions of NMA with different TMAO concentrations over a wide range of pressures relevant to protein denaturation. Hydration behavior of NMA is analyzed at different conditions chosen. It is observed that, hydrostatic pressure leads to a significant compression of hydration shell of nonpolar groups and increases hydration number. The compression is relatively insignificant in the vicinity of hydrogen bonding sites. TMAO can prevent pressure-induced enhanced hydration of NMA molecules. Interaction of TMAO with NMA and the structural and dynamical properties of water (site−site rdf, coordination number, hydrogen bond number and life-time) are also investigated to find the origin of the counteracting action of TMAO. Our results confirm that TMAO and pressure have counteracting effects on the water structural and dynamical properties, giving an explanation as to how TMAO counteracts pressure-conferred denaturation of proteins.

■ INTRODUCTION

As discussed in Part A of the present chapter, much attention has been directed toward understanding the hydration of NMA. However, the effects of pressure on NMA hydration are yet to be investigated thoroughly. Pressure-induced modifications of hydrogen bonding interactions between NMA molecules were studied recently for neat NMA, which represented a system of peptide groups only and hence peptide solvation was not addressed in that study [223]. The only mentionable investigation in this direction came from Takekiyo *et al.* [224] who employed DFT method to a trans-NMA dimer and a water molecule. The study showed that the $CO\cdots HO$ bond became stronger and the strength of the $CO\cdots HN$ bond reduced with increasing pressure.

In the work described in this part, we first investigate the hydration characteristics of NMA in pure water system at 1 bar and then extend it to systems with high pressure and high TMAO concentration to see how hydration of NMA atomic sites is affected by pressure and what is the role of TMAO on this pressure-induced modification of NMA hydration. After examining direct interaction between NMA and TMAO, we switch our attention to structural, energetic, and dynamical properties of water molecules in these different solution conditions.

The remainder of this part is organized into three sections. The models and simulation details are briefly described in the next section. This is followed by a section whereof we discuss our results, and our conclusions are summarized in the last section.

■ MODELS AND SIMULATION METHOD

Classical MD simulations were carried out for NMA in pure water as well as in binary solutions of increasing TMAO concentrations at five different hydrostatic pressures ranging from 1 bar to 8 kbar. In all of the simulated systems, the total number of solution species was kept fixed at 500, out of which 20 were the solute NMA (mole fraction of 0.04). Note that, while the central simulation cell for NMA−water system (denoted as NW) contained 20 NMA molecules immersed in 480 water molecules, TMAO solutions with TMAO mole fractions of 0.04, 0.06, and 0.08 ($NT2$, $NT3$, and $NT4$, respectively) were constructed by replacing water molecules with TMAO. The concentration of TMAO in these systems varied from 0 to 4 M. We used the popular SPC/E model [111] for water, and described TMAO and NMA with rigid version of models proposed by Kast *et al.* [113] and Jorgensen and Swenson [221], respectively. The interaction between atomic sites of two different

molecules was expressed using Eq. 2.3. The values of the LJ parameters and the partial charges for TMAO, water, and NMA were summarized in Tables 2A-2 and 4A-2.

The methods employed were identical to those described in **Chapter 2**.

■ RESULTS AND DISCUSSION

Hydration of NMA. The hydration characteristics of the NMA atomic sites in pure water at 1 bar were discussed in Part A of this chapter. Focusing on the effect of pressure, we find significant modification of water distribution in the vicinity of NMA methyl groups as pressure increases from 1 bar to 8 kbar (Figures 4B-1 and 4B-2). The water exclusion radius (the smallest distance at which $g(r) = 1$) decreases under pressure. This decrease, although can also be seen at 2 kbar, is easily visible at 8 kbar. At the same time, the first maximum and minimum shift to shorter distances, indicating inward movement of first hydration shell. For the amide methyl group, which has a relatively well-defined first hydration shell at 1 bar, the positions of the first peak and minimum at 8 kbar are ∼0.2

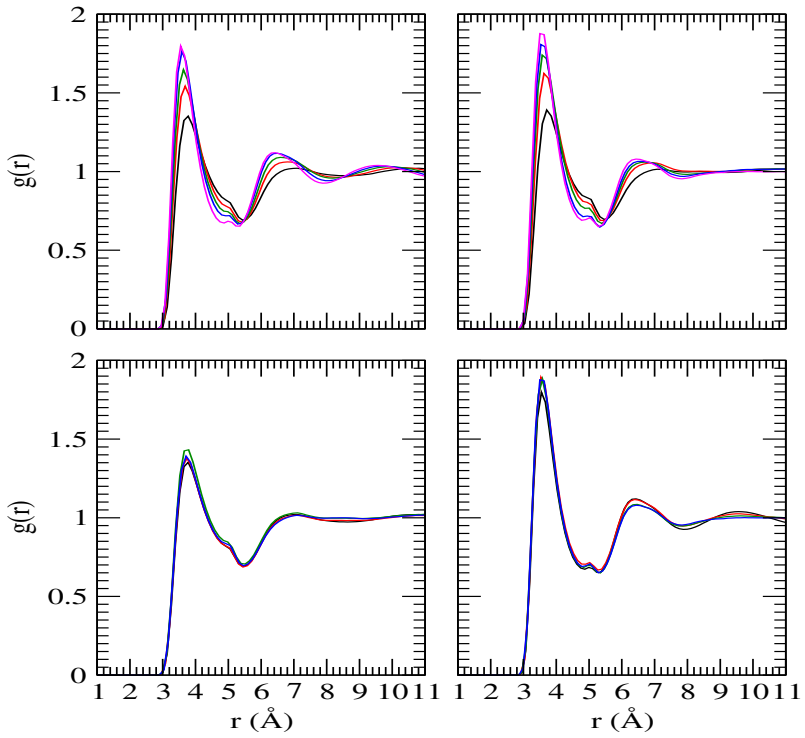

Figure 4B-1. *Site−site distribution functions involving NMA methyl group (Me_1) and water oxygen (Ow) for systems NW (left) and NT4 (right) at 1, 2000, 4000, 6000, and 8000 bar pressures (top) and also at 1 (left) and 8000 (right) bar pressures for systems NW, NT2, NT3, and NT4 (bottom).*

and ∼0.3 Å inward than those at 1 bar. Inward movements are observed also for successive hydration layers. These observations are clear indicators of highly compressed water shell in the vicinity of nonpolar groups. What seems to be more interesting is the monotonic increase in water density at the center of each hydration shell (the peak) and its decrease at the position which separates two hydration layers. These results imply a movement of water molecules from the large-r side in a particular shell toward its short-r side. The

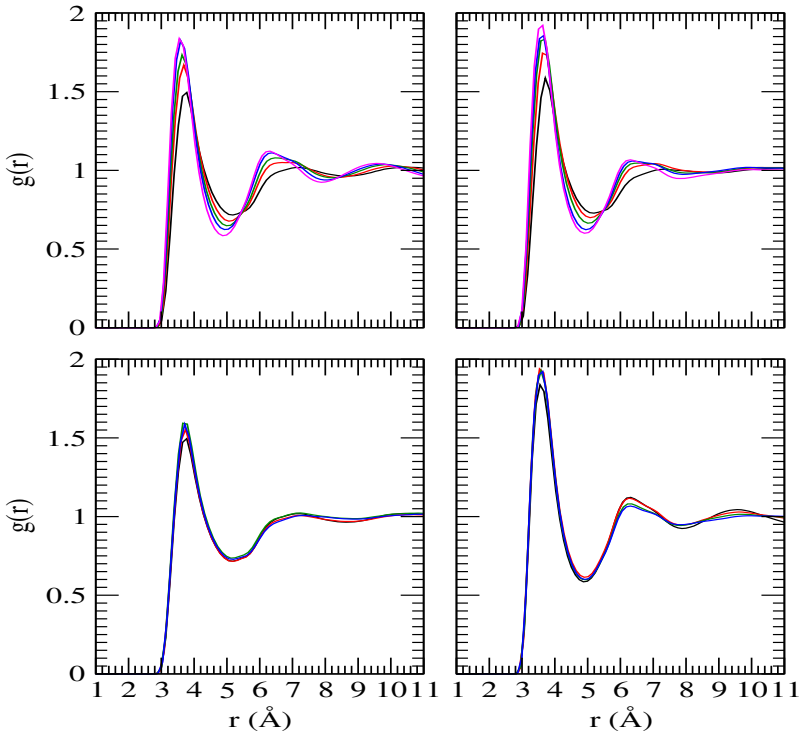

Figure 4B-2. *As in Figure 4B-1 except for the Me_2 group of NMA.*

water movement under pressure thus leads to a reduction in empty spaces in the vicinity of hydrophobic group with higher water density in this region and also makes the hydration shell more structured. Because existence of well-defined hydration layer surrounding a solute is directly related to its dissolution, solvent-separation of hydrophobic contacts at high pressure becomes clear from these results. Note that, more efficient packing of water molecules around hydrophobic solute at high pressures and consequent pressure-induced relative stabilization of the water-separated configuration of nonpolar solute as compared to its associated state were observed in cases of methane (**Chapter 2**) and neopentane (**Chapter 3**) and has also been reported extensively in the literature [7, 99, 141].

The average number of water molecules around selected atomic sites in NMA at

different perturbing conditions chosen are assembled in Table 4B-1. As expected from the behavior of methyl−water rdf, which shows a monotonic increase in the height of the first peak with pressure with significantly compressed water shell, the average number of water molecules in the close proximity of methyl group increases as the pressure is increased. It can be seen that, in the absence of TMAO, as pressure increases from 1 bar through 4000 to 8000 bar, the hydration number for Me_1 increases from 4.9 through 6.5 to 7.7. So, at 8 kbar, there is about 57% increase in hydration number. Similarly, for Me_2 group, high hydrostatic pressure (8 kbar) leads to about 52% increase (from 5.4 to 8.2) of hydration

Table 4B-1. Hydration Number for Selected Atomic Sites of NMA[a]

system	P (MPa)	Me_1	Me_2	O	H
NW	0.1	4.9	5.4	3.8	4.2
	200	6.3	6.8	4.7	5.0
	400	6.5	7.0	4.8	5.0
	600	6.8	7.2	5.1	5.1
	800	7.7	8.2	5.6	5.7
$NT2$	0.1	4.3	4.8	3.2	3.8
	200	5.6	6.1	4.0	4.5
	400	5.9	6.3	4.2	4.6
	600	6.8	7.2	4.7	5.1
	800	7.1	7.6	5.0	5.3
$NT3$	0.1	3.7	4.2	2.8	3.4
	200	4.8	5.2	3.4	3.9
	400	5.1	5.5	3.6	4.1
	600	6.1	6.5	4.2	4.7
	800	7.0	7.4	4.7	5.2
$NT4$	0.1	3.7	4.2	2.7	3.4
	200	4.1	4.5	2.9	3.5
	400	5.1	5.6	3.5	4.1
	600	6.1	6.4	4.0	4.6
	800	6.2	6.5	4.1	4.6

[a]Hydration numbers are obtained by integrating the rdf to 4.0 Å.

number. These observations are in good agreement with general findings that high pressure structures of proteins have more water molecules in its interior than the low pressure structures [13].

TMAO affects water distribution near NMA methyl group only slightly (Figures 4B-1 and 4B-2). The only notable feature about TMAO effect is the prevention of a more structured second hydration shell of methyl groups at high pressure. Although water density in the vicinity of a methyl group is not affected by TMAO, it indeed reduces average hydration number of hydrophobic moiety (Table 4B-1). For the highest TMAO concentration considered (system $NT4$), a 24% decrease of the average hydration number of the carbonyl methyl group (from 4.9 for NW to 3.7 for $NT4$) at 1 bar is observed in this study. The hydration number of methyl group is largely dependent on TMAO concentration at a particular pressure.

Figures 4B-3 and 4B-4 show influences of pressure on the hydration of NMA hydrogen bonding sites in solutions of increasing TMAO concentrations. We find that the first peak in $O-Hw$ and $H-Ow$ rdf profiles does not change its location on application of pressure and the peak height reduces slightly. Also, the first minimum shows an upward movement. The $O-Ow$ rdf follows similar trends with a much more pronounced upward movement at high pressure. These findings reveal a tendency of part of the hydration water to move toward large-r side of the first shell at high pressure. This behavior is quite different from that in the vicinity of nonpolar surfaces where water molecules move from large-r side of the first shell toward its short-r side. Hence, the water shell is much more compressed in the vicinity of nonpolar groups relative to the water shells surrounding hydrogen bonding sites. In fact, it has been reported that while exposure of hydrophobic groups to water is highly favored under pressure, high pressures have little effect on the tendency of a protein to form hydrogen bonds [225]. Enhanced hydration of these hydrogen bonding sites at high pressure can be inferred from Table 4B-1. TMAO leads to enhancement of first peak (Figures 4B-3 and 4B-4) and removes water molecules from the solvation shell (Table 4B-1), indicating its counterbalancing effect against pressure.

The structural, energetic, and dynamical properties of NMA−water hydrogen bonds were investigated for further characterization of NMA hydration. As mentioned earlier, we defined a hydrogen bond by imposing cut-off distances of r_{DA} for $D-A$ (where D is donor and A is acceptor) and r_{AH} for $A-H$, and a simultaneous cut-off angle of 45° for $H-D-A$. Note that, the cut-off distances were determined from the positions of the first minimum in the corresponding rdf at 1 bar for pure water system and these distances

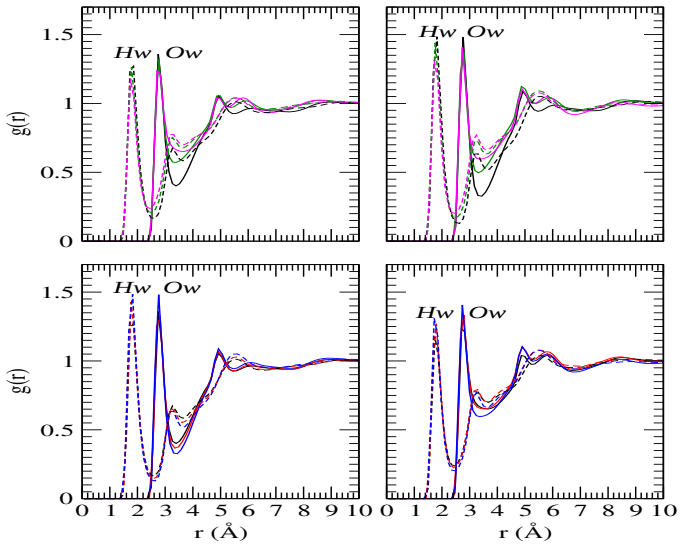

Figure 4B-3. *Site−site distribution functions involving NMA oxygen (O) and oxygen (Ow) and hydrogen (Hw) atoms of water as a function of pressure (top) for systems NW (left) and NT4 (right) and also as a function of TMAO concentration (bottom) for 1 bar (left) and 8 kbar (right) pressures. Color codes are as in Figure 4B-1.*

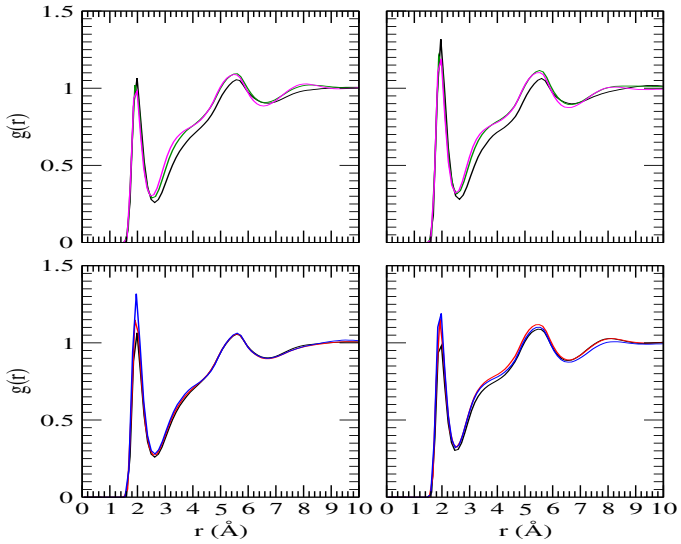

Figure 4B-4. *Site−site distribution functions involving NMA hydrogen (H) and water oxygen (Ow) as a function of pressure (top) for systems NW (left) and NT4 (right) and also as a function of TMAO concentration (bottom) for 1 bar (left) and 8 kbar (right) pressures. Color codes are as in Figure 4B-1.*

were listed in Table 4A-3. Hydrogen bond dynamics were investigated by defining a continuous hydrogen bond correlation function, $S_{HB}(t)$, as discussed in **Chapter 2** (Eq. 2.8).

The average number of NMA−water hydrogen bonds per NMA molecule at different conditions chosen are presented in Table 4B-2 together with their energies and life-times. Some points are particularly interesting to be noted here. (a) In presence of water only, NMA oxygen can form about 1.7 hydrogen bonds with water which is about 2 times larger

Table 4B-2. NMA−Water Hydrogen Bond Properties[a]

		$O-Hw$			$H-Ow$		
system	P (MPa)	n_{HB}	E_{HB}	τ_{HB}	n_{HB}	E_{HB}	τ_{HB}
NW	0.1	1.69	-20.02	1.20	0.75	-19.64	0.71
	200	1.74	-19.73	1.18	0.79	-19.20	0.72
	400	1.75	-19.45	1.13	0.82	-18.94	0.84
	600	1.74	-19.26	1.11	0.83	-18.78	0.87
	800	1.80	-18.97	1.00	0.88	-18.31	0.94
$NT2$	0.1	1.55	-20.30	1.53	0.75	-19.86	0.79
	200	1.58	-20.02	1.53	0.77	-19.41	0.87
	400	1.57	-19.79	1.45	0.79	-18.94	0.91
	600	1.60	-19.53	1.42	0.82	-18.70	0.94
	800	1.60	-19.35	1.31	0.83	-18.56	0.96
$NT3$	0.1	1.42	-20.48	1.75	0.69	-20.07	0.88
	200	1.51	-20.22	1.65	0.74	-19.41	0.91
	400	1.51	-19.97	1.54	0.77	-19.09	0.97
	600	1.43	-19.69	1.66	0.74	-18.81	1.09
	800	1.49	-19.48	1.60	0.79	-18.63	1.18
$NT4$	0.1	1.35	-20.75	1.91	0.70	-20.09	0.88
	200	1.38	-20.38	1.95	0.71	-19.62	1.03
	400	1.43	-20.03	1.90	0.76	-19.10	1.06
	600	1.46	-19.80	1.79	0.78	-18.74	1.08
	800	1.45	-19.74	1.59	0.81	-18.57	1.18

[a] n_{HB}, E_{HB}, and τ_{HB} represent average number, energy (in kJ mol^{-1}), and life-time (in ps), respectively.

than the average number of $NH \cdots OwHw$ bonds. Hydrogen bond life-time is also much smaller for the latter, although these hydrogen bonds are approximately isoenergetic. (b) For both types of hydrogen bonds, hydrogen bond number increases with increasing pressure and the attractive interaction reduces. Unlike these similar trends for number and energy, hydrogen bond life-time follows opposite trend with pressure reducing life-time of $CO \cdots HwOw$ bond and enhancing $NH \cdots OwHw$ bond life-time. Influence of pressure on hydrogen bond properties is, however, not very significant. (c) TMAO reduces number of NMA−water hydrogen bonds, makes these hydrogen bonds energetically attractive, and enhances their life-times. The carbonyl oxygen shows higher sensitivity to the presence of TMAO. Corroborative evidence for higher life-time of $CO \cdots HwOw$ hydrogen bond as compared to that of $NH \cdots OwHw$, and TMAO-induced enhancement of these hydrogen bonds can be seen in Figure 4B-5, which illustrates slower relaxation of $S_{HB}(t)$.

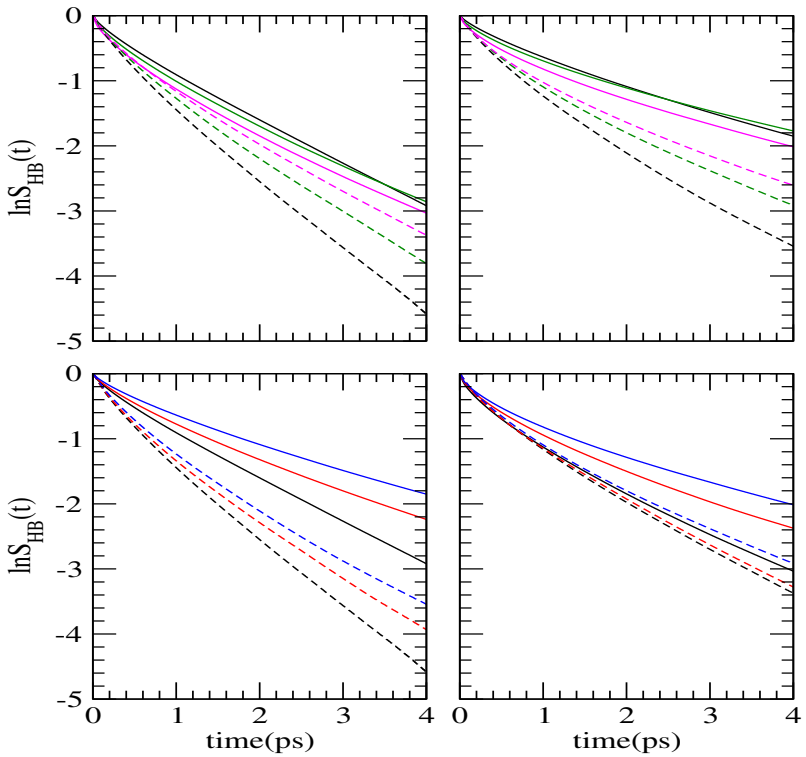

Figure 4B-5. *Time dependence of the continuous NMA−water hydrogen bond correlation function, $S_{HB}(t)$, as a function of pressure (top) for systems NW (left) and NT4 (right) and also as a function of TMAO concentration (bottom) for 1 bar (left) and 8 kbar (right) pressures. Color codes are as in Figure 4B-1. Solid and dashed lines are for $CO \cdots HwOw$ and $NH \cdots OwHw$ hydrogen bonds, respectively.*

To present the effects of TMAO on hydrogen bond energy under high pressure conditions, the probability distributions of NMA−water hydrogen bond energies are shown in Figures 4B-6 and 4B-7. We first notice that, the distribution is not uniform with the maximum probability at about -23 kJ mol^{-1} for $CO \cdots HwOw$ and $NH \cdots OwHw$ hydrogen bonds for the system NW at 1 bar. Also, the energy distribution is relatively broader for amide hydrogen bond. Clearly, applied pressure increases probability in the low energy (less negative) region and at the same time, decreases probability in the high energy (more negative) region. Therefore, the evidence here is that NMA−water hydrogen bonds are destabilized at high pressure. Figure 4B-6 shows that TMAO stabilizes hydrogen bonds between carbonyl oxygen and water. This is indicated by higher probabilities in the high energy region and lower probabilities in the low energy region compared to those with the pure water system. However, energy distribution of $NH \cdots OwHw$ hydrogen bond changes barely when TMAO is added to the system.

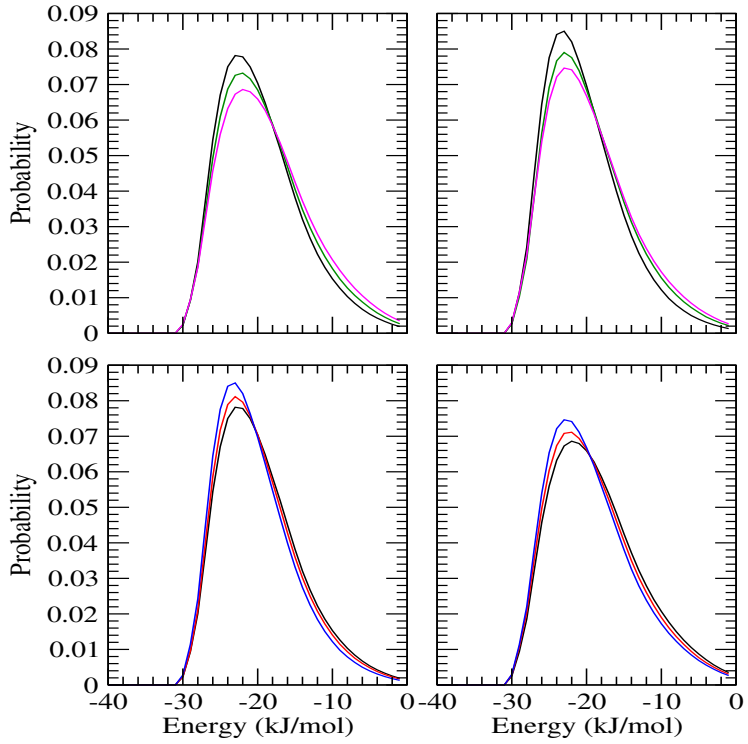

Figure 4B-6. *Probability distribution of $CO \cdots HwOw$ hydrogen bond energies as a function of pressure (top) for systems NW (left) and NT4 (right) and also as a function of TMAO concentration (bottom) for 1 bar (left) and 8 kbar (right) pressures. Color codes are as in Figure 4B-1.*

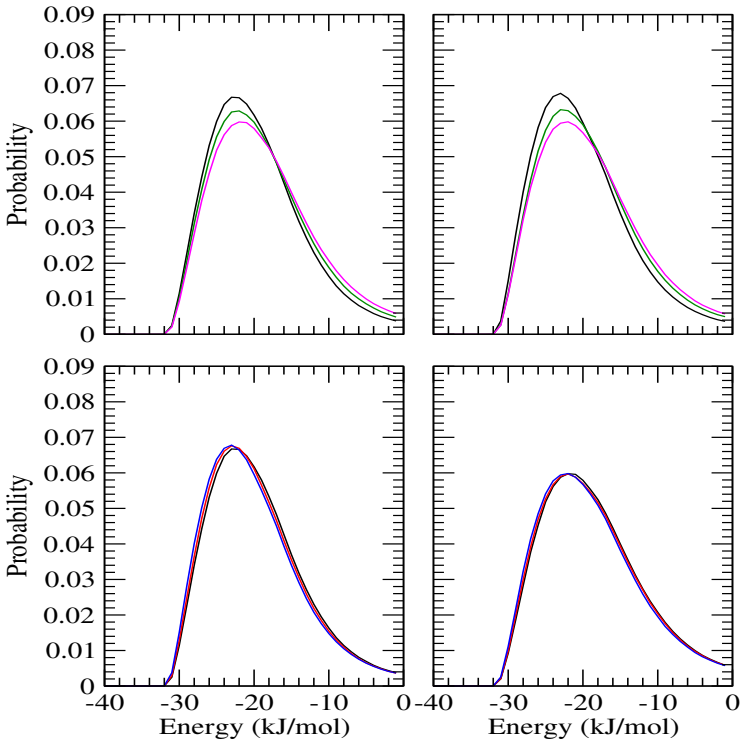

Figure 4B-7. *As in Figure 4B-6 except for $NH \cdots OwHw$ hydrogen bond.*

Thus a thorough investigation of the hydration characteristics of different atomic sites in NMA in pure water and in aqueous solutions of TMAO at different pressure conditions reveals that, application of high pressure leads to significant compression of hydration layers of hydrophobic groups and the number of water molecules in the vicinity of both nonpolar groups and hydrogen bonding sites increases. Some new hydrogen bonds between NMA and water start to form and the relative population of weaker hydrogen bonds increases at the extreme pressure condition. TMAO, on the other hand, can offset the pressure-induced enhanced hydration of NMA atomic sites. It reduces number of NMA−water hydrogen bonds, makes these hydrogen bonds energetically stronger, and also slows down the decay of these hydrogen bonds with time. All these findings are consistent with protein denaturation at high pressure and TMAO-induced counteraction. Two possible ways to investigate the underlying mechanism by which protein hydration is influenced by TMAO under high pressure conditions are to examine the direct interaction of TMAO with protein residues (which eventually competes with water) and also the indirect effect of TMAO on water structure. In the following, we have discussed both of these two possibilities in aqueous NMA solutions at different environments.

Direct Interaction of TMAO with NMA. Selected rdfs between atomic centers of NMA and TMAO are shown in Figure 4B-8. For system $NT2$ at 1 bar, the rdf between the TMAO carbon (Ct) and the carbonyl methyl group (Me_1) in NMA has a first peak at about 3.9 Å with peak magnitude 1.4. Similar observations are made for amide methyl group (Me_2) in NMA. These show that TMAO can interact directly with hydrophobic residue through its methyl groups. TMAO interaction occurs also with NMA oxygen through its methyl groups, though hydrogen bonding interaction between these two is unlikely. On the other hand, while rdf profiles reveal a strong tendency of TMAO oxygen to form hydrogen bonds with amide N, the hydrogen bond number between NMA and TMAO is very small (see Part A of this chapter). Note that lack of hydrogen bonding sites for TMAO in peptide backbone have been suggested in a number of studies [72, 210]. TMAO was shown to form only 0.1 hydrogen bonds with amide N for glycine peptides (2 to 5 residues) [210], whereas 1.2 hydrogen bonds were found between TMAO and the fully extended configuration of a

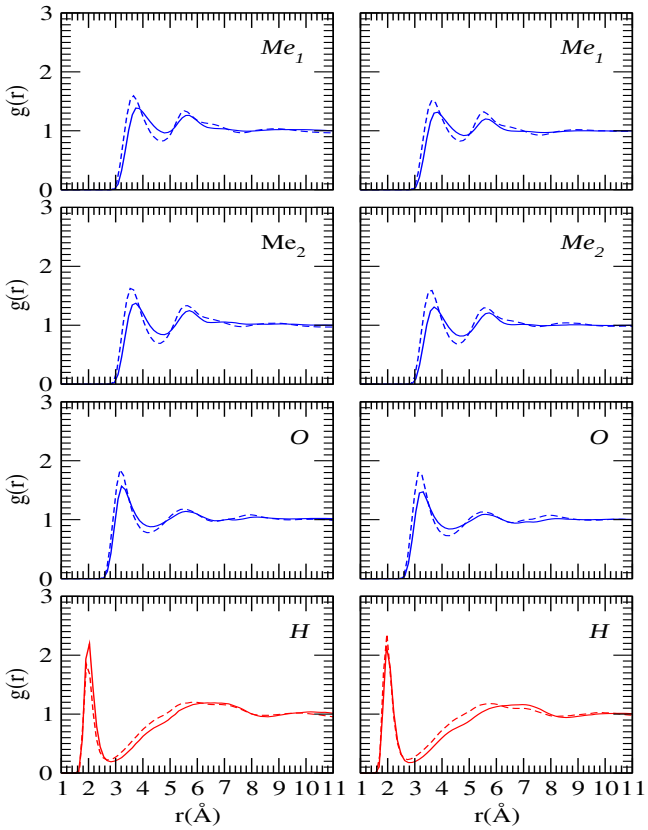

Figure 4B-8. *NMA−TMAO site−site distribution functions for systems NT2 (left) and NT4 (right) at 1 bar (solid) and 8 kbar (dashed) pressures. Red and blue lines are for TMAO oxygen (Ot) and carbon (Ct), respectively.*

decaalanine peptide [72].

To examine the solvation of NMA more closely, we calculated the time-averaged normalized ratio (τ_i) of component i using Eq. 2.7. Figure 4B-9 shows the τ_i values for different atomic sites in NMA as a function of distance. The points that emerge from this figure are relative accumulation of TMAO near NMA methyl groups and oxygen atom in a solvation shell beyond exclusion radius and TMAO's relative exclusion from the vicinity of amide hydrogen at low (1 bar) as well as at high pressure (8 kbar).

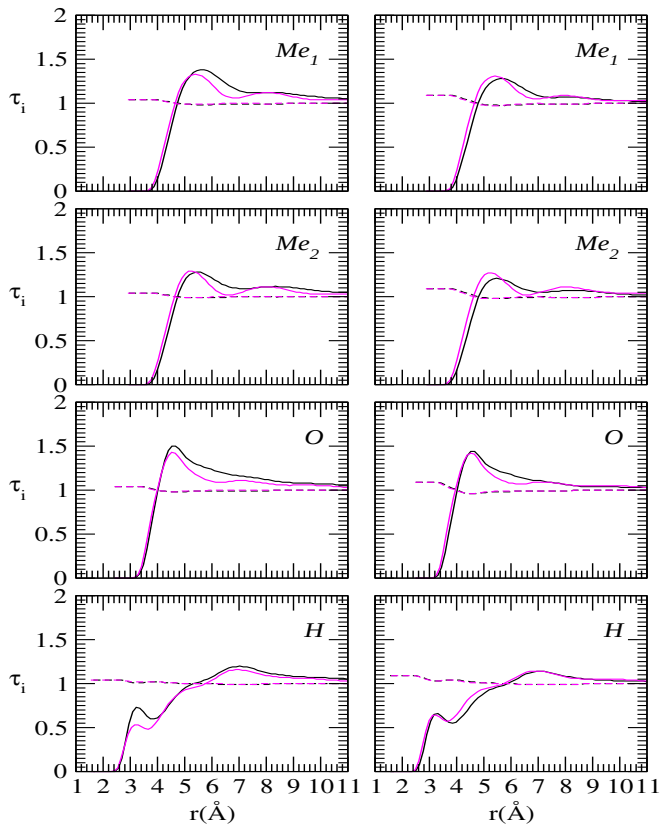

Figure 4B-9. *Time-averaged normalized fractions, τ_i, of water (dashed) and TMAO (solid) central atoms as a function of the distance from NMA atomic sites in NT2 (left) and NT4 (right) at 1 bar and 8 kbar pressures.*

Hence, TMAO is found to interact with NMA atomic sites through its methyl groups and oxygen atom. Additionally, although TMAO has some tendency to form hydrogen bonds with NMA hydrogen, the interaction efficiency is low, causing its relative exclusion near amide hydrogen. The existence of TMAO interaction sites in the vicinity of NMA sites can be expected to reduce hydration number of these sites, as observed in coordination number analysis.

Effect of TMAO on Water Properties at High Pressure. It has been suggested in the literature that TMAO can interact strongly with water to form di- and/or tri-hydrated TMAO complexes in solution [67, 68, 76-78]. In **Chapter 3**, we examined the behavior of water molecules in the vicinity of both hydrophobic (methyl) and hydrogen bonding (oxygen) sites in TMAO as a function of its concentration at different pressures. TMAO molecules were found to be well solvated by water molecules at ambient pressure conditions. Number of hydrogen bonded water molecules to TMAO oxygen enhanced slightly at high pressure. Moreover, total number of TMAO−water hydrogen bonds increased with increasing concentration of TMAO. We pointed out that the number of water molecules required to solvate all TMAO molecules present in the system increases at high TMAO contents.

To shed light on the indirect effect of TMAO solvation on water properties, we examined the structural and dynamical properties of water at different pressure conditions with increasing concentration of TMAO.

In Figure 4B-10, we have shown water oxygen−oxygen ($Ow-Ow$) rdf as a function

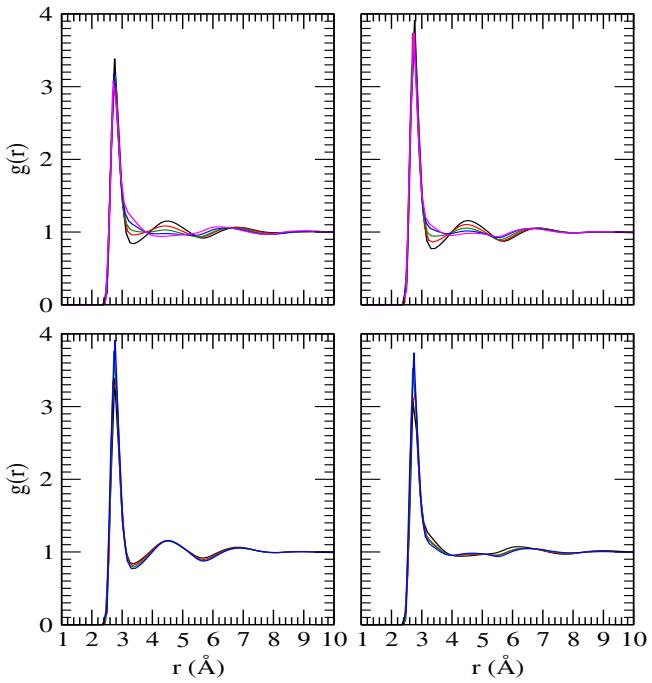

Figure 4B-10. *Water oxygen−oxygen site−site distribution functions as a function of pressure (top) for systems NW (left) and NT4 (right) and also as a function of TMAO concentration (bottom) for 1 bar (left) and 8 kbar (right) pressures. Color codes are as in Figure 4B-1.*

of pressure as well as of TMAO concentration. In pure water at 1 bar, the first and second peaks, that characterize the hydrogen bonded first neighbor and the tetrahedrally located second neighbor, appear at about 2.8 and 4.5 Å, respectively. On average, 4.7 identical neighbors are found for each water molecule by integrating the rdf to 3.4 Å (location of first minimum in the rdf). The average coordination number of water in the bulk was reported as 5.2 at 1 bar and 300 K [226]. With the facts that the number reduces in the vicinity of a large solute [226] and 20 large NMA molecules are present in our simulation system taken into consideration, the coordination number observed here agree quite well with that study.

There is a remarkable influence of pressure on water structure. To be specific, while the first peak does not show any significant pressure sensitivity, the changes in the first minimum (∼3.4 Å) and the second peak (∼4.5 Å) are easy to notice. These observations are consistent with both experiments [21] and computer simulations [21, 227] and are clear indicators for movement of part of the water molecules in the second shell toward the first shell, filling the empty spaces in this region. Thus, the first shell of water is crowded at high pressure and there is a collapse of second water hydration shell.

The counteracting effect of TMAO on pressure-induced water structure modification is reflected in Figure 4B-10. TMAO enhances the first peak and makes the first valley deeper. The first and second water shells are, therefore, more defined in the presence of TMAO. In other words, TMAO enhances water structure. It is important to be quite clear that, this water structure making property of TMAO is equally valid under high pressure conditions (see bottom-right panel in Figure 4B-10).

The pressure and TMAO concentration dependence of the local structure of water is elucidated further by tabulating the average number (N_H) of water oxygen around water oxygen within a shell of 3.4 Å for all simulated systems (Table 4B-3). The enhancement in the number of identical neighbors in the first shell of water can be seen immediately in this table. We observe that, in pure water, the coordination number increases from 4.67 at 1 bar to 6.33 at 8 kbar (an increase of about 35%). Table 4B-3 also reveals that, TMAO reduces the number of near neighbor water molecules. There is a decrease of coordination number by 20% at 1 bar as we move from pure water system (4.67) to the system containing 40 TMAO molecules (3.75). The decrease of coordination number for these two systems is found to be 29% at 8 kbar.

Table 4B-3 also depicts the average number, energy, and life-time of water−water hydrogen bonds for all of the systems considered. Among the 4.67 first shell water molecules

in pure water at 1 bar, 75% (n_{HB}=3.52) are hydrogen bonded to the central water molecule. The water−water average hydrogen bond energy is about -19 kJ mol^{-1}, which is weaker than those between NMA and water by about 1 kJ mol^{-1} (see Table 4B-2). In addition, while the life-time of water−water hydrogen bond (1.25 ps) is similar to that of $CO\cdots HwOw$ (1.20 ps), it is much higher than that of $NH\cdots OwHw$ (0.71 ps). High pressure increases the number of hydrogen bonds, as expected from increased water crowding. For example,

Table 4B-3. Properties of Water First Shell[a]

system	P (MPa)	N_H	n_{HB}	E_{HB}	τ_{HB}
NW	0.1	4.67	3.52	-19.17	1.25
	200	5.29	3.60	-18.80	1.23
	400	5.35	3.64	-18.54	1.21
	600	5.48	3.72	-18.28	1.18
	800	6.33	3.74	-18.07	1.19
$NT2$	0.1	4.20	3.35	-19.41	1.47
	200	4.71	3.44	-19.14	1.51
	400	4.80	3.48	-18.85	1.52
	600	4.90	3.48	-18.65	1.51
	800	5.56	3.54	-18.45	1.49
$NT3$	0.1	4.15	3.32	-19.53	1.60
	200	4.67	3.37	-19.28	1.66
	400	4.75	3.40	-19.02	1.65
	600	4.86	3.43	-18.78	1.66
	800	4.95	3.46	-18.61	1.65
$NT4$	0.1	3.75	3.20	-19.73	1.77
	200	4.17	3.25	-19.44	1.82
	400	4.69	3.29	-19.19	1.81
	600	4.83	3.31	-19.02	1.88
	800	4.89	3.36	-18.82	1.89

[a] N_H, n_{HB}, E_{HB}, and τ_{HB} represent average number of water oxygen around water oxygen within a shell of 3.4 Å, average number of hydrogen bonds, energy (in kJ mol^{-1}), and life-time (in ps) of water−water hydrogen bonds, respectively.

in the absence of TMAO, average hydrogen bond number increases from 3.52 to 3.64 and then to 3.74 as pressure increases from 1 through 4000 to 8000 bar. Slight reduction in hydrogen bond energy (less negative) and life-time of these hydrogen bonds are observed at high pressure. It is important to emphasize that, the fraction (n_{HB}/N_H) of hydrogen bonded water molecule in the first shell decreases at high pressure (Figure 4B-11). For the maximum pressure chosen, this decrease is found to be about 0.16. So, although number of nearest identical neighbors per water molecule increases at high pressure with consequent increase in average hydrogen bond number, a relatively higher fraction of first shell water molecules do not participate in these hydrogen bonds. This feature of water under high pressure is likely why pressure increases hydration of NMA molecules and, extended to proteins, leads to water penetration. Transferring water from its (water) first shell allows them to move freely in the bulk, giving an entropic profit to the system; and at the same time, it does not disturb water hydrogen bond network much (less energy loss). Our results are consistent with the notion that translational entropy relaxation in bulk water is an important factor in water penetration and consequent protein denaturation at high pressure [17-19].

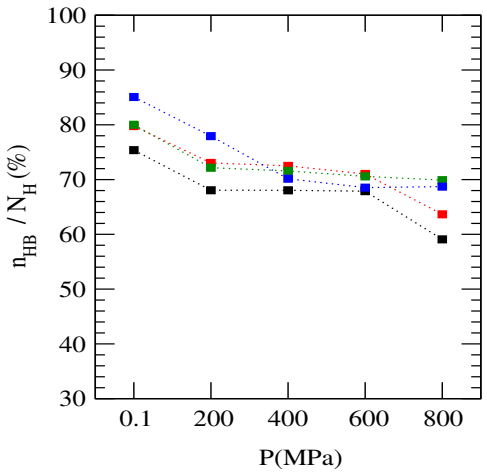

Figure 4B-11. *Fraction of hydrogen bonded water molecules in the radial shells of 3.4 Å as a function of pressure for systems NW, NT2, NT3, and NT4.*

Focusing on the influence of TMAO on water hydrogen bonding network, we find reduced number of hydrogen bonded water molecule. Few additional points that are of importance are: TMAO makes hydrogen bonds more attractive, leads to a slower relaxation of water hydrogen bond network, and enhances the fraction (n_{HB}/N_H) of hydrogen bonded

water molecule in the first shell at a particular pressure (Figure 4B-11). At 1 bar, the difference in fraction of hydrogen bonded water molecule between systems NW and $NT4$ is 0.10. Thus, TMAO shows a tendency to increase the fraction of hydrogen bonded water molecules. Since the first shell water molecules are largely associated through strong hydrogen bonds in the presence of TMAO, the penalty of removing a water molecule from the water solvation shell will increase (due to large energy loss) and hence, the NMA hydration process will be decelerated. The reduced number of hydrogen bonded water molecule in the presence of TMAO can be viewed in terms of less number of first shell water molecules. Previous simulation study by Zou *et al.* [67] showed water structure enhancement by TMAO in the form of a slight increase in the number of water−water hydrogen bonds per water molecule, whereas the data obtained by Pettitt and co-workers [70, 72] demonstrated no evidence for an increase in the water hydrogen bonding structure caused by the addition of TMAO. Though our hydrogen bond analysis agree with the results obtained by Pettitt and co-workers, it also suggests that, TMAO does enhance water hydrogen bonding network by increasing fraction of hydrogen bonded first shell water molecules and making these hydrogen bonds stronger.

Slight changes in water−water hydrogen bond life-time at high pressure and TMAO-induced enhancement of the same is reflected in the slight change in the hydrogen bond correlation function, $S_{HB}(t)$, as displayed in Figure 4B-12. The probability distributions of water−water hydrogen bond energies are shown in Figure 4B-13. Pressure-induced destabilization of water hydrogen bonding network and the counteracting effect of TMAO can be suggested immediately from this figure. We observe that, probability of water−water hydrogen bonds with high energy (more negative) reduces on application of pressure and more and more low energy (less negative) hydrogen bonds form under such conditions. When TMAO is added to the system, the energy distribution shift toward higher energy side, indicating hydrogen bond network stabilization by TMAO.

In Figure 4B-14, we have shown the fraction (f_n) of water molecules that engage in n number of hydrogen bonds with identical species as a function of TMAO concentration as well as of pressure. In the absence of TMAO, most of the water molecules are 3- and 4-coordinated and there are small fractions of 2- and 5-coordinated water molecules. Application of pressure increases the fraction of 5-coordinated water molecules and reduces the fraction of 2- and 3-coordinated water molecules. The observed pressure-induced enhancement of higher coordinated water molecules is in excellent agreement with previous MC simulation results for methane−water system at different pressures [136]. An opposite

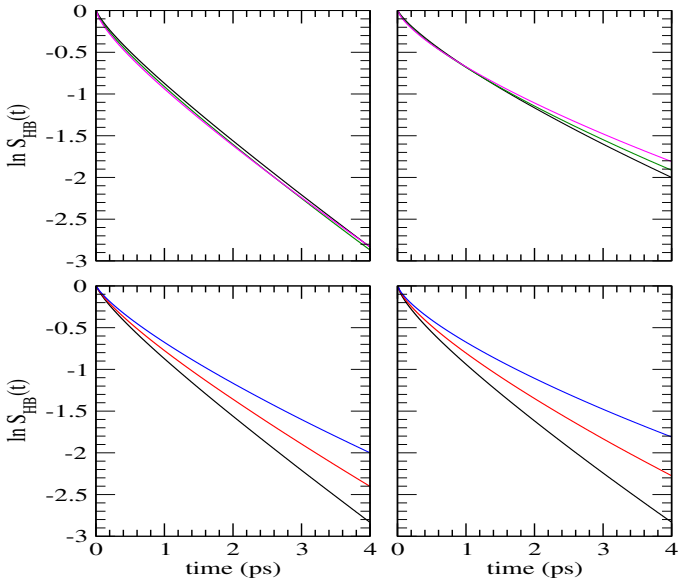

Figure 4B-12. *Time dependence of the continuous water−water hydrogen bond correlation function, $S_{HB}(t)$, as a function of pressure (top) for systems NW (left) and NT4 (right) and also as a function of TMAO concentration (bottom) for 1 bar (left) and 8 kbar (right) pressures. Color codes are as in Figure 4B-1.*

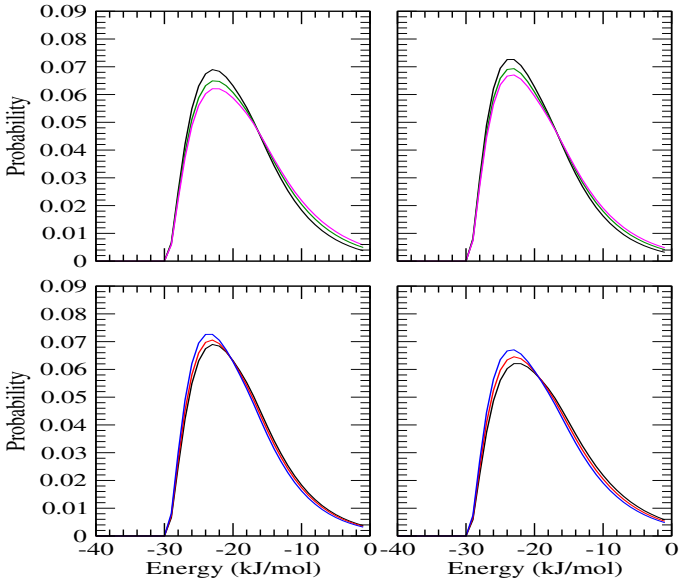

Figure 4B-13. *Probability distributions of water−water hydrogen bond energies as a function of pressure (top) for systems NW (left) and NT4 (right) and also as a function of TMAO concentration (bottom) for 1 bar (left) and 8 kbar (right) pressures. Color codes are as in Figure 4B-1.*

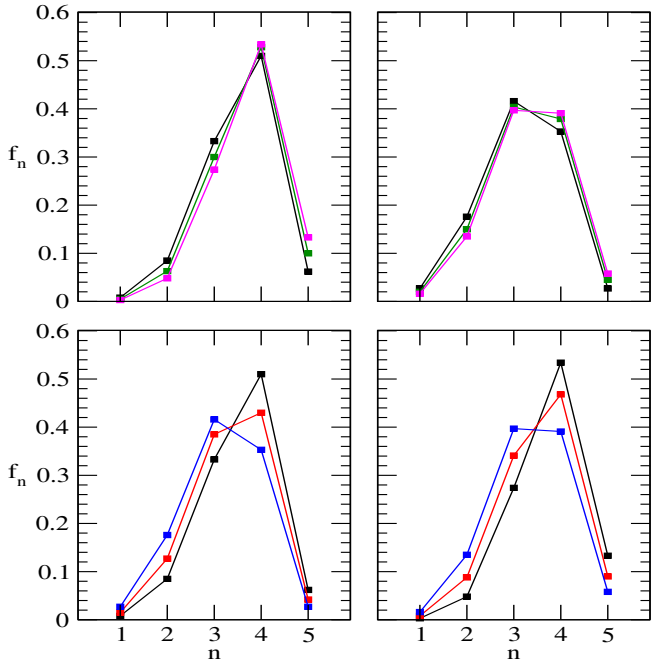

Figure 4B-14. *Fraction of water molecules with n number of hydrogen bonds with identical species as a function of pressure (top) for systems NW (left) and NT4 (right) and also as a function of TMAO concentration (bottom) for 1 bar (left) and 8 kbar (right) pressures. Color codes are as in Figure 4B-1.*

effect of TMAO can be seen in this figure. It reduces number of higher coordinated (4 and 5) water molecules and increases fraction of 2- and 3-coordinated water molecules. Thus, water molecules are mostly separated in the presence of TMAO and this is due to the solvation of large TMAO molecules. Note that, to accommodate a solute, water molecules must have to create a cavity first which is associated with alteration of water hydrogen bonding network. While a small molecule can be accommodated easily without any significant perturbation of hydrogen bond network, water cannot maintain this network in the presence of a large solute and loses higher coordinated identical neighbors. The effect was previously discussed in **Chapter 3**. The total number of water molecules that solvate TMAO increases with increasing TMAO concentration and this is reflected in enhancement of lower coordinated water molecules with reduction of higher coordinated water molecules with increasing TMAO concentration.

■ SUMMARY AND CONCLUSIONS

Employing the MD simulation technique, hydration characteristics of hydrophobic and hydrogen bonding sites in NMA were investigated in aqueous solutions of increasing TMAO

concentration each at five different pressures ranging from 1 bar to 8 kbar. The goal of this study was to understand the mechanism of protein protection by TMAO under high pressure conditions. Computing site−site rdfs, we made following observations at high pressure: (a) In the vicinity of hydrophobic group, water molecules move from large-r side of the first shell toward its short-r side, filling empty spaces in this region and at the same time, making the hydration shell more defined. (b) The behavior is different near the hydrogen bonding sites in that part of the hydration water is transferred to large-r side of the first shell. These observations are consistent with the suggestion that the water shell is much more compressed in the vicinity of nonpolar groups as compared to that of hydrogen bonding sites [228, 229] and also with the notion that, while exposure of hydrophobic groups to water is highly favored under pressure, high pressure has little effect on the tendency of a protein to form hydrogen bonds [225]. TMAO did not affect the water distribution much. Nonetheless, the hydration number of NMA sites which showed enhancement at high pressure, was found to be smaller upon addition of TMAO. Solvation characteristics of NMA sites were further explored in terms of NMA−water hydrogen bonds imposing geometric criteria. It was observed that, the number of hydrogen bonds formed by NMA oxygen with water is about 2 times larger than that by NMA hydrogen and although these hydrogen bonds have similar energy, the hydrogen bond relaxation is much slower for the former. Pressure-induced enhancement in hydrogen bond number and its reduction in the presence of TMAO were also observed. It was evident from analysis of hydrogen bond energy distribution that pressure destabilizes NMA−water hydrogen bonds, whereas TMAO increases population of more stable hydrogen bonds. TMAO was also seen to slow down the decay of NMA−water hydrogen bonds. All these results revealed counteracting effect of pressure and TMAO on NMA hydration.

To shed light on the counteracting mechanism, we then examined interaction of TMAO with NMA and the structural and dynamical properties of water at different pressure conditions with increasing concentration of TMAO. TMAO was found to interact directly with NMA atomic sites through its methyl groups and oxygen atom. Significant changes in water structure were observed both at high pressure and in the presence of TMAO. In particular, water molecules in the second shell were transferred to the first shell under high pressure conditions, leading to collapse of the second water shell and enhancement in the number of nearest neighbor water molecules. High pressure enhanced number of nearest identical neighbors per water molecule with consequent increase in average hydrogen bond number. Number of higher coordinated (5) water molecules were found to

increase with reduction in the number of lower coordinated (2 and 3) water molecules. The findings that, the relative number of water molecules that do not participate in hydrogen bonding increases and the population of more stable hydrogen bonds reduces with increasing pressure, were of significant interest. These findings suggest that water molecules are crowded at high pressure with a relatively destabilized hydrogen bond network. On the contrary, TMAO influenced water properties in a manner that oppose the effects of pressure. Compared to that for pure water, the first and second shells of water were found to be more defined in the presence of TMAO. TMAO not only reduced number of nearest identical neighbors of water but also enhanced relative number of first shell water molecules that participate in water hydrogen bond network. Additionally, population of more stable hydrogen bonds was found to increase upon addition of TMAO and hydrogen bonds relaxed slowly in these systems, which agree with other simulation findings that TMAO enhances water−water hydrogen bond life-time [73]. The effects of pressure and TMAO on water properties are thus consistent with their role on NMA hydration.

The observed water crowding at high pressure with some 'free' water molecules and a relatively destabilized hydrogen bond network explains the reason behind water penetration into the protein interior at high pressure. Without neglecting the essential role of the direct interaction between TMAO and backbone oxygen in protein stabilization, we conclude this part by suggesting that the counteracting effects of TMAO and pressure on the water structural properties play a crucial role in the ability of TMAO to offset protein denaturation under high pressure conditions.

Chapter 5

Solvation of Polypeptide Residues

"....the transfer of the peptide conformations to binary urea solution is dominated by the favorable vdW contribution, which overcomes the unfavorable electrostatic contribution and creates a better solution environment for the peptide. This is in contrast with the binary TMAO solution that does not have a significant favorable contribution from the vdW component to balance the strongly unfavorable electrostatic component and causes the TMAO solution to be an unfavorable solution environment for the peptide."

– H. Kokubo, C. Y. Hu, and B. M. Pettitt *J. Am. Chem. Soc.* **133**, 1849 (2011)

So far, our focus has been on the effects of pressure and osmolyte on solvation of hydrophobic and amide groups. We found pressure-induced dissolution of nonpolar group and, additionally, much more compression of water molecules in the close proximity of hydrophobic groups than the hydrogen bonding sites, in general agreement with the suggestion that the water shell is much more compressed in the vicinity of nonpolar groups as compared to that of hydrogen bonding sites [228, 229] and also with the notion that, while exposure of hydrophobic groups to water is highly favored under pressure, high pressure has little effect on the tendency of a protein to form hydrogen bonds [225]. On the other hand, osmolytes interacted directly with both hydrophobic and hydrogen bonding sites of solute molecules, causing dehydration. Aggregate of large hydrophobic solute formed in pure water was seen to dissolve in presence of the denaturant urea, and urea showed significant tendency to act both as hydrogen bond donor and acceptor. The protein protectant TMAO, in contrast, seemed to be neutral towards hydrophobic interaction and reduced efficiency of amide oxygen to form favorable hydrogen bonds with solution species. Although these findings provide a molecular level explanation of TMAO-induced protein stabilization and counteraction of pressure- and urea-conferred protein denaturation, it is necessary to extend the investigation to more realistic protein systems. The work presented in this chapter is motivated by this necessity.

The chapter is divided into two parts. In Part A, we focus on interaction of protein residues with solution species in the presence and absence of urea and TMAO at 1 bar. Part B, on the other hand, concentrates on TMAO's influence on polypeptide solvation at high pressure.

Part A:

Solvation of Polypeptide in Water and Aqueous Solutions of Urea and TMAO

Overview: To provide a molecular level understanding of how TMAO protects proteins in highly concentrated urea solution, we report here MD simulation results of a 15-residue model peptide in the presence and absence of urea and TMAO. Analysis of solvation characteristics reveals direct interactions of urea and TMAO with peptide residues. Preferential accumulation of urea near the peptide surface and preferential exclusion of TMAO from the peptide surface are observed. Solvation of peptide residues are investigated more closely by calculating the number of hydrogen bonds between the peptide and solution species. It is found that number of hydrogen bonds formed by the peptide with solution species increases in binary urea solution (relative to pure water) and this relative enhancement in hydrogen bond number reduces upon addition of TMAO. Comparison of total number of heavy atom contacts and the hydrogen bond number between the peptide and solution species in binary and ternary solutions of urea indicates TMAO's ability to offset urea-induced relative stabilization of the extended state over the folded state. Our simulation results also suggest that, in the ternary solution, the peptide solvation layer is better mixed in terms of water and urea as compared to binary urea solution. We discuss how these results give an explanation for the strong ability of TMAO to protect proteins in highly concentrated urea solution.

■ INTRODUCTION

A major topic of research in recent years has been the behavior of protein in aqueous solutions of urea and/or TMAO. Classical MD simulations were undertaken extensively to study the urea-mediated denaturation of a number of proteins and polypeptides [32, 35, 48-50, 120, 230-236]. Simulations of the protein CI2 in 8 M urea at 60°C by Bennion and Daggett [50] showed rapid protein unfolding through expansion of the hydrophobic core. Urea interacted directly with the peptide backbone, and the average residence times for urea around protein hydrophobic and hydrophilic residues were found to be greater than the corresponding water residence times [50]. Using the extensive (μs) MD trajectory of hen egg-white lysozyme in 8 M urea, Berne and co-workers [35] found stronger dispersion interactions between urea and the protein fractions (the backbone and side-chains) than those for water, causing intrusion of urea into the protein interior and to urea's preferential binding to all regions of the protein. To reduce the complexity in the interactions between solution species and protein residues, many simulations focused on small peptides, providing useful informations [49, 72, 237, 238]. Pettitt and co-workers [72] simulated a decaalanine peptide in multiple conformations of the denatured ensemble in binary urea solution to show the importance of the vdW contribution to the solvation effect of urea as seen previously [35, 210]. Addition of urea to pure water was shown to stabilize the extended states more than the compact helix through enhancement of more favorable protein−urea vdW interactions [72]. Also demontrated in the literature was better solution environment for a 'side-chainless' peptide backbone model, oligoglycine, in binary urea solution, forcing the peptide to adopt significantly more swollen states as compared to the model in pure water [238].

Focusing on the effect of TMAO, the favorable vdW contribution of TMAO to the solvation effect of decaalanine peptide was found to overcome by its unfavorable electrostatic contribution and, consequently, it was suggested that TMAO stabilizes the compact helix more than the extended states through reduction of less favorable protein−TMAO electrostatic interactions [72]. Similarly, Hu *et al.* [70] observed shifting of protein backbone (a oligoglycine model) towards a more collapsed state in TMAO solution as compared to pure water due to preferential exclusion of TMAO from the local region surrounding the backbone. Although there is general agreement on the preferential TMAO exclusion from the protein surface [63-66, 69], TMAO interaction with the peptide backbone and positively charged side-chains has also been reported in the literature [73-75]. In particular, utilizing

all-atom MD simulations of a number of model dipeptides and an intrinsically disordered $A\beta_{16-22}$ monomer in aqueous TMAO solution, Cho *et al.* [74] showed TMAO's tendency to form hydrogen bonds preferentially with the positively charged side-chains and the exposed dipeptide backbone; the $A\beta_{16-22}$ monomer, however, shifted from random coil to α-helical secondary structure at high TMAO concentrations.

Herein, to provide a molecular level understanding of how TMAO protects proteins in highly concentrated urea solution, we have reported MD simulation results on a 15-residue model peptide in pure water as well as in binary and ternary solutions of urea and TMAO. Computationally, it is difficult to capture complete unfolding of protein by urea due to high protein unfolding times and often high temperature has to be used to observe protein unfolding. So to see the interactions of these two osmolytes with folded and unfolded proteins, we have used here two different conformations of the model peptide. The first (denoted as **F**) is designed to maximize helicity and represents typical α-helix of proteins where backbone cannot interact freely with the surrounding solution species. The second (denoted as **U**) is the fully extended conformation of the peptide and represents unfolded state of proteins. We have allowed the peptide to fluctuate (i.e. flexible model) in aqueous solutions and so the **F** and **U** states are ensembles of conformations which are 'folded' and 'unfolded', respectively. It is also needed to mention that, for the **F** state of the peptide, only residues $4-12$ are in α-helical regions. That is why, our focus is mainly on these 9 residues. Two of these residues are positively charged (LYS7 and ARG10) and one is negatively charged (GLU11). We have first examined various site−site rdfs to see the solution structure around the peptide. Thereafter, we have given a close look on the solution compositions around the peptide. Finally, hydrogen bonding interactions between solution species and peptide residues are investigated.

The organization of the rest of the chapter is as follows. We first present the models and details of simulations. Results are discussed thereafter, and the last section includes concluding remarks with a brief summary.

■ MODELS AND SIMULATION METHOD

We carried out classical MD simulations of the model polypeptide in four different solvent systems: pure water, aqueous urea, aqueous TMAO, and mixed urea/TMAO. An overview of the systems simulated are presented in Table 5A-1. In all of the simulations, the SPC/E model [111] was used for water, the Smith model [239] was adopted for urea, and TMAO was described with the flexible model proposed by Kast *et al.* [113] Note that, atomic sites

Table 5A-1. Overview of Simulations[a]

state	system	Np	Nw	Nu	Nt	Mu	Mt	V(nm^3)
F	PW	1	1500	—	—	—	—	46.288-47.304
	PU	1	1000	250	—	8.3	—	49.265-50.235
	PT	1	1100	—	100	—	3.7	44.445-45.453
	PUT	1	650	250	100	8.2	3.3	49.893-51.019
U	PW	1	1500	—	—	—	—	46.253-47.328
	PU	1	1000	250	—	8.3	—	49.221-50.211
	PT	1	1100	—	100	—	3.7	44.452-45.415
	PUT	1	650	250	100	8.2	3.3	49.873-50.958

[a] N, M, and V represent number of molecules, average molar concentration, and volume (minimum and maximum), respectively. p, w, u, and t, respectively, refer to peptide, water, urea, and TMAO.

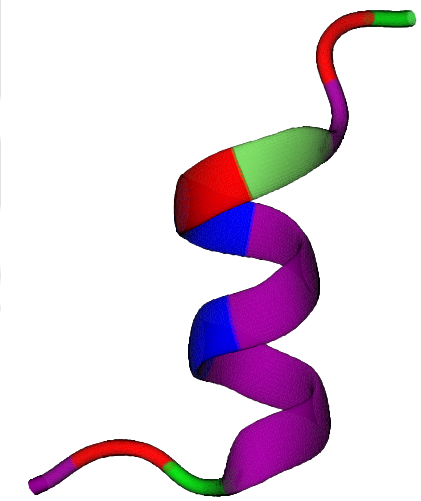

Figure 5A-1. *Initial structure of the helical peptide. Blue, red, and purple colors are for positive, negative, and nonpolar residues, respectively. The peptide sequence is:*

ALA-GLU-THR-ALA-ALA-ALA-LYS-PHE-LEU-ARG-GLU-HIS-MET-ASP-SER

in these molecules are abbreviated here as Im where I is the conventional atomic symbol of that particular atomic site and m can be w (for water), u (for urea), and t (for TMAO). For the helical structure of peptide, the initial coordinates were taken from the X-ray structure of Ribonuclease S (PDB code: 2RNS) [240]. After extracting the first 15 residues, we made few minor modifications (replacement of residues LYS1, GLU9, and GLN11 by ALA1, LEU9, and GLU11, followed by protonation to give a zwitterionic form with N-terminal NH_3^+ and C-terminal COO^- groups) to obtain a good starting structure for our simulations. The initial structure of this helix is shown in Figure 5A-1 with the sequence of amino acids. Histidine was deprotonated and the peptide was neutralised by using a Na^+ ion. The extended structure of the peptide (not shown) was generated using xleap program of AMBER 10 [241]. All atom parameter set AMBER ff99SB [241] was used to describe this model peptide.

The solution properties were investigated by carrying out MD simulations at 298 K. All MD runs were performed using the AMBER 10 suite of programs [241]. To obtain a reasonable initial structure, we first performed energy minimization (2500 steps of steepest descent method followed by 2500 steps of conjugate gradient method) of the system which was generated using packmol program [242]. We note that, the energy minimization (which relieves bad vdW contacts) was performed in two steps, first holding the peptide fixed by using harmonic restraints (force constant = 500.0 kcal mol^{-1} $Å^{-2}$) and then removing the restraints on the peptide. After that, each system was heated slowly from 0 to 298 K (to avoid void formation) for 50 ps in the NVT ensemble with weak restraints (force constant = 10.0 kcal mol^{-1} $Å^{-2}$) on the peptide and then equilibrated for 1 ns at the desired pressure in the NPT ensemble without any restriction on the peptide. The Berendsen barostat [116] was used to maintain the physical pressure with a pressure relaxation time of 2 ps. Temperature was controlled by Langevin dynamics method with the collision frequency of 1 ps^{-1} and a time step of 2 fs was used in all of the simulations. Bonds involving hydrogen were constrained by applying SHAKE algorithm. To remove edge effects, we used periodic boundary conditions. A cut-off radius of 12 Å was applied for non bonding interactions and the long-range electrostatic interactions were treated using the particle mesh Ewald method [243, 244]. After equilibration of 1 ns, simulations were continued for further 10 ns and the reported results are from these last 10 ns of simulation periods.

■ RESULTS AND DISCUSSION

Site−Site Radial Distribution Functions. Site−site rdfs between the peptide and solution species were computed to investigate solvation of the peptide residues in different chemical environments. Figure 5A-2 depicts the distributions of solution species (considering central atom only) around the peptide heavy atoms (residues $4-12$). Focusing on hydration of the peptide in the absence of osmolyte first (Figure 5A-2a), we see a small first peak at about 2.8 Å, reflecting existence of hydrogen bonding interaction between the peptide and water. The water density near the peptide is significantly lower than that in the bulk and there arises a positive gradient in water rdf at longer separations. This is a clear indicator of water exclusion near the peptide. The hydration pattern is qualitatively similar for both the **F** and **U** states. However, for the **U** state, the water density in the close proximity of the peptide is noticeably higher and, additionally, the magnitude of the

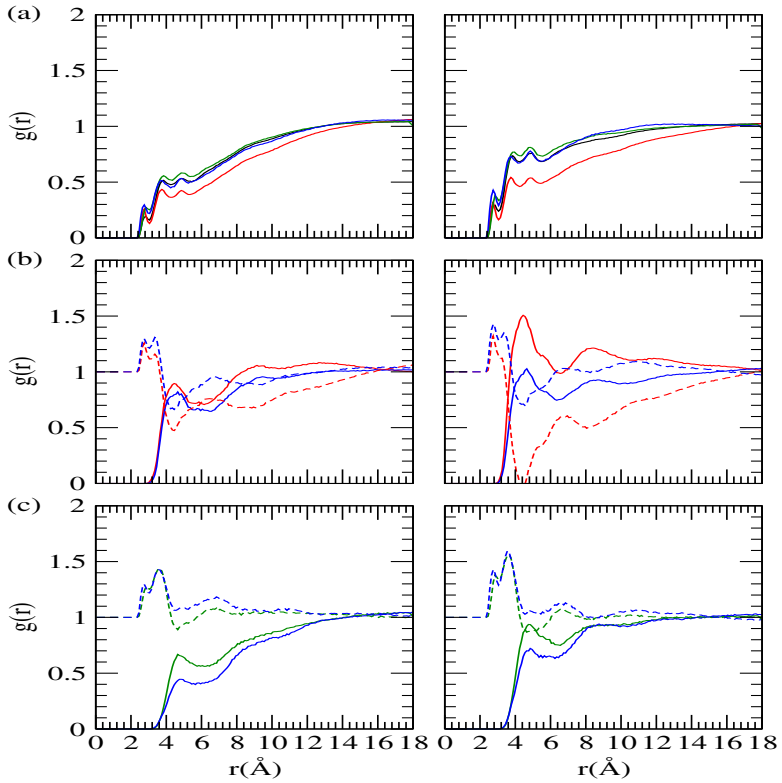

Figure 5A-2. *Distributions of water, urea, and TMAO central atoms (from a-c, respectively) around the peptide heavy atoms for the* **F** *(left) and* **U** *(right) states in water, aqueous urea, aqueous TMAO, and mixed urea/TMAO solutions. Dashed lines represent relative distributions of water to osmolyte. For clarity, relative distribution values are shifted by 1.*

gradient appearing at longer distances is smaller. All these observations suggest enhanced hydration of the peptide **U** state. Nonetheless, water exclusion around the peptide is observed regardless of whether the peptide is in the **F** or **U** state. The observed water exclusion is consistent with the notion that proteins fold spontaneously in nature as water itself is a slightly bad solvent.

Comparing water distribution around the peptide residues in water and binary urea solution, we find significant reduction of water density beyond 4 Å (Figure 5A-2a). We can also see that a large number of urea molecules are distributed around the peptide (Figure 5A-2b). Due to the larger excluded volume for a urea molecule (vdW radii for water and urea are about 1.5 and 2.2 Å [119], respectively), the urea density around the peptide starts to rise from zero at a longer distance (relative to water). But its density increases sharply and is significantly higher than the water density for both the **F** and **U** states. The relative distribution of water to urea (g_{Ow}-g_{Cu}) is included in Figure 5A-2b to present the effect of urea more clearly. Dominant occupancy of urea in a large portion of the peptide solvation shell can be seen immediately. This solvation pattern makes sense, because it strongly suggests urea's ability to reduce water density and to occupy the depleted hole created by water, making preferential interaction with the peptide residues. What is more, in binary urea solution, preference for urea over water is much higher in the **U** state than the **F** state.

TMAO, on the other hand, slightly increases the water density around the peptide (Figure 5A-2a). Again, although TMAO molecules are distributed at a relatively longer distance as compared to water, density of TMAO is similar to water density at longer separations ($r \geq 6$ Å). From the relative distribution of water to TMAO (g_{Ow}-g_{Nt}) curve included in Figure 5A-2c, we see higher water distribution in the close proximity of the peptide mostly due to the larger excluded volume for a TMAO molecule (vdW radius for TMAO is 2.95 Å [119] against ∼1.5 Å [119] for water). The relative distribution of water to TMAO then starts to decrease and approaches a value which is very similar to the ideal solution. Thus, while urea reduces water density around the peptide and occupies the depleted hole created by water; in binary solution of TMAO, the peptide residues do not show any preference for water or TMAO.

Interestingly, addition of TMAO to urea system makes the water density pure water like which is higher than that of the binary urea solution (Figure 5A-2a). Moreover, TMAO reduces the urea density around the peptide and the relative distribution of water to urea is more ideal like in the urea/TMAO mixture as compared to the binary urea solution

(Figure 5A-2b). Similarly, the density of TMAO near the peptide decreases upon addition of urea to TMAO system. However, relative distribution of water to TMAO does not deviate much from the ideal distribution (Figure 5A-2c). Overall, in urea/TMAO mixture, the preference of the peptide residues for urea over water decreases and the peptide solvation layer is better mixed in terms of solution species as compared to that in the absence of TMAO.

The details of peptide interactions with solution species can be obtained from site−site distribution functions between atom pairs involved in hydrogen bonding interactions, shown in Figures 5A-3−5A-6. Comparison of water pair functions suggests that the backbone hydrogens are not easily accessible to water as compared to other hydrogen bonding sites in the peptide. Water density around the backbone oxygen (Figure 5A-3a) is higher than that around the backbone hydrogen (Figure 5A-4a) and since water consists of only 1 oxygen against 2 hydrogen atoms, it is clear that hydrogen bonding between peptide backbone and water is solely dominated by backbone oxygen. While the positively charged side-chains of the peptide also participate in hydrogen bonding interactions with water (Figure 5A-5a), among the hydrogen bonding sites in the peptide, the negatively charged side-chain has the strongest tendency for hydrogen bond formation (Figure 5A-6a). The general features of the urea distribution functions around the peptide hydrogen bonding sites are similar to the water distribution functions for both the **F** and **U** states (Figures 5A-3−5A-6). The qualitative similarity of these rdf pairs indicates that urea can form hydrogen bonds with peptide atomic sites as do water molecules. On the other hand, although the general features of the distribution curves for water and TMAO oxygen atoms around the peptide hydrogen bonding sites are similar (Figures 5A-4 and 5A-5), indicating TMAO's ability to form hydrogen bonds with these atomic sites; the rdf profiles do not indicate any hydrogen bonding interaction of TMAO with backbone oxygen and negative side-chain (Figures 5A-3 and 5A-6). Thus, just like water and urea oxygens, TMAO oxygen can form hydrogen bonds with backbone hydrogen and positive side-chains. While methyl groups show a tendency to occupy the space near the backbone oxygen and negative side-chains, reducing their availability to form hydrogen bonds with water (and urea in urea/TMAO mixture); TMAO does not donate its hydrogen to these hydrogen bonding sites. In other words, interaction efficiency of the peptide hydrogen bond acceptor sites with solution species reduces in the presence of TMAO, as we mentioned in **Chapter 4** and, in all likelihood, it is this inefficiency that plays the crucial role in protein stabilization. Here we note that our observations are supported by various other lines of research. For

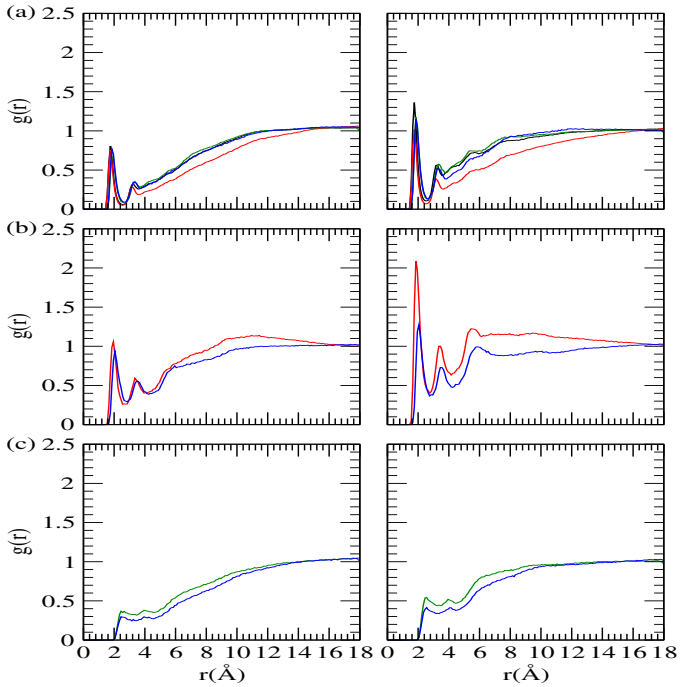

Figure 5A-3. *Site−site rdfs that show interactions of backbone oxygen (residues* $4-12$*) with water, urea, and TMAO hydrogens (from a-c, respectively) for the* **F** *(left) and* **U** *(right) states in water, aqueous urea, aqueous TMAO, and mixed urea/TMAO solutions.*

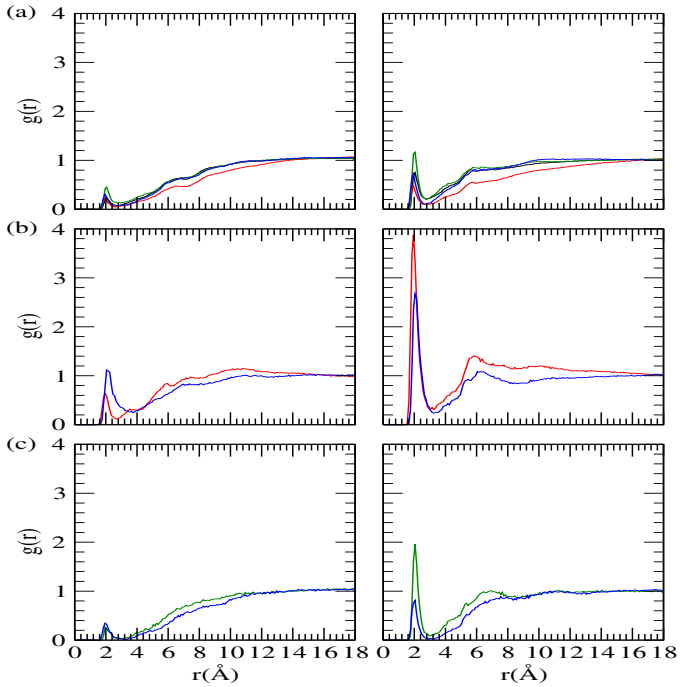

Figure 5A-4. *As in Figure 5A-3 except for interactions of backbone hydrogen (residues* $4-12$*) with water, urea, and TMAO oxygens (from a-c, respectively).*

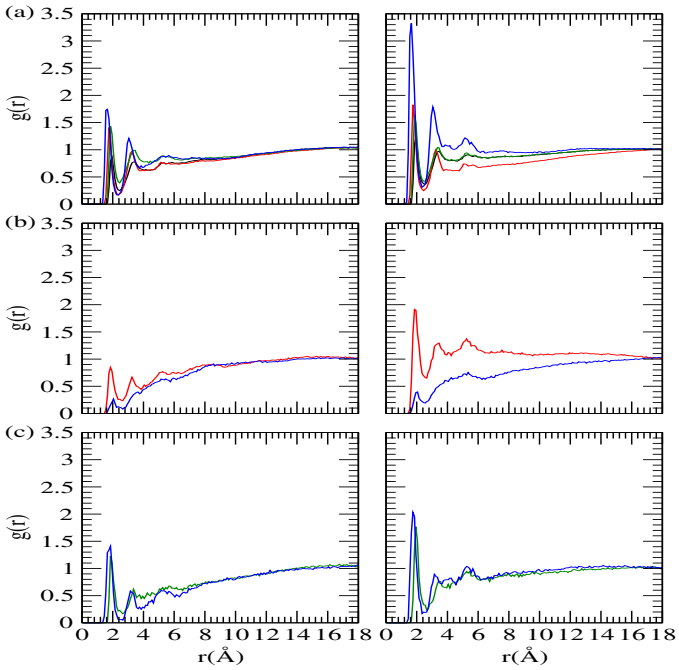

Figure 5A-5. *Site−site rdfs for atom pairs of positively charged peptide side-chains (LYS7 and ARG10) and water, urea, and TMAO oxygens (from a-c, respectively) that are likely to be engaged in hydrogen bonding interactions in water, aqueous urea, aqueous TMAO, and mixed urea/TMAO solutions. Results are for the* **F** *(left) and* **U** *(right) states.*

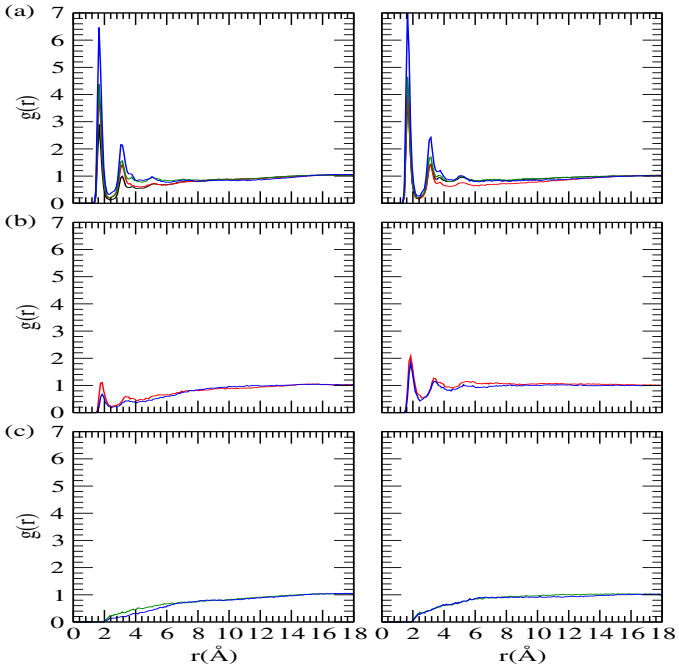

Figure 5A-6. *As in Figure 5A-5 except for atom pairs of negatively charged peptide side-chain (GLU11) and water, urea, and TMAO hydrogens (from a-c, respectively).*

example, NMR experiments [75] and MD study [74] indicated direct interaction of peptide backbone with TMAO oxygen through its amide nitrogen. The latter study also showed a clear and significant preference of TMAO for the positively charged lysine side-chain. On the other hand, transfer free energy measurements suggested that interaction of TMAO with protein backbone, which plays the dominating role in determining the extent of protein stabilization or destabilization [54, 208, 209], is highly unfavorable; and this leads to significant destabilization of the solvent-exposed state of protein.

Thus, examination of the solvation characteristics of peptide atomic sites in pure water and in binary and ternary solutions of urea and TMAO reveals direct interaction of the peptide residues with osmolyte. In binary solution of urea, the peptide residues are found to show significant preference for urea over water. In contrast to urea, the peptide residues do not show any preference for water or TMAO in its binary solution. Although TMAO forms hydrogen bonds with backbone hydrogen and positive side-chains, hydrogen bonding interaction of backbone oxygen and negative side-chains with TMAO is unlikely. However, a small fraction of TMAO methyl groups shows tendency to occupy the space near these hydrogen bonding sites. These methyl groups prevent the peptide hydrogen bond acceptor sites from interacting efficiently with other hydrogen bonding sites in the solution, providing a possible explanation for TMAO-induced protein stabilization and counteraction. In urea/TMAO mixture, TMAO is observed to reduce the preference of the peptide residues for urea over water (by enhancing water density and reducing urea density) and the solvation layer of the peptide is better mixed in terms of solution species as compared to that in absence of TMAO.

Osmolyte Accumulation Near Peptide. Accumulation of osmolyte near the peptide surface was investigated by calculating the time-averaged normalized fractions (τ_i) of water oxygen, urea carbon, and TMAO nitrogen, as defined in **Chapter 2** (Eq. 2.7). Two different methods were employed to calculate the number of water and osmolyte molecules around the peptide residues. First, from site−site rdfs using Eq. 2.6. While Eq. 2.6 is useful for calculating solvation number of a single atom; due to sharing of solution species, the solvation number for the entire peptide cannot be obtained accurately by simple multiplication of the so obtained number with the number of peptide's atom. Sharing of solution species by atoms comprising the peptide increases with cut-off distance, thereby increasing the deviation between the calculated value and the actual solvation number (as shown below). To prevent this deviation, we adopted the second method whereof we

considered each molecule of component i in the solvation shell of only one peptide atom (i.e., excluded that particular molecule from the solvation shell of remaining atoms). The peptide atom that saw the solution species in its solvation shell was determined by finding the minimum distance between the solution species and the peptide atom.

The average number of solution species around the heavy atoms of the entire peptide are shown in Figure 5A-7. When evaluation is carried out by excluding the solution species from the solvation shell of remaining heavy atoms of the peptide, number of water and osmolyte molecules in the solvation shell approaches the total number of solution species in the simulation box (1000 water in *PU*, e.g.) at half box width. In contrast, significantly lower solvation number for the peptide is obtained when the number is evaluated using Eq. 2.6. This is obvious as it includes only a single heavy atom of the peptide. Also, sharing of solution species among the peptide atoms is reflected in Figure 5A-7, showing

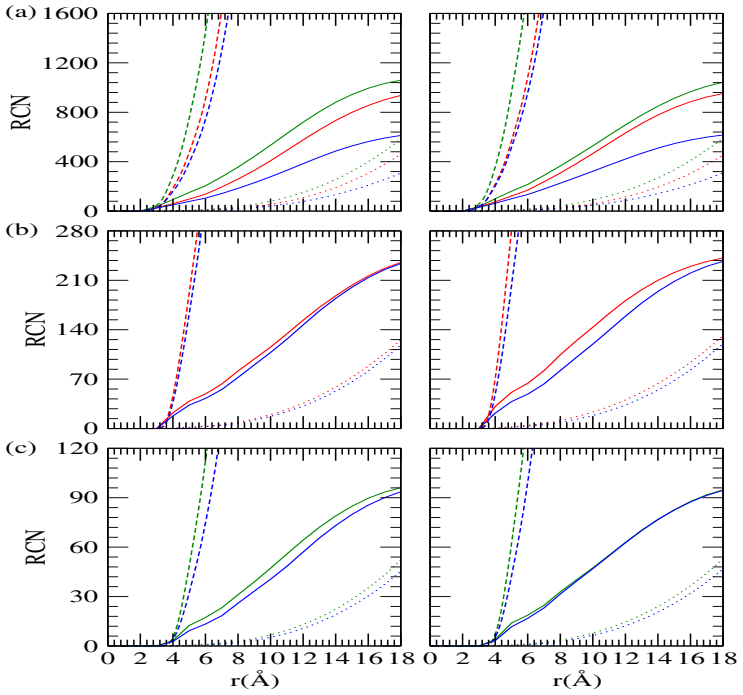

Figure 5A-7. *Running coordination numbers for water, urea, and TMAO central atoms (from a-c, respectively) around the heavy atoms of the entire peptide for the* **F** *(left) and* **U** *(right) states in aqueous urea, aqueous TMAO, and mixed urea/TMAO solutions. Solid: RCN around the peptide heavy atoms computed by counting each molecule of component i for a single time. Dotted: RCN for a single heavy atom of the peptide computed using Eq. 2.6. Dashed: RCN computed by multiplying RCN for the single heavy atom with total number of heavy atoms (117) comprising the peptide.*

much higher solvation number for the peptide when the number obtained for a single heavy atom (using Eq. 2.6) is multiplied by the total number of heavy atoms (117) comprising the peptide.

Figure 5A-8 shows the time-averaged normalized fraction, τ_i, of component i as a function of the radius of the spherical volume that defines the local domain around the peptide in binary and ternary solutions of urea and TMAO. In the presence of urea only, τ_{Ow} is greater than 1, whereas τ_{Cu} is lower than 1 below 4 Å, implying preferential accumulation of water in this region. However, urea dominantly occupies the peptide solvation shell beyond 4 Å. Comparing the component fractions of water and urea in the binary urea solution with the ternary solution, we find relative deficit of urea and excess of water around the peptide in the presence of TMAO. From the data in Figure 5A-8, it is not hard to suggest a much better mixed solvation layer of the peptide in terms of water

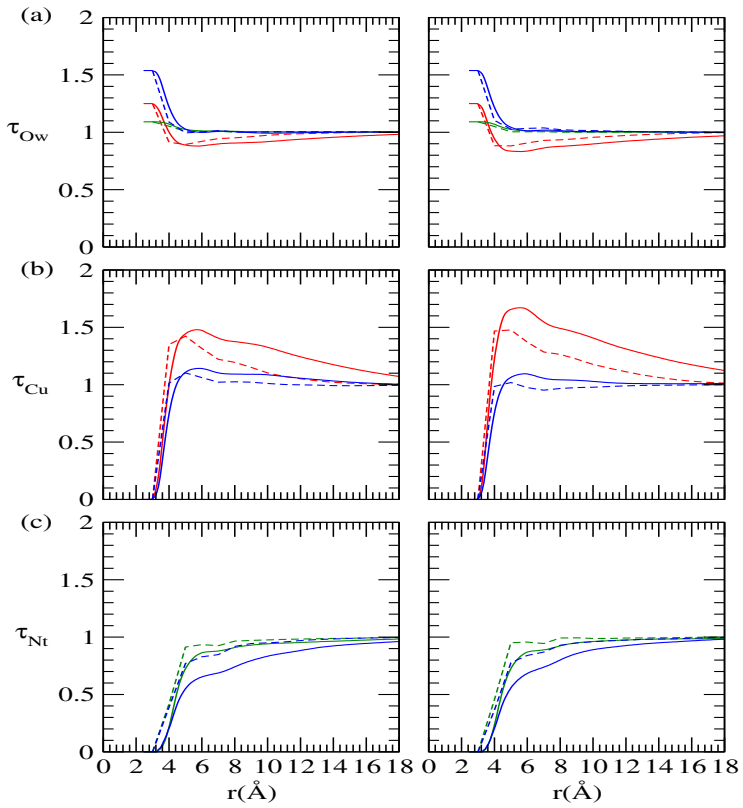

Figure 5A-8. *Time-averaged normalized fractions of water, urea, and TMAO central atoms (from a-c, respectively) as a function of the distance from the heavy atoms of the entire peptide for the* **F** *(left) and* **U** *(right) states in aqueous urea, aqueous TMAO, and mixed urea/TMAO solutions. Dashed: τ_i computed by counting each molecule of component i for a single time. Solid: τ_i computed using Eq. 2.6.*

and urea in the mixed osmolyte solution as compared to that in the absence of TMAO. TMAO is found to be excluded from the peptide surface and its relative exclusion increases in the urea/TMAO mixture (Figure 5A-8c). Note that, the magnitudes of τ_i depends to some extent on the method employed to calculate the number of solution species around the peptide residues. When the component fraction is evaluated by counting each molecule of component i only one time, τ_i shows better mixing of solution species in the peptide solvation shell. However, this difference in τ_i value alters none of our previous statements about preferential accumulation or depletion of osmolyte around the peptide. Thus, urea accumulates preferentially in the vicinity of the peptide, whereas TMAO is depleted slightly from the peptide surface. Similar observations regarding osmolyte accumulation near the peptide residues are made when component fractions are evaluated for residues $4-12$ (which is of primary importance in this study) using Eq. 2.6 (Figure not shown). Here we note that, our observations correspond well with previous MD simulation study [72] and also with the notion that urea interacts preferentially with protein residues [33-47]. In particular, Kokubo *et al.* [72] using a decaalanine peptide showed that there was excess of urea and strong deficit of water molecules around the peptide in binary urea solution, whereas the deficit of water was minimum in binary TMAO solution and the preferential solvation parameter of TMAO and the peptide was much smaller than that of urea (in fact, was close to the ideal zero value).

Again, although higher excluded volume of urea and TMAO do not allow their central atoms (Cu and Nt) to penetrate in a specific region around the peptide surface, these two osmolytes can interact with the peptide residues through other atomic sites (TMAO methyl groups, e.g.) as observed in site−site rdf calculations. To get an idea of the total number of heavy atom contacts between the peptide residues and the solution species, we calculated the average number of atomic sites in the first solvation shell (FSS) of the peptide. Number of atomic sites in the FSS was calculated first for each of the $4-12$ residues (using the method of exclusion to avoid sharing of atoms as much as possible) and the contact numbers reported here are obtained by simple addition of these numbers. A heavy atom of the solution species was considered to be inside the FSS when it fell within a distance of 3.5 Å from any heavy atom of the selected peptide residue.

Table 5A-2 presents the average number of water, urea, and TMAO heavy atoms in the FSS of the peptide. As expected from rdf calculations, we find more water molecules in the FSS of peptide residues in the **U** state. The hydration number decreases in the presence of osmolyte. It is seen that TMAO interacts with the peptide mainly through methyl

groups, whereas urea interaction occurs mostly through nitrogen atom. This is related to the atomic number density of osmolyte in the system (probability of finding an atom near a target molecule increases with concentration). Number of urea oxygen in the FSS of the

Table 5A-2. Solvent Heavy Atoms in the FSS of Peptide

state	system	N_{Ow}	N_{Cu}	N_{Nu}	N_{Ou}	N_{Nt}	N_{Ct}	N_{Ot}
F	PW	41.80	—	—	—	—	—	—
	PU	25.21	2.20	15.22	8.43	—	—	—
	PT	40.47	—	—	—	0.09	6.38	1.40
	PUT	22.16	1.40	13.57	7.53	0.10	4.22	1.12
U	PW	60.32	—	—	—	—	—	—
	PU	30.49	4.45	23.99	16.49	—	—	—
	PT	54.05	—	—	—	0.13	8.53	3.02
	PUT	30.01	2.62	17.32	10.44	0.14	6.29	1.98

peptide is also in the higher side. The presence of all these heavy atoms increases the total number of heavy atom contacts, N_{CON}, between the peptide and solution species upon addition of osmolyte (Figure 5A-9). We find that, for both the **F** and **U** states of the peptide, enhancement of N_{CON} is bounded by the maximum in binary urea solution and the minimum in binary TMAO solution. Figure 5A-9 also includes the difference in N_{CON} between the **F** and **U** states, i.e., $\Delta N_{CON} = N^U_{CON} - N^F_{CON}$. In the presence of urea only, the osmolyte-induced enhancement of N_{CON} (relative to pure water) is higher for the **U** state than the **F** state, which is an indication of accumulation of interacting sites next to the extended form relative to the folded form. The evidence here is that, while the addition of urea to pure water enhances short-range vdW interactions between the peptide and solution species for both the **F** and **U** states, relative enhancement is higher for the extended form. In contrast, TMAO-induced relative enhancement is slightly higher for the **F** state. Recent replica-exchange λ sampling simulations indicated osmolyte-induced stabilization of both the **F** and **U** states through short-range interactions. Although both urea and TMAO were found to enhance the favorable vdW solvation free energy of decaalanine peptide for helix and denatured conformations [72], relative stabilization of the **U** state through vdW inter-

actions between peptide and solution species was higher in binary urea solution (relative to pure water) and lower in binary TMAO solution. In the mixed osmolyte solution, there is much higher preference of urea over TMAO in the FSS of the peptide, as expected (Table 5A-2). But, due to the inclusion of few TMAO interacting sites in the FSS, the peptide loses some contacts with urea molecules upon addition of TMAO. As a result, enhancement of N_{CON} in the ternary solution is lower than that in the binary urea solution (Figure 5A-9). Moreover, addition of TMAO to urea system reduces the difference in N_{CON} between the **F** and **U** states dramatically and the value of ΔN_{CON} approaches that of the value in pure water. On these grounds, we can infer that, TMAO can reduce urea-induced enhancement of short-range interactions between peptide and solution species and the **U** state does not gain much net stabilization over the **F** state in urea/TMAO mixture through vdW interactions.

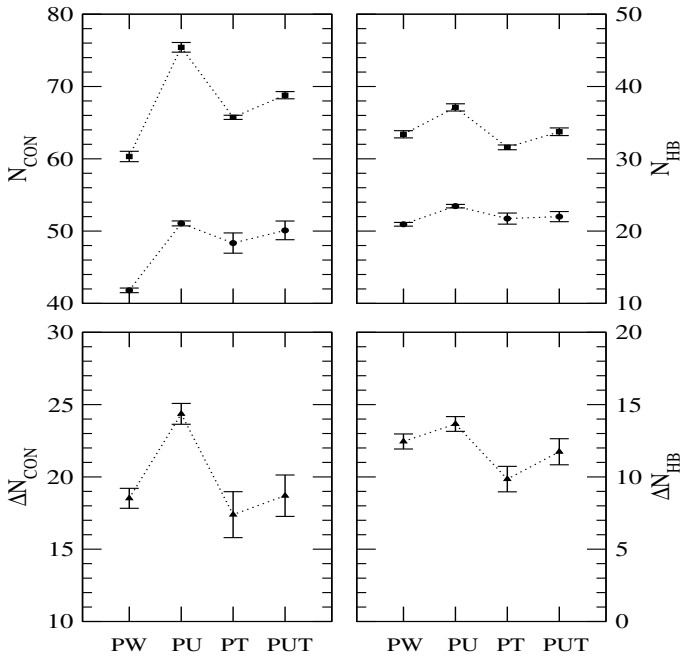

Figure 5A-9. *Top: Total number of contacts between the peptide and solution species (left) and total number of hydrogen bonds formed by the peptide with solution species (right) for the* **F** *(•) and* **U** *(■) states. Bottom: Difference between* **U** *and* **F** *states. Standard errors of the mean are included.*

Hydrogen Bonding Interaction. Numbers of hydrogen bonds formed by the peptide with solution species were calculated to investigate the peptide solvation more closely. A hydrogen bond, D-H $\cdots$ A, was defined by a maximal distance of 3.5 Å for D-A (where D is donor and A is acceptor) and a maximal angle of 45° for H-D-A. The hydrogen bond num-

bers were calculated using VMD [245] and the results obtained are tabulated in Table 5A-3. In pure water, number of peptide−water hydrogen bonds increases by about 12 for the **U** state. Urea molecules form large number of hydrogen bonds with the peptide residues, reducing the number of peptide−water hydrogen bonds significantly. This is consistent with previously reported higher hydrogen bonds formed by protein with solution species in aqueous urea solution as compared to pure water [72, 73]. Remarkably, the total number of hydrogen bonds formed by the peptide with solution constituents (N_{HB}) increases in binary urea solution (Figure 5A-9). This relative enhancement of total hydrogen bond number upon addition of urea is higher for the **U** state of the peptide (compare magnitudes of $\Delta N_{HB} = N_{HB}^{U} - N_{HB}^{F}$ in Figure 5A-9), indicating urea's ability to cause relatively higher stabilization of the extended form through hydrogen bonding interactions.

Table 5A-3. Hydrogen Bond Number between Peptide and Solution Species[a]

state	bond type	PW	PU	PT	PUT
F	n_{HB}^{w}	20.94±0.26	14.55±0.61	21.19±0.72	13.18±0.54
	n_{HB}^{u}	—	8.90±0.55	—	8.12±0.51
	n_{HB}^{t}	—	—	0.54±0.08	0.70±0.16
U	n_{HB}^{w}	33.39±0.50	18.23±0.52	30.08±0.35	19.27±0.46
	n_{HB}^{u}	—	18.88±0.58	—	13.34±0.98
	n_{HB}^{t}	—	—	1.50±0.22	1.13±0.25

[a]Superscripts w, u, and t represent water, urea, and TMAO, respectively. Standard deviations were calculated by considering 10 independent blocks of 1 ns each and the values shown after the average are the standard errors of the mean obtained by dividing standard deviation with square root of the block number.

In contrast to the osmolyte urea, which forms large number of hydrogen bonds with peptide and stabilizes the extended form through relative enrichment of hydrogen bonds between the peptide and solution species, TMAO rarely forms hydrogen bond with peptide residues and destabilizes the extended state by reducing its ability to form hydrogen bonds with solution species (Figure 5A-9). The counteracting effect of TMAO is also evident from Figure 5A-9, in that the total number of hydrogen bonds formed by the

peptide with solution species in urea/TMAO mixture is similar to that in pure water solution, which is lower than that in binary urea solution. What these findings suggest is that TMAO prevents the peptide hydrogen bonding sites from interacting efficiently with solution species, providing the pathway for TMAO-induced protein stabilization and counteraction.

■ SUMMARY AND CONCLUSIONS

To provide a molecular level understanding of how TMAO stabilizes proteins and counteracts urea-conferred protein denaturation, employing the MD simulation technique, solvation characteristics of a 15-residue model peptide were investigated. Two different conformations (**F** and **U**) of the peptide were used and for both conformations, simulations were carried out in pure water as well as in binary and ternary solutions of urea and TMAO. Computations of site−site rdfs showed exclusion of water molecules from the vicinity of the peptide, the depletion effect being more pronounced for the **F** state. The backbone hydrogens were not easily accessible to water as compared to other hydrogen bonding sites in the peptide and hydrogen bonding between peptide backbone and water was solely dominated by backbone oxygen.

Urea reduced water density near the peptide in its binary solution and occupied the depleted hole created by water, making preferential interaction with the peptide residues. While the peptide was dehydrated with consequent reduction of peptide−water hydrogen bonds, total number of heavy atom contacts as well as the hydrogen bond number between the peptide and solution species increased in the presence of urea due to the direct interaction of urea with the peptide residues. Urea-induced relative enhancement of both the heavy atom contact and hydrogen bond number were found to be higher for the **U** state as compared to the **F** state, causing better stabilization of the extended state.

TMAO also replaced water molecules in the peptide solvation shell and although slight depletion of TMAO from the peptide surface was observed; because of the existence of TMAO atomic sites (methyl groups in particular) in the close proximity of the peptide, total number of heavy atom contacts between the peptide and solution species increased upon addition of TMAO. Nonetheless, enhancement in heavy atom contact was slightly lower for the **U** state relative to the **F** state. Besides, TMAO reduced hydrogen bonding interaction efficiency of the peptide hydrogen bond acceptor sites by occupying the space near these atomic sites. Consequent relatively higher reduction of hydrogen bonding interaction between the peptide and solution species for the **U** state favors the **F** state.

For the ternary solution, the water density around the peptide was found to be pure water like. Addition of TMAO to urea system, on the other hand, reduced the urea density significantly, making the relative distribution of water to urea more ideal like in the urea/TMAO mixture as compared to the binary urea solution. In other words, TMAO reduced the preference of peptide residues for urea (over water) and the peptide solvation layer was better mixed in terms of solution species as compared to that in absence of TMAO. Comparison of total number of heavy atom contacts and the hydrogen bond number between the peptide and solution species in binary and ternary solutions of urea indicated TMAO's ability to offset urea-induced relative stabilization of the extended state over the folded state.

Although urea reduces the number of protein hydration waters, the short-range vdW as well as the hydrogen bonding interactions between the peptide and solution species increases in binary urea solution as compared to pure water and since the relative stabilization through these interactions is higher for the unfolded state than the folded state, importance of direct protein−urea interaction in urea-conferred protein denaturation is well-captured by our simulations. Our simulations also suggest that TMAO can prevent protein hydrogen bond acceptor sites from interacting efficiently with solution species and shifts the folded⇌unfolded equilibrium in favor of the folded state by reduction of short-range vdW as well as the hydrogen bonding interactions of the unfolded state relative to the folded state.

Part B:

TMAO's Effect on Polypeptide Solvation at High Pressure

Overview: Solvation characteristics of a 15-residue polypeptide and also the structure of the solution in the presence and absence of TMAO are investigated under high pressure conditions by employing the MD simulation technique. The goal is to provide a molecular level understanding of how TMAO protects proteins at elevated pressures. Two different conformations of the polypeptide are used: helix and extended. Analysis of peptide hydration characteristics reveals that pressure-induced enhancement of hydration number is higher for the extended state as compared to the helix. TMAO shows an opposite effect and causes more dehydration of the extended state. Total number of atomic sites that solvate peptide residues increases in the presence of TMAO, whereas the number of hydrogen bonds formed by peptide with solution species reduces due to the inability of TMAO to donate its hydrogen to peptide hydrogen bonding sites. In solution, both hydrophobic and hydrogen bonding sites of TMAO are found to be well solvated by water molecules and solvation of TMAO enhances water structure and reduces number of nearest identical neighbors for water. Pressure and TMAO are seen to have counteracting effects on water structural properties. Implications of these results for counteracting mechanism of TMAO are discussed.

■ INTRODUCTION

The protein denaturing effect under high hydrostatic pressure is a subject of long-standing interest [246]. Experimental studies such as compressibility measurement [247, 248], high resolution NMR spectroscopy [249-253], optical [254, 255] and vibrational [256] spectroscopy, and small angle X-ray scattering [1] have been carried out to investigate the structural changes occurring in proteins at high pressure. It has been suggested that in contrast to the extended configurations of proteins denatured by high temperature or chemical reagents, pressure-denatured proteins are relatively compact [1, 257-259]. Two-dimensional ^{1}H NMR study of basic pancreatic trypsin inhibitor (BPTI) in an aqueous environment by Li *et al.* [253] indicated hydrogen bond formation by most of the amide groups either with carbonyls or with water and pressure-induced shortening of these hydrogen bonds. Investigating the pressure-dependence of the folding/unfolding relaxation kinetics of staphylococcal nuclease (SNase), Vidugiris *et al.* [143] found that the transition state has larger volume than either the folded or unfolded states and furthermore, the activation volume of folding is much larger than that of unfolding. In a NMR study, Lasalle *et al.* [5] observed pressure-induced enhancement of hydrogen exchange rate of proteins, suggesting penetration of water molecules into the tightly packed hydrophobic core of proteins at high pressure.

To provide atomistic changes involved in pressure-induced protein structural transformations, MD simulations and other theoretical methods have also been performed extensively [9, 13-19, 226, 260-262]. Focusing on the structural changes occurring in hydrated BPTI at varying hydrostatic pressure, Marchi and Akasaka [261] reported that high pressure does not cause any significant increase in the number of intra-protein hydrogen bonds, supporting the Li *et al.*'s [253] interpretation of the ^{1}H NMR shifts as distance shortening, without increase in hydrogen bond number. Several theoretical and simulation studies [13-17], on the other hand, supported the experimentally [5] observed pressure-induced water penetration into the protein interior. The MD simulations of the protein ubiquitin by Day and García [13] showed that the high pressure structure has more penetrating water molecules than the low pressure structure, providing evidence for water penetration model; but they did not observe any structural transition of proteins. In a recent MD simulation study, Imai and Sugita [15] reproduced the experimentally observed pressure-induced structural transition of ubiquitin. Combining their results with those in a previous thermodynamic study [16], they concluded that water penetration is the primary driving force for protein denaturation under high pressure. Previous investigations of the pressure-induced

folding/unfolding transition of SNase by Paliwal *et al.* [9] also suggested the requirement of water insertions into the hydrophobic core to induce protein unfolding.

Changes in the partial molar volume (PMV) associated with the structural transition due to water penetration at elevated pressures have also been studied. In their three-dimensional reference interaction site model (3D-RISM) theoretical study of low-pressure and high-pressure structure of ubiquitin, Imai *et al.* [16] concluded that water penetration reduces the PMV by eliminating the structural voids in the region against the volume expansion due to the additional hydration effect. Investigations in this direction by Harano *et al.* [17] showed enhancement of the solvent accessible surface area upon pressure denaturation, while the PMV reduces. In a series of studies, this group argued that water penetration into the protein interior increases the total entropy of water molecules in the system, favoring the denatured structure at high pressure [17-19]. Recently, Grigera and McCarthy [14] have raised the importance of weakening of water hydrogen bond network in protein unfolding at high pressure.

As discussed above, considerable effort has been made both experimentally [1, 5, 143, 247-259] and theoretically [9, 13-19, 226, 260-262] to understand the protein denaturation induced by high hydrostatic pressures. Nevertheless, due to the complexity in the interactions between water and different groups (hydrophobic and hydrophilic side-chains and the backbone) of proteins, there is still no definitive generally accepted mechanism that underlines this denaturation. Again, switching our attention to TMAO, although well-known for preventing the pressure-induced unfolding of proteins [59, 61, 62], the molecular mechanism of protein protection by TMAO at elevated pressures is yet to be investigated thoroughly with model protein systems under high pressure conditions.

In this study, to investigate the solvation characteristics of protein residues in binary solution of TMAO at high pressure, we have undertaken MD simulations for a 15-residue model peptide in the presence and absence of TMAO both at low and high pressures. Note that pressure-denatured proteins are reported to be relatively compact as compared to heat-denatured proteins and, unlike in case of high temperature, the molecule cannot be described as a fully extended random coil [1]. However, to investigate the solvation characteristics of folded and unfolded proteins under high pressure conditions and the role of TMAO on this protein solvation, we have used here two different conformations of the model peptide: helix (denoted as **F**) and extended (denoted as **U**). During the simulation, the peptide is allowed to fluctuate (i.e., flexible model) and so the **F** and **U** states are ensembles of conformations which are 'folded' and 'unfolded', respectively. Also important

to note is that only 9 residues $(4-12)$ of the helix are in α-helical regions. Therefore, we focus on solvation of residues $4-12$ only and, in this part, the results reported for peptide solvation exclude the remaining 6 residues. Following important issues are addressed. First, what is the role of TMAO on the pressure-induced modification of peptide hydration? Can TMAO offset enhanced hydration of the peptide under pressure conditions? Second, how does TMAO interact with peptide residues and water molecules at high pressure and what is the implication of TMAO solvation by water in pressure-induced modification of water structural properties?

Simulations were carried out in pure water and binary TMAO solution (∼4M in strength) at three different hydrostatic pressures: 1, 4000, and 8000 bar. The models and simulation methods employed were identical to those described in Part A of the current chapter; the results are from last 10 ns of simulation periods.

■ RESULTS AND DISCUSSION

Hydration of Peptide Residues. To obtain molecular details of peptide hydration at different pressures in the presence and absence of TMAO, we calculated site−site rdfs between peptide and water. Water distribution around the peptide heavy atoms is shown in Figure 5B-1. The small first peak at about 2.8 Å, which is indicator of hydrogen bonding interaction between water and peptide residues, is unaffected by high pressure. On the other hand, increasing the pressure from 1 bar to 8 kbar leads to a significant modification of second peak. To be specific, the peak position shifts to shorter distance and the peak magnitude increases monotonically with pressure. These findings reveal negligible effect of high pressure on the tendency of a protein to form hydrogen bonds with water and a compressed water shell in the vicinity of non-hydrogen bonding sites, in accord with the suggestion that the water shell is much more compressed in the vicinity of nonpolar groups as compared to that of hydrogen bonding sites [228, 229].

Comparison of water pair function around the peptide residues in water and binary TMAO solution does not reveal any counteracting effect of TMAO against pressure. TMAO rather enhances water density near the peptide both at low and high pressures (Figure 5B-1). Water density enhancement by TMAO near the peptide, however, does not necessarily imply more water molecules in the close proximity of the peptide upon addition of TMAO. It only suggests, if anything, that the number ratio of vicinal water to bulk water is higher in binary TMAO solution as compared to pure water. Despite the higher water density in the nearby region of peptide, dehydration of peptide occurs (as shown later) in the presence

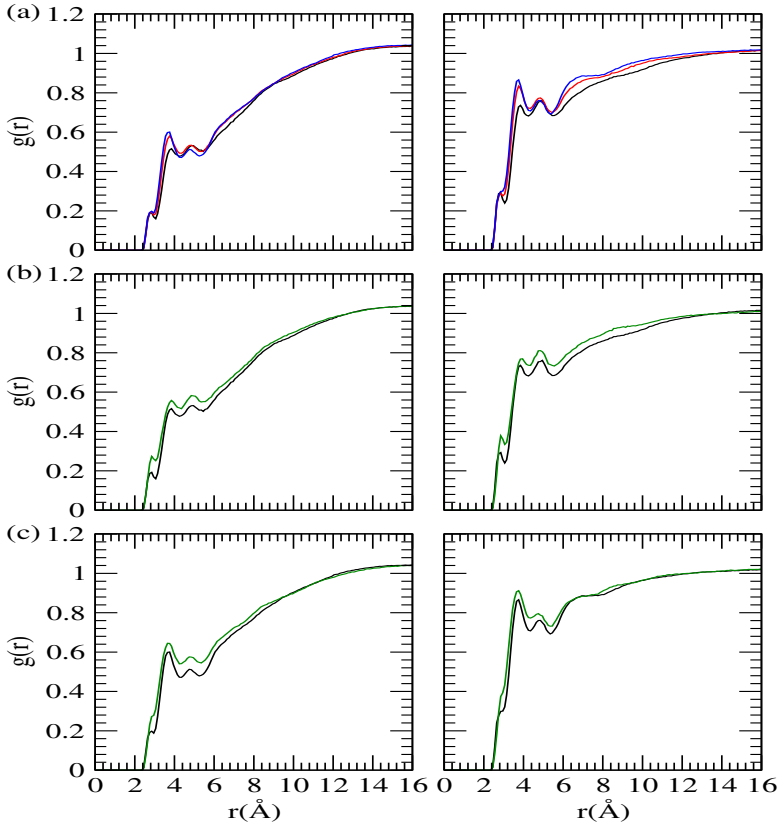

Figure 5B-1. *Distributions of water oxygen around the peptide heavy atoms (residues 4-12) in pure water (a) at 1, 4000, and 8000 bar pressures and also at 1 bar (b) and 8 kbar (c) pressures for systems PW and PT. Left and right panels are for the* **F** *and* **U** *states, respectively.*

of TMAO.

The hydration characteristics of the peptide residues were probed further by calculating the number of water molecules around the peptide residues and the number of peptide−water hydrogen bonds in different environments. Number of water in the first solvation shell (FSS) was calculated first for each of the $4-12$ residues and then those numbers were added to obtain total hydration number. A water molecule was considered to be inside the FSS when its oxygen atom fell within a distance of 3.5 Å from any heavy atom of the selected peptide residue. On the other hand, a hydrogen bond, D-H $\cdots$ A, was defined by a maximal distance of 3.5 Å for D-A (where D is donor and A is acceptor) and a maximal angle of 45° for H-D-A.

The average number of water molecules in the FSS of the peptide are assembled in Table 5B-1. As expected from peptide−water rdf, we find more water molecules in the

Table 5B-1. Heavy Atom Contacts between Peptide and Solution Species[a]

		F			**U**		
system	number	1	4000	8000	1	4000	8000
PW	N_W	41.80	54.96	64.25	60.32	78.17	91.74
PT	N_W	40.47	50.08	58.71	54.05	65.18	80.86
	N_N	0.09	0.17	0.24	0.13	0.30	0.36
	N_C	6.38	8.66	10.61	8.53	11.74	12.46
	N_O	1.40	2.17	2.19	3.02	3.53	3.19

[a]Subscripts W, N, C, and O represent water oxygen, and nitrogen, carbon, and oxygen of TMAO, respectively. Pressure is in the unit of bar.

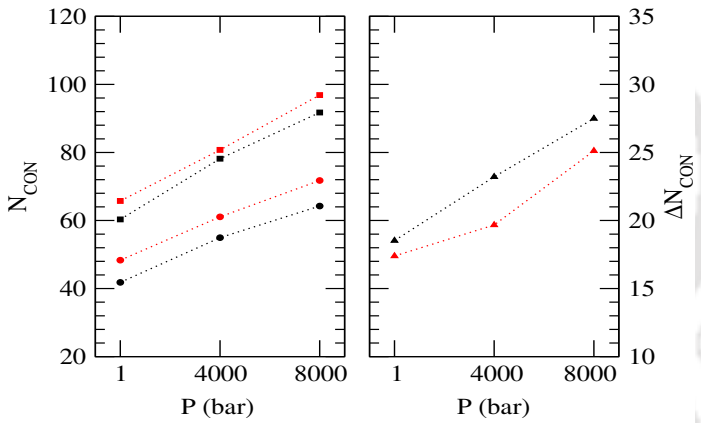

Figure 5B-2. *Left: Total number of contacts between peptide and solution species (left) for the* **F** *(•) and* **U** *(■) states in pure water and binary TMAO solution. Right: Difference between* **U** *and* **F** *states.*

FSS of peptide residues in the **U** state. The hydration number increases with pressure for both the **F** and **U** states. Interestingly, pressure-induced enhancement of peptide hydration is higher for the **U** state, which is clearly demonstrated in Figure 5B-2. For our model peptide, the hydration number in pure water enhances by about 22 and 31, respectively, for the **F** and **U** states as the pressure increases from 1 bar to 8 kbar (Table 5B-1). On these grounds, we can infer that, high pressure stabilizes both the **F** and **U** states through enhancement of short-range interactions with water molecules and the relative stabilization is higher for the latter conformation. It is remarkable here that, extensive MD simulations

on proteins suggested pressure-denaturation due to higher compressibility of the hydration shells of unfolded proteins than the folded ones [229]. Table 5B-1 shows TMAO's ability to remove water molecules from the close proximity of the peptide. While TMAO-induced dehydration occurs regardless of whether the peptide is folded or unfolded, for a particular pressure, the effect is relatively higher for the **U** state (Table 5B-1). Thus, TMAO can offset the pressure-induced relatively higher stabilization of the extended state as compared to the compact state by causing more reduction of short-range interactions with water molecules for the former.

In Table 5B-2, we have presented the number of peptide−water hydrogen bonds together with the relative population of water oxygen in the FSS of peptide residues that are engaged in hydrogen bonding interactions with the peptide. The peptide−water hydrogen bond number is higher for the **U** state, as expected from enhanced hydration. Also consistent with the effect of pressure on hydration of peptide residues is the observation that, in pure water, the hydrogen bond number increases with pressure. The enhancement in hydrogen bond number, however, does not differ much for the **F** and **U** states, as shown in Figure 5B-3. It is also important to emphasize that the relative population of hydrogen bonded water molecule in the FSS decreases with pressure for both conformations of the peptide (Table 5B-2). Thus, the **U** state does not gain much net stabilization over the **F**

Table 5B-2. Hydrogen Bond Number between Peptide and Solution Species[a]

		F		**U**	
system	P (bar)	n^w_{HB}	n^t_{HB}	n^w_{HB}	n^t_{HB}
PW	1	20.94(50)	—	33.39(55)	—
	4000	22.65(41)	—	35.20(45)	—
	8000	23.58(37)	—	37.66(41)	—
PT	1	21.19(52)	0.54(39)	30.08(56)	1.50(50)
	4000	20.91(42)	0.61(28)	29.08(45)	1.37(39)
	8000	21.21(36)	0.44(20)	30.58(38)	0.89(28)

[a] n^w_{HB} and n^t_{HB} are the number of hydrogen bonds formed by peptide residues (4−12) with water and TMAO, respectively. Numbers in parentheses give relative populations (in percentage) of water and TMAO oxygen in the FSS of peptide residues that are engaged in hydrogen bonding interactions with peptide.

state at high pressure from peptide−water hydrogen bonding interactions. In other words, intra-protein hydrogen bonds are likely to be preserved even at elevated pressure. This is consistent with the observation that pressure-denatured structures are much more compact than the thermally-denatured structures [1]. On the other hand, hydration of peptide residues is higher for the extended state (as discussed above). This leads us to suggest that protein-denaturation by high pressure is caused by the enhanced hydration of non-hydrogen bonding sites. Note that, in our previous chapters, we showed efficient packing of water molecules around hydrophobic solute at high pressures and consequent pressure-induced relative stabilization of the water-separated configuration of nonpolar solute as compared to its associated state. Also, it has been reported in the literature that while exposure of hydrophobic groups to water is highly favored under pressure, high pressure has little effect on the tendency of a protein to form hydrogen bonds [225].

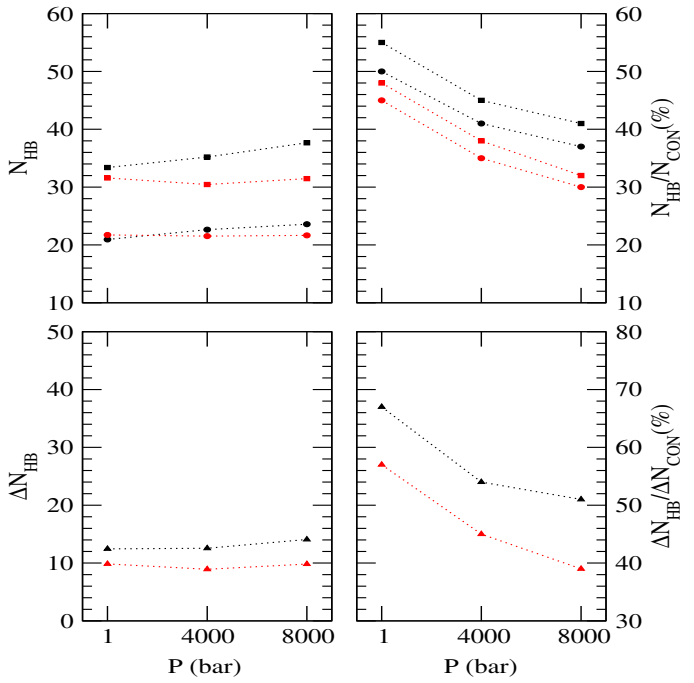

Figure 5B-3. *Top: Total number of hydrogen bonds (N_{HB}) formed by peptide residues with solution species (left) and the relative population of heavy atoms in the FSS of peptide residues that are engaged in hydrogen bonding interaction with peptide (right) for the* **F** *(•) and* **U** *(■) states in pure water and binary TMAO solution. Bottom: Difference between* **U** *and* **F** *states.*

Variation in peptide−water hydrogen bond number with pressure is insignificant in the presence of TMAO, though there is clear reduction in relative population of hydrogen

bonded water molecule in the FSS at high pressure for both the **F** and **U** states (Table 5B-2). TMAO shows a tendency to reduce the efficiency of the peptide atomic sites to form hydrogen bond with water molecules. The effect is higher for the **U** state and increases with pressure. Thus, through its effect on peptide hydration, TMAO can cause relatively higher destabilization of the **U** state both at low and high pressures. Though this is consistent with TMAO-induced protein stabilization, for a more clear picture, one needs to consider interaction between protein and TMAO as well and what follows is the discussion of this interaction.

TMAO's Interaction with Peptide Residues. Time-averaged normalized fractions (τ_i) of water oxygen and TMAO nitrogen were calculated (using Eq. 2.7) to investigate the accumulation of osmolyte near the peptide surface. Eq. 2.6 was used to calculate the number of water and TMAO molecules around the peptide residues (residues $4-12$). As suggested in Part A of this chapter, water accumulates preferentially in the vicinity of the peptide, whereas TMAO is depleted in this region (Figure 5B-4). We note that, for both conformations, relative exclusion of TMAO is higher at 8 kbar.

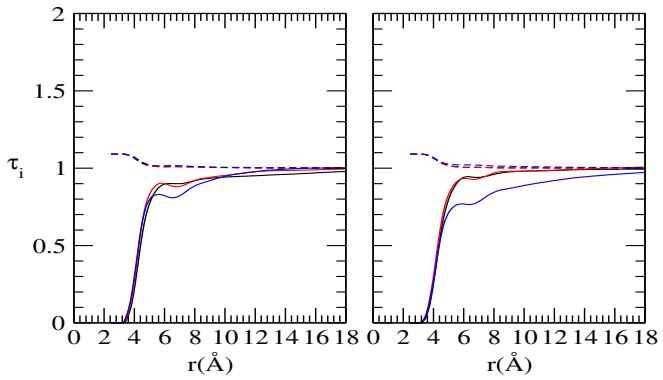

Figure 5B-4. *Time-averaged normalized fractions of water (dashed) and TMAO (solid) central atoms as a function of the distance from the peptide heavy atoms (residues* $4-12$*) for the* **F** *(left) and* **U** *(right) states at 1, 4000, and 8000 bar pressures.*

Solvation of peptide residues by TMAO was probed further by calculating the number of TMAO atomic sites within a distance of 3.5 Å from any heavy atom of the selected peptide residue. Table 5B-1 presents the total number of TMAO atomic sites in the FSS of the peptide. We first concentrate on nitrogen atom of TMAO, which being the central atom of this osmolyte, is generally considered to describe the interaction of protein

residues with TMAO molecule. Number of TMAO nitrogen in the FSS of each residue is very small and, overall, there is only about 0.1 nitrogen in the close proximity of the peptide at 1 bar (Table 5B-1). This number is much smaller than the number of water molecules in the FSS and is related not only to the lower number density of TMAO in the system (probability of finding a molecule near a target molecule increases with concentration), but also to the relative exclusion of TMAO near the peptide. TMAO interacts with the peptide residues mainly through methyl groups (Table 5B-1). Number of oxygen atom in the FSS of peptide residues is also significantly higher than that of nitrogen atom. The presence of all these sites increases the total number of heavy atoms, N_{CON}, in the FSS in binary TMAO solution than in pure water (Figure 5B-2). Nonetheless, the relative enhancement in N_{CON} is lower in the **U** state as compared to that in the **F** state (compare magnitudes of $\Delta N_{CON} = N^U_{CON} - N^F_{CON}$ in Figure 5B-2), which is an indication of depletion of interacting sites next to extended form relative to the folded form. Therefore, while the addition of TMAO to pure water seems to enhance short-range interactions between the peptide and solution species for both the **F** and **U** states, the relative enhancement is higher for the helix as compared to the extended form. This looks surprising at first instance, but corresponds well with the data obtained by Kokubo *et al.* [72] performing solvation free energy calculations. Their replica-exchange λ sampling simulations clearly showed TMAO-induced enhancement of the favorable vdW solvation free energy of decaalanine peptide for helix and denatured conformations, the helix being the more stable form in binary TMAO solution vs water [72].

In **Chapter 3** and Part A of this chapter, using NMA and a 15-residue model peptide, we showed that TMAO can interact with backbone oxygen through its methyl groups. Hydrogen bonding interactions between these atomic sites are, however, unlikely. We predicted that, due to the presence of TMAO methyl groups near these hydrogen bonding sites, their efficiency for hydrogen bond formation decreases. On the other hand, TMAO oxygen is expected to form some hydrogen bonds with backbone nitrogen and positive side-chains of peptide residues. We, therefore, calculated hydrogen bond numbers between TMAO oxygen and peptide residues both at low and high pressures using the geometric criteria defined for peptide−water hydrogen bond calculations. Table 5B-2 presents the numbers obtained for the peptide residues. We can see only a small number of hydrogen bonds between peptide and TMAO. Probability of TMAO oxygen in the FSS to engage in hydrogen bonding interaction with peptide residues increases for the **U** state and the probability decreases with pressure (see relative population in Table 5B-2). Because

TMAO does not donate its hydrogen to peptide hydrogen bond acceptor sites, total number of hydrogen bonds (N_{HB}) formed by peptide residues with solution species decreases mostly in the presence of TMAO (Figure 5B-3). Figure 5B-3 shows TMAO-induced noticeable decrease in relative population of heavy atom that make direct contact with peptide residues through hydrogen bonding interactions. Additionally, TMAO-induced reduction in N_{HB} is higher in the **U** state as compared to that in the **F** state (compare magnitudes of $\Delta N_{HB} = N_{HB}^{U} - N_{HB}^{F}$), implying relatively higher destabilization of the extended state. Thus, the enhancement of short-range vdW interactions in TMAO solution is likely to stabilize the peptide, whereas the peptide is destabilized by reduction of hydrogen bonding interactions. The most significant observation is that both these factors favor the folded state over the extended state.

Solvation of TMAO and Its Effect on Water Structural Properties. To obtain information regarding the counteracting mechanism, we also investigated TMAO solvation by water molecules and its indirect effect on water structural properties. Both hydrophobic and hydrogen bonding sites of TMAO are well solvated by water molecules and the effects of pressure on hydration of TMAO atomic sites are found to be similar to those described in **Chapter 3**. Similarly, our observations on pressure- or TMAO-induced alteration of water structural properties (**Chapter 4**) does not alter in these systems. These similarity provide further support for the importance of TMAO solvation and its indirect effect on water structure in protein stabilization by TMAO under high pressure conditions. Avoiding a detail discussion of our findings here, we simply note the following observations:

- Hydration number for both hydrophobic and hydrogen bonding sites of TMAO increases with pressure, though the enhancement is much lower for TMAO oxygen; and TMAO-water hydrogen bond number is almost unaffected by pressure (Table 5B-3).

- At 1 bar, majority of TMAO oxygens have either 2 or 3 hydrogen bonds to water (Figure 5B-5). High pressure decreases relative population of 2-coordinated water molecule and increases those of 3- and 4-coordinated water molecule for TMAO oxygen. Nonetheless, the relative population of water molecules in the close proximity of TMAO oxygen that participate in hydrogen bonding interaction with this atomic site decreases with increasing pressure (Table 5B-3).

- The data in Table 5B-4 and Figure 5B-6 shows counteracting effects of TMAO and pressure on water structural properties. High pressure enhances number of near-

est neighbor water molecules and although water−water hydrogen bond number increases, relative number of first shell water molecules that participate in hydrogen bonding interactions reduces with increasing pressure, indicating pressure-induced crowding of water molecules with a relatively destabilized water hydrogen bond network. On the contrary, TMAO not only reduces number of nearest identical neighbors of water but also enhances the relative population of first shell water molecules that participate in water hydrogen bond network.

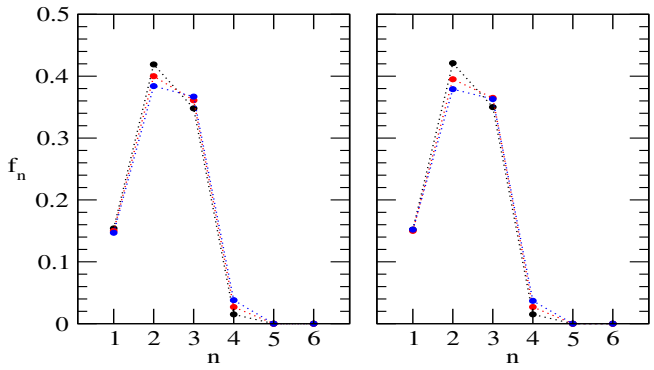

Figure 5B-5. *Fraction of TMAO molecules that engage in n number of hydrogen bonds with water molecules for the* **F** *(left) and* **U** *(right) states at 1, 4000, and 8000 bar pressure.*

Table 5B-3. TMAO Hydration Properties[a]

state	P (bar)	N_{Ct}	N_{Ot}	n_{HB}	n_{HB}/N_{Ot}
F	1	2.40	2.75	2.10	0.76
	4000	3.16	3.03	2.14	0.71
	8000	3.73	3.33	2.17	0.65
U	1	2.40	2.74	2.10	0.77
	4000	3.15	3.03	2.14	0.71
	8000	3.72	3.32	2.15	0.65

[a] N_{Ct} and N_{Ot} represent average number of water molecules within 3.5 Å of TMAO carbon and oxygen, respectively. n_{HB} is the number of hydrogen bonds between TMAO oxygen and water computed by imposing cut-off distances of 2.5 and 3.5 Å, respectively, for $Ot - Hw$ and $Ot - Ow$, and a simultaneous cut-off angle of 45° for $Hw - Ow - Ot$.

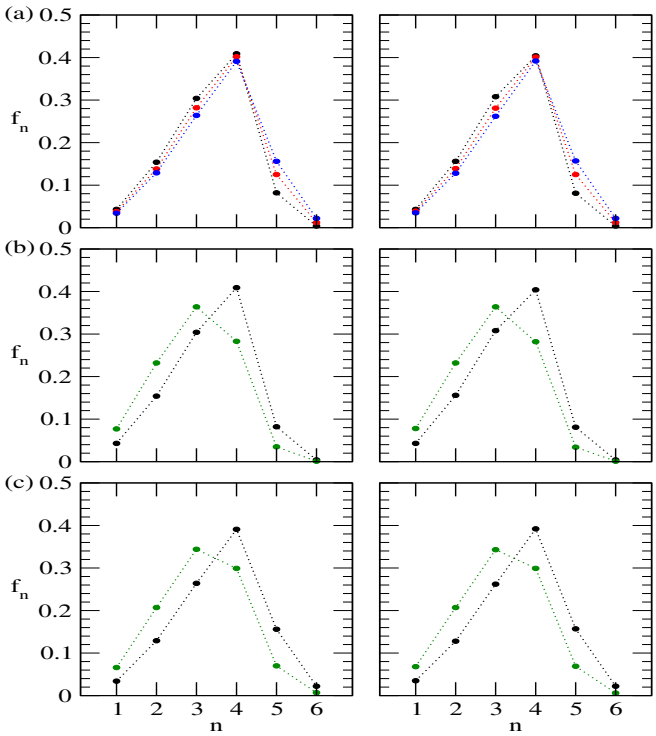

Figure 5B-6. *Fraction of water molecules that engage in n number of hydrogen bonds with identical species as a function of pressure in pure water (a) and also as a function of TMAO concentration at 1 bar (b) and 8 kbar (c) pressures for the* **F** *(left) and* **U** *(right) states. Color codes are as in Figure 5B-1.*

Table 5B-4. Characteristics of Water First Shell[a]

		F			**U**		
system	P(bar)	N_H	n_{HB}	n_{HB}/N_H	N_H	n_{HB}	n_{HB}/N_H
PW	1	5.07	3.33	0.66	5.06	3.32	0.66
	4000	6.09	3.47	0.57	6.06	3.46	0.57
	8000	6.90	3.56	0.52	6.87	3.56	0.52
PT	1	4.24	2.95	0.70	4.22	2.94	0.70
	4000	4.90	3.03	0.62	4.88	3.02	0.62
	8000	5.48	3.10	0.57	5.44	3.09	0.57

[a] N_H and n_{HB}, respectively, represent average number of water molecules within 3.5 Å of water oxygen and the number of water−water hydrogen bonds computed by imposing cut-off distances of 2.5 and 3.5 Å, respectively, for $Ow-Hw$ and $Ow-Ow$, and a simultaneous cut-off angle of 45° for $Hw-Ow-Ow$.

■ SUMMARY AND CONCLUSIONS

Employing the MD simulation technique, solvation characteristics of a polypeptide and also the structure of the solution in the presence and absence of TMAO were investigated under different pressure conditions to explore the mechanism of protein protection by TMAO both at low and high pressures. Computations of site−site rdfs indicated negligible effect of high pressure on the tendency of a protein to form hydrogen bonds with water and a compressed water shell in the close proximity of non-hydrogen bonding sites. Pressure-induced enhancement of hydration number was found to be higher for the **U** state as compared to the **F** state. These observations are consistent with the suggested much higher compressibility of the water shell in the vicinity of nonpolar groups as compared to that of hydrogen bonding sites [228, 229] and also with the notion that the hydration shells of unfolded proteins are more compressible than those of folded ones contributing to pressure denaturation [229]. However, for our model peptide, we did not observe much difference in peptide−water hydrogen bond number enhancement between the **F** and **U** states, making pressure-induced protein denaturation through enhancement of protein−water hydrogen bonds an unlikely possibility. Instead, we observed negligible effect of pressure on the tendency of a protein to form hydrogen bonds as was indicated previously [225]. TMAO did not prevent pressure-induced enhancement of water density in the close proximity of the peptide residues. But there were less number of water molecules in the peptide hydration shell in aqueous solution of TMAO and the number of hydrogen bonds between peptide and water reduced.

TMAO was found to be excluded from the peptide surface both at low and high pressures regardless of whether the peptide is folded or unfolded. Our simulations, however, showed TMAO interacting directly with peptide residues through its methyl groups and oxygen atom, and the total number of heavy atom contacts between peptide and solution species increased in the presence of TMAO. Relative enhancement in heavy atom contact was lower for the **U** state, contributing to relative stabilization of the **F** state. On the other hand, TMAO was observed to reduce efficiency of the peptide to form hydrogen bonds with solution species. The reduction was higher for the **U** state (relative to the **F** state), thereby favoring the folded state further.

From our systematic investigation, we believe that the movement of water molecules to the vicinity of protein better stabilizes the unfolded state through enhancement of short-range vdW interactions. Hydrogen bonding interactions between protein and water may

not affect the folded⇌unfolded equilibrium under these harsh conditions and protein denaturation by high pressure is most likely to be associated with enhanced hydration of non-hydrogen bonding sites, which results in a relatively compact structure as compared to thermally-denatured structure. On the other hand, TMAO protects proteins both at low and high pressures by preventing the protein residues from being hydrated. As shown clearly in previous chapters, TMAO forms some strong hydrogen bonds with water in the bulk and solvation of TMAO makes the water hydrogen bonding network stronger. This reduces the availability of water molecules that solvate protein residues. Besides the dehydrating effect, TMAO is capable to stabilize proteins through its direct interaction with protein residues, of which TMAO shifts the folded⇌unfolded equilibrium toward the folded state by relatively higher destabilization of the unfolded state.

Chapter 6

Summary and Our View on TMAO's Protein Protecting Action

"Hence, without excluding the importance of direct interaction of TMAO with water (and urea in urea/TMAO mixture) and its indirect effect on water structure enhancement, we conclude that the ability of TMAO to protect proteins in the presence or absence of urea at different pressures is a consequence of more inefficient interactions of protein hydrogen bond acceptor sites with solution species on unfolding."

To explore the underlying mechanism of protein stabilization by TMAO at low and high pressures in the presence and absence of the protein denaturant urea, employing the MD simulation technique, we systematically investigated solvation characteristics of various functional groups comprising proteins. We started our investigations using methane as model hydrophobic group and then extended to a larger hydrocarbon, neopentane. Preferential exclusion of urea from the solvation shell of methane and its preferential accumulation near the larger hydrophobic moiety were observed. Nevertheless, dehydration of nonpolar groups occurred and some urea molecules appeared in the close proximity of these groups in binary urea solution regardless of whether the solute is small or large. Additionally, although association of methane molecules were not affected much by the presence of urea, urea-induced dispersion of neopentane molecules was clear from our simulations. Investigation of structural, energetic, and dynamical properties of NMA (the smallest amide that represents the solvent-exposed protein backbone) hydrogen bonds with solution species showed the replacement of NMA−water hydrogen bonds by NMA−urea hydrogen bonds. The two solvation sites in NMA oxygen (which were occupied by water alone in pure water) were shared by water and urea in binary urea solution. Hydrogen bonds between NMA and urea were found to be more attractive than those between NMA and water and the hydrogen bond relaxation was also slower for the former. These results indicated direct interaction of urea with protein residues in urea-conferred protein denaturation. That the direct protein−urea interaction plays an important role in protein denaturation by urea was confirmed from simulations of the polypeptide. In binary solution of urea, water density reduced near the peptide and urea occupied the depleted hole created by water, making preferential interaction with the peptide residues. While the peptide was dehydrated with consequent reduction of peptide−water hydrogen bonds, total number of heavy atom contacts as well as the hydrogen bond number between the peptide and solution species increased in the presence of urea due to the direct interaction of urea with the peptide residues. Of significant importance in the context of urea-induced protein denaturation was the observation that the relative enhancement of both the heavy atom contact and hydrogen bond number are higher for the unfolded state than the compact state of protein, causing better stabilization of the extended state.

The hydration shell of hydrophobic groups (methane, neopentane, and NMA methyl groups) was significantly compressed at high pressure. Correlated with pressure-induced enhanced hydration of nonpolar groups were the observations that high pressure stabilizes the solvent-separated state of methane relative to its associated state and dis-

solves the aggregate of neopentane. In contrast to the highly compressed water shell in the vicinity of nonpolar groups at high pressure, the water compression was found to be much weaker near the hydrogen bonding sites. Again, although application of pressure enhanced slightly the number of hydrogen bonds between NMA and water, it was evident from analysis of hydrogen bond energy distribution that pressure destabilizes NMA−water hydrogen bonds. Our simulations of the polypeptide confirmed weak effect of high pressure on the tendency of a protein to form hydrogen bonds with water and a compressed water shell in the close proximity of non-hydrogen bonding sites. Relative population of water molecules in the solvation shell of polypeptide that are involved in hydrogen bonding interactions with the polypeptide residues reduced at high pressure. Moreover, while pressure-induced enhancement of hydration number was found to be higher for the unfolded state as compared to the folded state of the polypeptide, we did not observe much difference in peptide−water hydrogen bond number enhancement between the folded and unfolded states, making the pressure-induced protein denaturation through enhancement of hydrogen bonds between protein and water an unlikely possibility.

Just like the protein denaturing osmolyte urea, TMAO was observed to remove water molecules from the solvation shell of hydrophobic groups and interact directly with these solutes both at low and high pressures. TMAO's effect on propensity of hydrophobic association was, however, insignificant, and it did not show any tendency to prevent the pressure- and urea-induced dissolution of neopentane aggregate. TMAO formed few energetically strong hydrogen bonds with NMA hydrogen. Our simulation results also indicated existence of hydrogen bonding interaction between TMAO oxygen and protein hydrogen bond donating sites. On the other hand, despite the unlikely hydrogen bonding interactions, TMAO methyl groups occupied the space around backbone oxygen (and other hydrogen bond acceptor sites in protein), reducing efficiency of these atomic sites to form hydrogen bonds with solution species dramatically. Consequent TMAO-induced reduction in hydrogen bond number between protein and solution species was observed in simulations of NMA as well as the polypeptide. The observed TMAO-induced higher reduction in hydrogen bond number for the unfolded state than the folded state of protein can be taken as evidence of relatively higher destabilization of the extended state in the presence of TMAO.

To shed light on the mechanism of protein (de)stabilization, we also examined various structural, energetic, and dynamical properties of the aqueous solutions. Computations of site−site rdfs showed a slight collapse of the water second shell in the presence of urea,

indicating urea's ability to act as a water structure breaker. On the other hand, our analysis of hydrogen bond properties did not provide any evidence for the water structure breaking capacity of urea. Rather, urea was found to slightly increase water−water hydrogen bond energy and life-time. Water did lose some hydrogen bonds to identical species upon addition of urea, but those hydrogen bonds were replaced by water−urea hydrogen bonds, and urea appeared to fit well in the water cavities. In contrast, significant changes in water structure were observed both at high pressure and in the presence of TMAO. In particular, high pressure caused crowding of water molecules, destabilized water hydrogen bonding network, and increased population of first shell water molecules that are not engaged in hydrogen bonding interactions with the central water molecule. TMAO influenced water properties in a manner that opposes the effects of pressure. It not only reduced number of nearest identical neighbors of water but also increased population of more stable hydrogen bonds and the relative number of first shell water molecules that participate in water hydrogen bonding network. While the effects of pressure and TMAO on water properties are consistent with their role on hydration of protein residues, our simulations do not provide strong support for the indirect mechanism of urea-conferred protein denaturation that presumes urea as a structure breaker for water, making water molecules free to interact with protein residues.

Investigation of solvation characteristics of TMAO by solution species revealed TMAO solvation by both water and urea. TMAO molecules, which participated in 2 to 3 hydrogen bonds with water in its binary solution, showed its inability to maintain these hydrogen bonds as urea was added and these hydrogen bonds were replaced by TMAO−urea hydrogen bonds. We observed that hydrogen bonds formed by TMAO with water and urea were very strong. The hydration number for both hydrophobic and hydrogen bonding sites of TMAO increased with pressure, though the enhancement was much lower for TMAO oxygen, and the TMAO−water hydrogen bond number was almost unaffected by pressure.

We mention here that the observed water crowding at high pressure with some 'free' water molecules and a relatively destabilized hydrogen bond network explains the reason behind pressure-induced enhanced hydration of protein residues. Extreme water crowding at high pressure restricts water movement in the bulk, and for translational relaxation, the relatively 'free' water molecules in the water first shell move to the protein surface. The process gives an overall entropic profit (due to relaxation in water movement) to the system and allows water to form a relatively stable hydrogen bond network. Note that the dominating contribution of translational entropy gain from relaxation of water

molecules far away from the protein surface in overall entropic gain in the system upon pressure denaturation was suggested in the literature [17]. Consequent enhancement of short-range vdW interactions between protein and water stabilizes the folded state as well, but the relative enhancement of these interactions is higher for the pressure-denatured structure. Hydrogen bonding interactions between protein and water may not affect the folded⇌unfolded equilibrium under these harsh conditions and protein denaturation by high pressure is most likely to be associated with enhanced hydration of non-hydrogen bonding sites, which results in a relatively compact structure as compared to thermally-denatured structure.

The protein denaturing osmolyte urea, on the other hand, operates mainly through its direct interaction with protein residues. Although urea causes a slight collapse of the water second shell, by no means can the water structure breaking property of urea which, in turn, increases protein hydration, be considered to be a primary factor in urea-conferred protein denaturation. Urea removes water molecules from the protein solvation shell, and makes significant number of direct contacts with protein residues. Consequent enhancement of short-range vdW as well as the hydrogen bonding interactions stabilize both the folded and unfolded states. However, stabilization is higher for the extended state, forcing protein to adopt a solvent-exposed structure in the presence of urea.

Protein loses hydration waters also in the presence of TMAO. However, as compared to urea, TMAO interactions with protein residues are weaker. While urea can share the backbone oxygen and hydrogen bonding sites of negatively charged side-chains with water, TMAO cannot donate its hydrogen to these atomic sites. Tendency of TMAO's methyl groups to occupy the nearby space of protein hydrogen bond acceptor sites, on the other hand, reduces number of hydrogen bonds between protein and solution species. In other words, the surrounding environment of protein is inefficient to stabilize the protein through hydrogen bonding interactions, and it is obvious that, TMAO-induced destabilization is higher for the extended state. Protein adopts the compact state to reduce the number of inefficient interaction with solution species and to increase the number of efficient intra-protein interactions. Note that protein folding also allows TMAO to maximize the number of favorable contacts with water in the bulk and to stabilize water hydrogen bonding network, giving further stability to the system that contains the folded protein. What is important to mention as well is the fact that solvation of TMAO molecules by water in the bulk prevents pressure-induced crowding of water molecules (in terms of identical neighbors), and this indirect effect of TMAO on water structure greatly reduces the need

of water molecules to move to the protein surface. Hence, without excluding the importance of direct interaction of TMAO with water (and urea in urea/TMAO mixture) and its indirect effect on water structure enhancement, we conclude that the ability of TMAO to protect proteins in the presence or absence of urea at different pressures is a consequence of more inefficient interactions of protein hydrogen bond acceptor sites with solution species on unfolding.

Bibliography

1. G. Panick, R. Malessa, R. Winter, G. Rapp, K. J. Frye, and C. A. Royer *J. Mol. Biol.* **275**, 389 (1998).

2. C. A. Royer *Biochim. Biophys. Acta* **1595**, 201 (2002).

3. N. Ando, B. Barstow, W. A. Baase, A. Fields, B. W. Matthews, and S. M. Gruner *Biochemistry* **47**, 11097 (2008).

4. J. Roche, J. A. Caro, D. R. Norberto, P. Barthe, C. Roumestand, J. L. Schlessman, A. E. Garcia, E. B. Garcíia-Moreno, and C. A. Royer *Proc. Natl. Acad. Sci. U.S.A.* **109**, 6945 (2012).

5. M. W. Lassalle, H. Yamada, and K. Akasaka *J. Mol. Biol.* **298**, 293 (2000).

6. J. L. Silva and G. Weber *Annu. Rev. Phys. Chem.* **44**, 89 (1993).

7. G. Hummer, S. Garde, A. E. García, M. E. Paulaitis, and L. R. Pratt *Proc. Natl. Acad. Sci. U.S.A.* **95**, 1552 (1998).

8. C. Balny, P. Masson, and K. Heremans *Biochim. Biophys. Acta* **1595**, 3 (2002).

9. A. Paliwal, D. Asthagiri, D. P. Bossev, and M. E. Paulaitis *Biophys. J.* **87**, 3479 (2004).

10. H. Lesch, J. Schlichter, J. Friedrich, and J. M. Vanderkooi *Biophys. J.* **86**, 467 (2004).

11. D. Paschek and A. E. Garcíia *Phys. Rev. Lett.* **93**, 238105 (2004).

12. M. D. Collins, G. Hummer, M. L. Quillin, B. W. Matthews, and S. M. Gruner *Proc. Natl. Acad. Sci. U.S.A.* **102**, 16668 (2005).

13. R. Day and A. E. Garcíia *Proteins: Struct., Funct., Bioinf.* **70**, 1175 (2008).

14. J. R. Grigera and A. N. McCarthy *Biophys. J.* **98**, 1626 (2010).

15. T. Imai and Y. Sugita *J. Phys. Chem. B* **114**, 2281 (2010).

16. T. Imai, S. Ohyama, A. Kovalenko, and F. Hirata *Protein Sci.* **16**, 1927 (2007).

17. Y. Harano and M. Kinoshita *J. Chem. Phys.* **125**, 024910 (2006).

18. Y. Harano, T. Yoshidome, and M. Kinoshita *J. Chem. Phys.* **129**, 145103 (2008).

19. T. Yoshidome, Y. Harano, and M. Kinoshita *Phys. Rev. E* **79**, 011912 (2009).

20. G. Weck, J. Eggert, P. Loubeyre, N. Desbiens, E. Bourasseau, J.-B. Maillet, M. Mezouar, and M. Hanfland *Phys. Rev. B* **80**, 180202 (2009).

21. Y. Katayama, T. Hattori, H. Saitoh, T. Ikeda, and K. Aoki *Phys. Rev. B* **81**, 014109 (2010).

22. M. A. Schroer, J. Markgraf, D. C. F. Wieland, C. J. Sahle, J. Möller, M. Paulus, M. Tolan, and R. Winter *Phys. Rev. Lett.* **106**, 178102 (2011).

23. V. Daggett *Chem. Rev.* **106**, 1898 (2006).

24. A. Kumar and P. Venkatesu *Chem. Rev.* **112**, 4283 (2012).

25. D. B. Watlaufer, S. K. Malik, L. Stoller, and R. L. Coffin *J. Am. Chem. Soc.* **86**, 508 (1964).

26. E. G. Finer, F. Franks, and M. J. Tait *J. Am. Chem. Soc.* **94**, 4424 (1972).

27. A. Das and C. Mukhopadhyay *J. Phys. Chem. B* **113**, 12816 (2009).

28. H. S. Frank and F. Franks *J. Chem. Phys.* **48**, 4746 (1968).

29. F. Vanzi, B. Madan, and K. Sharp *J. Am. Chem. Soc.* **120**, 10748 (1998).

30. A. Idrissi, E. Cinar, S. Longelin, and P. Damay *J. Mol. Liq.* **110**, 201 (2004).

31. L. Yang and Y. Q. Gao *J. Am. Chem. Soc.* **132**, 842 (2010).

32. H. Wei, Y. Fan, and Y. Q. Gao *J. Phys. Chem. B* **114**, 557 (2010).

33. D. R. Robinson and W. P. Jencks *J. Am. Chem. Soc.* **87**, 2462 (1965).

34. W. K. Lim, J. Rösgen, and S. W. Englander *Proc. Natl. Acad. Sci. U.S.A.* **106**, 2595 (2009).

35. L. Hua, R. Zhou, D. Thirumalai, and B. J. Berne *Proc. Natl. Acad. Sci. U.S.A.* **105**, 16928 (2008).

36. B. J. Bennion, M. L. DeMarco, and V. Daggett *Biochemistry* **43**, 12955 (2004).

37. E. P. O'Brien, R. I. Dima, B. Brooks, and D. Thirumalai *J. Am. Chem. Soc.* **129**, 7346 (2007).

38. R. D. Mountain and D. Thirumalai *J. Am. Chem. Soc.* **125**, 1950 (2003).

39. G. I. Makhatadze and P. L. Privalov *J. Mol. Biol.* **226**, 491 (1992).

40. C. Oostenbrink and W. F. v. Gunsteren *Phys. Chem. Chem. Phys.* **7**, 53 (2005).

41. Y. Nozaki and C. Tanford *J. Biol. Chem.* **238**, 4074 (1963).

42. P. Das and R. Zhou *J. Phys. Chem. B* **114**, 5427 (2010).

43. R. Zangi, R. Zhou, and B. J. Berne *J. Am. Chem. Soc.* **131**, 1535 (2009).

44. M.-E. Lee and N. F. A. van der Vegt *J. Am. Chem. Soc.* **128**, 4948 (2006).

45. E. M. Duffy, P. J. Kowalczyk, and W. L. Jorgensen *J. Am. Chem. Soc.* **115**, 9271 (1993).

46. D. O. Alonso and K. A. Dill *Biochemistry* **30**, 5974 (1991).

47. M. C. Stumpe and H. Grubmüller *Biophys. J.* **96**, 3744 (2009).

48. H. Wei, Q. Shao, and Y. Q. Gao *Phys. Chem. Chem. Phys.* **12**, 9292 (2010).

49. H. Wei, L. Yang, and Y. Q. Gao *J. Phys. Chem. B* **114**, 11820 (2010).

50. B. J. Bennion and V. Daggett *Proc. Natl. Acad. Sci. U.S.A.* **100**, 5142 (2003).

51. L. J. Borowitzka and A. D. Brown *Arch. Microbiol.* **96**, 3752 (1974).

52. R. D. Bowlus and G. N. Somero *J. Exp. Zool.* **208**, 137 (1979).

53. T.-Y. Lin and S. N. Timasheff *Biochemistry* **33**, 12695 (1994).

54. M. Auton and D. W. Bolen *Proc. Natl. Acad. Sci. U.S.A.* **102**, 15065 (2005).

55. T. C. Gluick and S. Yadav *J. Am. Chem. Soc.* **125**, 4418 (2003).

56. J. Tatzelt, S. Prusiner, and W. Welch *EMBO J.* **15**, 6363 (1996).

57. C. Brown, L. Q. Hong-Brown, and W. Welch *Bioenerg. Biomembr.* **29**, 491 (1997).

58. P. Venkatesu, M.-J. Lee, and H.-m. Lin *J. Phys. Chem. B* **113**, 5327 (2009).

59. C. Krywka, C. Sternemann, M. Paulus, M. Tolen, C. Royer, and R. Winter *Chem. Phys. Chem.* **9**, 2809 (2008).

60. P. H. Yancey and G. N. Somero *J. Exp. Zool.* **212**, 205 (1980).

61. P. H. Yancey *J. Exp. Biol.* **208**, 2819 (2005).

62. M. A. Schroer, Y. Zhai, D. C. F. Wieland, C. J. Sahle, J. Nase, M. Paulus, M. Tolan, and R. Winter *Angew. Chem. Int. Ed.* **50**, 11413 (2011).

63. E. S. Courtenay, M. W. Capp, C. F. Anderson, and M. T. Record Jr. *Biochemistry* **39**, 4455 (2000).

64. D. W. Bolen and I. V. Baskakov *J. Mol. Biol.* **310**, 955 (2001).

65. M. Aburi and P. E. Smith *J. Phys. Chem. B* **108**, 7382 (2004).

66. S. Shimizu *Proc. Natl. Acad. Sci. U.S.A.* **101**, 1195 (2004).

67. Q. Zou, B. J. Bennion, V. Daggett, and K. P. Murphy *J. Am. Chem. Soc.* **124**, 1192 (2002).

68. S. Paul and G. N. Patey *J. Am. Chem. Soc.* **129**, 4476 (2007).

69. A. Wang and D. W. Bolen *Biochemistry* **36**, 9101 (1997).

70. C. Y. Hu, G. C. Lynch, H. Kokubo, and B. M. Pettitt *Proteins* **78**, 695 (2010).

71. M. V. Athawale, J. S. Dordick, and S. Garde *Biophys. J.* **89**, 858 (2005).

72. H. Kokubo, C. Y. Hu, and B. M. Pettitt *J. Am. Chem. Soc.* **133**, 1849 (2011).

73. B. J. Bennion and V. Daggett *Proc. Natl. Acad. Sci. U.S.A.* **101**, 6433 (2004).

74. S. S. Cho, G. Reddy, J. E. Straub, and D. Thirumalai *J. Phys. Chem. B* **115**, 13401 (2011).

75. K. G. Hovagimyan and J. T. Gerig *J. Phys. Chem. B* **109**, 24142 (2005).

76. J. Rösgen and R. Jackson-Atogi *J. Am. Chem. Soc.* **134**, 3590 (2012).

77. C. Sternemann, J. T. Hynes, and D. Laage *J. Phys. Chem. B* **114**, 3052 (2010).

78. J. Hunger, K.-J. Tielrooij, R. Buchner, M. Bonn, and H. J. Bakker *J. Phys. Chem. B* **116**, 4783 (2012).

79. C. C. Mello and D. Barrick *Protein Sci.* **12**, 1522 (2003).

80. L. M. F. Holthauzen and D. W. Bolen *Protein Sci.* **16**, 293 (2007).

81. Y. L. A. Rezus and H. J. Bakker *Phys. Rev. Lett.* **99**, 148301 (2007).

82. J. Qvist and B. Halle *J. Am. Chem. Soc.* **130**, 10345 (2008).

83. Y. L. A. Rezus and H. J. Bakker *J. Phys. Chem. B* **113**, 4038 (2009).

84. D. Laage, G. Stirnemann, and J. T. Hynes *J. Phys. Chem. B* **113**, 2428 (2009).

85. M. P. Allen and D. J. Tildesley *Computer Simulation of Liquids*; Clarendon Press: Oxford, 1987.

86. D. J. Evans *Mol. Phys.* **34**, 317 (1977).

87. D. J. Evans and S. Murad *Mol. Phys.* **34**, 327 (1977).

88. D. Fincham *CCP5 Quarterly* **2**, 6 (1981).

89. C. Tanford *The Hydrophobic Effect: Formation of Micelles and Biological Membranes*; Wiley: New York, 1973.

90. D. Chandler *Nature* **437**, 640 (2005).

91. N. Choudhury and B. M. Pettitt *J. Am. Chem. Soc.* **129**, 4847 (2007).

92. N. T. Southall, K. A. Dill, and A. D. J. Haymet *J. Phys. Chem. B* **106**, 521 (2002).

93. L. R. Pratt *Ann. Rev. Phys. Chem.* **53**, 409 (2002).

94. B. Widom, P. Bhimalapuram, and K. Koga *Phys. Chem. Chem. Phys.* **5**, 3085 (2003).

95. N. T. Southall and K. A. Dill *Biophys. Chem.* **101**, 295 (2002).

96. Y. Zhang and J. A. McCammon *J. Chem. Phys.* **118**, 1821 (2003).

97. S. Shimizu and H. S. Chan *Proteins* **48**, 15 (2002).

98. C. Czaplewski, S. Rodziewicz-Motowidlo, M. Dabal, A. Liwo, D. R. Ripoll, and H. A. Scheraga *Biophys. Chem.* **105**, 339 (2003).

99. T. Ghosh, A. E. Garcíia, and S. Garde *J. Am. Chem. Soc.* **123**, 10997 (2001).

100. T. Ghosh, A. E. Garcíia, and S. Garde *J. Chem. Phys.* **116**, 2480 (2002).

101. T. Ghosh, A. E. Garcíia, and S. Garde *J. Phys. Chem. B* **107**, 612 (2003).

102. T. M. Raschke, J. Tsai, and M. Levitt *Proc. Natl. Acad. Sci. U.S.A.* **98**, 5965 (2001).

103. J.-P. Ryckaert, G. Ciccotti, and H. J. C. Berendsen *J. Comput. Phys.* **23**, 327 (1977).

104. G. Graziano *J. Chem. Soc., Faraday. Trans.* **94**, 3345 (1998).

105. N. F. A. van der Vegt and W. F. van Gunsteren *J. Phys. Chem. B* **108**, 1056 (2004).

106. D. Trzesniak, N. F. A. van der Vegt, and W. F. van Gunsteren *Phys. Chem. Chem. Phys.* **6**, 697 (2004).

107. A. Wallqvist, D. G. Covell, and D. Thirumalai *J. Am. Chem. Soc.* **120**, 427 (1998).

108. M. Ikeguchi, S. Nakamura, and K. Shimizu *J. Am. Chem. Soc.* **123**, 677 (2001).

109. S. Shimizu and H. S. Chan *Proteins* **49**, 560 (2002).

110. G. Graziano *J. Phys. Chem. B* **105**, 2632 (2001).

111. H. J. C. Berendsen, J. R. Grigera, and T. P. Straatsma *J. Phys. Chem.* **91**, 6269 (1987).

112. E. M. Duffy, D. L. Severance, and W. L. Jorgensen *Israel J. Chem.* **33**, 323 (1993).

113. K. M. Kast, J. Brickmann, S. M. Kast, and R. S. Berry *J. Phys. Chem. A* **107**, 5342 (2003).

114. W. L. Jorgensen and J. Tirado-Rives *J. Am. Chem. Soc.* **110**, 1657 (1988).

115. H. Stassen *J. Mol. Struct.: THEOCHEM* **464**, 107 (1999).

116. H. J. C. Berendsen, J. P. M. Postma, W. F. van Gunsteren, A. DiNola, and J. R. Haak *J. Chem. Phys.* **81**, 3684 (1984).

117. H. L. Martinez, R. Ravi, and S. C. Tucker *J. Chem. Phys.* **104**, 1067 (1996).

118. H. Kokubo and B. M. Pettitt *J. Phys. Chem. B* **111**, 5233 (2007).

119. J. A. Schellman *Biophys. J.* **85**, 108 (2003).

120. N. Zhang, F.-F. Liu, X.-Y. Dong, and Y. Sun *J. Phys. Chem. B* **116**, 7040 (2012).

121. R. L. Mancera, A. D. Buckingham, and N. T. Skipper *J. Chem. Soc., Faraday Trans.* **93**, 2263 (1997).

122. S. Garde, G. Hummer, and M. E. Paulaitis *Faraday Discuss.* **103**, 125 (1996).

123. S. Garde, G. Hummer, and M. E. Paulaitis *J. Chem. Phys.* **108**, 1552 (1998).

124. S. Rajamani, T. Ghosh, and S. Garde *J. Chem. Phys.* **120**, 4457 (2004).

125. F. Meersman, D. Bowron, A. K. Soper, and M. H. J. Koch *Biophys. J.* **97**, 2559 (2009).

126. A. Luzar and D. Chandler *Nature (London)* **379**, 53 (1996); *Phys. Rev. Lett.* **76**, 928 (1996).

127. A. Luzar *J. Chem. Phys.* **113**, 10663 (2000).

128. A. Chandra *Phys. Rev. Lett.* **85**, 768 (2000); *J. Phys. Chem. B* **107**, 3899 (2003).

129. S. Balasubramanian, S. Pal, and B. Bagchi *Phys. Rev. Lett.* **89**, 115505 (2002).

130. S. Paul and A. Chandra *Chem. Phys. Lett.* **386**, 218 (2004).

131. D. Rapaport *Mol. Phys.* **50**, 1151 (1983).

132. S. Paul and A. Chandra *J. Chem. Phys.* **123**, 184706 (2005).

133. C. Y. Lee, J. A. McCammon, and P. J. Rossky *J. Chem. Phys.* **80**, 4448 (1984).

134. S. Paul and A. Chandra *J. Phys. Chem. B* **109**, 20558 (2005).

135. S. Paul and A. Chandra *J. Chem. Theory Comput.* **1**, 1221 (2005).

136. P.-L. Chau and R. L. Mancera *Mol. Phys.* **96**, 109 (1999).

137. S. W. Rick *J. Phys. Chem. B* **104**, 6884 (2000).

138. A. Wallqvist *J. Chem. Phys.* **96**, 1655 (1992).

139. A. Wallqvist *Chem. Phys. Lett.* **182**, 237 (1991).

140. A. Wallqvist *J. Phys. Chem.* **95**, 8921 (1991).

141. V. A. Payne, N. Matubayasi, L. R. Murphy, and R. M. Levy *J. Phys. Chem. B* **101**, 2054 (1997).

142. J. A. Rank and D. Baker *Protein Sci.* **6**, 347 (1997).

143. G. J. A. Vidugiris, J. L. Markley, and C. A. Royer *Biochemistry* **34**, 4909 (1995).

144. H. Herberhold, C. A. Royer, and R. Winter *Biochemistry* **43**, 3336 (2004).

145. K. Lum, D. Chandler, and J. D. Weeks *J. Phys. Chem. B* **103**, 4570 (1999).

146. D. M. Huang and D. Chandler *J. Phys. Chem. B* **106**, 2047 (2002).

147. F. H. Stillinger *J. Solution. Chem.* **2**, 141 (1973).

148. G. Hummer, J. C. Rasaiah, and J. P. Noworyta *Nature* **414**, 188 (2001).

149. A. Wallqvist and B. J. Berne *J. Phys. Chem.* **99**, 2885 (1995).

150. A. Wallqvist and B. J. Berne *J. Phys. Chem.* **99**, 2893 (1995).

151. A. Wallqvist, E. Gallicchio, and R. M. Levy *J. Phys. Chem. B* **105**, 6745 (2001).

152. X. Huang, C. J. Margulis, and B. J. Berne *J. Phys. Chem. B* **107**, 11742 (2003).

153. E. Sobolewski, M. Makowski, C. Czaplewski, A. Liwo, S. Oldziej, and H. A. Scheraga *J. Phys. Chem. B* **111**, 10765 (2007).

154. N. Choudhury and B. M. Pettitt *J. Phys. Chem. B* **110**, 8459 (2006).

155. R. D. Mountain and D. Thirumalai *Proc. Natl. Acad. Sci. U.S.A.* **95**, 8436 (1998).

156. R. Zangi *J. Phys. Chem. B* **115**, 2303 (2011).

157. P. Setny, R. Baron, and J. A. McCammon *J. Chem. Theory Comput.* **6**, 2866 (2010).

158. H. S. Ashbaugh and L. R. Pratt *Rev. Mod. Phys.* **78**, 159 (2006).

159. M. Dijkstra, R. van Roij, R. Roth, and A. Fortini *Phys. Rev. E* **73**, 041404 (2006).

160. T. M. Truskett, P. G. Debenedetti, and S. Torquato *J. Chem. Phys.* **114**, 2401 (2001).

161. H. S. Ashbaugh, L. R. Pratt, M. E. Paulaitis, J. Clohecy, and T. L. Beck *J. Am. Chem. Soc.* **127**, 2808 (2005).

162. S. Singh, J. Houston, F. van Swol, and C. J. Brinker *Nature* **442**, 526 (2006).

163. A. Poynor, L. Hong, I. K. Robinson, and S. Granick *Phys. Rev. Lett.* **97**, 266101 (2006).

164. F. Bresme and A. Wynveen *J. Chem. Phys.* **126**, 044501 (2007).

165. P. Ball *Nature* **423**, 25 (2003).

166. S. H. Lee and P. J. Rossky *J. Chem. Phys.* **100**, 3334 (1994).

167. T. Koishi, S. Yoo, K. Yasuoka, X. C. Zeng, T. Narumi, R. Susukita, A. Kawai, H. Furusawa, A. Suenaga, N. Okimoto, N. Futatsugi, and T. Ebisuzaki *Phys. Rev. Lett.* **93**, 185701 (2004).

168. T. Koishi, K. Yasuoka, T. Ebisuzaki, S. Yoo, and X. C. Zeng *J. Chem. Phys.* **123**, 204707 (2005).

169. M. S. P. Sansom and P. C. Biggin *Nature* **414**, 156 (2001).

170. H. S. Ashbaugh and M. E. Paulaitis *J. Am. Chem. Soc.* **123**, 10721 (2001).

171. N. Choudhury and B. M. Pettitt *J. Am. Chem. Soc.* **127**, 3556 (2005).

172. O. Beckstein and M. S. P. Sansom *Proc. Natl. Acad. Sci. U.S.A.* **100**, 7063 (2003).

173. C. Pangali, M. Rao, and B. J. Berne *J. Chem. Phys.* **71**, 2975 (1979).

174. G. Hummer, S. Garde, A. E. García, A. Pohorille, and L. R. Pratt *Proc. Natl. Acad. Sci. U.S.A.* **93**, 8951 (1996).

175. J. Perkyns and B. M. Pettitt *J. Phys. Chem.* **100**, 1323 (1996).

176. G. Hummer and S. Garde *Phys. Rev. Lett.* **80**, 4193 (1998).

177. D. E. Smith and A. D. J. Haymet *J. Chem. Phys.* **98**, 6445 (1993).

178. D. E. Smith, L. Zhang, and A. D. J. Haymet *J. Am. Chem. Soc.* **114**, 5875 (1992).

179. S. Shimizu and H. S. Chan *J. Am. Chem. Soc.* **123**, 2083 (2001).

180. S. W. Rick and B. J. Berne *J. Phys. Chem. B* **101**, 10488 (1997).

181. D. Chandler *Phys. Rev. E* **48**, 2898 (1993).

182. G. Hummer, S. Garde, A. E. García, M. E. Paulaitis, and L. R. Pratt *J. Phys. Chem. B* **102**, 10469 (1998).

183. T. R. Jensen, M. Ø. Jensen, N. Reitzel, K. Balashev, G. H. Peters, K. Kjaer, and T. Bjørnholm *Phys. Rev. Lett.* **90**, 086101 (2003).

184. T. Young, R. Abel, B. Kim, B. J. Berne, and R. A. Friesner *Proc. Natl. Acad. Sci. U.S.A.* **104**, 808 (2007).

185. J. Qvist, M. Davidovic, D. Hamelberg, and B. Halle *Proc. Natl. Acad. Sci. U.S.A.* **105**, 6296 (2008).

186. P. Ball *Chem. Rev.* **108**, 74 (2008).

187. B. J. Berne, J. D. Weeks, and R. Zhou *Annu. Rev. Phys. Chem.* **60**, 85 (2009).

188. S. Lüdemann, R. Abseher, H. Schreiber, and O. Steinhauser *J. Am. Chem. Soc.* **119**, 4206 (1997).

189. S. Shimizu and H. S. Chan *J. Chem. Phys.* **113**, 4683 (2000).

190. L. D. Schuler, X. Daura. and W. F. van Gunsteren *J. Comput. Chem.* **22**, 1205 (2001).

191. C. Pangali, M. Rao, and B. J. Berne *J. Chem. Phys.* **71**, 2982 (1979).

192. S. Paul and G. N. Patey *J. Phys. Chem. B* **111**, 7932 (2007).

193. S. Paul and G. N. Patey *J. Phys. Chem. B* **112**, 11106 (2008).

194. H. Chen, J. Xu, and G. A. Voth *J. Phys. Chem. B* **113**, 7291 (2009).

195. R. A. Kuharski and P. J. Rossky *J. Am. Chem. Soc.* **106**, 5794 (1984).

196. W. L. Jorgensen, J. D. Madura, and C. J. Swenson *J. Am. Chem. Soc.* **106**, 6638 (1984).

197. R. Zangi and B. J. Berne *J. Phys. Chem. B* **110**, 22736 (2006).

198. G. S. Chryssomallis, P. M. Torgerson, H. G. D. Drickamer, and G. Weber *Biochemistry* **20**, 3955 (1981).

199. C. Cléry, F. Renault, and P. Masson *Febs. Lett.* **370**, 212 (1995).

200. B. Wroblowski, José, F. Díaz, K. Heremans, and Y. Engelborghs *Proteins: Struct. Funct. Bioinf.* **25**, 446 (1996).

201. G. Panick, G. J. A. Vidugiris, R. Malessa, G. Rapp, R. Winter, and C. A. Royer *Biochemistry* **38**, 4157 (1999).

202. J. Woenckhaus, R. Kōhling, P. Thiyagarajan, K. C. Littrell, S. Seifert, C. A. Royer, and R. Winter *Biophys. J.* **80**, 1518 (2001).

203. S. Paul and G. N. Patey *J. Phys. Chem. B* **110**, 10514 (2006).

204. F. Meersman, D. Bowron, A. K. Soper, and M. H. J. Koch *Phys. Chem. Chem. Phys.* **13**, 13765 (2011).

205. A. Panuszko, P. Bruździak, J. Zielkiewicz, D. Wyrzykowski, and J. Stangret *J. Phys. Chem. B* **113**, 14797 (2009).

206. K. L. Munroe, D. H. Magers, and N. I. Hammer *J. Phys. Chem. B* **115**, 7699 (2011).

207. G. D. Rose, P. J. Fleming, J. R. Banavar, and A. Maritan *Proc. Natl. Acad. Sci. U.S.A.* **103**, 16623 (2006).

208. Y. Liu and D. W. Bolen *Biochemistry* **34**, 12884 (1995).

209. M. Auton and D. W. Bolen *Biochemistry* **43**, 1329 (2004).

210. C. Y. Hu, H. Kokubo, G. C. Lynch, D. W. Bolen, and B. M. Pettitt *Protein Sci.* **19**, 1011 (2010).

211. L. Pauling, R. B. Corey, and H. R. Branson *Proc. Natl. Acad. Sci. U.S.A.* **37**, 205 (1951).

212. H. Guo and M. Karplus *J. Phys. Chem.* **98**, 7104 (1994).

213. L. C. Mayne, L. D. Ziegler, and B. Hudson *J. Phys. Chem.* **89**, 3395 (1985).

214. G. P. Harhay and B. S. Hudson *J. Phys. Chem.* **97**, 8158 (1993).

215. Y. Wang, R. Purrello, T. Jordan, and T. G. Spiro *J. Am. Chem. Soc.* **113**, 6359 (1991).

216. Y. Wang, R. Purrello, S. Georgiou, and T. G. Spiro *J. Am. Chem. Soc.* **113**, 6368 (1991).

217. N. G. Mirkin and S. Krimm *J. Am. Chem. Soc.* **113**, 9742 (1991).

218. T. Köddermann and R. Ludwig *Phys. Chem. Chem. Phys.* **6**, 1867 (2004).

219. J. N. Spencer, S. K. Berger, C. R. Powell, B. D. Henning, G. S. Furman, W. M. Loffredo, E. M. Rydberg, R. A. Neubert, C. E. Shoop, and D. N. Blauch *J. Phys. Chem.* **85**, 1236 (1981).

220. J. B. O. Mitchell and S. L. Price *Chem. Phys. Lett.* **180**, 517 (1991).

221. W. L. Jorgensen and C. J. Swenson *J. Am. Chem. Soc.* **107**, 569 (1985).

222. L. R. Pratt and D. Chandler *J. Chem. Phys.* **73**, 3430 (1980).

223. S. K. Pattanayak, N. Prashar, and S. Chowdhuri *J. Chem. Phys.* **134**, 154506 (2011).

224. T. Takekiyo, Y. Yoshimura, A. Shimizu, T. Koizumi, M. Kato, and Y. Taniguchi *J. Phys. Condens. Mat.* **19**, 425212 (2007).

225. T. W. Randolph, M. Seefeldt, and J. F. Carpenter *Biochim. Biophys. Acta* **1595**, 224 (2002).

226. N. Smolin and R. Winter *J. Phys. Chem. B* **112**, 997 (2008).

227. K. Bagchi, S. Balasubramanian, and M. L. Klein *J. Chem. Phys.* **107**, 8561 (1997).

228. N. Smolin and R. Winter *Biochim. Biophys. Acta* **1764**, 522 (2006).

229. S. Sarupria and S. Garde *Phys. Rev. Lett.* **103**, 037803 (2009).

230. C. Camilloni, A. Guerini Rocco, I. Eberini, E. Gianazza, R.A. Broglia, and G. Tiana *Biophys. J.* **94**, 4654 (2008).

231. A. Das and C. Mukhopadhyay *J. Phys. Chem. B* **112**, 7903 (2008).

232. E. P. O'Brien, G. Ziv, G. Haren, B. R. Brooks, and D. Thirumalai *Proc. Natl. Acad. Sci. U.S.A.* **105**, 13403 (2008).

233. J. Tirado-Rives, M. Orozco, and W. L. Jorgensen *Biochemistry* **36**, 7313 (1997).

234. D. K. Klimov, J. E. Straub, and D. Thirumalai *Proc. Natl. Acad. Sci. U.S.A.* **101**, 14760 (2004).

235. M. Gao, Z.-S. She, and R. Zhou *J. Phys. Chem. B* **114**, 15687 (2010).

236. M. Eleftheriou, R. S. Germain, A. K. Royyuru, and R. Zhou *J. Am. Chem. Soc.* **128**, 13388 (2006).

237. A. Caballero-Herrera, K. Nordstrand, K. D. Berndt, and L. Nilsson *Biophys. J.* **89**, 842 (2005).

238. H. T. Tran, A. Mao, and R. V. Pappu *J. Am. Chem. Soc.* **130**, 7380 (2008).

239. L. J. Smith, H. J. C. Berendsen, and W. F. van Gunsteren *J. Phys. Chem. B* **108**, 1065 (2004).

240. E. E. Kim, R. Varadarajan, H. W. Wyckoff, and F. M. Richards *Biochemistry* **31**, 12304 (1992).

241. D. A. Case, T. A. Darden, T. E. Cheatham III, C. L. Simmerling, J. Wang, R. E. Duke, R. Luo, M. Crowley, R. C. Walker, W. Zhang, K. M. Merz, B. Wang, S. Hayik, A. Roitberg, G. Seabra, I. Kolossváry, K. F. Wong, F. Paesani, J. Vanicek, X. Wu, S. R. Brozell, T. Steinbrecher, H. Gohlke, L. Yang, C. Tan, J. Mongan, V. Hornak, G. Cui, D. H. Mathews, M. G. Seetin, C. Sagui, V. Babin, and P. A. Kollman, AMBER 10, University of California, San Francisco (2008).

242. L. Martínez, R. Andrade, E. G. Birgin, and J. M. Martínez, *J. Comput. Chem.* **30**, 2157 (2009).

243. T. Darden, D. York, and L. Pedersen *J. Chem. Phys.* **98**, 10089 (1993).

244. U. Essmann, L. Perera, M. L. Berkowitz, T. Darden, H. Lee, and L. G. Pedersen *J. Chem. Phys.* **103**, 8577 (1995).

245. W. Humphrey, A. Dalke, and K. Schulten, J. Molec. Graphics **14**(1), 33 (1996).

246. P. Cioni and E. Gabellieri *Biochim. Biophys. Acta* **1814**, 934 (2011).

247. K. Gekko and H. Noguchi *J. Phys. Chem.* **83**, 2706 (1979).

248. K. Gekko and Y. Hasegawa *Biochemistry* **25**, 6563 (1986).

249. S. D. Samarasinghe, D. M. Campbell, A. Jonas, and J. Jonas *Biochemistry* **31**, 7773 (1992).

250. K. Akasaka, T. Tezuka, and H. Yamada *J. Mol. Biol.* **271**, 671 (1997).

251. H. Li, H. Yamada, and K. Akasaka *Biophys. J.* **77**, 2801 (1999).

252. K. Akasaka, H. Li, H. Yamada, R. Li, T. Thoresen, and C. K. Woodward *Protein Sci.* **8** 1946 (1999).

253. H. Li, H. Yamada, and K. Akasaka *Biochemistry* **37**, 1167 (1998).

254. S. A. Hawley *Biochemistry* **10**, 2436 (1971).

255. A. Zipp and W. Kauzmann *Biochemistry* **12**, 4217 (1973).

256. N. Takeda, M. Kato, and Y. Taniguchi *Biochemistry* **34**, 5980 (1995).

257. K. Goossens, L. Smeller, J. Frank, and K. Heremans *Eur. J. Biochem.* **236**, 254 (1996).

258. K. Inoue, H. Yamada, K. Akasaka, C. Herrmann, W. Kremer, T. Maurer, R. Doeker, and H. R. Kalbitzer *Nat. Struct. Biol.* **7**, 547 (2000).

259. F. Pincet, E. Perez, and G. Belfort *Macromolecules* **27**, 3424 (1994).

260. W. B. Floriano, M. A. Nascimento, G. B. Domont, and W. A. Goddard, 3rd *Protein Sci.* **7**, 2301 (1998).

261. M. Marchi and K. Akasaka *J. Phys. Chem. B* **105**, 711 (2001).

262. N. Hillson, J. N. Onuchic, and A. E. García *Proc. Natl. Acad. Sci. U.S.A.* **96**, 14848 (1999).

List of Publications

1. Rahul Sarma and Sandip Paul, *J. Chem. Phys.* **135**, 174501-1−174501-13 (2011).
2. Rahul Sarma and Sandip Paul, *J. Phys. Chem. B* **116**, 2831−2841 (2012).
3. Rahul Sarma and Sandip Paul, *J. Chem. Phys.* **136**, 114510-1−114510-10 (2012).
4. Rahul Sarma and Sandip Paul, *J. Chem. Phys.* **137**, 094502-1−094502-11 (2012).
5. Rahul Sarma and Sandip Paul, *J. Chem. Phys.* **137**, 114503-1−114503-10 (2012).
6. Rahul Sarma and Sandip Paul, *Chem. Phys.* **407**, 115−123 (2012).
7. Rahul Sarma and Sandip Paul, *J. Phys. Chem. B* **117**, 677−689 (2013).
8. Rahul Sarma and Sandip Paul, *J. Phys. Chem. B* **117**, 5691−5704 (2013).
9. Rahul Sarma and Sandip Paul, *J. Chem. Phys.* **139**, 034504-1−034504-10 (2013).
10. Rahul Sarma and Sandip Paul, *J. Phys. Chem. B* **117**, 9056−9066 (2013).

Conferences Attended

1. Poster presented in the conference *Frontiers in Chemical Sciences (FICS)* held at Department of Chemistry, IIT Guwahati during 3-4 December, 2010.

2. Poster presented in the conference *Theoretical Chemistry Symposium (TCS)* held at Department of Chemistry, IIT Kanpur during 8-12 December, 2010.

3. Poster presented in the conference *Current Trends in Computational Chemistry (CTCC)* held at Department of Chemistry, North-eastern Hill University, Shillong during 16-17 March, 2012.

4. Poster presented in the conference *Theoretical Chemistry Symposium (TCS)* held at Department of Chemistry, IIT Guwahati during 19-23 December, 2012.